

Microfluidic-based organoid vascularization in PDMS devices replicated from 3D printed molds



Alia Alameri

alia.alameri@mail.mcgill.ca

Department of Biomedical Engineering

McGill University, Montreal

April 2022

A thesis submitted to McGill University

In partial fulfilment of the requirements of the degree of

Master of Engineering

In Biological and Biomedical Engineering

TABLE OF CONTENT

1. Abstract.....	1
1.1 English Abstract.....	1
1.2 French Abstract.....	2
2. Acknowledgements.....	3
3. Contribution of Authors.....	4
4. Project Description.....	5
4.1 Motivation.....	5
4.2 Project Goals.....	6
4.3 Declaration of Novelty.....	7
5. Introduction.....	7
5.1 2D and 3D cell culture techniques in tissue engineering.....	7
5.1.1 Cell culture overview and historical background.....	7
5.1.2 2D cell culture definition and properties.....	9
5.1.2.1 <i>Significance of missing cell-cell and cell-ECM interactions in 2D cultures</i>	9
5.1.3 3D cell culture definition, methods, and properties.....	14
5.1.4 Microfluidic cell culture systems for physiological studies.....	19
5.1.4.1 <i>Microphysiological systems: Organoid- and organ-on-a-chip platforms</i>	24
5.2 Brain organoids as models for neuroscience research.....	30
5.2.1 Biological models for neuroscience research: challenges and opportunities.....	31
5.2.2 Applications of brain organoids.....	40
5.2.2.1 <i>Midbrain organoids characteristics and applications</i>	45
5.2.3 Challenges facing current brain organoid models.....	49
5.2.3.1 <i>Vascularization and oxygen and nutrient supplementation</i>	50
5.2.3.2 <i>Non-neuronal cell diversity</i>	60
5.2.3.3 <i>Maturity and aging in brain organoids</i>	62
5.2.3.4 <i>Variability in brain organoid cultures</i>	64
5.3 Vascularization in tissue engineering.....	65
5.3.1 Vascularization in vivo.....	68
5.3.1.1 <i>Vasculogenesis</i>	68
5.3.1.2 <i>Angiogenesis and vascular remodeling</i>	70
5.3.1.3 <i>Examples of biomechanical and biochemical signaling in vascularization</i>	73
5.3.2 Microvascular tissue engineering considerations.....	77
5.3.2.1 <i>Endothelial cell types</i>	77
5.3.2.2 <i>Signaling molecules</i>	79
5.3.2.3 <i>Hydrogel composition and biomechanical cues</i>	80
5.3.3 Brain organoid vascularization.....	80
5.3.3.1 <i>Brain vascularization</i>	80
5.3.3.2 <i>Recent methods for brain organoid vascularization</i>	83
5.3.3.3 <i>Ethical implications of vascularized brain organoids</i>	90
5.3.4 Microphysiological systems of the vasculature.....	96
5.3.4.1 <i>3D wall patterning methods</i>	97
5.3.4.2 <i>3D self-morphogenesis methods</i>	101
5.4 Summary.....	108

6. Microfluidic-based organoid vascularization in PDMS devices replicated from 3D printed molds.....	108
6.1 Abstract.....	109
6.2 Introduction.....	109
6.3 Methods and Materials.....	115
6.3.1 Fabrication of microfluidic-based organoid vascularization devices.....	115
6.3.2 Fabrication of funnel structures for organoid pipetting.....	118
6.3.3 Fluidic tests and diffusion experiments.....	118
6.3.4 Endothelial cell culture.....	119
6.3.5 Midbrain organoid generation.....	119
6.3.6 Midbrain organoid and endothelial cell seeding in MOV devices.....	121
6.3.7 Freezing and cryosectioning organoids.....	122
6.3.8 Immunofluorescence staining and live cell labeling.....	123
6.3.9 Hypoxia and cell death characterization.....	124
6.3.10 Fluorescent dye perfusion.....	125
6.4 Results and Discussion.....	126
6.4.1 Device fabrication, characterization and optimization.....	126
6.4.2 CellTracker-labeled HUVECs integrate into midbrain organoids.....	131
6.4.3 Monitoring vascular sprouting of mCherry-HUVECs and CellTracker-HUVECs.....	136
6.4.4 Vascular-like networks are partially perfusable.....	140
6.4.5 Midbrain organoids express hypoxia and cell death markers.....	141
6.5 Conclusion	143
6.6 Supplementary information.....	144
6.6.1 3D positive molds and PDMS replicas of funnel structures.....	144
6.6.2 Characterization of diffusion in a fibrin-collagen filled chamber.....	145
6.6.3 Final differentiation medium composition.....	145
7. Extended discussion.....	145
7.1 Device fabrication and design.....	145
7.2 Cell and organoid seeding.....	146
7.3 Vascular network formation.....	147
7.4 Hypoxia and cell death.....	148
8. Conclusion and Future Work.....	149
9. References.....	150

LIST OF FIGURES

Figure 1	Hanging drop technique for culturing tissue explants.....	8
Figure 2	Cell-cell interactions and cell-ECM interactions in the <i>in vivo</i> environment.....	10
Figure 3	Tissues of the human body have unique stiffnesses and often softer than plastic.....	11
Figure 4	Distinctions between cells grown in 2D vs. 3D space.....	13
Figure 5	3D cell culture methods.....	14
Figure 6	Organoid 3D cell cultures replicating various organs.....	16
Figure 7	Differences in morphology of cells in 2D, 3D scaffolds, spheroids, organoids.....	16
Figure 8	Methods for liquid transport in microfluidic cell culture platforms.....	22
Figure 9	Lung-on-a-chip system.....	25
Figure 10	BBB-on-a-chip system.....	26
Figure 11	Kidney organoid-on-a-chip.....	28
Figure 12	Brain organoid-on-a-chip in comparison to conventionally grown brain organoids.....	29
Figure 13	Cell death in the core of brain organoids from two different reports.....	51
Figure 14	Organoid slicing method for reducing hypoxia and cell death in brain organoids.....	55
Figure 15	Milifluidic approach vs. shaking for reducing cell death in brain organoids.....	57
Figure 16	Spherical model for development of hypoxia in cerebral organoids.....	58
Figure 17	Steps of angiogenesis; formation of new blood vessels from a preexisting vessel.....	70
Figure 18	Brain vascularization during <i>in vivo</i> fetal development.....	81
Figure 19	Human cerebral organoids implanted in mice brains get vascularized.....	84
Figure 20	Human cerebral organoids embedded in a mix of Matrigel and hiPSC-ECs.....	86
Figure 21	Vascularized human cortical organoids.....	87
Figure 22	Vascularization of human cortical organoids by mixing ECs prior to aggregation.....	88
Figure 23	Vascularization of neuro-mesenchymal assembled organoids by a fusion method.....	89
Figure 24	3D wall patterning methods for modeling the microvasculature <i>in vitro</i>	97
Figure 25	Self-morphogenesis methods for modeling the microvasculature <i>in vitro</i>	101
Figure 26	Motor neuron spheroids co-cultured with ECs show increased neurite length.....	105
Figure 27	Overview of MOV device design and operation.....	121
Figure 28	Fabrication, sterilization, and assembly of MOV devices.....	126
Figure 29	Characterization of control and shell/MOs for size and HUVEC integration.....	132
Figure 30	MOV device co-culture of HUVECs and MOs.....	137
Figure 31	Nuclear staining and partial dye perfusion of vascular-like networks.....	141
Figure 32	Immunohistochemical analysis of hypoxia and cell death in midbrain organoids.....	143
Figure S1	Funnel structures enable safe loading of MOs into MOV devices.....	144
Figure S2	Diffusion of 40-kDa dextran in fibrin-collagen filled MOV device.....	145

LIST OF TABLES

Table 1	Spheroid vs. organoid culture.....	17
Table 2	Conventional and emerging biological models for neuroscience research.....	33
Table 3	Size, hypoxia and necrosis characterizations in reports of brain organoids.....	52
Table 4	Brain organoid vascularization reports.....	85
Table 5	Capillary stop valve function in response to various device configurations.....	128
Table 6	Media formulations for HUVEC shell/MO conditions tested.....	133
Table S1	Final differentiation medium composition.....	145

LIST OF ABBREVIATIONS

ECs	Endothelial cells
MOV	Microfluidic-based organoids vascularization
HUVECs	Human umbilical vein endothelial cells
MOs	Midbrain organoids
HIF1a	Hypoxia inducible factor 1 alpha
CC3	Cleaved caspase 3
TUNEL	Terminal deoxynucleotidyl transferase mediated dUTP nick end labeling
PDMS	Polydimethylsiloxane
3D	Three dimensional
2D	Two dimensional
CNS	Central nervous system
ECM	Extracellular matrix
GAGs	Glycoaminoglycans
PGs	Proteoglycans
RGD	Arginine-Glycine-Aspartic acid
MMPs	Metalloproteinases
EPCs	Endothelial progenitor cells
ESCs	Embryonic stem cells
hiPSC	Human induced pluripotent stem cells
iPSCs	Induced pluripotent stem cells
PSCs	Pluripotent stem cells
CC	Capillary circuits
h	Height
w	Width
L	Length
ΔP	Pressure difference
Q	Flow rate
R	Resistance of flow
η	Viscosity of fluid
γ	Surface tension
θ_s	Contact angle of a surface (s)
BSC	Biosafety cabinet
MPS	Microphysiological systems
AECs	Alveolar epithelial cells
PMECs	Pulmonary microvascular endothelial cells
BBB	Blood-brain barrier
ZO-1	Zona occludens 1
TEER	Transendothelial electric resistance
HBMEC	Human brain microvascular endothelial cells
HBVP	Human brain vascular pericytes
HA	Human astrocytes
EBs	Embryonic Bodies
TBR1	T-Box Brain Transcription Factor 1
CTIP2	COUP-TF-interacting protein 2
AD	Alzheimer's Disease
APP	Amyloid precursor protein
A β	Amyloid- β
RA	Retinoic acid
ALS	Amyotrophic lateral sclerosis
SOD1	Superoxide dismutase 1
SFEBq	Serum-free culture of embryoid body-like aggregates with quick re-aggregation
MCPH	Autosomal recessive primary microcephaly
RGCs	Radial glial cells
ZIKV	Zika virus

NPCs	Neural progenitor cells
COVID-19	2019 coronavirus disease
SARS-CoV-2	Novel severe acute respiratory syndrome coronavirus 2
ACE2	Angiotensin-converting enzyme 2
ROIs	Regions of interest
ASD	Autism spectrum disorder
FAD	Familial AD
SAD	Sporadic AD
DS	Down syndrome
APOE4	Apolipoprotein E4
PD	Parkinson's disease
α -syn	α -synuclein
mDA	Midbrain dopaminergic neurons
LRRK2	Leucine-rich repeat kinase 2
BMP	Bone morphogenic protein
TGF β	Transforming growth factor beta
SHH	Sonic Hedgehog
FGF8	Fibroblast growth factor 8
BDNF	Brain-derived neurotrophic factor
GDNF	Glial-derived neurotrophic factor
FOXA1/2	Forkhead box A transcription factor
LMX1A/B	LIM homeobox transcription factor
NURR1	Nuclear receptor related-1 protein
PITX3	Pituitary homeobox 3 transcription factor
TH	Tyrosine hydroxylase
hMOs	Human midbrain organoids (repetitive)
NM	Neuromelanin
IF	Immunofluorescent
DAPI	4',6-diamidino-2-phenylindole
scRNA-seq	Single cell RNA sequencing
SNO	Sliced neocortical organoids
ETV2	Human ETS variant 2
MLC	Microglia-like cells
Spin Ω	Miniaturized spinning bioreactors
VTE	Vascular tissue engineering
TEVG	Tissue engineering of vascular grafts
MVTE	Microvascular tissue engineering
VEGF	Vascular endothelial growth factor
Ang-1	Angiopoietin 1
VEGFR2/Flk-1	VEGF receptor
aFGF/FGF-1	Acidic fibroblast growth factor
Dll4	Delta-like ligand-4
NRP1	Neurophilin-1
vSMCs	Vascular smooth muscle cells
eNOS	Endothelial nitric oxide synthase
HIFs	Hypoxia-inducible factors
HIF β	Hypoxia-inducible factor beta
Ang-2	Angiopoietin 2
Tie-2	Tyrosine kinase with immunoglobulin-like loops and epidermal growth factor homology domains-2
HMVECs	Human microvascular endothelial cells
iPSC-ECs	Induced pluripotent stem cell derived endothelial cells
vWF	von Willebrand factor
CD34	Cluster of differentiation 34 (endothelial progenitor cells marker)
CD31	Cluster of differentiation 31 (also known as PECAM-1, endothelial cells marker)
hCD31	Human CD31
CM	Conditioned media
GW	Gestational week

SV	Subventricular
NVU	Neurovascular link
dpi	Days post implantation
NOD-SCID	Nonobese diabetic/severe combined immunodeficiency (mouse model)
NSG	NOD SCID Gamma (mouse model)
n/a	Not available
DOX	Doxycycline
hESC	Human embryonic stem cells
iPSC-MPC	iPSC-derived mesodermal progenitor cells
CDH5/CD144	Cadherin 5 (or VE-Cadherin)
P-gp	P-glycoprotein
IB4	Isolectin-B4
Col-IV	Collagen IV
SMA	Smooth muscle actin
PDGFR β	Platelet-derived growth factor receptor beta
EGFP	Enhanced green fluorescent protein
vhCOs	Vascularized human cortical organoids
BVOs	Blood vessel organoids
hBO	Human brain organoids
EEG	Electroencephalography
NCC	Neural correlates of consciousness
POMaC	Poly(octamethylene maleate (anhydride) citrate)
hLFs	Human lung fibroblasts
RPEs	Retinal pigment epithelial cells
WAT	White adipose tissue
hASCs	Human adipose-derived stem cells
hAMECs	Human adipose microvascular endothelial cells
MN	Motor neuron
MNS	Motor neuronal spheroids
CSVs	Capillary stop valves
cnCSVs	Continuous capillary stop valves
PT	Plasma treatment
FDM	Final differentiation media
EGM-2	Endothelial growth media
OCT	Optimal cutting temperature
CT	CellTracker dye
D	Diffusion coefficient
mCh-HUVEC	human umbilical vein endothelial cells expressing fluorescent mCherry protein
GFP-MO	Midbrain organoids expressing fluorescent green fluorescent protein
Shell-MO	Fibrin-EC embedded midbrain organoids
CellTracker-MO	CellTracker-labeled midbrain organoids
CellTracker-HUVEC	CellTracker-labeled human umbilical vein endothelial cells

1. Abstract

1.1 English Abstract

Brain organoids are three-dimensional multicellular structures capable of faithfully recapitulating the *in vivo* brain¹. Brain organoids grown from human induced pluripotent stem cells constitute promising tools for investigating mechanisms that underlie human neurodegenerative diseases and neurodevelopment^{1, 2}. A major challenge that hinders applications of brain organoids is their lack of vasculature, which leads to cell death at their core due to insufficient delivery of oxygen and nutrients once they exceed the diffusion limits that enable oxygenation and nutrient supply^{3, 4}. Attempts to vascularize brain organoids often include differentiation protocols performed in traditional well plates^{3, 5, 6}, which do not provide a straightforward method for perfusion of vascular networks due to a lack of spatial control of endothelial cells (ECs) within the culture. To address the need for spatially controlled vascularization systems, we developed a ‘Microfluidic-based Organoids Vascularization’ (MOV) device. The device leverages microfluidic principles by incorporating capillary stop valves that prevent hydrogel overflow from a middle chamber, where the organoid is added, to side channels where human umbilical vein ECs (HUVECs) are introduced. Digital light processing 3D printing was chosen to fabricate positive molds for fast and cost-effective fabrication of the PDMS device. MOV devices enabled monitoring vascular events during live culture, which we tested using midbrain organoids (MOs) and HUVECs that were either expressing fluorescent proteins or were labeled using a CellTracker dye. Our results showed vascular sprouting of HUVECs in co-culture with MOs, and partial formation of a vascular-like wall within MOV devices. Additionally, to determine the timeframe for vascularization, we characterized progression of hypoxia and cell death in MOs at four time points by immunostaining for hypoxia inducible factor-1 alpha (HIF1 α), cleaved caspase-3 (CC3), and for extensive DNA degradation using TUNEL assay. Our results showed that a dead core develops by the time MOs reach 1 month in culture, and expression of CC3 is directly proportional to the distance from the surface to the core of MOs. Additionally, we observed a pattern of hypoxia that resembled a ring that surrounded necrotic areas within MOs. Our report demonstrates a cost-effective device for studying midbrain vascularization with spatially controlled patterning of hydrogel and defined inlets and outlets, which has potential implications for future neurobiological studies.

1.2 French Abstract

Les organoïdes cérébraux sont des structures multicellulaires tridimensionnelles capables de reproduire fidèlement le cerveau *in vivo*¹. Les organoïdes cérébraux cultivés à partir de cellules souches pluripotentes humaines induites constituent des outils prometteurs pour l'étude des mécanismes qui sous-tendent les maladies neurodégénératives humaines et le neurodéveloppement^{1,2}. Un défi majeur qui entrave les applications des organoïdes cérébraux est leur absence de vascularisation, qui entraîne la mort des cellules en leur cœur en raison d'un apport insuffisant d'oxygène et de nutriments une fois que leur taille dépasse les limites de diffusion qui permettent l'oxygénation et l'apport de nutriments^{3,4}. Les stratégies existantes de vascularisation des organoïdes cérébraux incluent souvent des protocoles de différenciation réalisés dans des plaques à puits traditionnelles^{3, 5, 6}, qui ne fournissent pas une méthode directe pour la perfusion des réseaux vasculaires en raison d'un manque de contrôle spatial des cellules endothéliales (CE) dans la culture. Pour répondre au besoin de systèmes de vascularisation contrôlés dans l'espace, nous avons mis au point un dispositif de « vascularisation d'organoïdes basé sur la microfluidique » (VOM). Ce dispositif tire parti des principes microfluidiques en intégrant des vannes d'arrêt capillaires qui empêchent le débordement de l'hydrogel d'une chambre centrale, où l'organoïde est ajouté, vers les canaux latéraux où les CE de la veine ombilicale humaine (HUVEC) sont introduites. L'impression 3D par traitement numérique de la lumière a été choisie pour fabriquer des moules positifs permettant une fabrication rapide et économique du dispositif en PDMS. Les dispositifs VOM ont permis de suivre les événements vasculaires pendant la culture en temps réel, ce que nous avons testé en utilisant des organoïdes de cerveau moyen (OCM) et des cellules HUVEC qui exprimaient des protéines fluorescentes ou qui étaient marqués en utilisant un colorant CellTracker. Nos résultats ont montré une germination vasculaire des HUVEC en co-culture avec des OCM et la formation partielle d'une paroi de type vasculaire dans les dispositifs VOM. De plus, pour déterminer le délai de vascularisation, nous avons caractérisé la progression de l'hypoxie et de la mort cellulaire dans les OCM à quatre points dans le temps par immunomarquage pour le facteur inductible de l'hypoxie-1 alpha (HIF1 α), la caspase-3 clivée (CC3), et pour la dégradation étendue de l'ADN en utilisant le test TUNEL. Nos

résultats ont montré qu'un noyau mort se développe au moment où les OCM atteignent 1 mois de culture, et que l'expression de CC3 est directement proportionnelle à la distance entre la surface et le noyau des MO. De plus, nous avons observé un modèle d'hypoxie qui ressemble à un anneau entourant les zones nécrotiques des OCM. Notre rapport démontre l'existence d'un dispositif abordable pour étudier la vascularisation du mésencéphale avec une configuration contrôlée dans l'espace de l'hydrogel et des entrées et sorties définies, ce qui a des implications potentielles pour de futures études neurobiologiques.

2. Acknowledgements

I would like to acknowledge and give my sincerest thanks to my supervisor Dr. David Juncker for allowing me the opportunity to pursue my Masters degree in his lab where I gained valuable knowledge in the field of my research, and made wonderful friendships. I would like to also thank him for his guidance and mentorship throughout my journey in his lab, and for his inspiring passion towards science and his encouragement of my research goals. I also thank Dr. Andy Ng for always being available for feedback and mentorship during my Masters. I further express my warm thanks to our collaborators Dr. Thomas Durcan and Dr. Christopher Moraes for their immense support, dedication, and all their efforts in facilitating various aspects of our collaboration. I also thank Dr. Thomas Durcan and his students for allowing me to participate in the iPSC workshop organized by his lab where I had the chance to gain valuable hands-on knowledge about stem cell culture. I also extend many thanks to Dr. Arnold Hayer for his valuable insights and help even at times when I asked on short notice. I also express many thanks to Molly Shen, Camille Cassel de Camps, and Meghna Marthur for their help, dedication, and contributions to this project. I also thank Paula Lépine for training me on cryosectioning and histology, which provided me with valuable skills for this project and future ones.

I also express my thanks to all my colleagues and my friends at Juncker lab and McGill University. I express endless thanks to my bestest friend Molly Shen for her kindness, generosity, and selfless support that kept me going during many difficult times. I also thank her for joining my project and for her passion and excitement towards the proteomic and exosome studies we planned, and for the work she did for this project. While the proteomic results have not made it to this thesis, I

am hopeful that we will find a way to polish them for future publication. I also thank Edward Zhang for supporting me when I decided to pursue this project, his kindness and his support during my Masters journey, and for allowing me the chance to work with him on his Masters project as well.

I also express many thanks to Grant Ongo and Philippe DeCorwin-Martin for all their selfless efforts and the precious time they spent in setting-up the microscopy room at our lab and for their valuable microscopy training that made much of the work I present here possible. I also thank them, along with Vahid Karamzadeh, Zijie Jin, Nick Chahley, Andrew Tang, Rosalie Martel, Dr. Mohamed Yafia, and everyone at the Juncker lab for their scientific input on various aspects related to my research and lab work. I also thank Rosalie Martel for help with reviewing the French translation of the abstract. I also thank our lab managers over the years for helping ensure we had the resources we needed in the lab and their help with logistics, including Pammy Lo, Xuan Wang, Lorena Oliveira, and Katherine Turner.

I am immensely grateful for my close friends Molly Shen, Edward Zhang, Zijie Jin, Andrew Tan, Vahid Karamzadeh, Woojong Rho, and Abdulrahman Almusaabi, for being wonderful friends who constantly made me laugh and made my time in Montréal ever so memorable and sweet.

I am eternally grateful for my parents Laila and Ibrahim, and my sisters for their love and their patience during my time abroad. I am grateful for their endless support of my dreams. I would not have been able to get through many times of despair and hardship without their love and encouragement.

Lastly, the enriching academic, cultural, and life experiences I had in Montréal as an international student at McGill University would not have been possible without the generous support of the McGill-UAE fellowship who funded my Masters studies from 2017 to 2019, which I will always be immensely grateful for. I also express many thanks to the NSERC Discovery Grant for funding my stipend for the year 2020. I am also immensely grateful for the Biological and Biomedical Engineering Department for the excellence award they provided me in support of my academic studies.

3. Contribution of Authors

This thesis and manuscript were written by Alia Alameri, with feedback from Dr. David Juncker. The French version of the thesis abstract was edited by Rosalie Martel. All experiments were carried by Alia Alameri with the following exceptions. Midbrain organoid culture up to FD1 was done by

either Meghna Marthur or Camille Cassel de Camps. Culture of midbrain organoids used in **(Fig. 32)** was done by Camille Cassel de Camps, but cryosectioning and immunofluorescent staining was done by Alia Alameri. Fluorescent staining and perfusion imaging in **(Fig. 31)** was done by Molly Shen with remote feedback from Alia Alameri. Calculation of the diffusion coefficient in **(Fig. S2)** were done by Alia Alameri with help from Zijie Jin who provided code for the error function fitting.

4. Project Description

4.1 Motivation

Three-dimensional (3D) cell culture techniques have been recently recognized as more representative models of the spatial and chemical complexity of *in vivo* tissues than conventional two-dimensional (2D) cultures⁷. 3D cell culture can take many forms including the use of human induced pluripotent stem cells (hiPSC)-derived organoids; multi-cellular structures capable of self-organizing in 3D space to recapitulate various aspects of their *in vivo* organ-counterparts^{7, 8}. Organoids offer several advantages including the ability to derive them from multiple sources such as adult or embryonic tissues and human cells, which allows for modeling human diseases that are difficult to achieve in animal models and rare genetic mutations^{8, 9}. Additionally, organoids' ability to self-organize in 3D space allows for faithful representation of the cytoarchitecture of *in vivo* organs through morphogenesis⁷ (e.g. organoids with cerebral folds¹⁰, liver tubules¹¹, optic cup¹², villus-crypt structures¹³) which is missing in 2D models. Organoids can also differentiate into multiple cell types that exist in an organ of interest, and cells that do not exist in animal models, allowing researchers to account for cell-cell interactions in the microenvironment and accurately model human physiological conditions^{8, 14}.

Along with the advancement in 3D cell culture techniques and the stem cell field, hiPSC-derived brain organoids emerged as promising tools to study neurophysiology, neurodevelopment¹⁰, neurodegenerative diseases¹⁵ and conditions with unique genetic profiles^{16, 17}. Recently reported brain organoids models offer to advance our understanding of a wide range of devastating diseases of the central nervous system (CNS) including Zika virus-associated microcephaly¹⁸, autism spectrum disease¹⁹, Alzheimer's disease²⁰, Parkinson's disease²¹, and Schizophrenia^{9, 15}. Nevertheless, further applications of brain organoids are hindered by their lack of vasculature, which leads to cell death at

their core once their size exceeds the limits of oxygen and nutrient diffusion required for the cells' metabolic needs^{8-10, 20}.

In addition to the important tasks of oxygenation, nutrient delivery and waste removal, the vasculature has also been increasingly recognized for its instructive role to the maturation and maintenance of neuronal populations^{22, 23}. Several recent attempts to vascularize brain organoids in traditional well plates have generated successful results^{3, 6, 24}. However, brain organoid vascularization remains in preliminary stages of research. Despite evidence of formation of perfused vascular networks within these brain organoids^{3, 6, 24}, traditional 3D cell culture methods do not enable straightforward access to the microvasculature for continuous nutrient perfusion during live culture, due to a lack of spatial control of EC patterning which makes identifying a proper inlet and outlet to the microvascular network within the intact structure challenging.

Vascularization of spheroids has been achieved using *in vitro* microphysiological systems that allow spatial control of EC patterning and perfusion through defined inlets²⁵⁻²⁷. However, opportunities for brain organoid vascularization using microphysiological systems have not been fully explored. Furthermore, current methods employed in fabricating microfluidic devices for spheroid vascularization and organoid-on-a-chip applications have been extensively reliant on cleanroom microfabrication techniques, which are expensive, laborious, and time consuming^{25, 28, 29}.

4.2 Project Goals

We aimed to develop a PDMS microfluidic device replicated from 3D printed molds for studying the *in vitro* vascularization of midbrain organoids. Such device could offer control over the spatial distribution of endothelial cells relative to midbrain organoids while allowing a 3D culture with specific inlets and outlets for future perfusion of the vasculature. Device fabrication using PDMS, a transparent, gas permeable and biocompatible elastomer, from 3D printed molds offers a cost-effective and time-efficient fabrication method. In order to realize our project goal, the following aims were set:

- Design and fabrication of PDMS microfluidic devices from 3D printed molds for midbrain organoid vascularization.
- Characterization of hypoxia and necrosis progression in midbrain organoids.

- Co-culture endothelial cells and midbrain organoids in microfluidic devices, and monitor and live-image angiogenic processes.

4.3 Declaration of Novelty

Our approach leveraged 3D printing to fabricate positive molds for replicating PDMS microfluidic devices to be used as platforms for the co-culture of endothelial cells with midbrain organoids in 3D space to study *in vitro* vascularization processes. During this process, we also developed funnel structures that enabled us to solve newly identified challenges that were unique to the process of loading midbrain organoids into microfluidic devices, which have not been previously reported for spheroids and organoids. Additionally, we tested and developed several configurations of the device by alternating surface properties of the PDMS device and its seal, in order to allow two hydrogel-patterning formats applicable for the *in vitro* vascularization of spheroids and organoids in microphysiological systems.

5. Introduction

5.1 2D and 3D cell cultures in tissue engineering

5.1.1 Cell culture overview and historical background

Cell culture refers to a wide range of techniques frequently used in biomedical and clinical applications^{30, 31}. Animal and human cells grown *in vitro* have been utilized in various applications including biological studies to improve our understanding of mechanisms that underlie cell behavior (e.g. proliferation, migration, differentiation) and disease³⁰, cytotoxicity studies for drug development³², the generation of antibodies and development of vaccines^{33, 34}, cell-based therapies³⁵, biocompatibility studies of materials³⁶, and engineering transplantable cellular tissues and organs^{30, 37}. While, ideally, experiments involving cell culture for tissue engineering and physiological modeling should closely mimic cellular function and its microenvironment, recreating such conditions has been demanding due to the multifaceted complexity of *in vivo* conditions³⁰. Researchers have dedicated considerable efforts in recreating the cellular microenvironment through the construction of hydrogels representative of the extracellular matrix³⁸, the addition of spatiotemporal cues of biomolecules³⁹, varying growth media formulations based on cell type and stage of differentiation⁴⁰, surface modifications to account for cell-surface interactions^{41, 42}, co-cultures to account for cell-cell

interactions⁴³, and shifting towards 3D cell culture methods to better represent organs of interest^{30, 44}.

Current notions of cell culture started in the late 1800s through **animal tissue culture experiments** performed by embryologist and anatomist Ross Harrison whereby pieces of tissue were kept alive by maintaining them in test tubes with blood clots, agar or salt solutions as liquid

medium^{45, 46}. Harrison also invented the “hanging drop technique” whereby a small piece of tissue in a droplet of plasma was placed on a surface, and cells from the tissue migrated into the surrounding environment as illustrated in (**Fig. 1**)⁴⁵. Variations of this method is still used today as means for generating spheroids; compact cellular structures used as 3D models of physiological and pathological systems⁴⁷. The next revolution in cell culture that came after Harrison was by Alexis Carrel who developed techniques to allow tissues to keep growing on glass plates^{45, 46}. Cells that migrated from those tissues were then transferred serially several times to new glass plates; establishing early notions of continuous passages in cell culture⁴⁵. Carrel reportedly invented the first prototype of what we know today as tissue culture flasks which he called “D-flasks”⁴⁵. Carrel also showed that serum can be used instead of plasma as liquid medium, and emphasized the importance for sterile techniques by testing the use of small amounts of toluene to inhibit microbial contamination^{45, 46}. Carrel’s enormous contribution to tissue culture enabled him to receive the Nobel Prize in Medicine in 1912⁴⁵. Later on, in the 1950s, these **tissue culture** techniques developed into **cell culture** where cells are collected from various sources, digested by trypsin to detach from their environment, and grown into monolayers immersed with serum-based growth medium⁴⁵. Although frequently used interchangeably, “cell culture” as we know it today should be distinguished from “tissue culture” that was developed by Harrison and improved by Carrel and others later. Tissue culture involves culturing small pieces of tissue in an artificial environment that allows the cells to migrate out of the tissue onto a surface⁴⁵. Tissue cultures remain in use today for various applications^{48, 49}. Cell culture on the other hand, is the harvesting of individual cells from a specific tissue and maintaining them in a glass or plastic flask at physiologically-relevant conditions (*i.e.* body temperature at 37°C and in serum-based medium)⁴⁵.

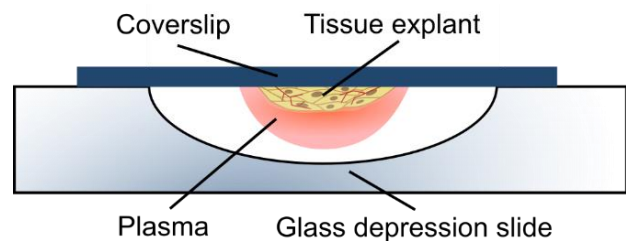


Fig. 1: Hanging drop technique for culturing tissue explants developed by Ross Harrison. *Reproduced by permission from Springer Nature. Viruses and Man: A History of Interactions. (Taylor M. W. 2014). Ref (45).*

Today, over 3600 cell lines are available from over 150 different species with various formulations of growth medium, which contributed to enhancing our understanding of biological systems and advancing medicine⁵⁰.

5.1.2 2D cell culture definition and properties

2D cell culture has been, for decades, the most popular method for maintaining adherent cells as *in vitro* models to study cell behavior in response to biochemical, mechanical, and physical stimuli⁵⁰. In **2D cultures, cells are maintained as a monolayer on a surface** that is most commonly a plastic flask or a petri dish. Such flasks have become a standard in cell culture for their low cost, wide availability, robustness, and simple cell handling protocols that reduce chances of contamination⁵⁰. Surfaces of these flasks can be easily functionalized with proteins, polymers, or other surfaces treatments to enhance cell adhesion, proliferation, and overall health⁵⁰. Due to the excellent optical properties of glass and certain plastics, monitoring cell health, morphology and proliferation throughout the culture period and imaging for post-analysis is easily done⁵⁰. Although 2D cell culture has significantly contributed to our current understanding of biology and cellular processes, in recent years, accumulating evidence has made it clear that **results from 2D cultures do not always reflect the conditions in the 3D microenvironment surrounding cells and organs *in vivo***, due to the missing cell-cell interactions and cell-extracellular matrix (ECM) interactions illustrated in (**Fig. 2**), with the most serious implication of this gap being presented in understanding human diseases, drug development, and translational medicine.

5.1.2.1 Significance of missing cell-cell and cell-ECM interactions in 2D cultures

In 2D cell cultures, a large area of the cell is exposed to the cell culture flask surface on its bottom side and growth media on its top side when in a monolayer, leading to reduced **contact area between adjacent cells connected via junctional proteins that mediate cell-cell interactions**. Indeed, reports have shown **reduced junctional proteins in 2D cultures than in 3D and their implication for cell morphology and behavior**⁵¹⁻⁵³. Intercellular junctions, illustrated in (**Fig. 2**), are mediated mainly by cadherins at adherens junctions, claudins and occludins at tight junctions, and connexons at gap junctions^{54, 55}. **Tight junctions** for instance, once thought to merely serve as permeability barriers to maintain epithelium integrity, are now known to be closely linked to

establishing epithelial apico-basal polarity and are important transmitters of signals to the cell interior to regulate the cytoskeleton, cell proliferation⁵⁶, differentiation⁵⁶, and gene expression^{57, 58}. **Adherens junctions** provide mechanical support for tissues through stabilizing cell-cell adhesive forces, control intracellular mass transport, and contribute significantly to various signaling pathways by responding to and activating Rho, Rac, and Cdc42 which have known roles in regulating the dynamics of the actin cytoskeleton, cell movement and growth, among other cellular processes^{54, 59, 60}. **Gap junctions** are 2-4 nm gaps spanned by protein channels that form pores between cells and play significant communicative roles by transporting ions, biomolecules, and electrical signals from one cell to the other^{54, 61}. Gap junctions are crucial for a wide range of biological functions, including development, differentiation, neuronal activity, hormone-receptor signaling, and immune reactions⁶¹. Therefore, reduced numbers of junctional molecules in 2D cultures is alarming when the research deals with modeling physiology and cellular responses to drugs, as evident by studies reporting differences in cell behavior in 2D cultures compared to 3D cultures⁵¹⁻⁵³.

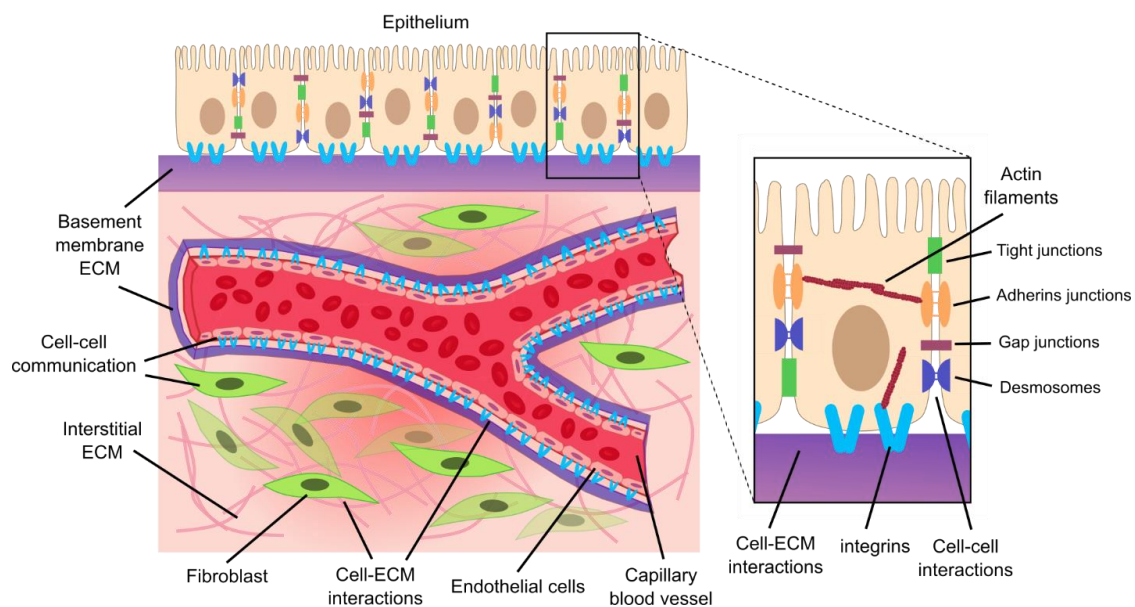


Fig. 2: The *in vivo* environment of cells allow cell-cell interactions through junctional molecules and cell-ECM interactions through integrins that relay cues from the ECM to the cell interior. Reproduced by permission from Springer Nature. Springer eBook (Ariza et al. 2018), Ref (72), and Nature Reviews Molecular Cell Biology. (Matter et al. 2003), Ref (55).

Furthermore, **traditional 2D cell cultures lack physiologically relevant cell types that exist in the vicinity of a cell of interest**^{62, 63}. This removes crucial extracellular signaling pathways that occur through paracrine, endocrine, and synaptic signaling *in vivo*⁶⁴. Creative **2D co-culture methods**

have been proposed through the use of transwells⁴³, micropatterning⁶⁵, sandwich cultures⁶⁶, and microfluidics⁶⁷ to address those challenges and showed physiological relevance and significant implications for drug discovery, but many of those methods remain constraint by the number of cell types that can be introduced, lack of cytoarchitecture, limited formats that allow direct contact between two different cell types, long fabrication protocols, and lack of 3D cell-ECM interactions.

2D cultures and many formats of 2D co-cultures are traditionally carried out on stiff substrates that are not representative of the mechanical and biochemical properties of **the extracellular matrix; a highly dynamic 3D network of fibrous proteins, glycoproteins, proteoglycans, polysaccharides, enzymes and growth factors, that comprises the non-cellular compartment of tissues and provides structural and biochemical support to cells**⁶⁸. The striking difference in stiffness between a plastic or glass petri dish and human tissues is illustrated in (**Fig. 3**), showing that plastic or glass at 2-4 GPa is almost six orders of magnitude stiffer than the human brain; one of the softest tissues in the human body at 1-4 kPa⁶⁹⁻⁷¹.

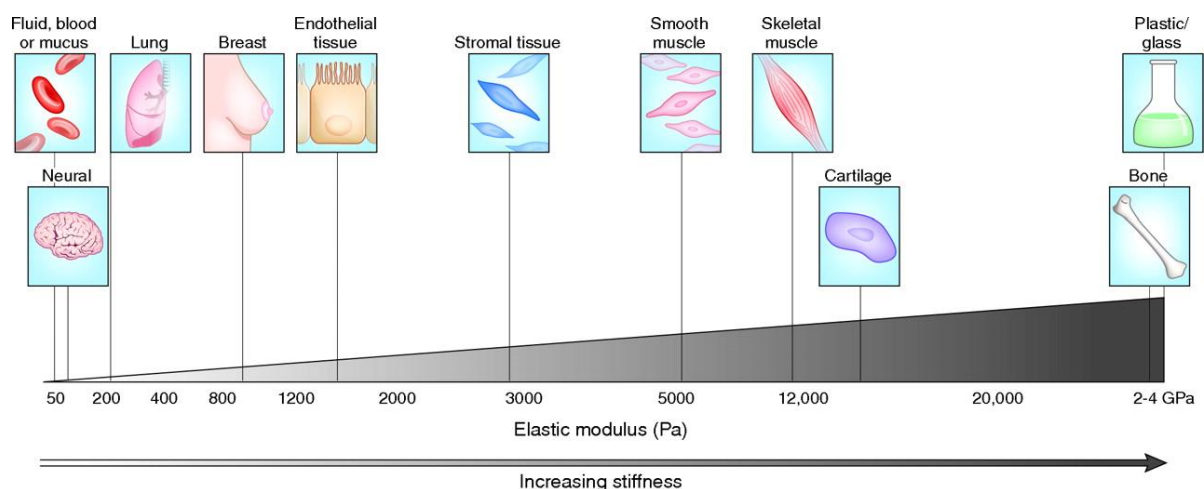


Fig. 3: Tissues of the human body have unique stiffnesses and are several orders of magnitude softer than plastic or glass with the exception of bone. *Reprinted by permission from The Company of Biologists Ltd. Disease Models & Mechanisms. (Thomas R. Cox, Janine T. Erler., copyright 2011). Ref (69).*

The ECM can be categorized based on its location *in vivo* to interstitial ECM and basement membrane ECM as illustrated in (**Fig. 2**), both of which have their unique protein compositions, mechanical and biochemical properties, and mechanical inputs⁷². Mechanical properties of the ECM include **material stiffness**; a measure of its resistance to deformation in response to an applied force, **strength**; a measure of its resistance to damage or failure, and **elasticity**; its ability to return to its

original geometry upon unloading of forces without dissipating energy^{71, 73}. These mechanical properties of the ECM are mainly dictated by the concentration and composition of three constituents of the ECM: **elastic fibers** (e.g. elastin) which provide extensibility and resilience to the ECM, **fibrillar collagens** (e.g. collagen type I and III) which contribute to ECM stiffness and strength, **glycosaminoglycans** (GAGs), and **proteoglycans** (PGs) which attach to ECM proteins cores and provide various functions such as sequestering of growth factors and ECM hydration^{72, 73}. Cells sense the ECM mainly through transmembrane proteins called **integrins** that are connected to cytoskeletal actin filaments through their intracellular domain and focal adhesions, and to epitopes of ECM proteins such as RGD through their extracellular domain⁷³. Mechanical inputs in the ECM can take many forms including gravity, shear stresses, and tensile and compressive forces or cellular forces applied to the matrix⁷¹. Cells sense their environment by applying traction forces that pull the ECM through actin-myosin contractility, and respond to mechanical inputs in various ways depending on the cell type and the developmental stage of the tissue⁷³. **Biochemical components** that do not directly contribute to the mechanical properties of the ECM include laminins, fibronectin, tenascins, growth factors, and matrix metalloproteinases (MMPs), are of equal importance to processes such as cell adhesion to the matrix, cell migration decisions, and ECM degradation⁷⁴. Disturbance of ECM mechanical and biochemical properties causes diverse physiological responses of cells ranging from differentiation, tissue organization and development, cell migration, cell division, homeostasis, and gene expression⁷³. For instance, studies have demonstrated that **stem cell shape and lineage specification are influenced by mechanical inputs of the ECM** that modulate Rho-dependent cell contractility⁷⁰. More specifically, soft matrices, such as that of the brain, have been found to differentiate stem cells into a neurogenic lineage, whereas stiffer matrices, such as that of the muscle, push them into myogenic and osteogenic lineages^{70, 75}.

Numerous reports show the influence of the ECM stiffness on **morphogenesis and cell behavior** including that of neural, muscle, and endothelial cell types. For instance, endothelial cells branch into small capillary-like vessel when cultured on compliant gels, but form large vessels with bigger lumens when cultured on stiffer substrates with a lower rate of endothelial cell sprouting, however, those results differ when the cells are cultured in 3D versus 2D or when other cell types such

as fibroblasts are introduced^{70, 76}. Additionally, the formation of new blood vessels requires ECM degradation by MMPs which are secreted by endothelial progenitor cells (EPCs); a key step in tissue repair and neovascularization. This process allow EPCs to migrate from their niche to target tissues that require repair. MMPs production rate is also influenced by the ECM stiffness, demonstrating that ECM mechanical properties and biochemical compositions are closely linked and are key factors in **cell migration and gene expression**⁷⁷.

The above examples of cell-ECM interactions follow the principle of **dynamic reciprocity** which refers to the continuous bidirectional interaction between cells and their ECM⁷⁸. Continuous remodeling of the ECM modifies biomolecules near the cell membrane and exerts mechanical forces on cells, thereby initiating signaling cascades that lead to changes in gene expression and cell behavior⁷⁸. Consecutively, cellular changes affect the composition and organization of ECM components⁷⁸. These ongoing interactions define the dynamic reciprocity between cells and their microenvironment, and its critical role in development and adult tissue homeostasis⁷⁸.

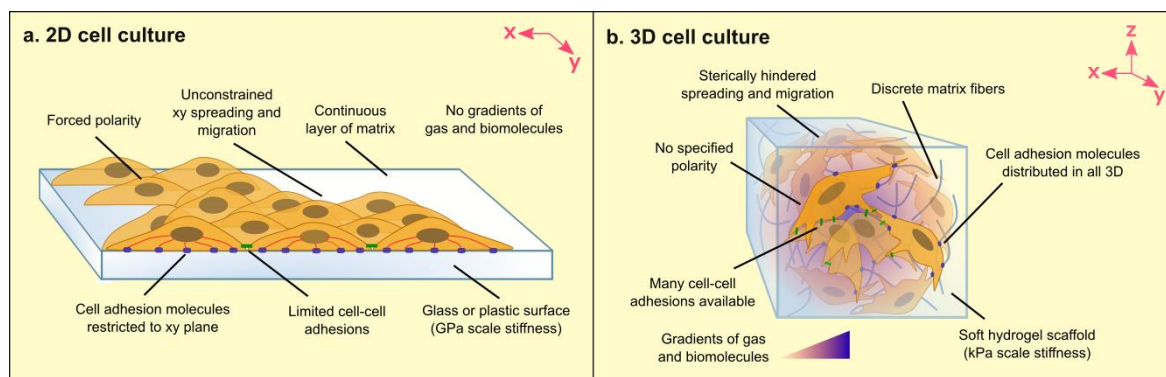


Fig. 4: Distinctions between cells grown in 2D vs. 3D space in morphology, behavior and mechanical and biochemical cues experienced. *Reproduced by permission from The Company of Biologists Ltd. Journal of Cell Science. (Baker, B. M. and Chen C. S., 2012). Ref (79).*

In addition, the 3D nature of the ECM, the unique distribution of cells in tissues, ECM remodeling by cells, the thickness of 3D tissues and the secretion of molecules by cells of each tissue into 3D space lead to generating **gradients of gas and molecules** in the ECM and **gradients of stiffness** with various **surface topography**³¹. All of which are crucial factors that influence cell behavior and are typically removed when cells are transferred from 3D to a 2D space where oxygen and nutrients supply is unlimited and one continuous matrix is available rather than discrete fibers of ECM proteins^{30, 31}. The microenvironmental differences between cells in 2D compared to 3D,

summarized in (Fig. 4), become especially important when studying phenomena that are strongly dependent on such factors such as development, cell migration, cancer progression, and many other cellular processes^{30, 31, 79}. Due to the above shortcomings of 2D culture, alternative methods emerged for culturing cells in 3D systems that more closely mimic *in vivo* conditions.

5.1.3 3D cell culture definition, methods, and properties

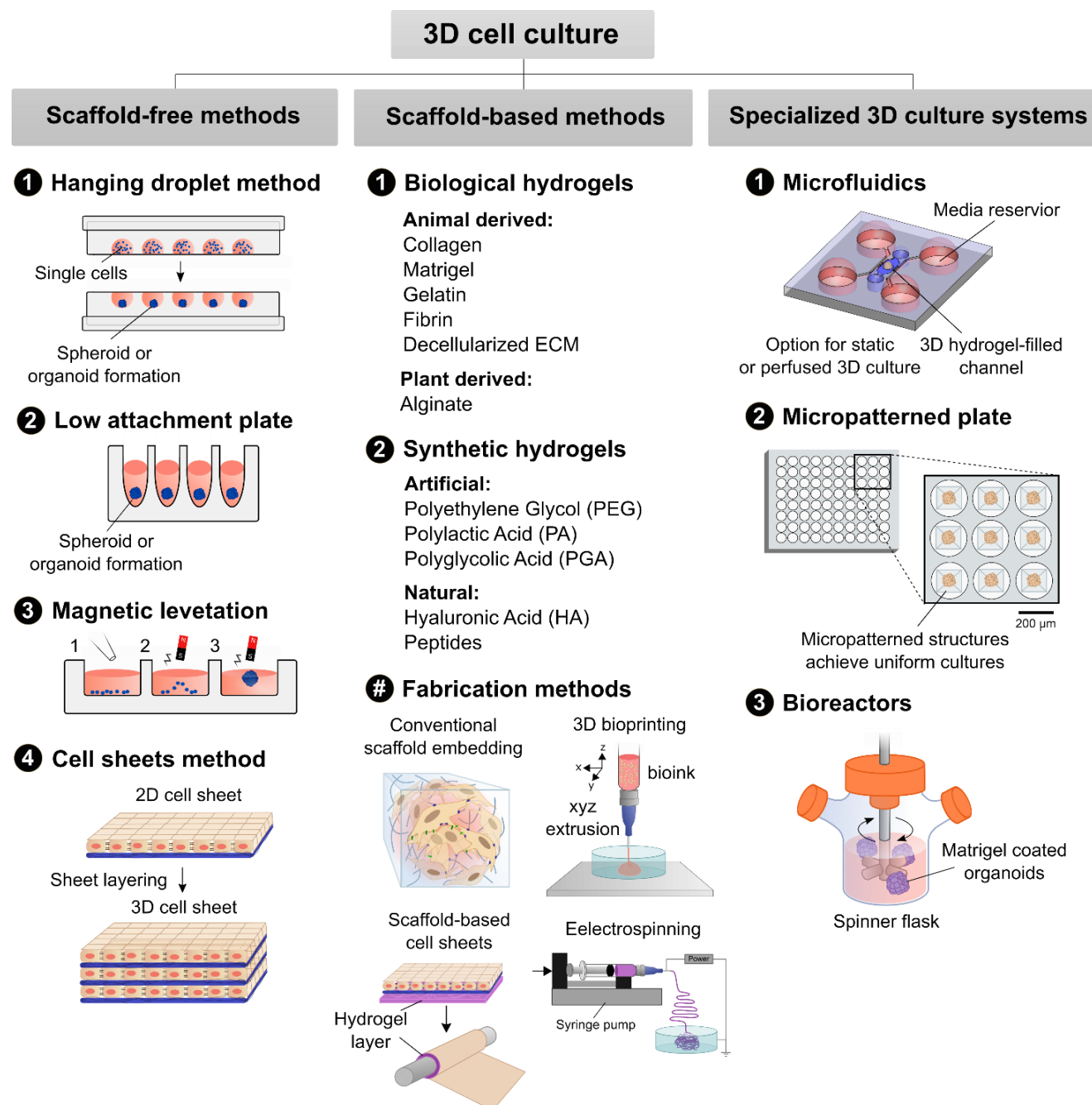


Fig. 5: 3D cell culture methods are categorized into: scaffold-free methods, scaffold-based methods, and specialized 3D culture systems. Most frequent methods for 3D cell culture are summarized below each category. *Reproduced/adapted under the terms of the Creative Commons Attribution License. Frontiers in Pharmacology. (Langhans S. A. 2018). Ref (80).*

Novel 3D cell culture techniques emerged with the increasing interest in replicating *in vivo* conditions for tissue engineering applications. **A 3D cell culture can be defined as any appropriate *in vitro* platform that allows cells to proliferate in all three directions**, unlike planar 2D cultures that limit cells proliferation to a single surface⁵⁰. Various formats of 3D cell culture exist and mainly include spheroid cultures, organoid cultures, 3D bioprinted cellular structures, conventional cellular scaffolds, cell sheets, and microfluidic cell cultures^{30, 80, 81}. These formats of 3D cell culture are often categorized into 1) scaffold-free methods, 2) scaffold-based methods, and 3) specialized 3D culture systems as summarized in **(Fig. 5)**^{30, 80}.

An ideal 3D cell culture system must closely mimic physiological or pathological conditions, where cells are allowed to proliferate, migrate, and differentiate in a microenvironment that includes physiologically relevant forms of cell-cell interactions, cell-ECM interactions, and gradients of stiffness, oxygen, nutrients and metabolic waste⁸⁰. Each of those methods meets some of those requirements thus has its own advantages and limitations making each method suitable for certain applications more so than others.

Spheroid and organoid 3D cell cultures

Scaffold-free methods such as the hanging droplet method, low attachment plate, and magnetic levitation allow the formation of **cell aggregates** from an initial number of single cells which makes them suitable for generating spheroids and organoids that can be used for physiological and pathophysiological modeling, and high throughput screening of drug agents for developing therapeutics and personalized medicine^{30, 80}.

Spheroids are distinguished from organoids in that spheroids are cellular aggregates formed from either one or more cell type that are not necessarily capable of self-organization or differentiation into additional subpopulations^{82, 83}. On the other hand, organoids are 3D cell aggregates derived from either embryonic stem cells (ESC), induced pluripotent stem cells (iPSC), primary cells, or primary tissues that are capable of self-renewal and self-organization to resemble *in vivo* organs^{8, 80}. Organoids provide the advantage of replicating organs architecture on a micro- to a millimeter scale⁸. This is important because organ structure and cell organization define its function and response to stimuli⁸. Spheroids replicate cell-cell interactions but lack the level of cell

organization and differentiation organoids provide⁸³. Both spheroids and organoids have been used as 3D models of normal physiological conditions and as disease models^{8, 82, 83}. However, spheroid cultures are most frequently used to generate models of 3D tumors generated from cancer cells or tumor biopsies^{82, 84}, while organoids are more frequently used for generating 3D models of *in vivo* organs in health and disease and rarely used for generating tumor models^{8, 80}. **Spheroids** are typically more compact and form more regular shaped spheres than **organoids** which have a high order of complexity and form irregular shapes with folds, rosettes, buddings, or gyrations based on the type of organ modeled, as illustrated in (Fig. 6) of various organoids including cerebral organoids¹⁰, lung bud organoids⁸⁵, intestinal organoids⁸⁶, and cardiac organoids⁸⁷.

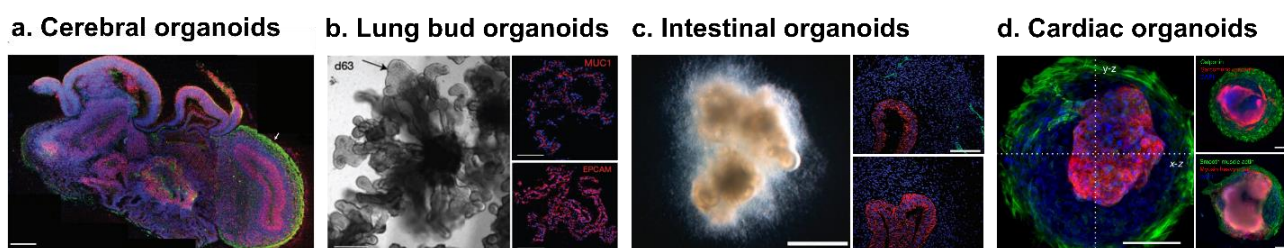


Fig. 6: Organoid 3D cell cultures replicating various organs: (a) **Brain organoids** self-organize to form cerebral folds with heterogeneous regions containing neural progenitors (red) and neurons (green). (Lancaster *et al.* 2013), Ref (10). (b) **Lung bud organoids** as models for lung development show alveoli budding and alveolar epithelial cell type II markers (red). (Chen Y. W. *et al.* 2017), Ref (85). (c) **Intestinal organoids** showing early villi structures stained for the epithelium layer (red). (Workman M. J. *et al.* 2016), Ref (86). (d) **Cardiac organoids** show organization of cardiac cells (red) in the center and myofibroblasts (green) on the periphery resulting in beating heart organoids. (Ma *et al.* 2015), Ref (87). All images were reprinted by permission from their respective publishers.

The difference between organoids and spheroids is illustrated in (Fig. 7) in comparison to traditional 2D cell culture and 3D cell culture where cells are directly embedded in a scaffold⁸³. Despite several distinctions between organoids and spheroids, both are frequently illustrated as spheres for simplicity, and the two terms are sometimes used interchangeably in literature. Peer reviewed articles that summarize or systematically study those distinctions are lacking, despite observable differences

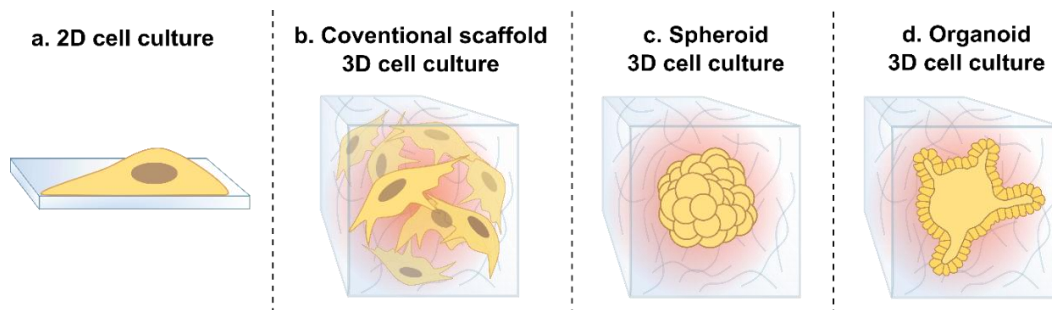


Fig. 7: Differences in morphology and shape of cells cultured using traditional 2D cell culture (a), and the main three 3D cell culture formats: conventional scaffold embedding (b), spheroid culture (c), and organoid culture (d). Reproduced by permission from Cambridge University Press. MRS Communications. (Carter S. D. 2017), Ref (83).

from research articles of spheroids and organoids of the same models. Here we summarize notable differences between spheroids and organoids in (**Table 1**).

Table 1: Spheroid vs. organoid 3D cell culture

	Spheroids	Organoids
Source	Cell lines, primary cells, primary tissues ^{31, 84}	Stem cells, primary cells, primary tissues ⁸
Shape	Regular spheres ⁸³	Irregular shapes ⁸⁸
Biological resemblance	Cell-cell interactions, limited self-renewal, lack cell-organization ⁸⁰	Cell-cell interactions, self-renewal, self-organization, differentiation ^{8, 80}
Culture length	Weeks ⁸⁹	Months ⁸⁸
Frequent applications	Cancer biology, drug screening ³¹	Physiological and pathological modeling, development, drug screening ⁸

3D cell sheets

Contrary to high throughput methods for generating organoids and spheroids, methods such as scaffold-free cell sheets⁹⁰ and scaffold-based ones⁹¹ have not been demonstrated for high throughput applications due to their laborious steps and high dependence on the skill of the lab member which leads to variations in resulted structures. Scaffold-free 3D cell sheets are generated from a confluent single layer of cells cultured using traditional 2D cell culture methods⁹⁰. Multiple layers of confluent cultures are then manually manipulated using tweezers to layer them on top of one another or rolled around a rod to generate 3D tubular structures⁹⁰. Scaffold-based 3D cell sheets are similarly layered on top of one another or rolled around a rod with the exception of a scaffold layer added at first⁹¹. This method is a viable option for engineering tissues composed of organized layers of cells such as cardiac tissues and blood vessels. Cell sheet methods have been successfully applied for vascular tissue engineering, neuronal cultures, and generating a tumor microenvironment, among other methods⁹⁰⁻⁹². Cardiac tissues generated using cell sheet methods have been proposed as transplantable structures and have been tested for *in vivo* transplantation in infarcted porcine hearts⁹³. Similarly, blood vessels generated using cell sheet techniques have been proposed as transplantable small vessel grafts, and as microphysiological systems for *in vitro* drug testing^{90, 94}. Tumor cell sheets have been proposed for pathological modeling and analysis⁹¹. Generally, **scaffold-free methods** allow culturing cells in an environment that account for cell-cell interactions, 3D organization of cells, and naturally occurring gradients of oxygen and nutrients within 3D structures once they exceed a certain size. On the other hand, **scaffold-based methods** allow those same advantages in addition to cell-ECM interactions.

Therefore each method is suitable for applications that require either one or both interactions to be accounted for.

Scaffold-based methods

Methods for seeding cells in scaffold-based 3D cultures involve: 1) generating a scaffold then introducing cells on top of it, 2) generating the scaffold then perfusing cells through it, 3) using spinner flasks or rotating chambers with suspended cells to aid with seeding, 4) embedding cells in the scaffold by mixing them with the hydrogel pre-polymer then polymerizing the whole mixture, or 5) generating a 3D cell culture (*e.g.* organoids, spheroids) then embedding it in a hydrogel in a well or a microchamber^{84, 95}. Conventional methods for generating cellular scaffolds and electrospinning methods are typically done in well plates and do not offer precise control over tissue structure or cell organization. 3D bioprinting on the other hand provides the option for layer-by-layer fabrication that replicates the macro architecture of organs with bioinks of interest and patterning of different cell types within the structure⁹⁶. However various bioprinting methods such as extrusion-based, light-based stereolithography, and laser-based bioprinting have their own advantages and limitations in terms of resolution, cell viability, and speed which is reviewed elsewhere⁹⁶.

Specialized 3D cell culture methods

Scaffold-free and scaffold-based 3D cell culture methods offer great opportunities for studying cellular responses in a 3D environment that resembles *in vivo* conditions. However, those methods can have certain limitations due to high costs, time consuming protocols, lack of uniformity and reproducibility of the generated 3D cultures, and lack of control over 3D cell patterning⁸⁰. Thus, **specialized 3D cell culture methods** have been proposed to address some of those limitations which include microfluidic cell culture methods, micropatterned plates, and bioreactors^{30, 80}. Microfabrication technology generally refers to techniques that allow for manufacturing miniature units or devices with features at micrometer or submillimeter resolution⁹⁷. Such technologies have been employed in developing integrated, fast, and cost-effective cell culture systems that have the potential for high throughput probing, testing, and analysis⁹⁷. Biological applications involving microfabrication technologies are various and include detection assay development⁹⁸, surface patterning to study cell adhesion, shape, and migration⁹⁹, fabrication of microwells for entrapment of single cells¹⁰⁰, and the

development of microfluidic devices and micropatterned plates for 3D cell culture, among other applications⁹⁷. **Microfluidic cell culture** allows the use of small volumes of reagents, patterning cells of different types in microfluidic channels, and the generation of flow rate and concentration gradients among other advantages that will be discussed further in (Section 5.1.4.)^{97, 98}. **Micropatterned plates** are designed to include microstructures that allow seeded cells to aggregate in a uniform manner across all the wells in the plate⁸⁰. This overcomes the lack of uniformity of spheroids or organoids generated in the common well plates we describe in non-scaffold based methods. **Bioreactors** allow large scale production and efficient transport of nutrients^{30, 101}. Additionally, specialized 3D cell culture methods such as microfluidics and bioreactors allow for introducing mechanical inputs to the cells such as shear stress which furthers *in vivo* mimicry of those methods^{50, 101}.

Scaffold-free and scaffold-based methods illustrated in (Fig. 5) represent the main techniques used for generating the initial 3D cell culture. However, once cell aggregates such as organoids or spheroids are formed they can be then embedded into a scaffold, or transferred to a bioreactor or a microfluidic device to proliferate, mature, or differentiate for the remainder of the culture period. Organoids and cellular scaffolds have also been implanted *in vivo* to either mature further as physiological models, or to test their clinical effects *in vivo*^{93, 102}. Various additional formats of 3D cell culture exist but mainly stem from the methods illustrated in (Fig. 5).

5.1.4 Microfluidic cell culture systems for physiological studies

Microfluidics refers to the science and technology of developing miniaturized systems capable of manipulating microliter to femtoliter volumes of liquid, which enables additional characteristics that have been advantageous for biomedical applications¹⁰³⁻¹⁰⁵. This is achieved by the fabrication of channels with dimensions of tens to hundreds of micrometers which is realized with the increasing advancements of microfabrication technologies^{97, 103}. The requirement for **small volumes reduces consumption of reagents and precious samples therefore significantly reduces costs** associated with microfluidic systems. In addition to their low cost, microfluidic devices are **easy to automate, disposable and have small footprints**¹⁰⁵. The first applications that microfluidics have been recognized for have been in separation and detection assays which can be carried out with **high resolution and sensitivity** in microfluidic devices due to their small channel dimensions, **precise**

control over fluid flow profiles, mass transport and concentration of molecules in space and time, and short analysis time^{103, 105}.

Some of those features have been also recognized as advantageous for both 2D and 3D cell culture and tissue engineering^{50, 98}. As previously mentioned, close mimicry of *in vivo* conditions requires recreating cell-cell interactions, cell-ECM interactions, physiological levels of shear stresses and mechanical cues, and relevant *in vivo* gradients and temperature⁵⁰. Microfluidics allow realizing many of those requirements through cell patterning, introduction of flow, hydrogel embedding in channels, and precise control over device pressure and temperature, which many of the other 3D cell culture methods cannot achieve^{50, 98}. The ability to introduce flow in defined inlets in microfluidic devices enables creating physiologically relevant shear stresses, automated and continuous removal of waste and replenishing of nutrients which cannot be achieved using traditional well plate based cell culture platforms that require daily or bi-daily maintenance⁵⁰. Additionally, microfluidic devices for cell culture applications are frequently made of materials such as polydimethylsiloxane (PDMS), transparent thermoplastics and glass, allowing **favorable optical properties** that allow direct monitoring and on-chip analysis including fluorescent microscopy, Raman spectroscopy^{50, 106}. Additionally, the small footprint of microfluidic devices allows developing **multi-tasked platforms that integrate multiple laboratory processes** (*e.g.* single cell sequencing, protein or pathogen detection, separation of cells) in one device, rendering the terms lab-on-a-chip, or the term organ-on-a-chip and body-on-a-chip in case of physiological models of organs¹⁰⁴. The small footprint also allows **parallelization** of each device as a small units in a larger platform which is advantageous for applications that require **high throughput analysis** such as drug screening^{106, 107}.

The use of microfluidics for cell culture applications has unique considerations, much the foundations of which have been laid out in a key review by David Beebe and Edmond Young¹⁰⁸. These considerations mainly pertain to 1) device design and operation, and 2) control over the *in vitro* microenvironment¹⁰⁸. Control over the *in vitro* microenvironment requires considering a suitable method for loading the cells or tissue into the device, and providing suitable biochemical and biomechanical cues for the application of interest. This constitutes patterning of ECM-based hydrogel and growth factors to support the cells and requires considering factors that affect degradation of the

hydrogel and cells consumption of growth factors/biomolecules added such as evaporation of media, the effective culture time, the critical perfusion rate, and bubble formation that could hinder media flow¹⁰⁸. The design and operation of the device has several key components researchers consider as well, including the material of the device, the suitable fabrication method based on the design requirements, the geometries and surface properties of the device, and the mode of liquid transport via pumps or valves¹⁰⁸. Throughout this introduction chapter, we provide examples for how some of these considerations were factored into the development of microfluidic-based cell culture platforms.

Transport of aqueous solutions through microfluidic channels can be achieved either using active systems such as those incorporating pumps, or passive systems such as those relying on capillary forces and gravity^{105, 109, 110}. In active systems fluid is forced to behave in a manner that is unachievable through geometry alone hence require external peripheral control, while passive systems allow fluid flow through the geometry of microchannels, their surface tension and natural flow features that arise^{105, 111}. The term capillarics has been coined for capillary force-driven liquid manipulation in passive microfluidic systems recently¹⁰⁵. Passive microfluidic systems can be designed to incorporate elements that regulate fluid flow. Such designs are referred to as microfluidic circuits or “capillary circuits” (CC) in analogy to electrical circuits¹⁰⁵. For instance, resistance of flow, **R**, through microchannels is analogous to resistance in electrical wires. Similarly, flow of liquid, **Q**, is similar to “flow of charge”, although electrons are prefilled in electrical circuits but not in CCs. The voltage difference in electrical circuits is the pressure difference ΔP across a microchannel in CCs. Those analogies, allow us to calculate the resistance in microfluidic channels using the below equation:

$$R = \frac{\Delta P}{Q} = \frac{12\eta L}{h^3 w} \left[1 - 0.630 \frac{h}{w} \right]^{-1} \quad (1)$$

where η represents the viscosity of the liquid, and L, h, w represent the length, height, and width of the microfluidic channel respectively, and $(h < w)$ ¹⁰⁵. CCs are designed by combining “capillary circuit elements” which regulate fluid flow¹⁰⁵. The initial flow in microchannels is driven by **capillary pressure** but then maintained using CC elements called **capillary pumps**, various designs of which are reviewed by Olanrewaju *et al.*¹⁰⁵. Capillary pressure arises in microfluidic channels as a result of the geometry of the channel and the surface tension at the liquid-air interface¹⁰⁵.

It is therefore defined by the size of the microchannel and the contact angle of the surfaces of all of its sides, according to this equation:

$$P = -\gamma \left[\frac{\cos\theta_t + \cos\theta_b}{h} + \frac{\cos\theta_l + \cos\theta_r}{w} \right] \quad (2)$$

where γ is the surface tension of the liquid in the microchannel, and θ_t , θ_b , θ_l , and θ_r represent the contact angle of the top, bottom, left, and right surfaces of the microchannel¹⁰⁵. Thus surface modifications such as plasma treatment of devices made of hydrophobic materials, among other treatments, contribute to changing the profile of liquid flow in microchannels^{105, 112}. Additional CC elements such as flow resistors, trigger valves, stop valves, retention valves, and retention burst valves also regulate fluid flow in CCs¹⁰⁵. Such circuit elements and design principles have been utilized to transport liquid through microchannels, generate gradients, and pattern cells for numerous applications for on-chip 2D and 3D cell culture^{50, 106}.

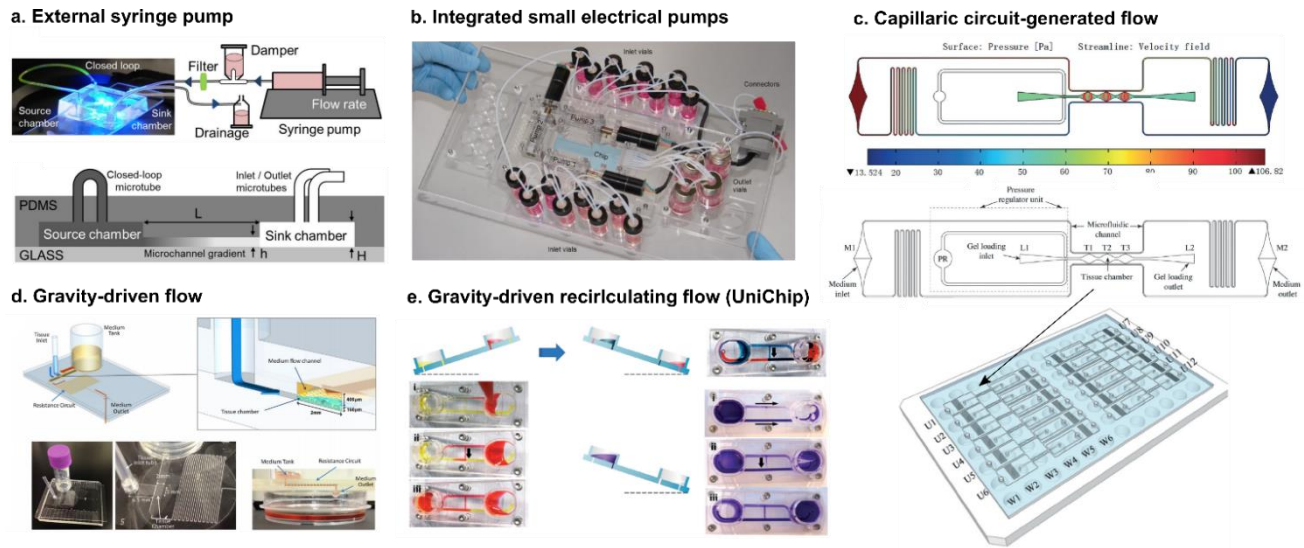


Fig. 8: Methods for liquid transport and generation of flow rates within microfluidic cell culture platforms. **(a) External syringe pump** directly control flow rates in microfluidic device. (Parittotokkaporn *et al.*, 2019), Ref (113). **(b) Integrated small electrical pumps** have been used in combination with capillary pumps to create a self-contained microfluidic device. (Skafte-Pedersen *et al.*, 2011) Ref (114). **(c) Capillary circuit-generated flow** incorporates pressure regulator structures that define the flow rate over time. (Phan *et al.*, 2018), Ref (117). **(d) Gravity-driven flow** across microchannels is possible through reservoirs of different heights at each end of the channel. (Komeya *et al.*, 2017), Ref (115). **(e) Gravity-driven recirculating flow (UniChip)** allows continuous flow by incorporating passive valves and placing the device on rocking platforms. (Wang and Shuler, 2018), Ref (116). All images were republished or reproduced by permission from their respective publishers.

In (Fig. 8) we summarized methods for liquid transport and control of flow rate in microfluidic channels. Syringe pumps offer a direct method to actively force liquid through microfluidic channels and control its flow rate, as shown in (Fig. 8a)¹¹³. Nonetheless, it can be cumbersome to use for cell culture applications where cells must be kept in sterile closed incubators at 37°C and 5% CO₂, and

handled in uncluttered biosafety cabinets (BSC). Tubing that connect a microfluidic device to an external syringe pump could be sources of contamination and could significantly complicate experimental setups with many moving parts to works with and tubes that trace to several inlets and outlets, which could reduce experimental throughput, especially if multiple devices are being tested. External syringe pumps have been replaced in some reports by small electrical pumps connected to tubes attached to containers outside the microfluidic device while being interconnected in one platform as shown in **(Fig. 8b)**, to introduce a flow rate¹¹⁴.

This improvement allows placing the whole platform in the incubator while eliminating moving parts and external connections to the outside of the incubator, and avoids overcrowding biosafety cabinets. Similarly, this setup can be used without electrical pumps by filling containers connected to a microchannel on opposing sides with liquids up to different heights thereby utilizing gravity to generate flow rates as shown in **(Fig. 8d)**¹¹⁵. However, the height difference must be re-introduced to maintain active flow. Wang and Schuler proposed a method to recirculate gravity-driven flow by utilizing passive valves and placing the device on a rocking platform¹¹⁶. This overcomes the need to maintain height difference between reservoirs. Despite the aforementioned advancements in liquid transport and generation of flow rates in microfluidic cell culture devices, many of those methods are not compatible with high-throughput screening which typically requires multi-channel pipetting, robotic equipment, or fluorescent plate readers, and are difficult to integrate with high quality live microscopy without risking contamination. Capillarics overcomes many of those complications by incorporating elements that allow **portable, autonomous, self-powered, and integrated designs**¹⁰⁵. As illustrated in **(Fig. 8c)**, Phan *et al.* developed a microfluidic platform that incorporates a pressure regulator unit to control flow velocity over time¹¹⁷. The device was used to generate vascular microtissues that were overlapped with a 96-well plate to allow high throughput screening of drug agents¹¹⁷. Hydrogel and media inlets and outlets were also designed to overlap with one well each to allow easy and fast pipetting steps in a format compatible with robotic and traditional pipetting, and common downstream analysis equipment¹¹⁷.

Microfluidic cell culture systems developed to model organs of interest *in vitro* are often referred to as microphysiological systems (MPS), which can incorporate 2D and 3D cell culture

formats based on a desired application that are often referred to as organ-on-a-chip and organoid-on-a-chip. We provide a general overview of how microfluidic techniques has been leveraged to meet experimental requirements of MPSs in the next section, and we show how these platforms have been specifically applied for microvascular tissue engineering at the end of this introduction chapter.

5.1.4.1 Microphysiological systems: Organ- and organoid-on-a-chip systems

The most recent developments in 3D cell culture have been interested in better mimicking the microstructure, mechanical and biochemical properties, and functionalities of whole living organs^{118, 119}. Previously introduced 3D cell culture methods such as organoid and spheroids cultures have been shown to replicate organ function to a higher degree than conventional 2D cell culture¹¹⁸. However, there remains certain shortcomings in organoids cultures, spheroid cultures and conventional 3D cell culture methods if not coupled with specialized 3D cell culture methods such as microfluidics, micropatterned plates, and bioreactors. While non-specialized 3D cell culture methods we described previously in **(Fig. 5)** offer cell-cell and cell-ECM interactions, **alone** they lack control over specific cell patterning in space, consistency between batches, tissue-tissue interfaces, and mechanical inputs such as shear stress^{118, 119}. **Organ- and organoid-on-a-chip systems** were developed to address some of those shortcomings by **integrating microfluidic technologies with living cells or organoids cultured within 3D devices developed using microfabrication methods inspired from the microchip industry and 3D printing**^{118, 119}. This has allowed scientists to study human physiology and disease through specialized *in vitro* models that **provide an organ-specific context**^{118, 119}.

Organ-on-a-chip design principle and examples

Organ-on-a-chip systems can be defined as **microfluidic cell culture devices designed to model the functional units of human organs *in vitro* developed through design principles that are based on a reductionist analysis of an organ of interest**¹¹⁹. The first step in developing an organ-on-a-chip system is to start with the anatomy of the organ of interest and reduce it to the basic elements responsible for physiological functioning¹¹⁸⁻¹²⁰. A “Functional unit” represents the building block of an organ where its most basic function occurs. For instance, nephrons in the kidney¹²¹, alveolar sacs in the lung¹¹⁹, and neurons in the brain¹²², all represent functional units of those organs. Functional units vastly differ between organs and are defined by key features such as cell types, structural

organization, and biochemical and mechanical properties of their ECM¹¹⁹. Once those features are identified, the researcher attempts to recreate them *in vitro* with the goal of replicating organ function for physiological analysis and drug testing which could potentially reduce animal experimentation and improve translational medicine^{118, 119}.

For example, the alveolar-capillary interface in alveolar sacs facilitates gas exchange in the lungs, as shown in **(Fig. 9a)** and consists of alveolar epithelial cells (AECs) and pulmonary microvascular endothelial cells (PMECs), both of which are present on opposing sides separated by a thin interstitium layer^{67, 119}. The epithelial side is exposed to mechanical forces from air flow (*e.g.* breathing-induced stretching), while the endothelial side is exposed to shear stresses due to blood flow^{67, 119}. Those features have been replicated for a lung-on-a-chip system by designing a microfluidic device with two layers separated by a thin porous membrane, where AECs are cultured on the bottom side of a top microchannel to model the wall of the alveolar sac, and PMECs are cultured on the top side of a bottom microchannel to model the capillary wall, as shown in **(Fig. 9a, 9b)**^{67, 119}. Cell culture media is flowed through the endothelial channel to model blood flow and air through the alveolar channel^{67, 119}. Vacuum is applied to side channels to simulate stretching forces on the capillary-alveolar interface layer^{67, 119}. This model was able to reproduce several *in vivo* organ responses including responses to bacteria and cytokines, accentuated inflammatory response to silica nanoparticles, and enhanced uptake of nanoparticles and transport into the bottom microvascular channel upon mechanical stimulation⁶⁷.

The neurovascular unit in the brain has been similarly modeled using reductionist organ-on-a-chip approaches to study the blood-brain barrier (BBB) by numerous reports, including most recently the work of Ahn *et al.* shown in **(Fig. 10)**^{63, 123, 124}. Modeling the BBB offers a great opportunity to test

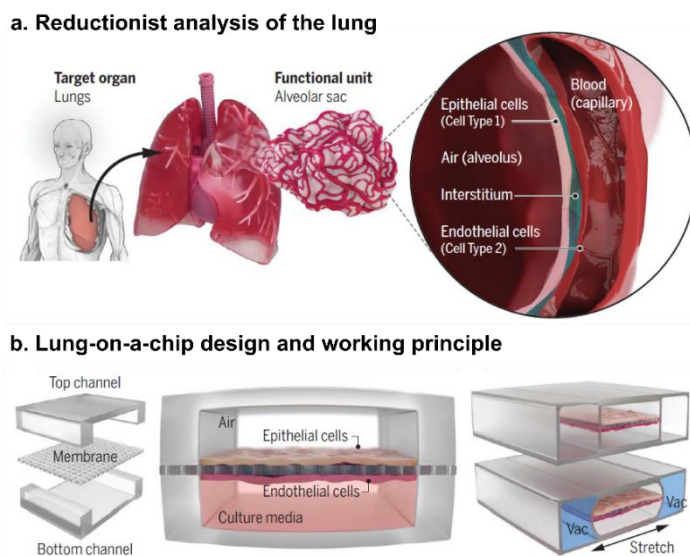


Fig. 9: Lung-on-a-chip system developed using micro-fabrication technologies to recreate lung function through a reductionist approach **(a)**. PMECs and AECs are introduced on opposing sides of a thin porous membrane to mimic the alveolar-capillary interface **(b)**. Reprinted by permission from AAAS, *Science* 364, Park, S. *et al.* copyrights 2019, Ref (119), [Illustration: BIOLines Lab].

neurological drug agents using improved and more accurate physiological settings. The BBB functions as a selective physical barrier to protect the brain against harmful compounds, and provides biochemical homeostasis for the brain necessary for optimal neuronal functioning^{63, 124}. The BBB is formed by specialized endothelial cells which line cerebral microvessels and connect together via complex tight junctions that force molecules to move transcellularly across the BBB rather than paracellularly in between the junctions as the rest of endothelial barriers across the body⁶³. The BBB supplies the brain with gas and nutrients, eliminates waste, restricts active and passive transport of molecules from the blood, and regulates the brain microenvironment due to its short diffusion distance from neurons^{63, 123, 124}. Tight junctions in the brain (*e.g.* ZO-1 and claudins) greatly restrict even the movement of small ions such as Na⁺ and Cl⁻, hence, the **transendothelial electric resistance (TEER)**; a measure of the electrical resistance across a monolayer of cells inversely proportional to permeability of barriers, is **significantly higher in brain endothelium (>1000 ohm.cm²)**, compared to **peripheral capillaries (2-20 ohm.cm²)**^{63, 123}. As a result large molecule drugs cannot cross the BBB and only 2% of small molecule drugs can¹²⁴. BBB function and maintenance is closely linked to its anatomy^{63, 124}. Brain capillaries are surrounded by pericytes and a basement membrane. Astrocytic end-feet surround the capillaries and are in close contact with microglia and neurons on its other ends^{63, 124}.

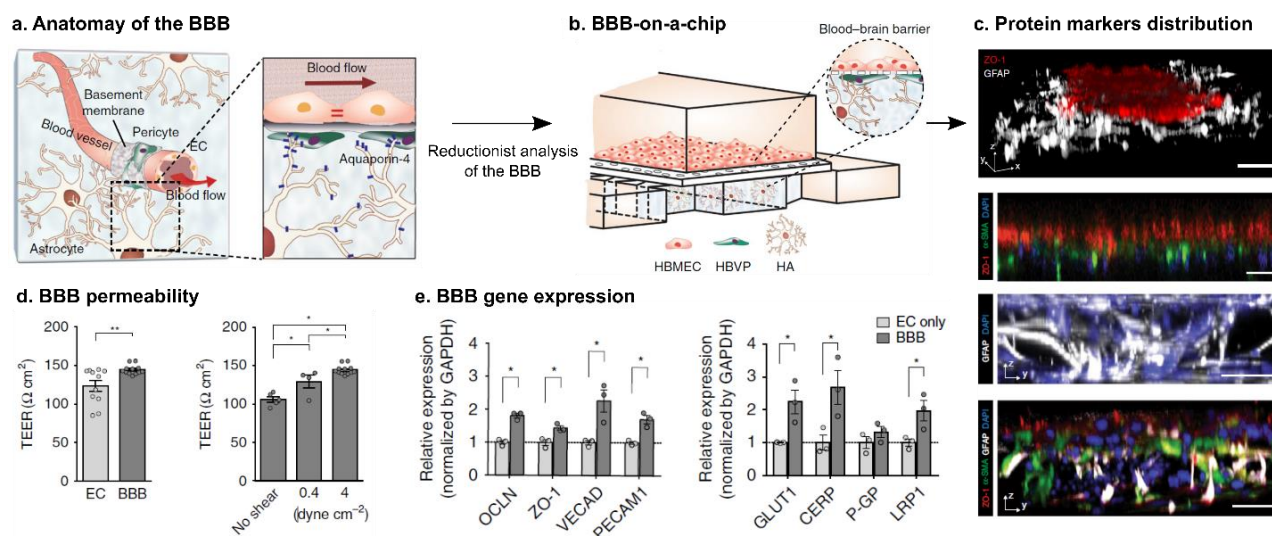


Fig. 10: BBB-on-a-chip replicates *in vivo* BBB anatomy using a tri-culture with defined distribution of HBMEC, HBVP and HA (a) and (b). Immunostaining shows distribution of BBB markers: ZO-1 (red) junctional protein in HBMEC. GFAP (white) astrocyte marker. α -SMA (green) HBVP marker (c). TEER value of the tri-culture is higher than a monoculture of ECs, and is increased with increasing shear stress. Gene expression of junctional proteins and cell receptors of endothelial cells is higher in the tri-culture compared to a monoculture. Reproduced under the terms of the Creative Commons license. Nature Communications. Ahn, S. I. et al. Copyright 2020. Ref (123).

Ahn *et al.* replicated several anatomical and functional aspects of the BBB in a microfluidic device where a tri-culture is introduced consisting of a 2D monolayer of human brain microvascular endothelial cells (HBMEC) cultured on top of a porous membrane with human brain vascular pericytes (HBVP) on its bottom side, and human astrocytes (HA) in a 3D Matrigel in a bottom channel¹²³. Interestingly, the device corroborated previously introduced features of the BBB by showing a significantly higher TEER value of the BBB tri-culture compared to a monolayer of ECs cultured with pericytes and astrocytes¹²³. Additionally, by introducing continuous fluid flow, which is unachievable without a specialized setting such as microfluidics, physiological values of shear stress were achieved which was shown to increase the TEER value of the BBB^{123, 125}. Expression of junctional proteins and endothelial cell receptors also increased similarly to what has been shown to occur *in vivo*^{123, 125}. This example well demonstrates the significance of microfluidic approaches in addressing the limitations of conventional cell culture methods. Petri-dish grown endothelial cells can be used to assess cytotoxicity of drugs. However it does not provide any accurate measure of drug delivery into the brain.

Organoid-on-a-chip compared to organ-on-a-chip systems

Traditional organoid cultures and organ-on-a-chip systems both developed with the same goal of recapitulating the complexity of *in vivo* organs^{119, 126}. The two technologies represent fundamentally different approaches^{119, 126}. Yet by combining aspects of each of those two technologies into **organoid-on-a-chip systems**, the two become complementary¹¹⁹. **Organ-on-a-chip technology** relies on engineering precisely controlled constructs of cells and their microenvironment to **replicate *in vivo* functions**¹¹⁹. In those systems the researcher makes decisions on the distribution of each cell type in the microfluidic device; be it introducing cells in a 2D monolayer, a 3D hydrogel, or a combination of both¹¹⁹. **Organoid-on-a-chip technology**, by contrast, relies on intrinsic developmental programs that allow stem cells to self-organize spontaneously to **recreate key functions and structural properties of *in vivo* organs**¹¹⁹. Such systems either introduce already aggregated organoids or spheroids into the microfluidic device or design micropatterend features that allow them to aggregate uniformly in the device. Controlled fluid flow in microchannels can then be introduced to improve the maturity of organoids, transport nutrients and remove waste, generate

biochemical gradients, or create fluid flow profiles desired for introducing spatially controlled growth factors. Organoid-on-a-chip technologies have been used to generate kidney organoids-on-a-chip¹²¹, brain organoids-on-a-chip¹²⁷, and a multiple organoid-on-a-chip system to model organ-organ interactions, among others¹²⁸.

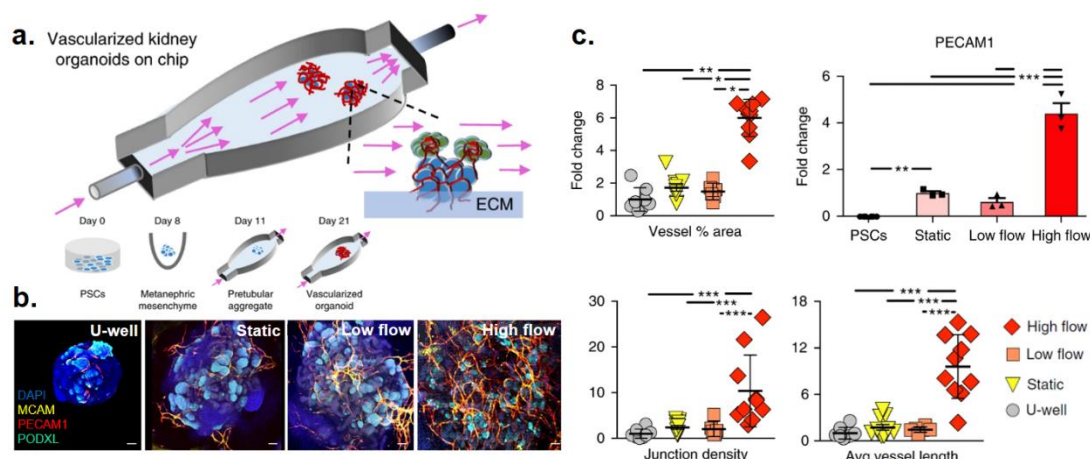


Fig. 11: (a, b) Kidney organoid-on-a-chip show the formation of PECAM1+ (red) and MCAM+ (yellow) vascular structures wrapped around PODXL+ (cyan) glomeruli-like compartments. (c) Vessel % area, junctional density, average vessel length, and PECAM1 expression were all significantly higher when organoids were cultured on-chip under high flow rates. *Reproduced by permission from Springer Nature. Nature Methods. Ref (121). Homan K. A. et al. Copyright 2019.*

In a kidney organoid-on-a-chip system developed by Homan *et al.* illustrated in (Fig. 11), kidney organoid pretubular aggregates derived from pluripotent stem cells are introduced in 3D printed microfluidic devices after their initial aggregation in U-wells¹²¹. The microfluidic device is connected with inlets and outlets for introducing fluid flow through its organoid channel¹²¹. High flow rates in the device increased the branching (junctional density), length, and area of PECAM1+/MCAM+ perfusable vascular structures during nephrogenesis¹²¹. The vascular structures are wrapped around glomeruli-like compartments that closely mimicked the structure of the glomerulus capsule (bowman's capsule) located in kidney nephrons where blood filtration occurs *in vivo*¹²¹. The newest wave of organoid-on-a-chip platforms integrate the best features of current organ- and organoid-on-a-chip systems to create more powerful synergetic *in vitro* models^{119, 126}. For instance, in the present example of kidney organoids-on-a-chip, the authors aimed to provide extensively characterized platform for vascularized kidneys. By integrating this platform with an organ-on-a-chip approach that connects the vascularized kidney organoids to endothelial cell-lined microfluidic channels, a more powerful platform could be achieved that allows controlled, directional perfusion of vascular networks for

disease modeling and drug testing applications.

Similarly, a brain organoid-on-a-chip system was developed by Wang et al. to enhance differentiation and *in situ* organization of brain organoids, as shown in (Fig. 12)¹²⁷. Among the many types of organoids developed in the recent years⁸, brain organoids have the most complex structure and exhibit the highest levels of organizational patterns with distinct functional regions and cortical structure^{1, 127}. While stem-cell derived brain organoids recapitulate several aspects of development and disease, differences between those organoids and the native brain remain¹²⁷. Additionally, the same batch of organoids generated with the same protocol is heterogeneous in terms of expression profiles of various markers of cell types in the developing brain, viability, size, shape, and not every single organoid is guaranteed to recapitulate *in vivo* function and structure^{8, 127}. Those challenges commonly occur in virtually any type of organoid generated using traditional organoid cultures⁸. This phenomenon suggests that

microenvironmental cues (*e.g.* biochemical and mechanical signals, and multicellular interactions) are either missing or presented inaccurately¹²⁷. In the example in (Fig. 12), embryonic bodies (EBs) suspended in Matrigel were immobilized and aligned in microchannels and introduced to neural induction medium followed by differentiation medium through a central perfused channel¹²⁷. The continuous flow of media in the central channel allowed controlled nutrient diffusion across the Matrigel-filled organoid channel¹²⁷. Supply of nutrients to the core of organoids was enhanced for the on-chip organoids in

comparison to petri-dish grown ones, as corroborated by increased viability of on-chip organoids and

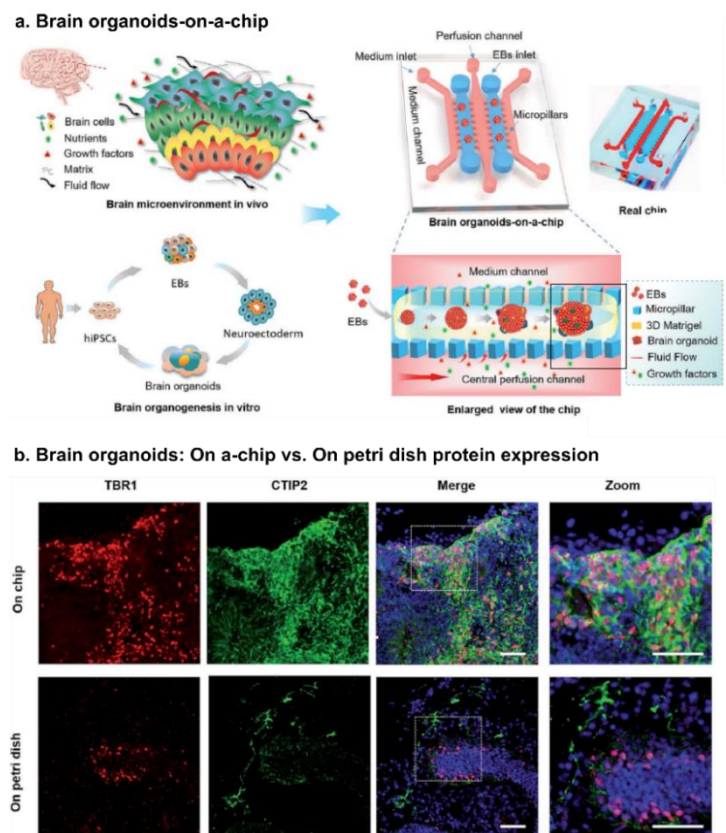


Fig. 12: Brain organoids differentiation and cell organization is improved using a perfused organoid-on-a-chip system in comparison to conventional petri-dish grown brain organoids. *Reproduced under a Creative Commons Attribution liscence. RSC Advances. Ref (127). Wang, Y. et al. Copyright 2018.*

reduced necrotic cell death at their cores¹²⁷. Additionally, the on-chip brain organoids showed higher expression of neural markers, brain regional markers, and the cortical layer markers (TBR1 and CTIP2) as shown in **(Fig. 12b)**¹²⁷.

Overall, the aforementioned examples demonstrate the capability of perfusable microfluidic organoid-on-a-chip platforms for providing improved biomimetic microenvironments and enhanced organ functionalities by recreating *in vivo* elements such as fluid flow, controlled cues, tissue architecture, and a 3D space.

5.2 Brain organoids as models for neuroscience research

The prevalence of dementia and neurodegenerative diseases is increasing rapidly in nations with increasing life expectancies¹⁵. Alzheimer's disease (AD), for instance; the most prevalent form of dementias, affects an estimate of 47 million people around the world¹²⁹. Despite decades of research, progressive neurodegenerative diseases such as AD, Parkinson's disease, and motor neuron diseases remain without a treatment that prevents or reverses the course of the disease, with treatments being limited to symptom management and palliative care¹⁵. While symptoms of neurodegenerative diseases are well-characterized, early pathophysiological events leading up to those conditions remain largely unknown^{1, 15}. Additionally, neurodevelopmental disorders such as autism spectrum disorder and neurodevelopmental diseases such as microcephaly manifest at embryonic and fetal stages, and have unique genetic and epigenetic programs, making them difficult to study using traditional models¹. Lack of understanding of those diseases, complexity of the brain, and limited access to human neural tissues represent main obstacles of neuroscience research^{14, 15}.

Various biological modeling methods emerged to allow scientists to unlock mysteries of the human brain, including cultures of dissociated neurons, tissue explants, and animal models^{14, 15}. Those models have been and remain commonly used in neuroscience, and while they have greatly advanced our understanding of neurophysiology and disease, each has its own long well-known limitations. Those traditional models have remained the gold standard for decades due to the lack of better alternatives. The recent advancements in the field of stem cell biology have made available: fetus-derived ESCs as first reported by Thomson *et al.* (1998)¹³⁰ and iPSCs reprogrammed from adult somatic cells by Takahashi and Yamakana (2006)^{14, 15, 131}. Those advances permitted a new generation

of *in vitro* models for neuroscience research; patient-derived tissues and brain organoids developed from patient samples using iPSC technologies^{14, 15}. **Brain organoids** are self-organizing neural structures capable of mimicking the development of the fetal human brain¹⁵. Such organoids have gained tremendous popularity because they preserve the genetic profile of patients and faithfully replicate tissue architectures, physiology and important pathological hallmarks found in neurological diseases and disorders^{14, 15}. The increasing technological advances in developing model systems, makes it crucial to understand and acknowledge the restrictions and benefits of each one of those system in order to appropriately utilize them in neuroscience research. In the next section, we discuss the emergence of brain organoids as complementary yet unique tools for neuroscience research that overcome certain limitations imposed by traditionally implemented *in vivo*, *ex vivo*, and *in vitro* models of the brain.





5.2.1 Biological models for neuroscience research: challenges and opportunities

In vivo models: A wide range of *in vivo* models, including vertebrates (e.g. zebra fish, rodents, non-human primates), and invertebrates (e.g. *C. elegans*, *drosophila*), have been used to model neurodevelopmental or neurodegenerative diseases¹³². Modifications to these animals to mimic symptoms of a disease of interest can be induced chemically by administration of neurotoxins such 6-hydroxydopamine which recreates symptoms of Parkinson's disease, or genetically through introducing mutations, overexpression, knock-out or -in of genes of interest¹³². For instance, mutations in Amyloid precursor protein (APP) and other proteins implicated in AD pathogenesis, have been used to mimic symptoms of AD¹²⁹. Animal models of the brain have been mostly comprised of rodents; mice and rats in particular¹³³. Rodent models of the brain have been tremendously advantageous over the years due to the *in vivo* context they offer through a **3D microenvironment, modeling neural-immune interactions, and access to functional tests of disease parameters** over an extended period of time by investigating cellular processes and whether modulation of molecular targets elicits therapeutic responses in the animal and/or behavioral changes. Nonetheless, a serious gap in clinical translation of animal models exists due to **species and age differences**¹³². For instance, in aging humans with AD, two molecules; tau and amyloid- β (A β) form crosslinked fibril aggregates¹²⁹. Such aggregates form lesions known as plaques that accumulate between neurons, disrupt their function,

and lead to cell death¹²⁹. Rodent models **do not naturally develop plaques nor do they live as long as humans**, thus those models are crossed to have an early onset of AD through mutations, as opposed to late onset AD which occurs in 90% of AD cases in humans with unknown aetiology¹²⁹. Many of AD transgenic rodents exhibit diffuse or fewer crosslinked fibrils, compared to A β plaques in the human brain¹²⁹. Additionally, transgenic rodent models are **inbred in lab housing and most are crossed to have single gene mutations**¹²⁹. This is not reflective of humans who have non-coding sequences, complex genetic backgrounds, and a diverse range of environmental factors affecting their epigenetics¹²⁹. Therefore, it is nearly impossible to faithfully model post-translational modifications or splice variants of human genetic material to be study their effect on pathogenesis of diseases in an animal model¹²⁹. This is also the cases with neurodevelopmental and neuropsychiatric disorders such as autism spectrum disorder, schizophrenia, and bipolar disorder which are presented with polygenic aetiology, genetic risk factors, and a high rate of comorbidity between them, making neuropsychiatric animal models of those disorders difficult to achieve¹. Additional limitations of animal models, summarized in **(Table 2)**, such as low throughput¹⁴, laborious practices¹³⁴, the cost of animal care and housing¹³⁴, when added to clinical translational gaps of those models, raise many practical and ethical questions on whether animal models should be used as often as they currently are in neuroscience when there is potential to use alternative models such as the *in vitro* and *ex vivo* ones we discuss next¹²⁹,

135, 136

Table 2: Conventional and emerging biological models for neuroscience research; limitations (grey)

				
	2D cell culture	Animal models	Brain tissues	Brain organoids
Sources	Human, animals ^{137, 138}	Often mice or rats ¹³³	Postmortum or biopsy of human brain, animals ¹³⁹	Human, animals ¹⁴
Human patient samples	Derivable from patient samples ^{14, 137}	Not applicable	Difficult to obtain ¹⁴⁰	Derivable from patient samples ¹⁴
Cost	Low ¹³⁴	High ¹³⁴	Relatively low ¹³⁴	Relatively low ¹⁴¹
Throughput	High ¹⁴	Low ¹⁴	Low ¹⁴	High ¹⁴¹
Handling/preparation	Easy ¹⁴	Difficult ¹³⁴	Difficult ¹³⁴	Relatively easy ¹⁴²
Genetic manipulation	Easy mostly ^{14, 143}	Difficult ¹⁴⁴	Difficult ¹⁴	Easy ¹
Cytoarchitecture	Missing ¹⁴	Present ¹⁴	Present ¹⁴	Present ^{10, 14}
3D microenvironment	Missing ¹⁴	Present ¹⁴	Present ¹⁴	Present ¹⁴
Human-unique cells	Missing ¹⁴	Largely missing ¹	Present ¹⁴	Present ^{1, 141}
Astrocytes and microglia	Missing ¹⁴	Present ¹⁴⁵	Present ¹⁴⁶	Present ^{145, 147}
Immune cells	Missing ¹⁴	Present	Missing ¹⁴⁸	Missing ^{14, 140}
Well-defined vasculature	Not present	Present	Present ^{134, 139}	Missing ¹⁴⁰
Endothelial cells	Missing ¹⁴	Present	Present ^{134, 139}	Present ^{3, 6, 149}
Behavioral testing	Not possible	Possible ¹⁴	Not possible	Could be possible if transplanted ¹⁰²
Length of use	Short	Long	Short or end point ¹³⁴	Long ¹³⁴
Cell death	Low ¹³⁸	Not applicable	High ¹⁴⁶	High in large organoids ¹⁴⁰
Brain maturity	Not present	Present	Not well defined ^{139, 150}	Lacking ^{14, 140}
Neural signals	Present ¹³⁸	Present	Present ¹⁴⁶	Present ¹⁵⁰
Batch variation	Present sometimes ¹³⁸	Present ¹⁵¹	Present ¹⁵¹	Present ¹⁵
Ethical concerns	Low mostly ¹⁴³	High	Relatively low ¹³⁴	Relatively low ¹⁵⁰

2D cell culture: *In vitro* and *ex vivo* models have been instrumental for studying brain physiology and disease, and complementary or alternatives to animal models used in pathophysiological modeling and drug screening¹³². *In vitro* models include 2D cell culture, and 3D brain organoid or neuronal spheroid cultures, while *ex vivo* models include brain tissue cultures^{14, 132}. **Cell culture** of neuronal cells is particularly challenging compared to cultures of other cell types because neurons do not undergo cell division once they mature¹⁴³. Yet neuroscientists developed methods to go around this challenge such as developing immortalized cell lines and devising surface coatings to enhance cell viability¹⁴³. Today, three main formats of **2D cell culture** of CNS cells exist, which include: cultures of **immortalized cell lines**, **primary cells**, and **pluripotent stem cell derived cells**^{132, 143}. CNS cell types including neurons, astrocytes, microglia and oligodendrocytes have been used as primary cells and cell lines in 2D cell culture to elucidate a wide range of processes such as

neurotoxicity, inflammation, and pathogenesis of neurological diseases¹³².

Secondary cell lines are derived from human or animal tumors and immortalized¹⁴³. Manipulation of cell culture conditions (*e.g.* adding specific growth factors) is done to induce a more neuronal phenotype of such cell lines¹⁴³. For instance, NT2 is a human neuronally committed teratocarcinoma derived from a metastatic pluripotent embryonal carcinoma¹⁴³. Treatment by retinoic acid (RA) and mitosis inhibitors induces NT2 lines into displaying neuronal morphologies (with cell bodies and processes), and expressing typical neuronal markers such as MAP2, NeuN, and GluR^{143, 152}. Those cells have been useful in testing neurotoxicity, and studying embryonic neurogenesis pathways due to their pluripotent nature before being induced¹⁴³. Cell lines have several advantages including the ability to generate an unlimited number of cells with minimal variability, and easy transfection¹⁴³. However, neuronal cell lines have been criticized for lack of physiological relevance as *in vitro* models for drug screening and translational research in comparison to **primary neurons**, in terms of recapitulating the same gene and protein expression profiles and neuronal subpopulations of *in vivo* differentiated neurons^{143, 153, 154}. The same types of neuron are also physiologically different from each other based on the cell type from which their cell line was derived¹⁴³.

Primary neurons can be isolated from human, rat, and mouse brains at embryonic or adult stages of development, either through whole brain dissections or biopsies¹³⁸. Primary neurons isolated from embryonic brains have historically been more desirable than neurons from adult brains due to their ease of isolation, increased viability, superior regenerative capacity, and reduced glial growth than their adult counterparts¹³⁸. Reduced glial growth is desired by researchers for preparation of homogenous and consistent cultures that are easy to stain and analyze¹³⁸. However, the lack of diverse cell populations represents one of the main caveats of conventional 2D cell culture which typically lack a biologically relevant microenvironment, leading to inaccurate physiological modeling of CNS responses¹³⁸. Additional considerations come up when working with primary cultures but not with cell lines. Unlike cell lines, the number of primary cells available throughout an experiment is much more limited, and primary cells are a lot harder to transfect than cell lines¹⁴³. Additionally, since primary neuronal cells are freshly isolated from human or animal brains, ethical approvals are required before preparing those cells¹⁴³. However, since primary cells are often isolated from sacrificed animals,

ethical concerns are less severe than those associated with animal models which involve experimenting with living animals for extended time periods and animal suffering.

One approach that combines some of the advantages of neuronal cell lines such as **ease of genetic manipulation and expandability of cells**, and advantages of primary neuronal cells such as **physiological relevance**, is **pluripotent stem cell (PSC)-derived neuronal cells**¹³⁷. PSCs include iPSCs and ESCs, both of which can be used to generate neuronal cells and neuronal stem cells from somatic cells of humans or animals by expression of defined factors^{137, 143}. ESC are cells that are isolated at early embryogenesis from the inner cell mass of animal or human blastocysts and are able to give rise to all cell types of the body. iPSCs are cells that start off as somatic cells isolated from various sources (*e.g.* blood, skin) and are then de-differentiated to a stem cell state by transfection with specific genes (described first by the Yamakana group as Oct4, Klf4, Sox2, and c-Myc for fibroblast reprogramming), using established transfection methods^{132, 137}. Similarly to ESCs, iPSCs are characterized by their capability to give rise to all three primitive germ layers (ectoderm, mesoderm, and endoderm)^{132, 137}. Since iPSCs and ESCs are types of stem cells, they both can be expanded *in vitro* without losing pluripotency which offers a great advantage for when those cells are isolated from precious patient samples and intended to be differentiated into a specific cell type of interest involved in a disease of question. Additionally, iPSCs isolated from patient samples **retain genetic signatures of patients** and can therefore be used to model neurological diseases and disorders with complex genetic backgrounds¹⁵⁵. For instance, amyotrophic lateral sclerosis (ALS) is a fatal neurodegenerative disease where upper and lower motor neurons are progressively lost¹⁵⁵. The familial form of ALS involves mutations in the superoxide dismutase 1 (SOD1) gene, in addition to an estimate of 30 genes that are thought to be directly linked to ALS pathophysiology¹⁵⁵. This form of ALS was recreated *in vitro* by differentiating skin fibroblasts from ALS patients into patient-specific iPSCs¹⁵⁶. These cells were directly differentiated into TUJ1 positive-motor neurons while still carrying the SOD1 mutation, upon adding RA and SHH to the culture medium¹⁵⁶. iPSCs therefore have great potential for personalized neuromedicine. Despite iPSCs being powerful disease modeling tools with capabilities that overcome many of the limitations of other *in vivo* and *in vitro* models, **batch-to-batch variability** remains a shortcoming of iPSC-generated neurons¹³⁷.

Overall, the main advantages that distinguish the aforementioned 2D cell culture formats from other biological models of the CNS in (Table 2) are their **robustness, fitness for high-throughput screening, and clinical relevance due to human origin of many neuronal cell types**, making them widely adopted and continuously improved¹³². However, it is well established that these 2D cell culture models, unless coupled with specialized cell culture methods such as microfluidics or within scaffolds, are **too simple to answer complex questions** due to a **lack of brain cytoarchitecture, and a 3D microenvironment** which encompasses neuron-ECM interactions, and chemical and functional interactions with other cell types such as cells of the BBB and immune cells, and must therefore be always complemented with animal models to validate findings¹²⁴.

Brain organotypic slice culture: One of the first attempts to bridge the gap between *in vivo* and *in vitro* CNS modeling platforms involved *ex vivo* brain tissue slice cultures¹³⁴. Such platform offers an *in vivo*-like frame of work with a **3D microenvironment with an intact map of brain circuits** and the **accessibility, cost-effectiveness, human origin, and controlled environment** typically offered by *in vitro* platforms¹³⁴. Brain tissues for slice culture is most often obtained from postnatal dissection of rat or mice brains, postmortem human brains, or biopsies and surgical procedures where pieces of brain tissue are removed to treat or diagnose human patients with conditions such as epilepsy or cancer^{134, 150}. These models have been used in a wide range of applications including drug testing¹⁵⁷, modeling neurodegenerative diseases¹⁵⁸ and cerebral ischemia¹⁵⁹, and study of neurogenesis and investigating neuronal cell therapy approaches by grafting neuronal cells into brain tissue slices and monitoring their integration into preexisting neuronal circuits^{134, 160}. Additionally, organotypic brain slices were demonstrated to retain neurovascular structures. Even in the absence of blood flow, brain capillaries were able to survive in tissue slice cultures. This finding was extremely useful in allowing direct access to the BBB *ex vivo* and characterizing neurovascular coupling; a mechanism that contributes to tight control over cerebral blood flow and nutrient supply and demand for neurons¹⁶¹. Additionally, culture medium and the tissue is directly accessible in slice culture for analysis of cell-secreted molecules and morphological changes, which not as easy to do in animal models. Moreover, compared to animal models, ethical concerns associated with brain slice culture are relatively low as it does not involve animal suffering¹⁵⁰.

However, this also related in part to some of the limitations and general characteristics of the current generation of brain slice cultures; such as **severed neuronal connections due to the dissection process and lack of sensory neuronal inputs and motor outputs**^{134, 150}. Thus the likelihood of higher-order functions or consciousness is very much off-chance¹⁵⁰. Additional challenges halt further applications of brain slice culture. **Cell viability** for one is a major challenge in brain slice culture and it is highly dependent on multiple factors such as source age, media composition, preparation speed, sterility, and health of the source donor¹³⁹. Brain slices are also very thin and fragile; ranging between 100-400 µm in thickness and can therefore be easily damaged, making them difficult to handle and only cultured for a few weeks¹³⁴. All of the above factors also affect the **reproducibility** of results obtained from brain tissue slice cultures by different research groups, halting their adaptation as standard models.

Brain organoids: Brain organoids represent the most recent tool developed for modeling CNS events. Brain organoids can be derived from iPSCs based on established protocols to generate either **whole brain organoids**; termed cerebral organoids, or **region-specific brain organoids**¹⁵. Protocols for generating brain organoids fall under two major categories: 1) self-patterning protocols (intrinsic patterning), and 2) pre-patterning protocols (using extrinsic signaling molecules)^{1, 162}. **Self-patterning** approaches rely on the intrinsic ability of stem cells to self-organize into an entire cerebrum, which has been the common approach for generating cerebral organoids. In **pre-patterning** approaches, on the other hand, the culture conditions are modified to include patterning factors that are added at different time points to direct the induction process towards a specific fate, which has been implemented in generating region-specific brain organoids¹⁶². The first established method for generating *in vitro* grown 3D neural tissues that were not brain slices was in 2008 by Yoshiki Sasai and colleagues¹⁶³. The method established, coined serum-free culture of embryoid body-like aggregates with quick re-aggregation (SFEBq), is based on the property that ESCs, when grown in suspension and in the absence of serum or neural differentiation inhibitors, have the tendency to aggregate into spheres and produce neural precursors through spontaneous neural differentiation^{1, 15, 163}. The neural EBs generated using this method showed the formation of self-organized apico-basally polarized **cortical tissues** with four distinct zones (ventricular, early and late cortical plate, and Cajal-

Retzius cell zones)¹⁶³. Later in 2011, with the emergence of **Matrigel as a laminin-rich ECM-based hydrogel**, Sasai and colleagues demonstrated that 3D ESCs embedded in Matrigel formed self-organizing optic cup-like structures with retinal architecture^{1, 12}. Few years later, building on these findings among other advances in organoid technologies, two main systems emerged that pioneered the field of brain organoids¹. First was the generation of self-patterned cerebral organoids that contained regions that resembled specific brain regions by Lancaster and colleagues¹⁰, and second was the demonstration that a specific brain region; the forebrain can be differentiated as a 3D structure from human ESCs using inductive signaling molecules, by Sasai's group¹⁶⁴. Since then, various forms of region-specific brain organoids were generated using similar technologies including hippocampal¹⁶⁵, hypothalamic¹⁴¹, cerebellar¹⁶⁶, and midbrain organoids^{1, 141}.

The attractiveness of brain organoids as models to investigate neuronal processes stems from the ability to utilize them to overcome many of the challenges associated with animal models, 2D cell culture, and *ex vivo* brain slice cultures. First, the **3D nature of brain organoids enables cellular, biochemical, and mechanical cues that are lacking in 2D cell culture systems**¹. Second, brain organoids can have **human origin** which lends clinical significance, in addition to the ability to generate them with high throughput unlike animal models and brain slice cultures^{1, 135}.

Species differences between animal models and humans led to a serious gap in clinical translation of results obtained from animal models, which fail to model diseases with intricate genetic factors or diseases that occur in aging humans but do not naturally occur in rats or mice. Brain organoids, which are derivable from healthy human or human patient samples, preserve genetic profiles and mutations from their human source cells that get passed down to the iPSCs then to the induced neural populations. For instance, the **cerebral organoids** previously mentioned by Lancaster *et al.* were used to model **autosomal recessive primary microcephaly (MCPH)**; a neurodevelopmental disorder characterized by abnormally smaller cerebral cortex in new born infants. Among twelve genes implicated in MCPH; most of which play a role in mitotic progress, is CDK5RAP2 which regulates centriole replication and impacts neural progenitor proliferation when lost. Yet, CDK5RAP2 mutant mice do not show a severely reduced brain size as seen with human patients, whereas MCPH patient fibroblast-derived cerebral organoids carried the gene mutation and

were smaller in size compared to health cerebral organoid controls. These patient-derived cerebral organoids demonstrated smaller neuroepithelial tissues, larger neuronal outgrowth compared to control, and very few neuronal progenitor regions that had impaired proliferation, which is thought to be responsible for the disease phenotype. This was also suggested to be the reason CDK5RAP2-deficient mice do not exhibit microcephaly with the same severity as humans, since mouse neural progenitors do not expand or proliferate to the same extent as in humans prior to neurogenesis to begin with¹⁴⁰. This demonstrates the capabilities of iPSC-derived brain organoids in recapitulating aspects of human disease that may not be possible using animal models. Additionally, the aforementioned cortical tissues by Sasai and colleagues, and other brain organoids since then, impressively, displayed key features of human corticogenesis during development including the presence of outer radial glial cells (RGCs), also known as basal radial glial cells, which are largely missing in mice models^{164, 167}. Thus, brain organoids can enable studying human-specific brain development features. Moreover, animal experimentation has been widely criticized for excessive use of animal models with very little translational benefits in clinical trials. While animal models might always be necessary in neuroscience, brain organoids have the potential to contribute to reducing the volume of animal experimentation and therefore reducing animal suffering. However, as brain organoid models become more sophisticated, there could be a chance for these organoids to become sentient entities and new regulations must take place to ensure standards of practice are set to have metrics that define organoid sophistication, legal status, and ethical handling and disposal procedures¹⁵⁰. However, this is not currently an issue with the status-quo brain organoids which have limitations in terms of brain maturity and necrotic cell death due to the lack of vasculature as these organoids grow bigger in size, which we discuss in more detail in **(Section 5.2.3)**. Batch-to-batch variation, similarly to most other biological models of the CNS, also remains a well-known challenge with brain organoids cultures. Pre-patterning approaches tend to generate organoids that are relatively more homogenous in cellular composition while self-patterning approaches where neural induction is more random tend to generate more heterogeneous batches of organoids¹⁶². Overall, batch-to-batch heterogeneity currently remains a challenge with all types of brain organoids, but it has been addressed by some researchers through the use of specialized cell culture technologies such as the use of mini-bioreactors¹⁴¹. In summary,

brain organoid technologies represent valuable tools for CNS modeling that overcome many of the limitations of other biological models, although their goal is not to replace other models of the CNS but rather to complement them in establishing experimental validity. As summarized in (**Table 2**) each biological model of the brains has its own strengths as it has its own weaknesses.

5.2.2 Applications of brain organoids

A wide range of applications have been reported, thus far, for stem cell-derived brain organoids^{2, 14}, which have been categorized in a review article by Qian *et al.* into²: 1) Structural recapitulation and brain malformation¹⁰, 2) human evolution¹⁶⁸ and neurophysiology¹⁶⁷, 3) major psychiatric disorders¹⁹, 4) neurodegenerative diseases²¹, and 5) development of therapeutics and toxicology research^{18, 141, 169-171}. The common process for applying brain organoids to a research problem begins with determining the appropriate model of brain organoid for an application of interest by consulting the available literature on the phenotypic, regional, and molecular manifestations of the condition as provided by previous *in vivo*, *in vitro*, and clinical data. Subsequently, a brain organoid model is generated and validated for whole or regional brain identity through immunohistochemical, genetic and proteomic analyses. The brain organoid model can then be applied to **elucidate** mechanisms underlying disease and physiology, **model** disease using patient-derived or genetically engineered organoids, and **test** brain response to **therapeutics** (*e.g.* gene therapy¹⁷⁰, antiviral drugs¹⁸, neurodegeneration suppressors¹⁷¹) or **environmental factors** (*e.g.* alcohol¹⁶⁹, nicotine²⁹, hypoxia¹⁷², Zika virus¹⁸). Numerous reports for applications of brain organoids demonstrate this process for modeling the brain and its disorders. Here, we highlight a few examples of common applications of brain organoid research.

Brain organoids for modeling environmental exposure to viruses: Neurotropic effects of environmental exposure to viruses have been modeled using brain organoids. Exposures to Zika virus (ZIKV)^{18, 141, 173}, herpes simplex virus¹⁷⁴, Japanese encephalitis virus¹⁷⁵, and the 2019 novel coronavirus¹⁷⁶, were modeled using cerebral^{18, 173, 174}, forebrain¹⁴¹, and cortical^{175, 176} organoids, of which the most extensively modeled has been ZIKV. ZIKV is a prenatal-acquired pathogen that spreads from infected pregnant females to their fetus and causes congenital defects characterized by severe microcephaly among other neurological disorders in newborns^{18, 177}. ZIKV neurotropism

studies by Qian *et al.*, performed using forebrain organoids, revealed selective viral localization with neural progenitor cells (NPCs) which has been confirmed in animal models and postmortem human fetal brain tissues^{141, 178}. NPC in ZIKV infected forebrain organoids were found to have disrupted cell cycle entry, hindered cell proliferation, and increased necrosis, which are thought to be the cause for microcephaly in infected newborns¹⁴¹. Additionally, ZIKV-forebrain organoids were significantly smaller than control forebrain organoids¹⁴¹; a phenotype that has been reproduced by several reports of ZIKV infected brain organoids^{18, 141, 173}, which was similarly found in Lancaster's genetic model of microcephaly discussed in **(Section 5.2.2)**¹⁰. Notably, Watanabe *et al.* used cerebral organoids to model ZIKV exposure and performed compound testing of antiviral treatments (*i.e.* up to six drug agents were tested, one to five doses per drug, and three to nine replicates per drug dose)¹⁸. The study identified candidate ZIKV receptors in the fetal brain model, and proposed compounds (Duramycin and Ivermectin) that could reduce ZIKV developmental manifestations¹⁸. While all six tested compounds have been long known to exhibit antiviral activity, studying their effects in context of a disease-specific 3D human brain organoid culture demonstrates a powerful capacity of brain organoids for high-throughput drug testing applications¹⁸.

More recently, brain organoids have been used to model the global 2019 coronavirus disease (COVID-19) pandemic caused by the novel severe acute respiratory syndrome coronavirus 2 (SARS-CoV-2), which to date, according to the world health organization has resulted in 122 million infections and devastating 2.7 million deaths globally¹⁷⁹. COVID-19 is well-known to cause respiratory manifestations primarily and systemic ones with fever, cough, and dyspnea being the top three most common symptoms respectively¹⁸⁰. Neurological symptoms such as headache, loss of smell and taste (anosmia and ageusia), and seizures have been reported in some COVID-19 cases as well^{176, 181}. Whether those neurological manifestations are **directly** resultant from severe SARS-CoV-2 neuroinvasion or **indirectly** caused by the respiratory syndrome is unclear. SARS-CoV-2 host invasion begins with binding of viral spike protein (α -Spike) to the angiotensin converting enzyme 2 (ACE2) host cell receptor, which stimulates innate immune response by the cell through phagocytosis and inflammatory response activation¹⁸². ACE2 is expressed in a wide range of organs including the skin, stomach, small intestine and the brain, with the lung being one of the highest ACE2 expressing tissues

and the brain being one of the lowest¹⁸². Song *et al.* explored the capacity of SARS-CoV-2 for neuroinvasion using three biological models including cortical organoids and postmortem COVID-19 patient brain tissues¹⁷⁶. The authors characterized cell death due to SARS-CoV-2 infection by staining for DNA degradation using terminal deoxynucleotidyl transferase mediated dUTP nick end labeling (TUNEL) assay¹⁷⁶. Micrographs of infected organoids were analyzed and plotted for the signal of TUNEL positive and negative cells in relation to SARS-CoV-2 positive cells taken from different regions-of-interest (ROIs) in the same organoid section¹⁷⁶. The authors reported neuroinvasiveness of SARS-CoV-2 in human brain organoids and extensive cell death in infected organoids¹⁷⁶. Yet, the majority of TUNEL-positive cells in infected organoids were **negative** for SARS-CoV-2, with the ROIs displayed in the article showing those necrotic SARS-CoV-2 negative cells in the core of the organoids¹⁷⁶. Based on those results, the authors concluded that SARS-CoV-2 infection **promotes death of nearby cells** in brain organoids¹⁷⁶. However, the use of brain organoids is flawed in this case and does not permit the conclusion made by authors with regard to infection-induced necrosis of nearby cells because the authors did not consider nor characterize hypoxia-induced necrosis in normal control organoids¹⁷⁶. Instead, we speculate those results to be a product of **hypoxia-induced necrosis in organoids cores due to a lack of vasculature** which an expected outcome in any 3D tissue culture that exceeds the limits of oxygen and nutrient diffusion in any dimension and has been reported in brain organoid sections by several groups^{10, 102, 147, 176, 183}. Therefore, attributing neuronal cell death to SARS-CoV-2 infection is not necessarily valid in this article. Additionally, the lack of an endothelium and immune cells present *in vivo* in these brain organoids significantly affects viral neuroinvasion efficiency¹⁸⁴. Thus, reporting neuroinvasiveness of SARS-CoV-2 using non-vascularized, immune-cell lacking brain organoids is not representative of *in vivo* physiology¹⁷⁶. Additionally, while human brain postmortem tissue characterization showed neurons positive for α -Spike, the authors failed to show negative controls of normal brain tissue or statistical significance tests of the number of SARS-CoV-2 infected neurons¹⁷⁶. The article also lacked reporting of any neurological symptoms or specific cause of death for the COVID-19 patients in the study that could support necrosis found in brain organoids or that could be attributed to viral infection or the ischemic injury found in infected regions of patients brains¹⁷⁶. This information is necessary because the human brain function is lost after

significant intervals of ischemic brain injury leading to permanent disability or death¹⁸⁵. Moreover, the blood brain barrier can be disrupted during ischemia and viral load can deposit in the brain, which could occur at a point where neuroinvasion is no longer relevant because the brain irreversibly ceased to function and the neurological symptoms under investigation cannot be reported by the patient nor verified¹⁸⁵. Furthermore, the well-known **high variability** of brain organoids renders it difficult to avoid experimental bias and selective choosing of ROIs when the same organoid section is used without careful characterization of necrosis in control organoids². This study potentially demonstrates some of the limitations of brain organoid models, when and why it can be inappropriate to make scientific conclusions using a flawed model, and the importance of carefully contextualizing conclusions in light of method limitations.

Note worthily, the ZIKV brain organoid models previously discussed¹⁸, despite having the limitations of organoid culture, presented a more appropriate experimental approach to model viral infection than the SARS-CoV-2 model for several reasons: First, the cerebral organoids generation protocol reported by Watanabe *et al.* was optimized and characterized in terms of reproducibility prior to modeling the disease¹⁸. Second, ZIKV infection has tangible phenotypic effects on the brain that can be measured *in vitro* (e.g. reduced brain size) but neurological symptoms from SARS-CoV-2 infection have sensory manifestations that require consciousness to report them, which is not possible with current brain organoids^{18, 176}. Third and most importantly, apoptotic marker cleaved-caspase 3 positive regions **in organoids' cores** were excluded from cell death count in the ZIKV study and were not attributed to the viral infection¹⁸. Only ROIs on the outer few cell layers of the organoid, where limits of oxygen and nutrient diffusion were not exceeded, were analyzed unlike the SARS-CoV-2 model where this distinction was not made^{18, 176}. We discuss the challenges and limitations of brain organoid models in more detail later in this chapter.

Brain organoids for modeling neuropsychiatric disorders: Major neuropsychiatric disorders, such as autism spectrum disorder (ASD), schizophrenia, and bipolar disorder, represent cognitive and behavioral human-unique, highly debilitating, complex conditions characterized by polygenic aetiology, variable symptoms, and comorbidity between them^{1, 162, 186}. Such characteristics make those conditions difficult to study in animal models due to the limitations discussed in **(Section 5.2.1)**^{1, 162}.

Additionally, neuropsychiatric disorders lack objective diagnostic biomarkers and therefore have been largely diagnosed based on patient interviews with many studies in the past focused on behavioral outcomes rather than molecular and cellular components involved in those disorders¹⁶². Advancements in genomics facilitated large-scale genomic studies in recent years that revealed a significant amount of genetic risk factors to be involved in neuropsychiatric disorders^{162, 187, 188}. Coincidentally, advancements in the ability to derive brain organoids from human patients' somatic cells and the readiness of brain organoids for easy genetic manipulation put them forward as attractive tools for modeling neuropsychiatric disorders, that are now better known for their genetic complexity, and proved them beneficial in identifying developmental abnormalities in these disorders^{19, 162}. For instance, ASD is a developmental brain disorder that manifests in defective social behaviors and lacks a well-defined etiology in 80% of the cases due to highly heterogeneous genetic variants that are thought to interact with other risk factors to cause ASD pathology, making it extremely difficult to model¹⁹. Mariani *et al.* generated idiopathic ASD telencephalic organoids derived from affected families to recapitulate molecular and cellular pathways involved in ASD pathology during first trimester human cortical development¹⁹. The authors found that upon overexpression of FOXP1, production of GABAergic inhibitory neurons is increased with no change in glutamate neurons which leads to the glutamate/GABA neuron ratio imbalance that has been involved in ASD pathogenesis¹⁹. The study highlights the benefit of using brain organoids in investigating molecular changes involved in selective vulnerability of specific human neuronal cell populations within a 3D human multicellular environment of the same genetic background¹⁹.

Brain organoids for modeling neurodegenerative disease: Neurodegenerative diseases are a group of untreatable terminal illnesses characterized by a progressive loss of certain neuronal cell populations in the brain^{15, 189}. The accumulation of harmful protein aggregates in the brain represents a common characteristic of these diseases and leads to the clinical symptoms of neurodegeneration such as dementia and decline in physical functions, which vary in severity based on the protein or brain region involved, and time course of the illness^{15, 189}. For the most part, modeling neurodegenerative diseases such as AD and Parkinson's disease using two-dimensional culture and rodent models has not translated well clinically^{15, 189}. Brain organoids represent complementary tools or, as some argue, better

alternatives for overcoming limitations of previous biological models, especially when used to model early events of disease, although organoid technology has challenges of its own that must be vetted as well^{15, 189}. Despite brain organoids being primarily developmental models, cerebral¹⁹⁰⁻¹⁹², cortical^{193, 194}, midbrain^{21, 195}, and motor nerve¹⁹⁶ organoids have been used to model numerous neurodegenerative diseases including AD^{192, 193}, Parkinson's disease^{21, 195}, frontotemporal dementia¹⁹⁰, Huntington's disease¹⁹⁴, hereditary spastic paraplegia¹⁹¹, and motor neuron disease¹⁹⁶. Interestingly, despite the immaturity of brain organoid models, they were able to recapitulate certain hallmarks of the aforementioned neurodegenerative diseases.

Gonzalez and colleagues produced cerebral organoids from familial AD (FAD) and Down syndrome (DS) patient-derived iPSCs and analyzed them comparatively with healthy control cerebral organoids¹⁹². Contrary to control organoids, DS and FAD organoids spontaneously produced amyloid plaque- and neurofibrillary tangle-like structures upon long term culture (110 days), as determined by immunofluorescence staining of 4G8 and 6E10 A β -specific antibodies¹⁹². Similar findings were reported by Choi and Kim *et al.* where plaque aggregates were produced after ESC-derived NPCs overexpressing several FAD mutations were 3D cultured for 90-days¹⁹⁷. Moreover, molecular outcomes of harnessing the apolipoprotein E4 (APOE4) allele; a prevalent risk factor for developing sporadic AD (SAD) later in life, were demonstrated by Meyer *et al.* who modeled sporadic AD (SAD) using cerebral organoids derived from APOE4⁺ gene-edited iPSCs¹⁹⁸. APOE4 organoids showed increased A β expression and phosphorylated tau¹⁹⁸, thus further illustrating genetic factors involved in AD and some possibility for brain organoids to model neurodegeneration.

5.2.2.1 Midbrain organoids characteristics and applications

Motivation for region-specific models of the brain: Region-specific brain organoids can be of particular interest in modeling neurological diseases as they aid in elucidating mechanisms that underlie **cell- and region-specific vulnerability to degeneration**¹⁸³. Neurodegenerative disorders that more severely affect certain brain regions such as the hippocampus in AD and the substantia nigra in Parkinson's disease¹⁸³, thus, represent important candidates for region-specific brain organoid models.

Parkinson's disease (PD) represents the second most common neurodegenerative disease after AD¹⁹⁹, with devastating symptoms ranging from movement abnormalities to psychiatric symptoms

including apathy, executive dysfunction, and depression^{199, 200}. PD affects 10 million individuals around the world; a prevalence that is on the rise due to increases in life expectancies¹⁹⁹. **Misfolding and toxic fibrillar aggregation of α -synuclein (α -syn)**; a protein involved in neurotransmitter release, vesicle trafficking, and membrane remodeling, represent key hallmarks of PD¹⁹⁹. Signaling pathway abnormalities resulting from α -syn aggregation and the resultant Lewy body inclusions, eventually lead to degeneration of vulnerable cell types in the brain^{199, 201}. Cellular characteristics linked to this vulnerability to degeneration include higher levels of **mitochondrial oxidative stress, elevated calcium concentrations, and extensive arborizations with many vesicular release sites enriched in α -syn**, all of which are characteristics **found in midbrain dopaminergic (mDA) neurons of the substantia nigra; the most affected type of neurons in PD**^{199, 201}. Additionally, neuroinflammatory processes mediated by neighboring glial cells have been found to play a role in PD progression¹⁹⁹. Furthermore, animal models mimicking PD-causing genetic mutations (*e.g.* LRRK2) failed to provide clear evidence for progressive loss of mDA neurons or formation of Lewy bodies, demonstrating an example of some of the limitations of animal models in studying PD^{195, 202}. **Thus, faithful modeling of human mDA neurons and the human brain microenvironment *in vitro* represents a key requirement for studying PD.**

***In vitro* 2D and 3D models of the midbrain:** Advancements in our understanding of **midbrain development** facilitated several protocols for generating *in vitro* **2D cultures of mDA neurons** from stem cells, which have been recently adapted for generating **3D cultures of midbrain organoids**¹⁹⁹. These protocols include the following key steps^{199, 203}: **1) dual SMAD inhibition**, which involves BMP and TGF β /activin/nodal pathway activation, that directs stem cells to a neuroectodermal fate^{199, 203}. **2) Midbrain floor plate identity** is then directed using a combination of **SHH, WNT, and FGF8 signaling**, which generates mDA progenitors^{199, 203}. **3) Differentiation and maturation of mDA progenitors** is then directed using **neurotrophic factors** (*e.g.* brain and glial-derived neurotrophic factors; BDNF and GDNF), and ascorbic acid as an antioxidant^{199, 203}. This specification process induces expression of a series of transcription factors (mainly; FOXA1/2 and subsequently LMX1A/B) required for **differentiation of mDA neurons** with diverse subtypes, which **upregulates expression of mDA neuronal identity markers** such as NURR1, PITX3, and tyrosine hydroxylase (TH)^{199, 203}.

As such, 2D cultures of mDA neurons have been differentiated from iPSCs of monogenic or sporadic forms of PD, and characterized in several studies^{199, 204}. In these studies, **2D cultures of mDA neurons reproduced several pathways linked to the aforementioned characteristics that contribute to neurodegeneration vulnerability**^{204, 205}. While hiPSC-derived mDA neurons were shown to be helpful *in vitro* models for studying PD, **only a few studies were able to reproduce degeneration of mDA neurons**^{199, 204}. Additional concerns of these 2D cultures, such as the lack of maturity of the differentiated mDA neurons and the lack of concurrent *in vitro* differentiation of other cell types present *in vivo* such as glial cells, warranted exploring 3D cultures as improved systems for modeling PD¹⁹⁹. Non-directed differentiation of hiPSCs into 3D cultures of **whole brain organoids** has been found to yield a proportion of cells positive for midbrain and mDA neuronal markers²⁰⁶. However, the proportion of those cells in whole brain organoids are typically small and variable^{199, 206}. Additionally, 75% of all dopaminergic (DA) neurons in the adult brain reside in the ventral midbrain²⁰⁰, which further motivates the need for **region-specific midbrain organoids (MOs)**.

Several protocols adapted the previously detailed steps for 2D cultures of mDA neurons in order to generate 3D human MOs (hMOs)^{141, 183, 201, 207, 208}. The first report of these protocols is by Tieng *et al.*, which proved that a 3D suspension of hiPSCs in microwells yields homogenous embryonic bodies that can be differentiated into mDA progenitor cells in a culture at liquid-air interface²⁰⁷. This demonstrated the generation of neurospheres containing >60% DA neurons of midbrain-like identity, characterized by expression of FOX2A, LMX1A, TH, and NURR1 positive cells after 3 weeks of culture²⁰⁷. Protocols following after for the generation of hMOs characterized these models more extensively and demonstrated methods for their long-term maintenance^{141, 183, 201, 208}. Two main strategies used in these protocols include either sequential²⁰⁸ or simultaneous^{141, 183, 207} use of morphogens to generate cells with midbrain floor plate identity¹⁹⁹. Organoids generated using these protocols share several features of midbrain floor plate organization including a ventricular zone with OTX2+/FOXA2+ cells, an intermediate LMX1A+/NURR1+ layer, and mantle layers with MAP2+/TH+ maturing neurons^{183, 201, 208, 209}. However, organoids generated using each of these protocols displayed variable percentages of those markers at similar time points. These differences in yield are thought to be a result of differences in differentiation protocols, estimation methods, and the

inherent variability of iPSC lines¹⁹⁹. The highest yield of MAP2+/TH+ cells has been recently reported by Kwak et al. as 86% of total cells, which was achieved upon optimization of SMAD and WNT signaling, thus achieving a more homogenous distribution of mDA neurons in hMOs²⁰⁹.

Interestingly, several studies reported the spontaneous appearance of neuromelanin (NM) granules in long-term cultures of human iPSC-derived MOs^{183, 201, 208, 209}. These structures resembled the ones found in SN tissues of the adult human brain, which have rarely been reported in 2D cultures of mDA neurons and have not been found in mouse MOs despite their presence in human MOs reported in the same study by Jo *et al.*^{199, 208}. These findings imply a unique advantage of human MOs. Additionally, the presence of inhibitory (*e.g.* GABAergic) and excitatory neurons, astrocytes, and oligodendrocytes, in some cultures of hMO, mimics midbrain composition and represents an advantageous characteristic missing from 2D cultures of mDA neurons^{199, 208, 209}. Overall, these reports support the use of hMOs to generate mDA neurons in a 3D environment that reflect certain cellular and biochemical characteristics of the human midbrain, paving the way for their use in neurodegenerative disease modeling.

Midbrain organoids as 3D models for Parkinson's disease: Advanced *in vitro* models of PD represent powerful tools to elucidate mechanisms underlying the neurodegenerative process^{21, 195, 199, 210}. Several reports modeled familial and sporadic forms of PD using hMOs, in recent years, using one or more of the following strategies: genetic editing of control hiPSC lines to express PD-causing mutations prior to deriving hMOs, derivation of hMOs from PD patient samples, and by studying correction of PD-causing mutations in patient-derived samples^{195, 210, 211}. Reports modeling PD using hMOs were able to recapitulate key phenotypes of the disease. Smits *et al.* demonstrated that long-term cultures of hMOs derived from PD patient samples carrying the common PD-associated LRRK2-G2019S mutation reproduced certain characteristics of PD including reduced number and complexity of mDA neurons, as identified from high-content image analysis of TH and FOXA2 expressing cells²¹¹.

In corroboration, Kim *et al.* demonstrated that identity markers for mDA neurons and neurite length were decreased in LRRK2-G2019S isogenic hMOs¹⁹⁵. Furthermore, LRRK2-G2019S hMOs displayed elevated levels of phosphorylated α -syn compared to healthy control hMOs, a key hallmark

of PD¹⁹⁵. Transcriptomic analysis of hMOs and 2D cultures of LRRK2-G2019S mDA neurons found differential expression of genes between the two culture methods, with genes enriched in LRRK2-G2019S hMOs being also found in *post-mortem* PD tissues¹⁹⁵. Additionally, expression of TXNIP; a protein proved to mediate LRRK2-associated pathology, was 4-folds higher in the isogenic hMOs compared to 2D cultures of mutant mDA neurons¹⁹⁵.

As stated previously, mitochondrial stress represents one of the key characteristics of PD-affected cells. Several studies using hMOs to model PD reported increased mitochondrial stress or mitophagy^{195, 210}. Ahfeldt *et al.* showed that by knocking out several PD loss-of-function genes in independent isogenic human pluripotent stem cells, oxidative stress and mitochondrial dysfunction increased in all lines²¹⁰. This was concluded from depletion of mitochondrial proteins and increased oxidative stress in TH+ cells²¹⁰.

Overall, these findings support the use of hMOs as improved research tools to model pathological processes of PD. To recap, up to this point in this chapter, we discussed the use of brain organoids as models for neurophysiology and disease in context with other commonly used biological models for neuroscience research. We aimed to highlight the advantages of using brain organoids through examples of applications in which brain organoids allowed either novel or improved recapitulation of disease and physiology. The motivation for region-specific models of the brain was then discussed through the example of using midbrain organoid models to study PD. Thus, based on the previously presented literature, it is clear that brain organoids represent valuable tools for neuroscience research. However, certain limitations of brain organoid culture call for caution when attempting to interpret results using brain organoid models. We discuss in further detail the challenges and limitations of brain organoid culture in the next section.

5.2.3 Challenges facing brain organoid models

While the previously mentioned advantages of brain organoids and their applications demonstrate their value as unprecedented research tools capable of recapitulating characteristics of the human brain while maintaining its genetic background, like other technologies brain organoids remain with certain limitations^{14, 15, 135, 199}. A key aim of organoid technology has been to **reproduce organogenesis in a dish** without the embryonic environment that is normally available *in vivo*¹³⁵.

While brain organoids provide the advantage of direct accessibility to analyze and monitor organogenesis *in vitro*, they lack the **elaborate well-controlled spatiotemporal developmental cues** present *in vivo* which allow for patterning a fully formed, vascularized, cell-type-diversified brain^{14, 135}. As such, methods for generating brain organoids, despite having the advantage of straightforward differentiation and cell maintenance protocols, compromise simplicity with **limitations in maturity, quality, and reproducibility of brain organoids**^{14, 15, 135, 199}. Additionally, artifacts from the unique 3D culture conditions used to grow and maintain brain organoids can interfere with data interpretation¹⁹⁹. Here, we highlight key challenges of brain organoid culture. We primarily focus on the lack of vascularization as one of the major drawbacks of brain organoids and discuss how it relates to the other challenges facing brain organoid cultures.

5.2.3.1 Vascularization and oxygen and nutrient supplementation

A mature human brain is a highly vascularized organ with an estimated vascular surface area of ~12 square meters made up of an order of 100 million capillaries²¹². The dense vascularization of the human brain attains to the biochemical needs of the brain, which ensure proper function and survival of neurons^{135, 177, 212}. The absence of functional vascular networks in the majority of brain organoid models reported thus far represents a major drawback of the technology and a frequently arising challenge in tissue engineering in general^{4, 135, 177}. For instance, impaired vascularization of embryonic brain can lead to pathological manifestations and developmental abnormalities²¹³. Mutations in the FLVCR2 gene lead to glomeruloid vasculopathy, which results in abnormally thickened and perforating vessels, hydrocephaly, and a thin cerebral cortex²¹³. Additionally, blood vessels play an instructive role in developing rodent brains by inducing neuronal differentiation, migration, and network formation; emphasizing the importance of brain organoid vascularization²¹³. Most cells *in vivo* are located no further than 200 μm away from a capillary to ensure sufficient oxygenation, nutrients supplementation, and waste clearance that maintain tissue viability^{4, 214}. Thus, **tissue engineered constructs that exceed the diffusion limitation distance (~100-200 μm) for oxygen and nutrients are at risk of becoming severely hypoxic and have been shown to experience apoptosis and necrosis, in the absence of perfused vascular networks**^{3, 4, 102, 214, 215}. The term ‘necrotic core or dead core’ is often used to refer to a region of dead cells that develops at the

utmost center of organoids, due to insufficient delivery of oxygen and nutrients, as the organoids grow in size without vascularization^{199, 216-218}. Here, we discuss methods used to characterize hypoxia and the necrotic core in brain organoids.

Methods for hypoxia and cell death characterization: Characterization of hypoxia and cell death due to inadequate supply of oxygen and nutrients, in reports of brain organoids has been largely overlooked in early years of development of the technology. While the majority of brain organoid articles reported recently still lack characterizations of cell death and hypoxia, a great number of reports did provide these characterizations, albeit often with limited comprehensiveness. The maximum size of brain organoids reached along with characterizations of hypoxia and necrosis in these reports are compiled in (Table 3).

Methods used for cell death characterization frequently include **nuclear staining, Immunofluorescent (IF) staining for apoptotic markers, and fluorescent assays that detect hallmarks of cell death**. Nuclear stains such as **DAPI and Hoechst** are applied on sections of brain organoids to identify aberrant nuclear morphology of necrotic cells characterized by pyknosis (DNA shrinkage), karyolysis (nuclear dissolution), or karyorrhexis (nuclear fragmentation)^{216, 217, 219}.

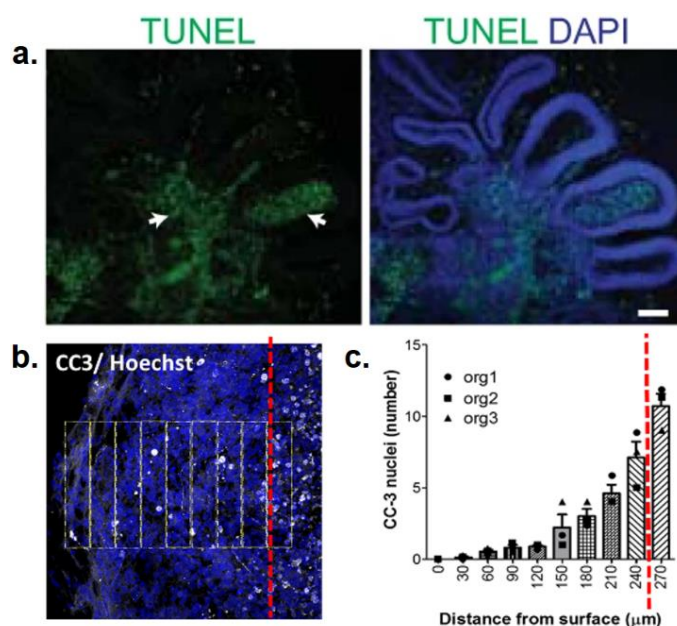


Fig. 13: micrographs of cell death in the core of brain organoids from two different reports. (a) TUNEL staining for DNA degradation in the core of cerebral organoids (*Lancaster et al. copyright 2013*), Ref (10). (b, c) Immunofluorescent staining and analysis of cleaved-caspase 3, CC3 (white) in neural organoids derived from Alzheimer's disease samples (c) Deeper regions of the organoid display increased CC3 expression (*Raja et al. copyrights 2016*), Ref (20). All figures reprinted with permission from publisher.

Table 3: Size, hypoxia and necrosis characterizations in reports of various brain organoid models over a 10-year period

First author	Organoid identity tested	Matrix	Max size	Culture (days)	Approach for reducing hypoxia	Hypoxia/cell death markers	Day/size tested hypoxia/necrosis	Ref
Eiraku <i>et al.</i> 2011	Optic cup	Matrigel	~2mm	14	None	-	-	12
Lancaster <i>et al.</i> , 2013	Cerebral	Matrigel	~4mm	15-60	Spinning bioreactor	TUNEL, DAPI	-	10
Muguruma <i>et al.</i> , 2015	Cerebellum	None	~0.5mm	21-35	None	-	-	166
Paşca <i>et al.</i> , 2015	Cortical	None	4mm	43-70	None	-	-	220
Qian <i>et al.</i> , 2016	Forebrain and ZIKV	Matrigel	~2mm	71-80	Mini-spinning bioreactor	DAPI, CC3	d28, ~0.3mm	141
Jo <i>et al.</i> , 2016	Midbrain	Matrigel	>2mm	30	Orbital shaker	-	-	208
Raja <i>et al.</i> 2016	AD vs. healthy	Matrigel	-	30-90	None	CC3	0.25mm	20
Quadrato* <i>et al.</i> 2017	Cortical	Matrigel	~1.5mm	15-273	Spinning bioreactor	HIF1 α , CC3	d273	206
Monzel <i>et al.</i> , 2017	Midbrain	Matrigel	1.3mm	20-61	Orbital shaker	CC3	d27, ~0.6mm	183
Lee* <i>et al.</i> , 2017	Cortical	hydrogel	~0.6mm	66	None	TUNEL, DAPI	d66, ~0.4mm	221
Ormel* <i>et al.</i> , 2018	Cerebral	Matrigel	~0.6mm	17-119	Spinning bioreactor	CC3	-	147
Mansour* <i>et al.</i> , 2018	Cerebral vs. vascularized	Matrigel	~1mm	40-279	Vascularization <i>in vivo</i>	TUNEL, DAPI	d31, ~0.5mm	102
Bian <i>et al.</i> , 2018	Cerebral and tumor	Matrigel	~3mm	15-30	Orbital shaker	-	-	222
Berger* <i>et al.</i> , 2018	Midbrain	GelTrex	~1mm	30	Millifluidics, shaking	Hoechst/cell debris	d30, ~1mm	217
Cakir* <i>et al.</i> , 2019	Cortical vs. vascularized	Matrigel	~4mm	30-120	Vascularization <i>in vitro</i>	TUNEL, DAPI	d30, 70, 120	3
Song <i>et al.</i> , 2020	Cerebral and SARS-CoV-2	None	-	63	Orbital shaking	TUNEL, HIF1 α	d63	176
Qian* <i>et al.</i> , 2020	Forebrain, neocortical	Matrigel	~1.5mm	60-150	Orbital shaking, slicing	Hypoxia dye, CC3	d60, 110, 140, 1-1.5mm	218
Nickels* <i>et al.</i> , 2020	Midbrain	GelTrex	~2.5mm	30	Accelerated patterning	ATP assay, Hoechst	d30, 2.5mm	216
Cai <i>et al.</i> , 2021	Cerebral	None	~2.5mm	35	Acoustofluidics	-	-	223
Ao* <i>et al.</i> , 2021	Cerebral, forebrain	Matrigel	-	16-35	Tubular culture, rocking	HIF1 α , live/dead	d7	215

*Starred articles reported minimal cell death in brain organoids generated using different approaches for enhancing transport of oxygen and nutrients or various optimizations/timelines for the differentiation protocol.

Apoptotic markers such as **CC3** and **Annexin-V** are involved in signaling cells to undergo apoptosis upon activation of cell death pathways²¹⁹. IF staining of brain organoid sections often targets CC3 and Annexin-V to characterize severity of the necrotic core^{20, 147, 183, 206, 218, 224, 225}. Immunostaining for apoptotic markers is often coupled with an additional characterization of cell death hallmarks to confirm findings. For instance, **TUNEL assay** uses terminal deoxynucleotidyl transferase to label blunt ends of DNA breaks, which allows for detecting cells that undergo extensive DNA fragmentation that occurs during late stages of apoptosis²¹⁹, and has been applied on sectioned brain organoids to characterize cell death^{3, 10, 102, 176, 221}. **Cell lysis** is another hallmark of cell death that can be observed using bright field imaging of brain organoid sections whereby the necrotic core of organoids appears as a region of sparse cell debris, especially at late stages of cell death²¹⁶.

Live/dead assays that identify apoptotic cells based on compromised cell membranes have

been used to detect cell death in intact brain organoids (>300 µm in diameter) in a few reports using confocal microscopy^{215, 226}. However, the main concern that arises from applying this method on intact brain organoids is potentially inadequate transport of the dye used in the assay to the core of organoids when the diffusion limitation distance of the dye is exceeded. Thus, characterization of cell death on intact brain organoids risks underestimating cell death at the core of the organoid where cell death has been shown to be greatest in multiple reports^{10, 20, 216, 217}.

Coupling cell death analyses with **characterization of hypoxia aids in inferring causes of spatially defined cell death in brain organoids and assessing the overall state of organoids**^{176, 206, 215, 218}. IF staining for hypoxia often targets hypoxia inducible factor 1-alpha (HIF1α); a protein complex that senses oxygen tension by stabilizing the complex in hypoxic conditions, and mediates cellular response to low oxygen concentrations through transcriptional activation of angiogenic pathways, cell proliferation, and regulation of apoptosis²²⁷. Methods such as qPCR and single-cell RNA sequencing (scRNA-seq) have also been applied to measure expression of HIF1α and apoptotic genes in brain organoid samples^{215, 228, 229}. However, a drawback of these methods is the loss of spatial information of cells expressing those markers within the brain organoid, as those methods require dissociating organoids into a cell suspension to perform measurements.

Hypoxic conditions in vivo and in vitro

Importantly, **stem cells naturally experience hypoxic conditions *in vivo*, in their specialized niche**^{230, 231}. The oxygen level in the majority of standard tissue culture systems used to generate brain organoids and in 2D cell culture, is that of environmental oxygen (20%) which is, in fact, considered hyperoxic in comparison to *in vivo* oxygen levels (1.5-8%) in the pre-implantation embryo²³⁰⁻²³². However, given the 3D nature of brain organoids, the inner cells of the organoid encounter oxygen concentrations that have been proposed to be exponentially lower than 20%, based on their distance from the organoid surface⁴. Therefore, traditionally generated brain organoids do experience hypoxia and/or apoptosis at various time points, as demonstrated in **(Table 3 and Fig. 13)**, which often occurs even with the use of tissue culture equipment that facilitate enhanced transport of oxygen and nutrients such as orbital shakers and bioreactors^{10, 20, 176, 183, 215, 218}. However, reported expression levels of hypoxic and apoptotic markers and the methods used to measure them in various reports are variable¹⁰.

Hypoxia alone in brain organoids is not necessarily disadvantageous at all stages of growing the organoid. Several *in vitro* studies demonstrated **enhanced survival of human CNS precursors and their improved differentiation under hypoxic conditions**^{231, 232}. Although other reports have suggested that rather than enhancing differentiation, hypoxic conditions act to **maintain pluripotency of stem cells**, which, in alternative cases, is necessary for their expansion^{230, 233}. Nonetheless, hypoxia is favorable rather than detrimental for stem cells and CNS precursor cells **during specific stages of development**²³⁰. Increasing oxygen tension during embryonic development is thought to act as a driving force that guides blastocyst migration and later contributes to initiating angiogenesis towards increasing oxygen gradients²³⁴. **It is, however, when hypoxia persists without vascularization, and is coupled with hypoglycemia, beyond an expected developmental stage does cell viability becomes threatened**^{235, 236}. Wang *et al.* demonstrated that neuronal stem cells exposed to long-term oxygen and glucose deprivation (6 and 8 hours) displayed decrease in cell survival, reduced differentiation and diminished neurite outgrowth of differentiated neurons²³⁵. Another report has shown repressed expression of forebrain, cortical, glial, and oligodendrocyte markers in 10-day old cerebral organoids cultured for 72 hours under hypoxic conditions (1-8%) without glucose deprivation²²⁴.

The detrimental effects of persistent oxygen deprivation on brain development *in vivo* are widely demonstrated in cases of prenatal hypoxic injury, which is a leading cause of neurological disability²³⁶. Immediate apoptotic cell damage and long-term dysfunction of NPCs can be caused by prenatal oxygen deprivation, which occurs due to factors such as placental insufficiency and umbilical cord occlusion, and leads to developmental abnormalities and increased risk for neurological disorders later in life²³⁶. Thus, brain organoid models experiencing hypoxia-induced cell death have serious concerns for the generated data if conclusions about physiology and disease are made under these conditions, without proper control, or without characterization of the necrotic core. **This poses the questions of how long and up to what size a brain organoid can grow without experiencing extensive cell death, under the current standard conditions of brain organoid culture.** A challenge arises when attempting to answer these questions because very few reports of brain organoid research

provided **all three characterizations of size, hypoxia and necrosis** in brain organoid^{4, 218}. We next discuss reports that provide insight on this topic.

Addressing hypoxia-induced cell death in brain organoid culture

Recently, several reports shifted from passively characterizing cell death in brain organoids to developing solutions to circumvent cell death directly in brain organoids through attempts of vascularization, accelerated patterning, sliced cultures, and using microfluidic systems to enhance transport of oxygen and nutrients to the core of organoids. Here is a review of hypoxia and cell death characterization in these reports.

Qian *et al.* aimed to generate cortical organoids that model features of late stages of cortical layer development, as shown in (Fig. 14)²¹⁸. The authors **cited cell death at the core of cortical organoids as a key limitation for generating a late stage model** because as the outer layers of cortical organoids

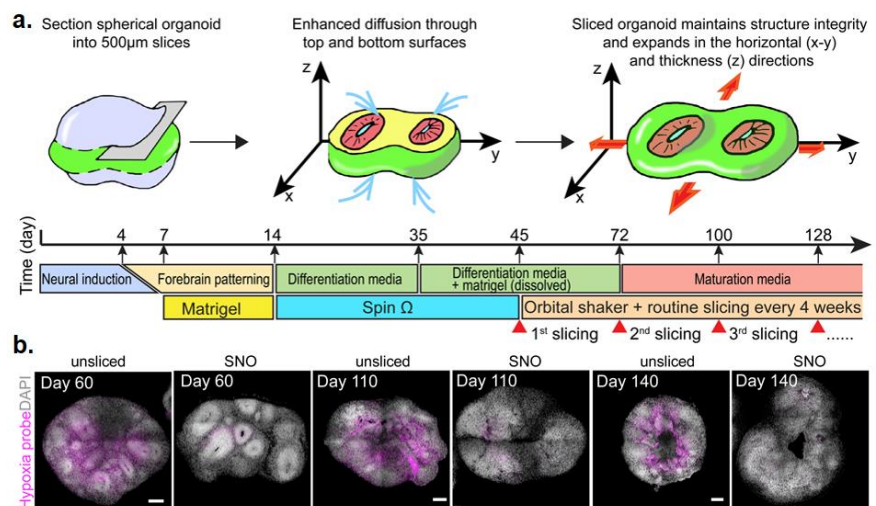


Fig. 14: Organoid slicing method proposed to reduce hypoxia and cell death in cortical organoids. The method models cortical layer formation. (a) Slicing protocol (b) Hypoxia and nuclear staining of sliced neocortical organoids (SNO) and unsliced controls. (Qian *et al.* copyrights 2020), Ref (218). Reprinted with permission from publisher.

thicken, proliferating progenitor zones that make up the core of the organoids are depleted continuously due to limited diffusion of oxygen and nutrients to the core²¹⁸. This **depletion of interior NPCs hinders further cell generation and leads to disorganized organoid architecture, thus making cortical organoids particularly vulnerable to the detrimental effects of a necrotic core**²¹⁸. To address this limitation, the authors developed a **slicing method** to cut cortical organoids into a disk shape, which exposes organoids' interior to oxygen and media, in order to facilitate oxygen/nutrient supplementation and neocortical layer specification²¹⁸. The authors used traditionally generated forebrain organoids, cultured with orbital shaking, as unsliced controls²¹⁸. Scale bars on micrographs of sliced neocortical organoids (SNOs) and unsliced organoids showed the organoids ranging in diameter between **1 to 1.5 mm** across three time points, albeit statistical comparisons for overall

diameter between the two conditions were not reported²¹⁸. As expected, unsliced organoids displayed a high signal for hypoxia with a **hypoxic area that ranged between 30-55% of the total organoid section**, which appeared primarily at inner regions of the organoids²¹⁸. On the other hand, SNOs displayed a significantly lower hypoxic area (<10%) across all three time points, and **a significantly lower expression of CC3 than unsliced organoids** across all measured time points²¹⁸. Additionally, characterizations of neurogenesis and radial migration of newborn neurons showed an increasing thickness of progenitor zones throughout a long-term culture of SNOs (70-150 days)²¹⁸. Whereas, unsliced organoids showed a decrease in progenitor zone thickness, which was significantly smaller than that of SNOs after day 100²¹⁸. Whether this slicing method is applicable to other types of brain organoids is not yet clear, since this model is aimed at modeling cortical layer development. However, **this report demonstrates several positive outcomes from resolving hypoxia-induced cell death at the core of organoids.**

Nickels *et al.* attempted to standardize and **improve MOs generation and analysis by reducing variability between organoids and minimizing cell death**²¹⁶. The researchers developed a protocol for **accelerated patterning of MOs** using a more committed cell type; human floor plate NPCs, as the starting cell type for the differentiation protocol, and employing shorter timing periods for each step of the protocol with each designated media for maintenance and differentiation²¹⁶. The authors hypothesized that this accelerated patterning approach will reduce tissue density within the organoids, thus facilitating better oxygen and nutrient supply to the core²¹⁶. Using the optimized version of the protocol, the authors reported reduced tissue density and smaller sized organoids compared to control²¹⁶. Furthermore, viability studies of the latest time point at **day 30** showed that MOs grown using accelerated patterning were able to grow up to **2.5 mm** with no visible necrotic core based on bright field imaging of MO sections, compared to control and one other tested condition²¹⁶. Although, coupling these results with more specific characterization of cell death markers as opposed to relying on bright field imaging would have strengthened the findings. Nonetheless, ATP production within the optimized MOs showed a 40% increase compared to controls and a FOX2A+ inner cell mass was also observed within these organoids²¹⁶. Despite size and density reduction using this protocol, MOs derived using this method demonstrated distinct spatial organization and were able to

generate different neuronal subtypes²¹⁶. The volume of TH within MOs was estimated using whole mount staining and 3D reconstruction, and was used as indicator of dopaminergic neurons²¹⁶. TH volume in MOs derived using optimized accelerated patterning was significantly higher than control MOs, which the authors attributed to an equal number of TH+ cells in a smaller organoid and fewer dead cells²¹⁶. Similarly, neuronal and glial markers were increased in MOs generated using the optimized protocol²¹⁶. Overall, this report **demonstrates the effect of tissue density on oxygen and nutrient transport to the core of organoids** and provides a framework for optimization steps of MO derivation protocols to address cell death within the organoid core without compromising the validity of MOs as research tools for modeling the midbrain.

In a study by Berger *et al.* the authors attempted to address the development of a necrotic core in MOs using a commercially available Quasi Vivo[®] millifluidic culture system that supplies media to organoids through continuous laminar flow, as shown in **(Fig. 15a)**²¹⁷. Compared to conventional shaking conditions, MOs under millifluidic culture displayed reduced necrotic core regions, although, the necrotic core was not completely eliminated in either cases, as shown in **(Fig. 15b, 15c)**²¹⁷. Additionally, millifluidic culture conditions showed increased dopaminergic differentiation compared to conventional culture²¹⁷. The report demonstrated an opportunity for improving MO quality by reducing cell death at the core of MOs through enhanced mass transport facilitated by culture under continuous laminar flow²¹⁷.

Overall, only a few articles that applied traditional methods for facilitating mass transport in brain organoid culture through the use of spinning bioreactors and orbital shaking, reported minimal cell death^{147, 206, 221}. However, in these traditional reports, as well as the majority of reports of specialized systems where cell death was in organoid cores was also minimal, such as millifluidics and sliced cultures^{102, 217, 218}, the maximum size shown

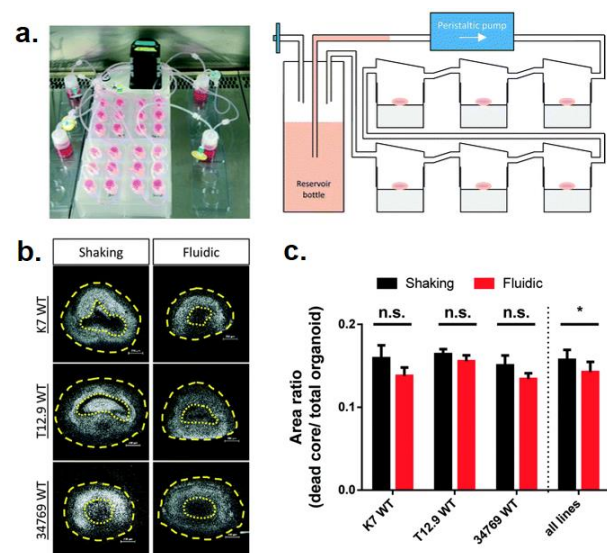


Fig. 15: Millifluidic approach vs. shaking for reducing cell death in brain organoids. **(a)** Millifluidics setup. **(b, c)** Millifluidics show reduced dead core in organoids relative to shaking but do not eliminate it (Berger *et al.* 2018), Ref (217). Reproduced with permission from publisher.

for the organoid in micrographs of cell death characterizations ranged between **0.6-1.5 mm**^{102, 147, 206, 217, 218, 221}. This could hint that methods that reduce organoid diameter or cell density provide a successful approach for reducing cell death, as has been observed with the accelerated patterning method discussed²¹⁶. Exceptionally, in a report by Cakir *et al.*, the authors constructed vascular-like structures within cortical organoids *in vitro*, by ectopically expressing human ETS variant 2 (ETV2); an essential vascular development transcription factor, and were able to demonstrate significantly reduced cell death in cortical organoids with vascular-like structures that appeared to reach up to 4 mm in diameter³. However, the vascular-like structures within these organoids still lacked long-term maturation due to the lack of blood flow inside the organoid^{3, 237}. A fully functional vascular network within brain organoids is thus yet to be developed. Reports of attempts to vascularize brain organoids are discussed in further detail in (Section 5.3.3.2).

Interestingly, as demonstrated in (Table 3) and discussed reports (Figs. 13 to 15), brain organoids are able to grow beyond the diffusion limitation distance for oxygen (200 μm), either without developing a necrotic core or despite possessing one. A report by McMurtrey provides a theoretical model that explains this phenomenon, where a cerebral organoid is modeled as a 3D spherical construct and the model is analytically solved for steady-state diffusion and metabolism under unlimited supply of gas and nutrients, as illustrated in (Fig. 16)⁴. In this model, based on diffusive transport, calculated cell density, and reportedly low metabolic rate for oxygen in cortical neurons, the author found that the maximal predicted diameter of cerebral organoids without central cell death is 1.4 mm, which is strikingly close to the majority of previous reports where cell death the core was reported to be negligible^{4, 102, 147, 206, 217, 218, 221}. Nonetheless, experimental data in this report

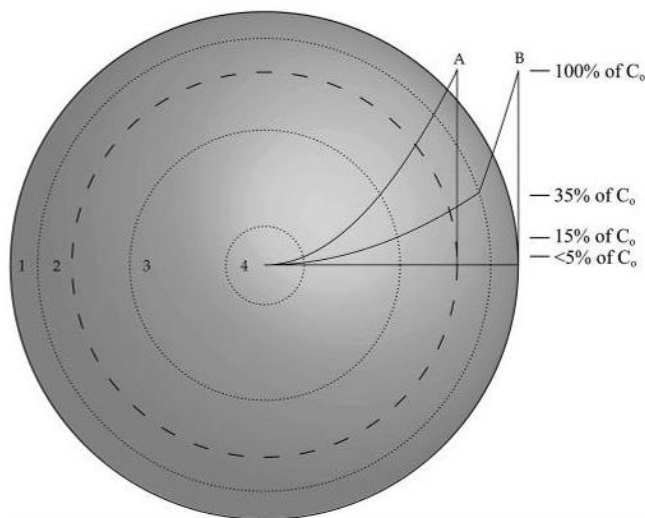


Fig. 16: Spherical model for development of hypoxia in cerebral organoids. Curve A shows a concentration profile for metabolized gas or nutrient and the maximal diameter of 1.4 mm (dashed line) when distribution of cells is homogenous. Curve B demonstrates the concentration profile for a modified maximum radius when a percentage of cells shifts into a denser outer layer (zone 1), with all other parameters maintained constant, the model predicts an enhanced maximal diameter of 1.8 mm (solid border), (McMurtrey 2016), Ref (4). Reprinted with permission from publisher.

showed that the average diameter of cerebral organoids over time, measured at the shortest axis, exceeded the predicted diameter and averaged at 1.8 mm by day 40⁴. The disparity between the predicted model and experimental data is attributed to the assumption that cell density within cerebral organoids is homogenous in the predicted model⁴. Thus, the author proposed an alternative multi-compartment model to describe oxygen consumption within cerebral organoids with four layers of variable cell density and neuronal regions, as shown in **(Fig. 16, curve B)**⁴. The model proposes that metabolically active cells shift away from the core to an outer layer to form a denser rim around the sphere (zone 1), while an intermediate region of progenitor cells may be present in zone 2⁴. Zone 3 is proposed to contain a region of multipotent cells preserved due to hypoxic conditions, while zone 4 represents a severely hypoxic region where cell viability is at risk⁴. This regionalization process is known to occur in early brain development, as well as in brain organoids through the migration of neuroglial precursor cells⁴. The multi-compartment model thus provides a plausible explanation for achieving an enhanced diameter in brain organoids despite possessing a necrotic core.

In addition to causing cell death at the core of brain organoids, the lack of vascularization poses serious limitations on the quality and maturity of brain organoids^{135, 177, 238}. While early *in vivo* development of the neocortex is able to progress without vascularization, later stages of brain development highly depend on vascularization of the subventricular zone^{135, 177, 238}. By 6 gestational weeks, a capillary plexus covers the entire cerebral cortex, and by 8 gestational weeks, the neurovascular network develops in a ventral-to-dorsal progression, to supply oxygen and nutrients and eliminate waste²³⁸. As the neurovascular network expands, it innervates deeper brain regions and contributes to the niche surrounding neuronal progenitor populations. Dynamic crosstalk between neuronal progenitors and the vascular network guides proliferation, migration, and differentiation of neuronal progenitors, and neuronal survival and maturation^{135, 177, 238}. This dynamic reciprocity between brain tissue and the vasculature remains crucial for maintenance and survival of neuronal populations throughout adulthood²². Therefore, lack of vascularization in brain organoids could potentially affect the aforementioned processes, interfering with normal development and physiology¹³⁵. The absence of vascular networks in brain organoids is thought to be likely responsible for shortage of progenitor populations and the inability to faithfully recapitulate cortical plate

formation in brain organoids thus far¹⁷⁷.

Furthermore, the interaction between brain tissue and the neurovasculature itself is an important one to model due to its potential for clinical applications and understanding neuropathology^{15, 135}. Drug delivery to brain tissues is a process controlled by BBB¹³⁵. Faithfully modeling the admission of drug agents to neurons through the BBB would enable us to improve drug transport efficiency and physiology¹³⁵. Additionally, BBB dysfunction is involved in the aging process and brain disorders¹³⁵. For instance, vascular pathology is a key contributor to two most common neurodegenerative disorders; AD and vascular dementia^{15, 135}. Moreover, vascularized brain organoids could potentially allow modeling the pre- and post-stroke adult brain, and better understanding neurological disease etiology¹³⁵. Evidently to the importance of neurovasculature proximity to neurons as not only conduits that deliver oxygen and nutrients to the brain, but as also contributors to the microenvironment^{22, 135}, it has been shown that approximately every neuron in a fully formed brain has its own capillary. The average *in vivo* distance between any neuron and a capillary in the human brain being 8-20 μm ²¹². As aforementioned, this proximity is far from superfluous for the brain microenvironment. However, it is unclear whether tissue-engineering approaches must replicate the same level of *in vivo* vascular density in order to generate faithful *in vitro* models of the brain. Nonetheless, functional vascularization of brain organoids is a crucial step towards generating improved models of brain physiology and disease.

5.2.3.2 Non-neuronal cell diversity

The human brain requires cellular and environmental complexity to perform its functions. This complexity emerges in part due to interactions between neuronal cell populations and glial cells, including astrocytes, oligodendrocytes, and microglial cells^{177, 238, 239}. Astrocytes and oligodendrocytes; collectively termed macroglia, constitute most of the cell types in the brain and perform key functions²³⁸. Astrocytes play a crucial role in synaptogenesis, regulating homeostasis, metabolism, maintenance of the BBB, and response to CNS damage, while oligodendrocytes produce myelin; a multilayer sheath crucial for rapid impulse propagation^{177, 240}. Microglia are specialized brain-resident innate immune cells that play a key role in brain development, homeostasis, function, and repair^{177, 189, 239}. They maintain brain homeostasis through phagocytosis of pathogens and damaged

cells, synapse elimination, and inflammatory response modulation^{177, 189, 239}. Derivation of these non-neuronal cells is necessary for upgrading the fidelity of brain organoid models.

During *in vivo* development, gliogenesis occurs after neurogenesis, starting mid-gestation and continuing after birth, which includes developmental stages that have proven challenging to replicate in brain organoids^{238, 241}. The initial temporal sequence of events for formation of glial cells following neurogenesis has been replicated in cerebral organoid cultures where astrocytes appeared much later in culture^{241, 242}. Induction of mature oligodendrocytes has been recently demonstrated in cortical organoids²⁴³, and oligodendrocyte organoids²⁴⁴, after 28 weeks and 30 weeks in culture, respectively. However, the level of functionality using these protocols remains limited. These studies demonstrated that formation of oligodendrocytes and astrocytes within 3D cultures while preserving neuronal cell populations is possible, which is not surprising given that, similarly to neuronal cells, oligodendrocytes and astrocytes originate from the neuroectoderm^{238, 243, 244}. In contrast, microglia are myeloid cells that uniquely originate outside the CNS from hematopoietic stem cells in the yolk sac, which then migrate through the circulatory system to inhabit the neuroectoderm; a process that occurs during week 5 of human gestation, after neurogenesis and prior to formation of macroglial cells^{177, 238, 239}. Given this non-ectodermal origin, microglia have been missing in the majority of hiPSC-derived brain organoid models and their incorporation into brain organoids has been challenging^{177, 238, 239}. Additionally, since morphogens are added to traditional brain organoid cultures through bath application, spatiotemporal cues required to attract non-ectodermal cell populations, such as microglia and endothelial cells, are almost completely absent²³⁸.

Recently, efforts have been made to integrate microglia-like cells (MLC) and iPSC-derived microglia into brain organoids^{147, 239}. Ormel *et al.* showed that cerebral organoids generated via an **unguided self-patterning approach** intrinsically developed microglia-like cells, which likely emerged from mesoderm contributors within the structure¹⁴⁷. While transcriptomic analysis showed partial similarities between these cells and the adult human microglia, it is unclear whether these MLCs resemble microglia that originate from the yolk sac^{147, 239}. Furthermore, generation of these MLCs within cerebral organoids has been variable and inconsistent, which necessitates further optimization of these protocols^{147, 239}. Due to varying germ layer lineage contributions in the brain, generating

microglia using **guided pre-patterning approaches** for region-specific brain organoids is extremely challenging, as these protocols include specific ectoderm patterning factors that are unfavorable for microglia differentiation, and strategies for *in vitro* generation of iPSC-derived microglia have only been recently available^{238, 239, 245, 246}. Efforts towards integrating iPSC-derived microglia into brain organoids have been made through co-culture approaches^{245, 246}. These studies have shown that exogenously generated microglia are able to integrate into cerebral organoids, participate in crosstalk with neuronal populations, and generate an immune response^{238, 239, 245, 246}. However, while the *in vitro* generated microglia possess a process-bearing ramified-like appearance, their morphology does not fully replicate the resting ramified state of *in vivo* microglia^{239, 245}. Further work is needed to optimize co-culture conditions in terms of the number of successfully and reproducibly integrated microglia, distribution and function of the cells, and the timing for their introduction, as those factors may influence differentiation, neuronal survival, and immune response^{238, 239}. Characterization of transcriptomic identity of iPSC-derived microglia in comparison to their mature resting *in vivo* counterparts is additionally needed to determine maturity^{238, 239}.

Survival of microglia within long-term brain organoid cultures is yet to be optimized, as the majority of protocols use short 1-week time points while 1 month is the longest time point reported^{238, 247}. Given that macroglia develop late in culture and microglia at earlier time points, long-term culture of microglia is required to comprehensively study neuroimmune interactions and replicate brain cytoarchitecture²³⁸. Furthermore, cell death at the core of organoids of later time points due to lacking vasculature will need to be resolved in order to generate brain organoid models with sufficient amounts of functional and viable glial populations to model the human brain during later stages of development and in disease. A human brain organoid model composed of mature glial populations would likely represent a useful, clinically relevant tool for modeling neurodegenerative diseases such PD and AD, where microglia and astrocyte-mediated neuroinflammation is known to play an important role in pathophysiology and disease progression^{189, 199}.

5.2.3.3 Maturity and aging in brain organoids

Current differentiation protocols only allow for generating brain organoids of early stages of development, which match molecular signatures of the human fetal cortex up to second trimester of

gestation¹⁵. This limits the ability to model later developmental stages or study diseases that arise during adulthood^{239, 248}. This lack of maturity has been mostly attributed to previously discussed limitations of brain organoids, including cell death and insufficient delivery of signaling molecules due to lacking vascular networks, absence of biochemical and biophysical gradients in the *in vitro* environment, and the lack of glial populations^{199, 238, 239}. Collectively, these limitations diminish complexity and long-term viability of brain organoids that are necessary to generate a mature brain model^{199, 238, 239}. In corroboration of missing *in vivo* interactions in brain organoid cultures, upon *in vivo* transplantation in mice, hiPSC-derived neurons showed improved functional maturation^{239, 249}. Additionally, Mansour *et al.* demonstrated that transplantation of human brain organoids into brains of immunodeficient mice allowed up to one-year survival, and showed vascular invasion from the host vasculature into the organoids¹⁰². The studies suggest possibility for long-term maturation upon exposure to *in vivo* factors^{102, 249}. However, transplantation of human cells in rodent models does not provide a clinically-relevant setting applicable to the human brain due to the surrounding rodent *in vivo* environment, and additional work is needed to investigate possibility for maturation towards postnatal developmental stages, information processing, and response to stimuli, which would have important ethical implications to consider²³⁹.

Although brain organoids are primarily neurodevelopmental models, their applications extend to age-related neurodegenerative diseases such as PD and AD as well, due to their ability to reproduce certain pathophysiological hallmarks of neurodegeneration using patient-derived or genetically edited hiPSCs^{15, 199}. However, modeling aging-related diseases using hiPSC-derived brain organoids must be carried with caution^{15, 199}. Reprogramming cells to an iPSC state has a well-known but often overlooked “rejuvenating” effect, where aging-related epigenetic markers are erased, telomeres are lengthened, and mitochondrial fitness is increased in reprogrammed cells, which eliminates benefits of using patient-derived cells^{15, 199, 239}. Additionally, certain hallmarks of neurodegeneration reproduced by brain organoids could potentially result from artifacts of culture conditions or could be by-products of limitations of brain organoid culture. Loss of dopaminergic neurons could result from cell death due to insufficient delivery of oxygen, nutrients in brain organoids, and must be interpreted with this consideration and tested with appropriate controls^{15, 199}. Moreover, brain organoid culture

have an upregulated reliance on glycolysis and increased endoplasmic reticulum stress, which has been shown minimize neuronal differentiation and impairs molecular subtype specification, reducing fidelity of brain organoids in modeling dopaminergic neuronal populations that are vulnerable in neurodegeneration^{199, 250}.

Certain strategies have been suggested for promoting aging in brain organoids, including overexpression of progeric genes, and inducing DNA damage and mitochondrial stress^{15, 199}. Furthermore, bypassing the pluripotent state through direct reprogramming of patient cells to neurons has been shown to better preserve aging hallmarks in human motor neurons, although it is unclear whether this method, if used to generate brain organoids, would permit the same spontaneous self-organization that occurs in iPSC-derived brain organoids^{15, 251}. Another alternative to induce aging in brain organoids is by manipulating oxidative stress using toxins or altering media composition¹⁹⁹. For instance, eliminating antioxidants from culture media of hMOs after 45 days in culture enabled differentiation of cells containing NM, expression of mature neurons, and increase in DNA damage^{195, 199}. Additionally, hMOs cultured without antioxidants were enriched for human midbrain transcripts associated with aging and genes found in post-mortem PD tissue^{195, 199}. Overall, providing a precisely controlled environment that mimics *in vivo* cues or using protocols that induce aging represent beneficial strategies for generating mature brain organoids^{15, 199, 239}.

5.2.3.4 Variability in brain organoid cultures

Brain organoid cultures are notoriously known for the “batch syndrome” where different batches of organoids show significantly variable quality and spatiotemporal organization of their cell populations^{135, 199, 237}. Reproducibility is a highly necessary requirement for accurately modeling biological events and testing therapeutics. However, it is challenging to achieve high reproducibility in brain organoid cultures because it requires production of cell types that 1) organize in a defined 3D architecture and 2) reproduce functional properties of the brain, while consistently fulfilling these requirements²³⁷. Several factors are responsible for high variability in brain organoid culture, including heterogeneous genetic background of iPSC lines, discrepancies in iPSC culture, and variations in differentiation protocols and the environment inside different bioreactors^{15, 199, 237}. Furthermore, animal-derived hydrogels such as Matrigel and Geltrex contribute to variability of the 3D network

surrounding organoids, thus synthetic biomaterials such as poly (lactide-co-glycolide) copolymer have been proposed as alternatives for enhancing reproducibility^{199, 252}. The effect of differentiation method on reproducibility has been characterized using scRNA-seq, which showed that whole brain organoids generated via self-patterning, where no exogenous factors are added, have greater variability than region-specific brain organoids derived using guided differentiation where media-supplemented growth factors tightly restrict cell fate²²⁸. Moreover, in effort to control growth conditions of brain organoids, Qian *et al.* developed 3D printed miniaturized spinning bioreactors (SpinΩ) that were able to reliably produce forebrain organoids with reduced heterogeneity in shape and size¹⁴¹. Improved reproducibility will likely aid in addressing other challenges of brain organoids such as lacking microglia and vascular networks, since high variability lead to inconsistent results and difficulty making conclusions when developing solutions for each of these challenges.

Overall, biological and technical solutions addressing challenges facing brain organoid models are rapidly evolving and benefitting from bioengineering advancements. The challenges discussed in this section are intertwined, as maturity of brain organoids is dependent on cell viability, vascularization, and non-neuronal cell diversity, and their low reproducibility hinders further advancements. Efforts addressing these challenges will have to combine to generate an improved brain organoid model that enables faithfully reproducing neurobiological events in health and disease.

5.3 Vascularization in tissue engineering

The field of tissue engineering developed to address two key biomedical needs. First, the shortage of organs for transplantation represents a key motivation for developing tissue engineered constructs that regenerate, or replace lost function²⁵³⁻²⁵⁵. Second, physiological modeling of human organs in health and disease is necessary for advancing our understanding of human biology and for developing, testing, and validating therapeutic agents in a clinically relevant humanized context²⁵⁴⁻²⁵⁷. While the field of tissue engineering has made significant advancements in recent years, scaling tissue-engineered constructs from short-term small sized tissues to long-term large-scale tissues for *in vitro* studies of mature organs or translation into clinical applications remains challenging largely due to lacking vascularization of engineered tissues^{253, 255, 257}.

The *in vivo* circulatory system plays a critical role in maintaining organ homeostasis and

vitality^{255, 257, 258}. This role is carried out by a hierarchy of blood vessels that include large blood vessels (>6 mm in diameter), small blood vessels (1-6 mm), and microvessels (<1 mm)^{255, 258, 259}. These blood vessels can be categorized based on their size into the macrovasculature and the microvasculature²⁵⁸. The macrovasculature consists of large blood vessels; arteries and veins, and is responsible for rapid movement of blood to and away from distant organs²⁵⁸. The microvasculature consists of a vast network composed of three types of microvessels; arterioles, venules, and capillaries, which exhibits a high surface area-to-volume ratio and is responsible for rapid local exchange of substances with surrounding tissues²⁵⁷⁻²⁵⁹. The role of the microvasculature has been long perceived as restricted to oxygen and nutrient delivery, regulation of thrombosis, clearance of metabolic waste, and contributing to immune responses^{22, 255, 257}. However, a recent paradigm shift has elevated the role of the microvasculature from passive conduits of molecules and cells to key regulators of homeostasis and metabolism, and directors of non-fibrotic regenerative responses by resident stem cells²². This instructive role has been studied and demonstrated for tissue-specific capillary ECs in proximity to epithelial, hematopoietic, mesenchymal and neuronal cells and their corresponding stem and progenitor cells, which is enabled through “angiocrine factors” that are paracrine-secreted by ECs and the resident cell types in response²².

The implication of the aforementioned critical physiological tasks of the microvasculature is that its absence from engineered tissues undermines both their viability and physiological mimicry. Modeling organ regeneration and stem cell behavior using avascular tissues paints an incomplete landscape of physiology due to missing organ-specific EC-tissue angiocrine crosstalk²². Additionally, as mentioned in a previous section, (**Section 5.2.3.1**), tissue engineered constructs that exceed a certain distance, particular to the type of tissue, required for oxygen diffusion (often 100-200 μm in any direction), become at risk of hypoxia and subsequent cell death rendering them nonviable for further applications^{4, 255, 257}. While an avascular tissue engineered implant could experience vascular invasion from the host as part of the foreign body response, this vascular invasion process requires days or weeks to take place²⁵³. This time frame is long enough for cell death to occur at the center of the implanted tissue due to insufficient oxygen or nutrient delivery, leading to poor tissue integration²⁵³. Thus, pre-vascularization of engineered tissues before implantation has been long proposed for

priming implants for perfusion by allowing the implant's vasculature to integrate by *in vivo* bridging or microsurgical attachment to the host vasculature²⁵³. Similarly, tissue engineered constructs for *in vitro* drug testing and physiological modeling require vascularization for their long-term maturation and viability^{3, 4, 117}. Perfusable microvascularization of engineered tissues remains a pressing challenge in tissue engineering to-date^{253, 255, 257}, although researchers demonstrated more success in vascularizing certain tissue types than other types, such as successful perfusion of vascularized tumor and fibroblast microtissues^{25, 256, 260, 261}.

Vascular tissue engineering (VTE) developed as a branch of tissue engineering to translate the knowledge of vascular biology and the multidisciplinary principles of tissue engineering into clinical applications to advance therapeutics, engineered implants, and physiological models of vascular structures^{255, 262}. VTE and vascular regenerative medicine currently have two main focus points: 1) producing artificial blood vessels, which is often associated with tissue engineering of vascular grafts (TEVG), and 2) generating vascularized tissue constructs, which is often referred to as microvascular tissue engineering (MVTE)^{255, 262, 263}. Both areas of VTE research overlap to some degree in the basic knowledge they derive from, despite their different end goals. They both generally include the following key considerations for developing their respective products: 1) cell sources, 2) appropriate biomaterials for the desired application, 3) biochemical and mechanical cues required for simulation, maintenance, and maturation of the engineered vascular structure, and 4) the technique for generating the vascular structure^{254, 257, 262, 264-266}.

Synthetic grafts for replacing large blood vessels have been generally acceptable as a therapeutic option despite their shortcomings, while engineered grafts for replacing small sized blood vessels remain a greater challenge for TEVG²⁶⁷⁻²⁶⁹. Principles and methodologies of TEVG for generating improved large and small blood vessel grafts are out of the scope of this thesis, and have been reviewed as referenced²⁶⁷⁻²⁶⁹. MVTE research includes three main topics including therapeutic vascularization, development of microphysiological *in vitro* systems, and vascularization of engineered tissues, reviewed as referenced^{256, 257, 261}. In this thesis, we provide a review of the latter two topics: microphysiological *in vitro* systems specifically for spheroid and organoid cultures, and tissue vascularization methods specifically for brain organoids. The difference between the two latter

topics generally lies in the use of microfluidic devices and cell-patterning methods to control the spatial distribution of endothelial cells when generating a microphysiological *in vitro* system^{25, 26, 256}. Whereas, vascularization of engineered tissues utilizes traditional well plates or *in vivo* models to achieve vascularization^{6, 102}, which typically eliminates spatial control of the vascularization process.

Approaches for MVTE are rooted in our understanding of angiogenic spatiotemporal cues^{256, 257}. Control of angiogenic spatiotemporal cues can be achieved through recapitulating cell-ECM and cell-cell interactions, and controlled release of pro-angiogenic factors, which must take into consideration tissue-specific cues present during *in vivo* biological processes (e.g. development, and cancer metastasis); where vascularization takes place^{256, 257, 270}. Recapitulating tissue-specific angiogenic cues specifically for spheroid and organoid models remains challenging due to the interdisciplinary characteristic of MVTE research²⁵⁶. Additionally, the ability to generate human iPSC-derived organoids and iPSC-derived endothelial cells is relatively recent and has only been recently integrated into the MVTE²⁵⁶. In the next sections, we discuss examples of microphysiological *in vitro* systems and engineered tissues where perfusable vascularization was achieved and how their respective applications are relevant to brain organoids.

5.3.1 Vascularization *in vivo*

As previously stated, the formation of vascular networks is an intriguing biological process to study and recapitulate for tissue engineering and regenerative medicine. The formation of vascular networks *in vivo* occurs through two fundamental processes angiogenesis and vasculogenesis²⁷¹. Angiogenesis is a morphogenic process by which new blood vessels form from preexisting blood vessels²⁷¹. It is distinguished from vasculogenesis in that vasculogenesis occurs through differentiation and assembly of initial vascular plexuses *de novo* from individual primitive endothelial cells^{265, 271}. Angiogenesis is well known to occur during both embryonic development and postnatal life. Vasculogenesis, on the other hand, was long thought to occur only during embryonic development, but increasing evidence that remains under debate, suggests that vasculogenesis also occurs during postnatal life, although less commonly than postnatal angiogenesis²⁷²⁻²⁷⁴.

5.3.1.1 Vasculogenesis

Vasculogenesis is a reoccurring process during mammalian embryogenesis that first occurs

in the mammalian yolk sac early in embryonic development^{272, 275, 276}. First, epiblasts in the primitive streak undergo epithelial to mesenchymal transition²⁷⁶. These now-mesenchymal multipotent cells migrate to occupy a region between the epiblast and the visceral endoderm and differentiate into mesoderm or definitive endoderm²⁷⁶. The visceral endoderm is thought to be responsible for the formation of the first differentiated cell types in the embryo; angioblasts and hematopoietic stem cells from their hemangioblast progenitors, by modulating soluble signals that generate these cell types from the underlying mesoderm^{276, 277}. ‘Blood islands’ are formed during this process, which consist of 1) hematopoietic stem cells that form a loose inner mass which can later differentiate into blood cells, and 2) angioblasts, alternatively termed primitive endothelial cells, that form the outer luminal layer of blood islands and can later differentiate into endothelial cells that line the walls of blood vessels²⁷². In blood islands, angioblasts fuse to form primitive capillary-like vascular networks and plexuses^{272, 276}. Subsequently, vascular remodeling and maturation of the primitive capillary plexus occur through the recruitment of mural cells, concurrently with hematopoiesis; the induction of mature circulating blood cells from hematopoietic stem cells^{272, 276}.

The aforementioned steps for vasculogenesis occur orderly during embryonic development, and are well-regulated by factors such as vascular endothelial growth factor (VEGF) and Angiopoietin 1 (Ang-1)^{272, 275}. Mice deficient for Ang-1 or with a deletion for its receptor Tie-2, or a deletion for VEGF receptor (VEGFR2, also known as Flk-1) have been shown to experience rapid death during embryogenesis²⁷².

While vasculogenesis is essential during embryogenesis for the provision of metabolic factors to developing tissues, it has been suggested that vasculogenesis may also play an instructive role in organogenesis^{275, 278, 279}. For instance, Matsumoto *et al.* showed that angioblasts may also contribute to inducing liver morphogenesis, even prior to vascular function²⁷⁸. The authors showed that *flk-1*^{-/-} mutant mice, which are unable to form ECs nor mature blood vessels but still form angioblasts with migratory defects, display defects in liver bud development during the morphogenic phase of liver organogenesis²⁷⁸. Lammert *et al.* also showed the role of the endothelium in inducing differentiation of insulin-expressing cells that are required for pancreatic organogenesis²⁷⁹. Thus, reproducing vasculogenesis in models of organs is likely to improve not only the health but also the biomimetic

properties of tissue-engineered constructs.

5.3.1.2 Angiogenesis and vascular remodeling

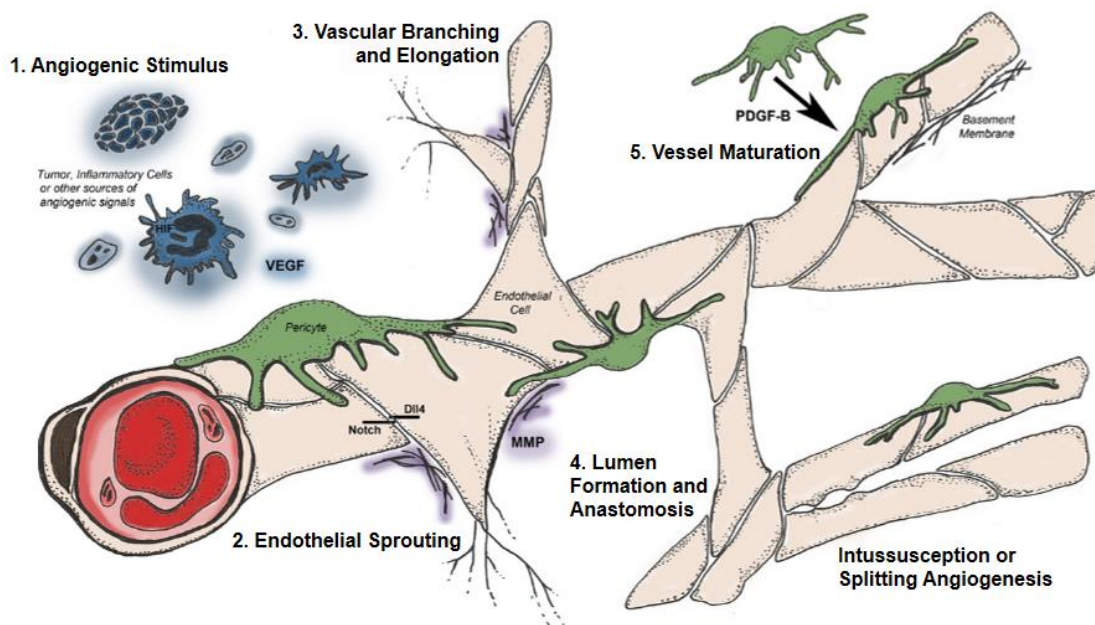


Fig. 17: Steps of angiogenesis; the formation of new blood vessels from a preexisting vessel upon angiogenic stimulus. (Logsdon et al. 2013), Ref (271). Reproduced with permission from publisher.

Angiogenesis is observed under several physiological conditions that require increased blood and oxygen supply such as embryogenesis, postnatal organ growth, wound healing, and exercise²⁷¹. Moreover, dysregulated angiogenesis is implicated in several pathologies including retinopathies, arthritis, psoriasis, primary pulmonary hypertension, and growth and metastasis of tumors²⁷¹. In contrast, other pathologies display a regression of blood vessels and could benefit from angiogenesis, such as Crohn's disease, atherosclerosis, and osteoporosis. Therefore, developing models of microvascularized tissues, and elucidating the mechanisms that underlie pro- and anti-angiogenic stimulation of tissues is valuable for biomedical research²⁷¹.

After vascular plexuses have formed through vasculogenesis, a transition to angiogenesis occurs during embryogenesis²⁷². Angiogenesis occurs after vascular maturation as well, under certain conditions during development or postnatal life²⁷². Two main mechanisms of angiogenesis have been described: sprouting and intussusceptive (splitting), illustrated in (**Fig. 17**), both of which occur in nearly all tissues^{271, 277}. Sprouting angiogenesis is the more discussed and classical form of angiogenesis as it has been discovered two centuries ago, while splitting angiogenesis has only been

described three decades ago²⁷⁷. A key difference between the two forms of angiogenesis lies in formation of ‘sprouts’ as one of key steps in sprouting angiogenesis but not splitting angiogenesis^{271, 277}. Sprouts are endothelial cells that follow a ‘tip/stalk’ morphology and usually proliferate towards angiogenic stimuli^{271, 277}. By contrast, in splitting angiogenesis, a process of interstitial tissue invasion occurs into the lumen of the existing blood vessel, causing one vessel to split into two^{271, 277}. Splitting angiogenesis is thought to be faster and more efficient than sprouting angiogenesis, as it initially only requires the reorganization of existing ECs as opposed to requiring their migration and proliferation as the case is in sprouting angiogenesis²⁷⁷.

Sprouting angiogenesis involves a series of key steps, illustrated in **(Fig. 17)**, including: angiogenic stimulus, sprouting, elongation and branching, tubulogenesis, anastomosis, and finally mural cell-driven stabilization, or regression^{271, 277}. First, an angiogenic stimulus initiates from distress signals such as hypoxia, and metabolic or mechanical stimuli, which results in secretion of pro-angiogenic factors such as VEGF and acidic fibroblast growth factor (aFGF or FGF-1)^{271, 277}.

Sprouting of ECs from the preexisting blood vessel occurs in response to the stimulus and the tissue develops gradients of pro- and anti-angiogenic signals that guide the newly formed sprouts towards a target tissue^{271, 277}. Additionally, substrate stiffness, ECM composition, and ECM fibers orientation and density have been shown to regulate other elements of sprouting such as EC migration speed and branching^{271, 280}.

Sprouting occurs concurrently with ECM degradation in order to clear a migratory path for the sprouting ECs^{271, 277}. ECM degradation is enabled by proteases such as MMPs that are secreted by ECs in response to angiogenic stimulus^{271, 277}. A ‘tip’ EC has a specific molecular signature that includes VEGFR2, VEGFR3, Delta-like ligand-4 (Dll4), neuropilin-1 (NRP1), among others²⁸¹. This molecular signature, along with long cellular structures termed ‘filopodia’ that characterize the highly polarized nature of tip cells, enable them to discern gradients of angiogenic cues, such as gradients of VEGF-A sensed by VEGFR2^{271, 277, 281}. The action of filopodia together with the contraction of actin filaments enables tip cells to pull towards the stimulus, secrete proteases, and sprout towards a specific direction^{277, 281}.

Tip cells usually do not form lumens and often possess minimal proliferative capacities²⁸¹.

Thus, lengthening of newly formed sprouts and their lumen formation is performed by proliferative ‘stalk cells’ that line up behind the tip cell and connect it to the circulation^{271, 277, 281}. During this step, Dll4/Notch signaling contributes to maintaining tip cells in the leading position while preventing the trailing stalk cells from leaving their position^{281, 282}. Computational models of elongation and branching during angiogenesis revealed that proliferation of stalk cells could determine the length of newly formed capillary, while elongation of stalk cells could determine how many branches are formed²⁷¹. Tubulogenesis, or lumen formation, occurs, as the next step of angiogenesis, when a series of stalk cells develop inter- or intracellular ‘vacuoles’ that coalesce together, which has been observed in 3D *in vitro* cultures of ECs, and a zebrafish model^{283, 284}.

In parallel with lumen formation, the sprouting capillary connects with another nearby capillary that is either sprouting as well or preexisting, in a process known as anastomosis^{271, 285}. Experimental and computational models of angiogenesis proposed mechanisms for anastomosis^{271, 282, 285}. For instance, Bentley *et al.* proposed the concept of a transient tip cell based on a spring-agent model, where the same Dll4-Notch signaling that maintains a tip cell in the leading position could revert its fate to a non-migratory stalk cell during anastomosis, upon a filopodia-driven feedback loop with VEGFR2 signaling^{271, 282}.

A third subtype of ECs aside from tip and stalk cells is ‘phalanx’ cells²⁸¹. Phalanx cells represent the most quiescent subtype of ECs and are characterized by their cobblestone morphology²⁸¹. These cells gain their quiescence during the last stage of angiogenesis once the new vessel has formed and stabilized²⁸¹. Maturation and stabilization of newly formed blood vessels as a final step of angiogenesis is achieved by the recruitment of mural cells, which mainly include pericytes and vascular smooth muscle cells (vSMCs)^{271, 286}. Pericytes associate with small vessels such as capillaries and venules, and perform critical roles in angiogenesis and long-term maintenance of vascular stability by regulating proliferation and migration of ECs, and depositing a basement membrane with ECs^{271, 286}. On the other hand, vSMCs associate with larger vessels such as arteries, and interact with ECs to strengthen the walls of maturing blood vessels in order to optimize flow, contractility, and shear stresses of the blood vessel^{271, 286}.

The primitive capillary plexus initially formed by vasculogenesis is composed of very basic

interconnected small vessels that are generally homogeneous in shape and size²⁸⁷. A process of vascular remodeling that occurs concurrently with angiogenesis is crucial for the subsequent hierarchical and functional organization of vessels into arteries and veins that ensures transport of necessary substances from and to the yolk sac and embryo during development²⁸⁷. Vascular remodeling is a dynamic morphogenic process by which blood vessels undergo changes in size and resistance by expanding, extending, and ‘pruning’; a process where unnecessary branches are eliminated^{271, 287}. Vascular remodeling is different from angiogenesis in that it does not involve the formation of new vessels, only the structural alteration of existing ones²⁸⁸. Regulated by molecular and biomechanical cues, vascular remodeling is critical for viability of the embryo and cardiovascular health in development and postnatal life^{287, 289}.

5.3.1.3 Examples of biomechanical and biochemical signaling in vascularization

Biomechanical forces play crucial roles during development and postnatal life. Regarding the vascular system, of relevance are hemodynamic forces that come into play when the heart beats and initiates fetal circulation at day 22-post fertilization for humans, and day E8.25 for mice^{287, 290}. Vascular remodeling occurs soon after circulation, around E8.5 and E9.5 in mice, which is thought to be modulated partly by blood flow²⁸⁷. Arterial-venous specification during vascular remodeling is genetically predetermined by vascular identity markers and is additionally modulated by hemodynamic forces²⁹¹. While vasculogenesis is thought to occur in mice without the need for hemodynamic forces, biomechanical forces have been found to promote hematopoiesis, and regulate vascular wall maintenance and endothelial function^{276, 287, 292}. The exact role of hemodynamic forces in angiogenesis on the other hand is more complicated^{271, 289}. Three types of hemodynamic forces are often relevant for alterations in size and morphology of the vasculature including shear stress, circumferential stress, and axial stress^{287, 289}. The effects of these hemodynamic forces on progression of various pathologies²⁸⁹, and on embryonic development²⁸⁷ are reviewed in detail by others.

Shear stress is the primary hemodynamic driving force for vascular remodeling^{287, 289}. Shear stress; the frictional force exerted by blood flowing in parallel to the vessel wall, is the product of multiplying the apparent viscosity of blood by the shear rate^{287, 289}. The shear rate is a function of the velocity gradient of blood flowing at the vessel wall and the radius of the vessel^{287, 289}. Understandably,

changes in blood viscosity and cardiac output, or abnormalities in cardiovascular development or hematopoiesis significantly influence shear rate^{287, 289}. Since ECs lining vessel walls are sensitive to mechanotransduction, their function and ability to engage in various steps of vascular remodeling is greatly influenced by changes in shear rate^{287, 289}. Mechanotransduction in ECs is possible through activation of mechanosensor proteins, signaling pathways, and expression of genes and proteins in response to mechanical stimuli^{287, 289, 293}.

For instance, evidence of a direct mechanical role of shear stress in vascular remodeling became available from *in vivo* experiments where primitive erythroblasts were sequestered to blood islands prior to initiation of blood flow, which resulted in reduced blood viscosity and reduced shear stress in wild type mice embryos^{287, 294}. This led to impaired vascular remodeling of the capillary plexus in the yolk sac and significant reduction in expression of endothelial nitric oxide synthase (eNOS); a mechanosensitive protein responsible for the production of nitric oxide and modulating vascular homeostasis and remodeling^{287, 294, 295}. Additionally, matured blood vessels can adapt to changes in shear stress throughout life and beyond the embryonic stage²⁸⁹. Thus, the role of hemodynamic forces in vascular remodeling is crucial beyond embryonic development²⁸⁹.

In terms of *in vivo* angiogenesis, the role of blood flow has been initially investigated several decades ago in models of chick embryo and frog larvae, where these studies demonstrated that blood velocity regulated capillary growth and regression^{271, 296}. Subsequently, the first theoretical model of blood flow was developed, relating tissue oxygenation with blood flow and capillary distribution and number²⁹⁷. Theoretical models supported by experimental data that came after became more sophisticated as they took into account the role of microvascular heterogeneities in influencing metabolic and hemodynamic signaling in angiogenesis and vascular remodeling^{271, 298}. Overall, widely cited research by Pries *et al.* led to consensus in recent years that local pro-angiogenic gradients mainly induce sprouting angiogenesis and blood flow induces vascular remodeling of the networks formed, whereas, splitting angiogenesis is thought to occur through both metabolic and hemodynamic signaling^{271, 298, 299}. An *in vivo* model of skeletal muscle contraction also suggested that high luminal shear stress induces splitting angiogenesis via an increase in eNOS expression and VEGF content, while longitudinal stretch, which was associated with increased VEGF staining, induces external

sprouting angiogenesis in skeletal muscles³⁰⁰. The aforementioned paradigm does not exclude the role of other types of hemodynamic forces (e.g. transmural flow) in inducing sprouting angiogenesis *in vivo*. However, studying such forces while excluding luminal shear stress is challenging to replicate in an *in vivo* setting with proper control.

In vitro experiments have shed further light on the effect of hemodynamic forces on sprouting angiogenesis, albeit the results are somewhat complicated³⁰¹⁻³⁰³. For instance, *in vitro* application of luminal shear stress has been shown to inhibit VEGF-induced angiogenic sprouting, whereas shear stress generated by transmural flow, which is directed in the direction exiting the blood vessel, has been widely accepted as a pro-angiogenic stimulus^{301, 302}. Subsequent research by Galie *et al.* attributed this difference in angiogenic sprouting between the two types of shear stress to low luminal shear stress being tested (3 dyn/cm²) and high transmural shear stress being tested in literature³⁰¹. Galie *et al.* demonstrated that shear stresses from luminal flow and transmural flow can both induce angiogenic sprouting *in vitro* when around or above a certain newly identified threshold (10 dyn/cm²), depending on environmental context³⁰¹. The authors also noted that since *in vitro* culture includes a high level of serum containing pro-angiogenic factors that *in vivo* plasma is deprived of, the true range required for inducing sprouting *in vivo* could be higher than previously appreciated due to angiogenic inhibitory factors available *in vivo*³⁰¹.

Nonetheless, some controversy remains with respect to application of shear stress *in vitro*. For instance, Colgan *et al.* demonstrated that upon application of relatively high shear stress (10-14 dyn/cm²), endothelial permeability was decreased³⁰⁴, which is typically associated with quiescent stable vessel phenotype^{305, 306}. Additionally, microfluidic studies have demonstrated *in vitro* vascular sprouting and subsequent network formation in 3D tissue models without incorporating or accounting for shear stress, which suggests that shear stress is not a requirement for initiation of sprouting angiogenesis^{25, 27, 260, 271}. In some of these studies, perfusion was applied only after angiogenesis and vascular network formation, and was found to increase eNOS production, which was used to confirm mechanotransduction and functional properties of ECs in these models^{27, 260}.

These various stimulatory and inhibitory roles of hemodynamic forces on sprouting angiogenesis seem to point to the importance of the context in which angiogenesis occurs. For

example, hypoxia-induced sprouting angiogenesis occurs in the absence blood flow in the rising capillary sprout³⁰⁷, and may not benefit from increased blood flow that may wash away hypoxia-induced biochemical factors required for angiogenic sprouting²⁷¹. This may be seen in clinical phenomena where interstitial tumor pressure blocks blood flow, thus increasing hypoxia, which initiates production of tumor-associated factors, angiogenesis, and tumor growth²⁷¹.

Hypoxia represents a key player in embryonic and postnatal vascularization through inducing biochemical responses such as increased expression of nitric oxide, hypoxia-inducible factors (HIFs) activation, among other pathways^{271, 308}. During vascular development, hypoxia is required for the differentiation of important progenitor cell types including the hemangioblasts that gives rise to cells involved in vasculogenesis, which occurs via expression of a group of genes upon ARNT (HIF β subunit) dimerization with HIF α subunit under hypoxic conditions^{308, 309}. On the other hand, *in vitro* hyperoxia; abnormally high oxygen, was shown to inhibit differentiation of angioblasts into ECs, which is required during formation of vascular plexuses³¹⁰. Additionally, early stages of vascular development are coordinated by HIF β , which modulates paracrine production of growth factors such as VEGF and Ang-1 by hematopoietic cells³⁰⁸.

Furthermore, HIFs are critical transcriptional regulators of several aspects of developmental, physiological, and pathological angiogenesis^{308, 311}. For instance, as a master pro-angiogenic factor; VEGF is a direct transcriptional target for HIF1 α and HIF2 α ³¹¹. Additionally, HIF1 α and HIF2 α are both involved in inducing expression of several pro-angiogenic genes, which are also used as biomarkers for tumor hypoxia in addition to *veg*f, such as *Ang-1*, *Ang-2*, and *Tie-2*³¹¹.

Overall, the role of HIF1 α is more centered towards stimulating EC sprouting, proliferation, and migration, recruitment of key other cell types involved in angiogenesis, and arterial-venous specification^{308, 311}. For instance, HIF1 α is a regulator of Hey2 and Dll4, which both inhibit venous specification thus promoting an arterial fate³¹¹. Additionally, HIF1 α stimulates recruitment of CD45⁺ myeloid cells, which possess pro-angiogenic capacities due to expressing CXCR4; a receptor for SDF-1 that plays a neovascularization role in ischemic tissues or tumors³⁰⁸. Recruitment of vSMCs that stabilize blood vessels is also suggested to be linked to an increase in HIF1 α expression³¹².

The role of HIF2 α on the other hand remains somewhat elusive and varies with animal genetic

background. Nonetheless, literature suggests that the role of HIF2 α is not redundant with HIF1 α , and appears centered towards morphogenesis, vascular remodeling, and vascular integrity³⁰⁸. For instance, in one murine strain, loss of HIF2 α causes defects in remodeling of vessels into larger ones, while in other murine backgrounds; its loss causes abnormal organogenesis without clear vascular defects³⁰⁸. Another study supporting the role of HIF2 α in vascular remodeling cite that HIF2 α but not HIF1 α , induce eNOS expression³⁰⁸. Another study suggests HIF2 α plays a role in controlling vascular integrity by increasing junction protein VE-Cadherin expression³⁰⁸.

Other biochemical and microenvironmental factors such as ECM composition and inflammation strongly influence various steps of vascularization and have been reviewed by others^{257, 271}. Overall, the aforementioned examples demonstrate the multi-faceted nature of the steps and signaling pathways involved in vascularization of tissues, which ideally must be considered while developing microvascularization tissue-engineering solutions.

5.3.2 Microvascular tissue engineering considerations

The main considerations in MTVE are: 1) cell sources, 2) appropriate biomaterials for the desired application, 3) biochemical and mechanical cues required for simulation, maintenance, and maturation of the engineered vascular structure, and 4) the technique vascular formation²⁵⁷.

5.3.2.1 Endothelial cell types

A key aspect of MVTE is the choice of cell source. EC sources can be divided into two types: 1) somatic cells; terminally differentiated ECs, and 2) stem cells and progenitor cells; pluripotent and multipotent cells, respectively, which can be differentiated into ECs under defined conditions^{254, 262, 313}.

Somatic ECs used in MVTE include HUVECs, and human microvascular ECs (HMVECs)^{257, 313}. HMVECs can be further classified based on the source tissue such dermal and lung microvascular ECs²⁵⁷, and human brain microvascular ECs¹²³. Stem cell and progenitor cell sources of ECs include ESC-derived ECs, iPSC-derived ECs (iPSC-ECs), mesenchymal stem cell-derived ECs, and EPCs^{254, 257, 313}. Among these, HUVECs, HMVECs, and iPSC-ECs are commonly used in MVTE^{257, 313}, and thus will be the focus of this review. Although, EPCs; reviewed by others^{257, 313}, must be considered as a source for neovascularization in MVTE applications due to evidence of circulating EPCs that

induce vasculogenesis during postnatal life^{273, 313}, and the ability of EPCs to induce vascularization *in vitro* and *in vivo*^{257, 313}.

There are differences between EC types based on surface markers and RNA profile³¹³, although they do often share angiogenic behavior and certain identity markers such as CD31 and vWF for HUVECs and HMVECs, and CD31 and CD34 for iPSC-ECs, among other important markers that overlap among these EC types such as growth factor receptors³¹³. Heterogeneity between EC types exists due to variable tissue sources, batch-to-batch variability, and chemical and mechanical differences in the bodily environment of different donors or culture protocol^{257, 313-315}. This could be controlled for by using one pooled sample for the entirety of the experiment, however, that is limited by availability of cells and could pose challenges on reproducibility of results across labs²⁵⁷. HUVECs and HMVECs are easily obtained from commercial sources^{257, 313}. However, the count of cells from the same vial could limit the expansion rate, which requires a certain initial seeding density³¹⁶.

On the other hand, iPSC-ECs are quasi-unlimited cells that can be differentiated to specific vascular subtypes from human patient samples^{254, 313}, but possess higher heterogeneity than HUVECs based on genetic and phenotypic studies of the two³¹⁵. A certain level of heterogeneity between iPSC-ECs should be expected and can be favorable^{314, 315}, because it could account for single-cell differences, EC subtypes, and patient-unique differences^{313, 315}. However, a high level of genetic and phenotypic heterogeneity could pose challenges for modeling small genetic variant effects³¹⁷, and could represent a manifestation of technical issues caused by the differentiation protocol itself and the pluripotent source of ECs rather than biological differences between cells and individuals³¹⁵.

Nonetheless, a powerful attraction of using iPSC-ECs in MVTE that HUVECs and HMVECs do not offer is the ability to derive them from human patient samples^{254, 313}. This allows generating ECs with the same genetic background as patients, which is advantageous for modeling vascular pathologies with a genetic component without the need for gene editing³¹⁸, and provides potential for testing therapeutics through a precision medicine approach³¹³.

Furthermore, patient-derived iPSC-ECs are considered an autologous cell source, which could eliminate concerns of immunogenicity if the iPSC-ECs are transplanted *in vivo*^{254, 262, 313}. While transplantation of ECs into a host falls more often under applications of therapeutic vascularization

and TEVG^{254, 257}, which we are not covering, a few MTVE approaches also utilized *in vivo* transplantation as a method to vascularize pre-engineered tissue constructs and subsequently extract the tissue for further analysis^{6, 102}. Another concern distinct to stem cell-derived ECs transplanted *in vivo* is tumorigenicity but that might not arise in short-term animal studies²⁵⁴.

HUVECs and HMVECs are more cost-effective to purchase and maintain, and their protocols are easier to handle than iPSC-ECs in terms of the length of the process³¹³. This could pose a challenge for the use of iPSC-ECs in engineering labs, given that MTVE requires multidisciplinary expertise. Additionally, HUVECs have been used in research for a longer period than iPSC-ECs, thus it is not surprising that HUVECs have been characterized more extensively and are the most commonly used EC source of all types²⁵⁷.

The use of other supporting cell types such as vSMCs, pericytes, and fibroblasts in co-culture with ECs for MTVE application is advantageous and recommended²⁵⁷. The choice of supporting cell types depends on each application, and has been suggested to improve modeling accuracy of the ECM and cell-cell interactions of the vascular niche²⁵⁷. Furthermore, supporting cell types are thought to improve vascularization through secretion of pro-angiogenic factors²⁶⁰, and enhance maturation of vascular networks^{257, 260}.

5.3.2.2 Signaling molecules

VEGF is commonly used in MTVE to induce sprouting given its well-known pro-angiogenic effects³¹⁹. In addition to VEGF, other growth factors have been commonly used in MTVE as are part of the secretome of tissues that induce angiogenesis³¹⁹. Growth media that involves the addition of factors based on the secretome of a tissue of interest is referred to as conditioned media. The use of conditioned media (CM) in MTVE has been applied using fibroblast-CM. In fact, fibroblasts are often co-cultured with ECs in MTVE applications to induce sprouting and lumen formation²⁵⁶, and were found to induce higher level of sprouting than when only fibroblast-CM is used³¹⁹.

Newman *et al.*, using a fibrin bead assay, investigated the role of fibroblast-secreted molecules in angiogenic signaling in 3D co-culture with ECs, and identified pro-angiogenic factors in fibroblast-CM³¹⁹. They were able to also distinguish a combination of factors involved in EC sprouting from those involved in lumen formation. Those factors included Ang-1, angiogenin, hepatocyte growth

factor, transforming growth factor- α , and tumor necrosis factor. The authors also identified fibroblast-derived matrix proteins that regulate matrix stiffness that is involved in formation of sprouts and lumens. Overall, the addition of stromal cells such as fibroblasts and pericytes and identifying secreted molecules that contribute to vascularization is a key aspect of MTVE applications.

5.3.2.3 Hydrogel composition and biomechanical cues

Another key aspect of MVTE is the choice of hydrogel. Two commonly used hydrogels for MTVE are collagen and fibrin, which have been repeatedly found to support microvascular network formation^{256, 261}. Mechanical properties of these hydrogels such as stiffness, permeability, fiber diameter, and degradation rate represent important parameters that have been found to regulate formation of vascular networks²⁶¹. For instance, stiffer hydrogels were found to generate smaller vessel lumens, and display reduced vascular invasion from sprouting ECs into their matrix than softer hydrogels²⁶¹. Moreover, the mechanical properties of collagen can be tailored by adjusting the temperature and pH, while the mechanical properties of fibrin can be modified by controlling fibrinogen and thrombin concentration²⁶¹.

Examples of biomechanical cues that affect the vasculature have been provided in previous sections, and have been applied in MTVE to study vascular parameters such as vessel alignment, branching and sprouting directionality^{256, 261}. This demonstrates a capacity within MTVE to tailor vessels for a desired application, based on accumulated knowledge of parameters that affect them.

5.3.3 Brain organoid vascularization

5.3.3.1 Brain vascularization

Early in human embryonic development from gestational week (GW) 2 to 4, oxygen and nutrients are supplied to neural tissues via diffusion from the amniotic fluid, as illustrated in **(Fig. 18)**^{213, 320}. From GW 4 to 5, upon time for its closure; the neural tube becomes surrounded on its surface by a dense mesenchymal tissue called the meninx primitiva, which contains primitive vascular loops (meningeal meshwork) that form via vasculogenesis and are connected to the primitive dorsal aorta and cardinal veins^{213, 320}. The meningeal meshwork begins to provide oxygen and nutrients to the neural tissue via diffusion^{213, 320}.

Subsequently, the brain continues to grow and forms the three main brain vesicles:

prosencephalic, mesencephalic, and rhombencephalic vesicles; the developmental regions that represent the forebrain, midbrain, and hindbrain, respectively³²⁰. In parallel to formation of these regions, the meninx primitiva expands into the roofs of the prosencephalic and rhombencephalic vesicles in order to improve supply of oxygen and nutrients to these regions³²⁰. This step occurs around GW 5 to 7, and leads to the initial formation of the choroid plexuses³²⁰. Differentiation of the choroid plexuses is important for the brain's vascular morphogenesis because it establishes a vascular pattern within the meningeal meshwork that will later evolve into all brain arteries³²⁰. To contextualize the increased need for vascularization at this stage in terms of size, it is noted that around GW 7, the diencephalon part of the forebrain reaches around 2.85mm in diameter²¹³. Additional cerebral

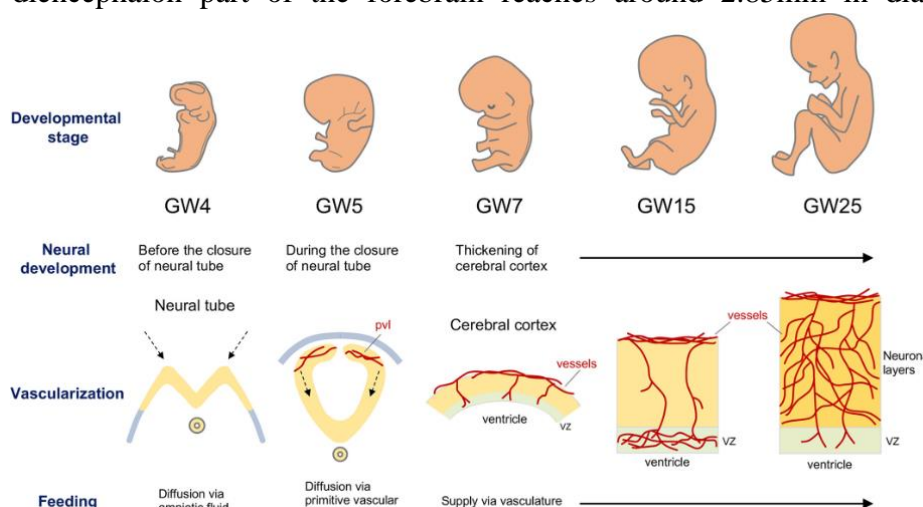


Fig. 18: Brain vascularization during *in vivo* fetal development. The neural tissue is initially supplied with oxygen and nutrients via diffusion of the amniotic fluid. Upon closure of the neural tube around GW 5, primitive vascular loops develop and feed the neural tissue via diffusion as well. Around GW 7 and beyond, the vasculature invades further layers and supplies the brain with oxygen and nutrients from fetal circulation (Matsui *et al.* 2021), Ref (213). Reprinted with permission from publisher.

measurements have been reported by others at different GWs³²¹.

GW 7 is thought to be the approximate time point of human embryonic CNS development at which the vascularization process shifts from vasculogenesis to angiogenesis²¹³. Angiogenesis in the CNS at that point occurs through sprouting of ECs from the surface capillary layer of the meningeal vascular meshwork, in response to increased cerebral size and hypoxia as diffusive transport of nutrients from the surface plexus formed via vasculogenesis becomes no longer sufficient^{213, 320}, as illustrated in (Fig. 18). After GW 12, the subventricular (SV) plexus subsequently forms²¹³. From GW 15 to 25, vascularization shifts to further neuronal layers²¹³. After GW 25, vascularization in the cortical neuronal layers increases²¹³.

The aforementioned developmental vascularization process occurs in parallel with CNS development^{213, 320}. The regional shift of vascularization through brain layers is thought to be a result

of increased metabolic demands by expanding and differentiating neural tissue, which has been modeled by Raybaud *et al.* in a segmentation model of brain developmental region^{213, 320}.

The role of vascular and neuronal interactions during CNS development and postnatal life has been increasingly appreciated since the establishment of the concept of the neurovascular unit (NVU) in 2001, at the Stroke Progress Review Group meeting of the National Institute of Neurological Disorders and Stroke²³. The concept of the NVU describes the relationship between cells comprising cerebral blood vessels and brain cells as interdependent, and suggests that neurovascular interactions influence developmental, functional, and structural properties of the brain²³. Structurally, cells comprising the NVU are diverse across the hierarchy of CNS vasculature²³. Briefly, cerebral arterioles are coupled with vSMCs that cover an EC-lined lumen, while the penetrating cerebral capillaries are associated with pericytes that cover a lumen of ECs, and both cerebral arterioles and capillaries are covered around their outside circumference with endfeet of astrocytes²³. Functionally, the NVU contributes to formation of the BBB and its maintenance, among other roles in immune surveillance and signal transduction²³.

The concept of the NVU is sustained for brain development as well, although much of this evidence has come from animal experiments²³. Proliferation, migration, differentiation of neural progenitors and vascular cells appear closely related to that of each other, and their reciprocity occurs during development and continues in postnatal life²³. For instance, early in mouse brain development, VEGF-A secreted by neural progenitors in the SV zone acts as a chemoattractant that guides migrating blood vessels from vascular plexuses that surround the brain²³. In reciprocity, ECs in the SV zone and hippocampal subgranular zone provide cues for the postnatal brain neurogenesis²³. Furthermore, BDNF secreted by cerebral ECs, in combination with VEGF signaling by astrocytes, allow the vasculature to act as a scaffold that guides neuronal progenitor migration²³. Similarly, migration of oligodendrocytes precursors responds to guidance cues from blood vessels, and in turn, oligodendrocytes precursors contribute to white matter postnatal vascularization²³. BDNF has also been implicated in neuronal growth and more recent studies demonstrated the role of BDNF in inducing secretion and nuclear translocation of angiogenin; a strong mediator of angiogenesis, in ECs³²².

In addition to VEGF and BDNF in the aforementioned examples, an appreciable commonality exists in signaling molecules that affect both the vascular and neural cellular processes, and such molecules have been termed ‘angioneurins’^{323, 324}. For instance, the angiogenic factor FGF-2, and vessel-derived factors such as Endothelin-3, Artemin, and its receptor GFRalpha3 have also been shown to be involved in neuronal development³²⁴.

Additionally, a few molecules have been identified as specific regulators of CNS angiogenesis, which include Wnt7a/b-Frizzled6, DR6/TROY, and GPR124³²⁴. The presence of such CNS-specific vascularization molecules is not surprising given the specialized vasculature of the CNS. The aforementioned molecules are also involved in differentiation and formation of the BBB, which is necessary for neuronal homeostasis, and demonstrate examples of CNS-derived instructive cues that have been previously predicted³²⁴.

Furthermore, molecular cues involved in guidance of axonal growth cones belonging to families of Netrins, Semaphorins, Ephrins, Slits, and their receptors, have been later found to exert repulsive or attractive guidance cues on endothelial tip cells as well, thus possessing the capacity to steer the direction of both growing axons and blood vessels in similar functional and structural manners³²⁴. These molecules are not expressed exclusively in the CNS and can exert either the same or opposite guidance cue on axons and vessels³²⁴. However, understanding their possible role in co-patterning of axons and vessels could be beneficial for tissue engineering, and developing therapeutics targeting vascular defects that precede several neurodegenerative diseases^{323, 324}.

5.3.3.2 Recent methods for brain organoid vascularization

Vascularization is essential for brain development, oxygen and nutrient supply, waste removal, and plays an instructive role for the differentiation and maintenance of neuronal populations^{23, 213}. Vascularization of brain organoid is a pressing challenge for improving their modeling capabilities beyond early developmental stages. Recently, several research groups attempted brain organoid vascularization, and their reports include an *in vivo* method¹⁰², entirely *in vitro* methods^{24, 325}, and reports that tested both *in vitro* and *in vivo* approaches along with combining steps from both^{3, 5, 6}. Methods and findings from the main reports of brain organoid vascularization thus far are summarized in (Table 4).

In 2018, Mansour *et al.* generated human cerebral organoids and attempted to vascularize them and improve their maturity by transplanting them into the retrosplenial cortex of immunodeficient mice, as shown in (**Fig. 19**)¹⁰². This was the first attempt at transplanting human brain organoids into a rodent brain. The host mouse vasculature was able to invade the transplanted cerebral organoid within two weeks¹⁰². The organoids were maintained up to 233 days and 85.4% of the grafted ones were vascularized¹⁰². The authors used two-photon imaging to demonstrate *in vivo* functional perfusion of the grafted vascularized organoids as early as 30 days post implantation (dpi) and later at 120 dpi¹⁰².

Additionally, initial cell death in the grafted organoids shown at 5 dpi was rescued after grafting, with grafted organoids in subsequent time points showing almost no cell death compared to significantly high cell death in non-grafted traditionally cultured organoids¹⁰². The authors also reported increased number of mature neurons in vascularized organoids compared to non-vascularized ones, as inferred from NeuN staining¹⁰². Furthermore, the authors reported invasion of mouse microglia from the host into the organoid, and expression of human GFAP+ cells within the grafted organoid, which indicates possible gliogenesis¹⁰².

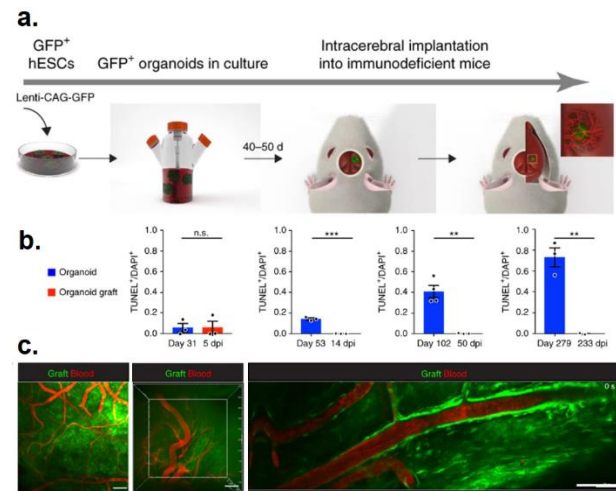


Fig. 19: Human cerebral organoids implanted in mice brains (**a**), become vascularized (**c**), and experience low to no cell death compared to non-grafted control (**b**) (Mansour *et al.* 2018). Ref (102). Reprinted with permission from publisher.

Table 4: Brain organoid vascularization publications

	Publication	<i>in vivo</i> model/ implant site	EC type used	Organoid (day of culture or implant)	Perfusion	Vessel characteristics
<i>in vivo</i>	Mansour <i>et al.</i> , 2018 Ref (102)	NOD-SCID mouse/ brain (retrosplenial cortex)	(n/a)	Cerebral organoids, implanted 40-50 days post <i>in vitro</i> culture	Functional perfusion by host mouse	mCD31+, mEndoglin+ sparse signal but good blood flow and vessel structure Neuronal activity present
	Pham <i>et al.</i> , 2018 Ref (6)	NSG mouse/ brain	iPSC-EC embedded in Matrigel surrounding the organoid	Cerebral organoids, embedded with iPSC-EC at day 34 for <i>in vitro</i> vascularization Cerebral organoids embedded with iPSC-ECs, were implanted <i>in vivo</i> at day 54	(n/a)	hCD31 + signal but most dense in outer organoid layers Vessels appear somewhat discontinuous
<i>in vivo and in vitro</i>	Cakir <i>et al.</i> , 2019 Ref (3)	Rag2 ^{-/-} GammaC ^{-/-} mouse/ hind limb	ETV2-expressing hESCs induced into ECs via DOX 20% ETV2-hESCs mixed with non- modified hESCs prior to aggregation	Cortical organoids ECs within organoids were induced at day 18 <i>in vivo</i> implantation done using organoids at day 40-50	<i>in vitro</i> : partial perfusion of dye (outer portion of organoid) <i>in vivo</i> : functional perfusion by host mouse	hCD31 (+ signal, but discontinuous, or in outer layers of organoid only) α -ZO1 and CDH5 (+ signal but in sparse spots) Increased gene expression of vessel morphogenesis and EC proliferation in vascularized cortical organoids Neuronal activity present (minimal)
	Shi <i>et al.</i> , 2020 Ref (5)	NOD-SCID mouse/ brain (S1-cortex)	HUVECs mixed with iPSC prior to organoid aggregation	<i>in vitro</i> vascular-cortical organoids kept at 42, 65, 200 days Implanted <i>in vivo</i> after 60 days in culture	<i>in vitro</i> (n/a) <i>in vivo</i> : functional perfusion by host mouse	Detected both human and mouse ECs by HUN+/- staining CD31 (+ signal but minimal characterization) Laminin, IB4 (+ signal) P-gp (+ signal later in culture, co- localized with IB4) Increased vessel morphogenesis gene expression in vascularized organoids Neuronal activity present
<i>in vitro only</i>	Wörsdörfer <i>et al.</i> , 2020 Ref (325)	(n/a)	iPSC-MPC organoid fused with iPSC-neural aggregates	Neural-mesodermal organoid assembled after 8 days in culture, maintained for 20-28 more days	(n/a)	CD31 (+ signal) Col-IV (+ signal) SMA (+ signal, minimal) CD31 co-localized with Col IV No apparent penetration of CD31+ cells into TUJ1+/MAP2+ neural organoid Good penetration of CD31+ cells into GFP neural organoid
	Ahn <i>et al.</i> , 2021 Ref (24)	(n/a)	Clumps dissociated from iPSC-derived blood vessel organoids at day 15, co-cultured with cerebral organoids	Cerebral organoids Co-culture starts at cerebral organoid day 5, then vascular-cerebral organoid is maintained up to day 50	Partial retention of dextran (upon incubation) in vascularized organoids vs. no retention in control	CD31 (+ signal) SMA (+ signal) PDGFR β (+ signal) Col-IV (+ signal) CD144 (+ signal) EGFP vascularized cerebral organoids tested CD31+, expressed BBB markers

The authors proposed based on this work that the *in vivo* physiological environment of the animal brain could allow human disease modeling under physiological conditions¹⁰². However, while the aforementioned findings support the role of vascularization in improving some aspects of brain

organoid models such as reducing cell death and improving maturation, several concerns arise from this approach. The use of an immunodeficient mouse model eliminates the role of peripheral immune system interactions with the brain or in response to potential drug testing studies, thus reducing physiological relevance of such model for immune-mediated brain disorders³²⁶. Additionally, the mouse origin of the vasculature and microglia invading the organoid compromise human and clinical relevance of this model by negating the initial purpose of using brain organoids derived from human samples for disease modeling¹. This becomes critical when taking into account the instructive role of neurovascular interactions in influencing developmental, functional, and structural properties of the brain²³, the role of the vasculature in neurodegenerative diseases³²³, and the unique characteristics of the human CNS that pose challenges for development of CNS therapeutics using results inferred from animal studies¹. An *in vivo* approach for inducing vascularization does not capitalize on other advantages of human brain organoid models as well, such as tissue accessibility, reduced cost, and higher throughput in comparison to animal models^{1, 14}.

Pham *et al.* developed a method for cerebral organoid vascularization, where after 34 days in culture, the cerebral organoids were embedded in a Matrigel coating that was premixed with hiPSC-ECs that were derived from the same patient samples used to generate the organoid⁶. The *in vitro* EC-coated organoids were transplanted into immunodeficient mice at day 54 of culture⁶. The coating resulted in vascularization of the organoids after 3 to 5 weeks *in vitro* and after 2 weeks *in vivo*⁶. The ECs in the coated organoid at day 54 prior to transplantation appeared to have already penetrated the outer layers of the organoid but it was not clear if a vessel-like morphology had formed throughout all the regions, although the ECs were positive for human CD31 vascular marker⁶. On the other hand, the ECs in the transplanted organoids displayed more tubular vascular structures within the cerebral organoid than the earlier *in vitro* time point, and were positive for human CD31, as shown in (Fig. 20)⁶. Penetration of ECs *in*

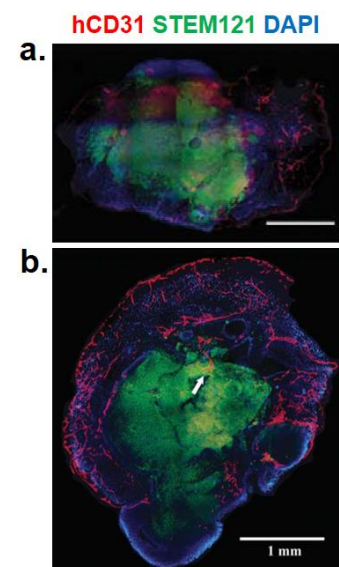


Fig. 20: Human cerebral organoids embedded in a mix of Matrigel and hiPSC-ECs. (a) *in vitro* vascularized at day 54 (20 days post embedding). (b) 2 weeks after transplantation of 54-day old organoid in immunodeficient mice (Pham *et al.* 2018), Ref (6). Reproduced with permission from publisher.

in vitro in absence of any perfusion suggests a possible mechanism for *in vitro* vascularization of brain organoids. The authors could not verify presence of mouse blood within the *in vivo* organoids, therefore, functionality of the formed vessels remains to be investigated⁶.

Cakir *et al.* devised a gene-editing method for vascularizing cortical organoids by first developing a hESC line that expressed *ETV2*; a gene that directly reprograms hESCs into ECs, which was engineered to be induced by addition of doxycycline³. Subsequently, the *ETV2*-expressing hESCs were mixed with non-modified hESCs before differentiating the aggregated mix into a cortical organoid³. Forced expression of *ETV2* in cortical organoids using this method led to formation of hCD31+ vascular-like structures within the vhCOs as early as day 30 of the protocol³.

Additionally, the authors demonstrated reduced cell death in the vascularized human cortical organoids (vhCO) compared to control human cortical organoids (hCO), which is interesting given that both organoids were maintained in the same format of spinning culture and the vascular structures were not perfused

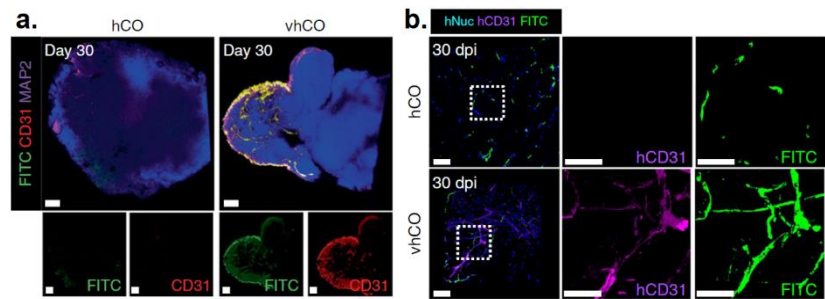


Fig. 21: Vascularized human cortical organoids (vhCO) compared to control (hCO). (a) *in vitro* expression of CD31 and FITC perfusion. (b) *in vivo* grafted vascularized cortical organoids express hCD31 shown perfused with FITC (Cakir *et al.* 2019), Ref (3). Reprinted with permission from publisher

continuously during live long-term culture³. This finding could suggest that vascular lumen formation may decrease cell density of vhCOs, thus enhancing diffusive properties of growth media into the organoid and enhancing survival even in absence of perfusion³. Alternatively, cell death may have been reduced due to enhanced retention of media that penetrates the vascular lumen via the spinning action, which would allow oxygen and small nutrients to diffuse from the vessel lumen into the vhCO in absence of flow³, which would resemble early stages of fetal brain vascularization *in vivo*, where feeding occurs via diffusion from the primitive vascular loops²¹³. The authors also demonstrated perfusability of the vhCOs *in vitro* and *in vivo* in short-term experiments, which supports lumen formation and suggests functionality of the vessel-like structures, as shown in (Fig. 21)³. Furthermore, the authors reported several BBB properties for the vhCOs such as increased expression of tight junction markers such as α -ZO1 and occludin, and trans-endothelial resistance³.

Interestingly, the authors also compared single-cell transcriptomic profiles of vhCOs and hCOs with those of developing human brain samples to determine maturity level of the organoids³. The authors found that neurons from vhCOs resembled neurons corresponding to GW 16 to 19 in the *in vivo* samples, while control hCO-derived neurons resembled ones from earlier time points of GW 10 to 12. Thus, the findings suggest that vascularization accelerates neuronal maturation in brain organoids, potentially increasing their fidelity as brain models³.

Shi *et al.* attempted a similar approach as Cakir *et al.* for vascularizing cortical organoids, with the exception of using HUVECs in a mix with iPSCs prior to aggregation instead of using hESC-derived ECs⁵. The results similarly showed reduced cell death, increased neurogenesis, and vessel morphogenesis, as characterized by differentially expressed genes and immunofluorescent staining⁵. Immunofluorescent staining of the vascularized cortical organoids did not clearly demonstrate a vascular-like structure for some of the samples, despite positive expression of vascular markers, as shown in (Fig. 22d)⁵.

Additionally, the use of laminin; the main component of the basement membrane of vessels, and IB4; an EC marker, for identifying ECs may not be highly specific since those two markers could be expressed by other cell types as well, including certain types of neurons^{327, 328}. Nonetheless, co-localization of

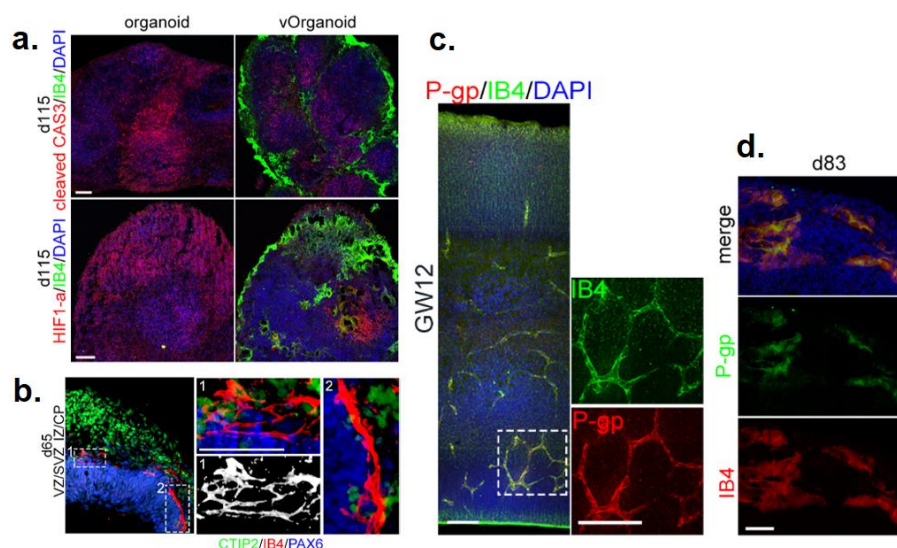


Fig. 22: Vascularized of human cortical organoids by mixing HUVECs with iPSCs prior to aggregation. (a) vascularized organoids (vOrganoids) express IB4 vascular marker (green) and show reduced cell death and hypoxia compared to control at day 115. (b) vOrganoids formed vascular-like structures that extended in CTIP2+/Newborn neurons at day 65. (c) Comparison of vascular structures and markers in vOrganoids at day 83, compared to fetal human brain sample at GW 12 (Shi *et al.* copyright 2020), Ref (5). Reproduced with permission from publisher.

IB4 and P-gp at day 83 strengthens analysis of the organoid vasculature, although when compared to co-localization of the two proteins in fetal brain tissue samples at GW12, as shown in (Fig. 22c, 22d)⁵.

One drawback of the ‘mixing-prior-to-aggregation’ approach is its inherent inability to control EC patterning within the organoids by simple mixing, as vascular networks may cluster on one

region of the organoid unpredictably, as seen in (**Fig. 21a and Fig. 22**). The implications of this drawback present a set of challenges. For instance, attempting to perfuse the organoids at a desired time point, in a high throughput format, as organoids grow larger may be challenging if vascular networks did not consistently cluster in a manner that allows for a vessel to be connected to the outer surface of the organoid where a perfusion inlet can be introduced. The possibility for straightforward perfusion is necessary when considering the role of mechanical stimulation in maturation and remodeling of the vasculature, and the potential use of vascularized brain organoids for drug testing. Additionally, neuronal maturation could include organoid-to-organoid spatially variability as a consequence of variable EC patterning. Inherent batch-to-batch variability of ESC-derived ECs added to the variability of vascularized organoids may exacerbate reproducibility issues and would benefit from further investigation.

Another approach to vascularize brain organoids, proposed by Wörsdörfer *et al.*, involves generating iPSC-derived neural aggregates and assembling them with aggregates of iPSC-derived mesodermal progenitor cells (iPSC-MPC); which can differentiate into all cell types of the vessel wall³²⁵. The assembly method involves transferring the iPSC-MPC organoid into a well containing a neural organoid, in a 96-well plate³²⁵. The co-culture leads to the two organoids fusing, and the assembled neuro-mesenchymal organoid is then transferred after one day to a 10-cm dish for the remaining culture period³²⁵. Characterization of the assembled organoids revealed penetration of CD31+ cells into the neural part of the GFP neural organoid, although the same vascular invasion phenotype is not clearly observed in TUJ1+/MAP2+ neural organoids in a separate experiment reported at the same time point of day 20, as shown in (**Fig. 23**), which may be due to organoid-to-organoid variability³²⁵.

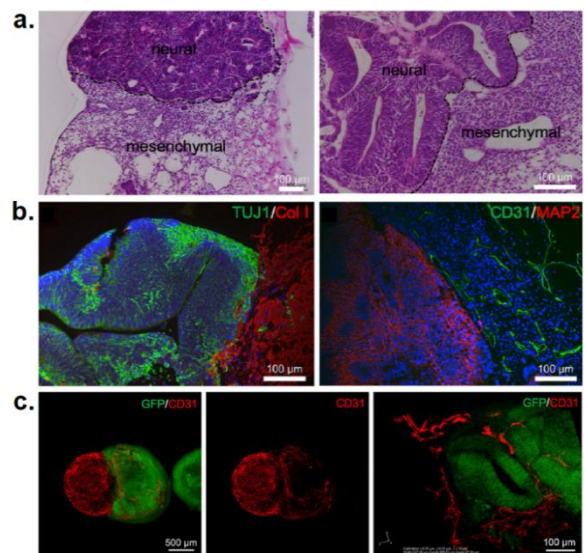


Fig. 23: Vascularization of neuro-mesenchymal assembled organoids at day 20 by fusion of neural aggregates with vascular organoids. **(a)** Histological staining, left image shows overall tissue, and right images shows higher magnification. The mesenchymal and the neural part are show differential characteristic morphology. **(b)** Immunofluorescence staining of organoids shows TUJ1+/Collagen I+ sections, and CD31+/MAP2+ sections. **(c)** CD31+ cells penetrate GFP neural organoid (Wörsdörfer *et al.* 2021), Ref (325). Reproduced with permission from publisher.

Building upon recent work that demonstrated that blood vessel organoids (BVOs) reproduce structural and functional properties of developing human vessels, Ahn *et al.* attempted to test adaptability of BVOs in vascularizing human cerebral organoids²⁴. The authors co-cultured clumps dissociated from BVOs with human cerebral organoids and reported vascular invasion of the cellular clumps into the cerebral organoids and formation of a vascular-like structure²⁴. The vasculature consisted of tubular structures of CD31+ ECs that were associated in their surroundings with SMA+ or PDGFR+ cells, which suggests presences of mural cells that stabilize vessels²⁴. Additionally, the vascularized brain organoids were able to retain fluorescent dextran upon incubation, while control organoids did not retain the dye, which suggests lumen formation within the vascularized organoids, although the results were not indicative of vessel permeability²⁴.

Overall, co-culture approaches, summarized in **(Table 4)**, that incorporate stem cell-derived ECs^{3, 6}, HUVECs⁵, assembly with EC precursors³²⁵, or clumps of ECs²⁴, provide promising methods to study neurovascular interactions, enhance neuronal maturation, and reduce cell death in brain organoid. However, further improvement of these approaches will require attempts to enhance control over EC patterning, reduce organoid spatial variability, and exploring formats in which perfusion inlets can be introduced, which are areas of improvement where microfluidic culture may assist with²¹³. Microfluidic-based vascularization systems are therefore reviewed in **(Section 5.3.4)**.

5.3.3.3 Ethical implications of vascularized brain organoids

While the previously outlined challenges facing brain organoids in **(Section 5.2.3)** remain a work-in-progress, complexity of brain organoids has been rapidly increasing in recent years. This increase in complexity may trigger additional challenges due to ethical concerns about the potential for generating consciousness in human brain organoids (hBO) that would be significant-enough to warrant them moral status^{150, 329-331}. Generating consciousness in hBOs may spark further ethical concerns down the line, such as issues pertaining to procurement of samples, donor consent, ownership of samples, data privacy, and post-research handling, which have been discussed as referenced^{150, 330}. Here, consciousness as the root of these concerns is mainly addressed, along with our perspective on the implications of recent developments in vascularization of brain organoids for generating consciousness.

Articles discussing ethics of hBO research have made efforts in defining ‘consciousness’ by citing key works from the field of philosophy of mind and neuroscience to set a framework that allows for identifying the moral status and ‘interests’ of animals based on the complexity of their consciousness³²⁹⁻³³². Discussions of moral status of animals in research often focus on two kinds of consciousness: self-consciousness and phenomenal consciousness³²⁹. Self-consciousness is the most sophisticated form of consciousness as it entails awareness of the self and complex cognitive abilities; characteristics that are exclusive to humans and non-human primates with higher brain functions, while phenomenal consciousness is characterized by experiences of subjective sensory qualities such as pain, pleasure, and perception, which is experienced by all animals³²⁹. As others discussed, a self-conscious human would have interests in sensing pleasure, avoiding pain, pursuing life goals, and reflecting on experiences, beliefs, and memories, and would have moral considerations as such³²⁹. On the other hand, lower animals, which mainly possess phenomenal consciousness, are likely only interested in experiencing pleasure and avoiding pain, and may arguably have a different set of moral considerations than humans and other cognitively complex animals³²⁹.

In biomedical research, the use of animals that mainly possess phenomenal consciousness has already been established under stringent and well-defined bioethical practices stemming from the ‘3R philosophy’ as referenced³³⁰. Yet, controversy of using animals in research remains, because many people ascribe moral significance to phenomenal consciousness even in absence of other forms of consciousness³²⁹. Human brain organoids may have the potential for reducing the use of animal models, while also improving our understanding and the treatment of devastating neurological diseases that impact people’s lives and burden the healthcare system, in a context that has not been possible before³²⁹. Therefore, from a consequentialist perspective, there is a moral drive for exploring the potential of hBOs as neurobiological models, but the stakes are also high for employing them ethically as they become more complex.

The key questions that emerge in this discussion include; are there currently any reported characteristics of hBOs that would be ethically concerning in terms of possibility for generating self- or phenomenal consciousness? What type of future hBO research should we be most vigilant about based on the latest understanding of the neuroscience of consciousness? And how do we evaluate

consciousness?

Evaluating consciousness in hBOs is quite challenging and not as straightforward as evaluating it in human subjects who are capable of providing qualitative feedback to describe an experience³³¹. However, inferences about consciousness in hBOs could be made based on established methods in neuroscience for measuring brain activity of vigilant subjects³³¹. A recent article by Lavazza laid out ways in which hBOs could provide insights into human consciousness and proposed a framework for evaluating their consciousness, as referenced³³¹. In terms of the experimental conditions that could lead to generating consciousness in hBOs, the majority of researchers agree that generating a level of consciousness within hBOs that would be complex enough to warrant them moral status is currently remote^{329, 330}, while others started to consider it a possibility^{150, 331}. Key research pertaining to each viewpoint is summarized as follows.

A recent study by Trujillo *et al.* showed that 6-month old hCOs were able to spontaneously generate periodic and regular oscillatory network activity that resembled features of electroencephalography (EEG) of 25-39 week-old premature human infants³³³. This work is often cited in ethical discussions of brain organoids due to concerns of whether those hCOs possess or could develop consciousness similar to how a normal human fetus develops into a conscious being, given the aforementioned similarity the researchers found. Others have questioned the interpretation of this finding and its ensued ethical concerns, stating that it is not possible to know if the activity observed in the hCOs is due to the same mechanisms occurring in the premature infants^{330, 334}. Moreover, genetic analysis of the hCOs did not fully reflect the same cell diversity expected in premature human infants^{333, 334}. Additionally, the authors did not provide analysis of overall viability of the hCOs, which is necessary given that cell death at the core of brain organoids is often a concern, especially in extended culture. Such analyses are necessary before stating concerns about the possibility for consciousness due to the following arguments.

The neural correlates of consciousness (NCC) are defined as “the minimum neural mechanisms sufficient for any one specific conscious percept”³³⁵. According to the global neuronal workspace theory, the NCC “are believed to be distributed across large and diverse anatomical regions of the cerebral cortex and involve multiple cell types” that must be present at minimum to provide a

possibility for consciousness^{330, 332, 335}. This is not thought to be the case for the hCOs reported by Trujillo *et al.*³³⁰. This notion of consciousness might also lessen ethical concerns about region-specific hBOs such as cerebellar organoids or midbrain organoids, compared to concerns regarding cortical and whole-brain organoids. However, given that region-specific hBOs contain regions of stem cells and progenitor cells that could differentiate into other cell types, further evidence is needed to determine if a region-specific hBO could be differentiated into a whole-brain organoid under certain conditions. If research shows that as a possibility, it might be necessary to include region-specific hBOs in ethical discussions as well, as most neuroethics articles have focused thus far on cortical organoids. Additionally, it is important to recognize that theories about the NCC remain debatable amongst researchers³³⁵⁻³⁴⁰. While many researchers generally accept that consciousness is localized in the cortex³³⁵⁻³³⁸, others have proposed that specific brain regions such as the midbrain may be sufficient to generate consciousness³³⁹. However, theories focusing on the cortex and thalamus³⁴⁰ are more widely supported than the midbrain³³⁷.

Sensory stimulus is also thought to be required as a basic element for the NCC; that it must appear in order for any form of cognitive processing to occur, which has been referred to by Northoff and Huang as the temporo-spatial theory of consciousness³⁴¹. Given that fusion of two organoids into a larger assembloid could allow for the long-distance connectivity described in the global neuronal network space theory, as well as the potential for fusion with sensory organoids, generating consciousness in assembloids has been proposed as a possibility^{330, 342}. However, neuronal maturity and complexity in assembloids remains lacking.

Researchers discussing ethics of hBOs also share the notion that a level of consciousness that would be complex enough to resemble human consciousness cannot emerge without proper sensory input, motor output, and nurturing environmental interactions and reactions, the combination of which; assembloids and hBOs currently lack^{329, 330}. Nonetheless, a recent article by Giandomenico *et al.* from Lancaster's group demonstrated possibility for generating motor output from cerebral organoids by innervating the organoids with *in vitro* mouse spinal cord explants³⁴³. The researchers recorded spontaneous and evoked contraction of adjacent muscle cells³⁴³. Such research is valuable for modeling debilitating diseases such spinal cord injury and ALS, but it could also push scientists

closer to replicating key aspects of consciousness in a lab. Nonetheless, it is important to recognize that demonstration of functional properties of a group of muscle cells or a limited number of neurons does not equate to organ level function nor indicate that purposeful thinking generated the motor output^{330, 331}. The aforementioned research, as well as research towards development of sensory organoids, such as brain organoids with light-sensitive photoreceptor cells²⁰⁶, are highly relevant for questions regarding consciousness but ethical concerns must not be exaggerated without examining the full requirements for the NCC.

Furthermore, none of the aforementioned hBOs in this section have reported signs of vascularization nor established the same level of cell diversity present in the human brain. As stated previously, brain vascularization is a crucial step in CNS development, and necessary for supplying nutrients, neuronal differentiation and maturation based on the concept of the NVU. Circumventing cell death in hBOs via vascularization is necessary to set the initial conditions for neurons and neuronal progenitors to be viable long enough to mature or differentiate and later establish neuronal network activity. For instance, transcriptomic analysis by Cakir *et al.* that showed that neurons in vhCOs resembled neurons of GW 16 to 19 while neurons in non-vascularized hCOs resembled neurons of earlier GWs, suggests a possibility for improved recapitulation of later stages of development by addressing the challenge of vascularization. It is thought that some characteristics of fetal consciousness emerge after GW 24 upon the establishment of thalamocortical connections from sense organs³³⁶. Therefore, the ability to more closely mimic later stages of human brain development would be relevant for questions about consciousness.

Nonetheless, current reports of *in vitro* hBO vascularization remain in a preliminary stage of research. The few reports that demonstrated presence of neuronal network activity, including the report by Cakir *et al.*, only showed minimal activity in a few neurons, not in a whole-brain organoid^{3, 5}. While the report by Mansour *et al.* of *in vivo* hBO vascularization demonstrated superior neuronal network activity than *in vitro* reports of hBO vascularization, the findings cannot provide inferences about human brain consciousness¹⁰². The *in vivo* hBO by Mansour *et al.* is grafted within anatomical features that do not match the human brain, and the size to which the hBO can grow to is restricted by the size of the host animal brain. When the researchers measured the spatial learning abilities of mice that

received an hBO graft to ones that did not, the researchers did not observe differences between the two groups, except for a minor decreased performance of the grafted mice in spatial memory testing, which could suggest a lack of beneficial outcome from such research for cognitive inferences. The possibility that mouse-*in vivo* vascularized hBOs would gain self-awareness or consciousness that resembles that of the human brain currently seems unlikely. Nonetheless, ethical concerns might arise from brain organoid chimeras depending on factors such as the ratio of human cells to animal cells, and the type of host animal in terms of species or developmental stage at which the engraftment was performed³⁴⁴. Ethical concerns regarding humanized chimeras have been discussed in more detail as referenced³⁴⁴.

As brain organoid models become increasingly advanced, it is possible that researchers may arrive at a model that combines technical developments that have solved individual limitations of hBOs into one model that overcomes several challenges of hBOs, and replicate consciousness in this process. An extreme version of such model for instance could include a perfusable vascularized assembloid or hBO with sensory input and motor output that displays complex neuronal activity, anatomical resemblance to the human brain, cellular diversity, and extended viability. However, it is important to recognize that tissue engineers are often interested in recreating certain features that reproduce and study a function of interest rather than creating a perfect functioning human brain. Additionally, the fact that ethical concerns that might emerge from hBOs research have already been addressed by researchers and neuroethicists is a positive indicator of an existing awareness that parallels technological developments.

Lavazza has contrasted the ‘precautionary principle’³³⁷ and a consequentialist perspective³³⁰ as two moral positions researchers discussed in light of recent advancements in hBO research. Based on the precautionary principle^{331, 337, 345}, in situations of uncertainty, decision-makers should refrain from actions that may risk harming the public or the environment “even if the harmfulness of these actions or policies has not been scientifically established beyond reasonable doubt”³⁴⁵. In the case of hBOs, if researchers suspect the organoids may become partially conscious then regulations should be instated to prevent further experimentation^{331, 337}. On the other hand, researchers adopting a more consequentialist view, generally see that the use of hBOs should be weighed against the research benefit, and do not perceive sufficient available evidence to attribute hBOs a moral status³³⁰.

Despite the contrast in views, researchers adopting either view have advocated for continued ethical discussions between researchers and regulators, and for the inclusion of bioethicists in various stages of research to advise researchers as projects proceed³²⁹⁻³³¹. Overall, hBOs are exciting research tools that could significantly advance human health and our understanding of human neurobiology. Their employment in research raises important ethical questions that may be difficult to resolve but ethical resolutions through well-regulated practices have been feasible in the past for similar issues such as ones brought up in discussions of animal research³⁴⁶, and resolutions should be feasible for hBOs as well.

5.3.4 Microphysiological systems of the vasculature

Microfluidic techniques have been used to engineer microphysiological systems that incorporate perfusable vascular networks inside microchannels^{25, 256, 261, 347}, which we have previously referenced as one of key topics in MTVE²⁵⁷. Such microphysiological systems have been generally used in applications that model the microvasculature itself as a tissue^{347, 348}, or model the microvasculature in conjunction with other organs of interest^{25, 26, 121}, which also belong to organ-on-a-chip and organoid-on-a-chip applications of microphysiological systems that we previously introduced^{119, 256}. Modeling the 3D structure and physiological function of the microvasculature using a suitable *in vitro* model is valuable for vascular biology and tissue engineering, as it enables various applications such as studying pathophysiology of the microvasculature^{117, 349}, cancer metastasis^{26, 117, 350}, and tissue vascularization^{25, 27, 121}.

After the first *in vitro* observation of angiogenesis, made in 1980, by Folkman and Haudenschild³⁵¹, other *in vitro* models of angiogenesis and vasculogenesis also emerged^{256, 352, 353}. A tube formation assay by Kubota *et al.* emerged soon after, where ECs plated on an ECM composed of basement membrane-like substrate form tubule connections³⁵². The assay became a gold standard that remains used to evaluate endothelial cell function and identity, known as tube-formation assay³⁵². A subsequent assay involved the use of a modified Boyden chamber that allows for studying ECs under pro-angiogenic conditions such as chemotactic cues from cancer cells³⁵³. These initial vascular studies were useful for understanding EC differentiation and morphogenesis²⁵⁶. However, the engineering design for those assays could not account for other key factors involved in angiogenesis,

vasculogenesis, and vascular remodeling such as gradient cues, mechanical cues, and spatial patterning of cells^{256, 257, 301}. Additionally, the 2D nature of the past *in vitro* model does not replicate the unique 3D structure of the microvasculature, which strongly influences its function^{289, 301}.

The use of microfluidic cell culture to model the microvasculature is advantageous over previous *in vitro* methods in that it enables the incorporation of the aforementioned factors^{256, 261}. Microfluidic techniques allow the addition of features relevant to applications of vascular biology and tissue engineering, such as parallelization that can enable high throughput testing of anti-cancer drugs¹¹⁷, compartmentalization of channels that can enable spatial patterning of signaling molecules and other cell types in the EC microenvironment^{25, 260}, and controlled flow that can enable testing mechanical cues^{117, 301, 303}. In order to achieve the desired features required to engineer the microvasculature as per application, microfluidic-based vascularization systems have utilized a wide range of fabrication methods such as photolithography, soft lithography, surface patterning, sacrificial micromolding, 3D bioprinting, and 3D printing, which have been reviewed by others^{261, 354, 355}. The choice of fabrication method often depends on the desired final microvessel model^{256, 261}. Microfluidic-based models of the microvasculature have been categorized based on their microvessel formation method into wall-patterning methods and self-morphogenesis methods^{256, 261}. Advantages and applications of the two methods are contrasted as follows.

5.3.4.1 3D wall patterning methods

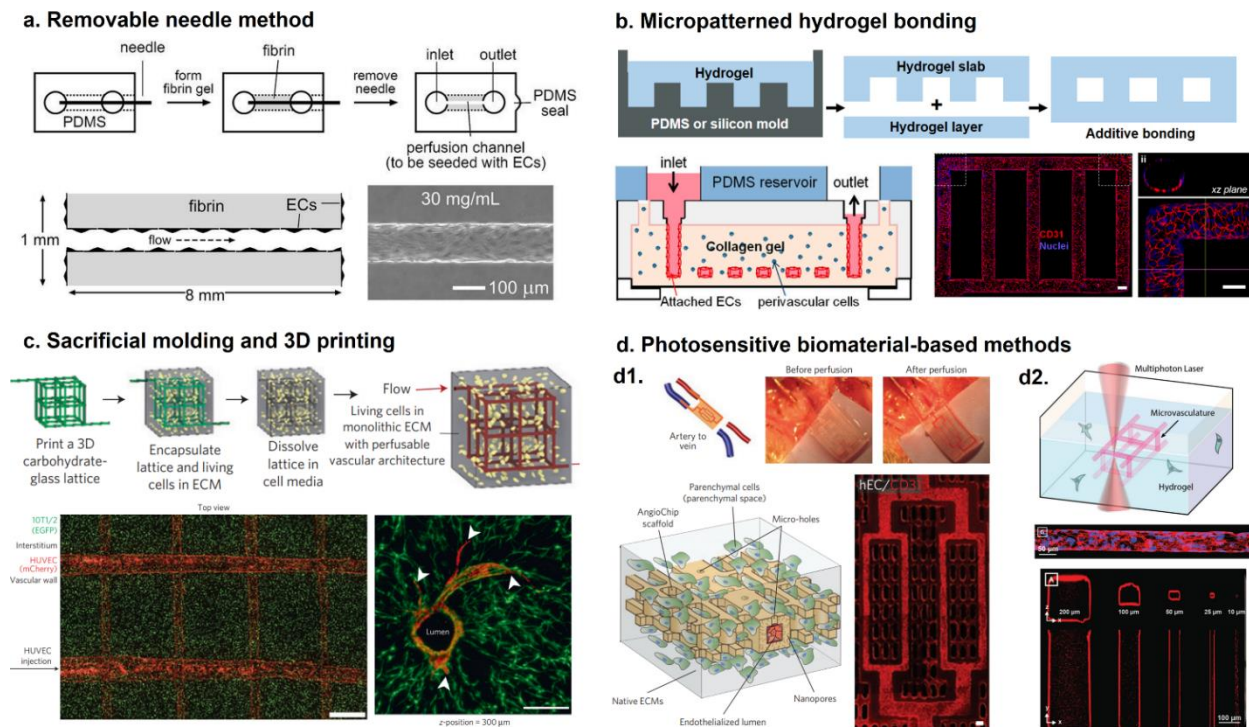


Fig. 24: 3D wall patterning methods with hydrogel coated microchannels for *in vitro* modeling of single microvessels (a), single-layer microvascular network (b), multi-layer microvascular networks (c, d) (adapted from Wang *et al.* copyright 2018), Ref (261). (a) Needle removal method (Wong *et al.* copyright 2012), Ref (356). (b) Micropatterned hydrogel bonding (Zheng *et al.* copyright 2012, National Academy of Sciences), Ref (). (c) Sacrificial molding and 3D printing of carbohydrate-glass lattice allows lumen formation and endothelial sprouting (Miller *et al.* 2012), Ref (358). (d1) AngioChip developed using PoMAC photocrosslinker and biodegradable polymer enable engineering multi-layered microvasculature that was successfully used for surgical anastomosis in rat hindlimbs (Zhang *et al.*, copyrights 2016), Ref (348). (d2) Multiphoton 3D printing using photodegradable polymer enables formation of microvessels and microvascular networks (Arakawa *et al.*, copyrights 2017), Ref (359). All images were reproduced or republished by permission from their respective publishers.

A simple form of wall patterning methods for *in vitro* microvessel models is to pattern a 2D endothelial layer in a microfluidic chamber^{67, 123, 256}. A common fabrication method of microfluidic devices for 2D endothelial layer models includes using photolithography for generating an SU-8 master positive mold of the device and using soft lithography to replicate a PDMS slab with the final device features^{67, 123}. The surface of the devices at which ECs are cultured on is decided by upside down orientation of the device during the initial cell seeding^{67, 123}. A thin surface coating with a basement membrane protein such as fibronectin can further facilitate surface attachment to the PDMS surface^{123, 261}. In this model, parameters that affect endothelial physiology such as shear stress due to laminar flow can be evaluated in terms of TEER, the permeability values produced by the model, and resemblance of the *in vitro* ECs protein expression to their *in vivo* counterparts^{67, 123, 256}. Examples of this 2D model of the endothelium used for BBB-on-a-chip and lung-on-a-chip applications were

discussed in (Section 5.1.4.1) and illustrated in (Fig. 9 and Fig. 10)^{67, 123}.

The second form of wall patterning methods used for modeling *in vitro* microvessels is 3D wall patterning, where ECs are patterned on all inner surfaces of a microchannel as opposed to one surface, thus creating a 3D lumen structure^{256, 261}. For instance, PDMS microchannels fabricated using photolithography and soft lithography were used by Li *et al.* to study endothelial cell response to 3D shear stresses in terms of morphology and proliferation, and were further able to quantify calcium concentration and NO production at the level of individual ECs in response to ATP³⁴⁷. The results of the study recapitulated key aspects of *in vivo* venules when compared to the *in vitro* model³⁴⁷.

The walls of the hollow microchannel or network of microchannels used for seeding ECs could be composed of a hydrogel coating as well instead of PDMS^{261, 356-358}. 3D wall patterning of ECs into hydrogel-based microchannels has been applied to model: 1) single microvessels, 2) a single-layer network of microvessels, or 3) a multi-layer network of microvessels. Fabrication of these models has been achieved in various reports using innovative methods, examples of the broad categories of these methods are compiled in (Fig. 24), and can be described as follows.

One simple approach to fabricating hydrogel-coated microchannels includes a **removable microneedle method** that has been used for modeling single microvessels³⁵⁶, as shown in (Fig. 24a). In this approach, a microneedle is inserted into a microchannel to maintain it hollow, followed by flowing a fibrin hydrogel, removing the microneedle after the hydrogel polymerizes, and flowing ECs subsequently to line the walls of the channel. For instance, Wong *et al.* used this method to model endothelial response to lymphatic drainage³⁵⁶.

Another approach for generating hydrogel-coated microchannels includes using microstructured PDMS to ‘micropattern’ a slab of collagen hydrogel that composes three sides of the microchannels onto a flat surface coated with the same hydrogel, which enables bonding the two layers to form networks of hydrogel-coated microchannels³⁵⁷. This **micropatterned hydrogel bonding method** was used to model a single-layer microvascular network³⁵⁷, as shown in (Fig. 24b). The researchers were also able to use the model to study the transition of ECs to a pro-thrombotic state during inflammation³⁵⁷.

A third approach includes the use of **sacrificial micromolding methods** to fabricate multi-

layer microvascular networks^{348, 358}, as shown in **(Fig. 24c)**. For instance, Miller *et al.* formulated a biocompatible carbohydrate glass and used it as a sacrificial material that was 3D printed into a network of filaments that were then encapsulated within an ECM mixed with mesodermal cells to model the interstitial space, and to provide structural support to the microchannel network³⁵⁸. The filaments were then dissolved in cell media and HUVECs were injected into the hollow channels to line the walls of the microchannel network³⁵⁸. The authors demonstrated ability to control network geometry and interconnectedness, which is advantageous for modeling vascular networks that consist of a hierarchy of microvessel diameters³⁵⁸. The authors also showed enhanced metabolic function for liver tissue engineered constructs that were comprised of ECM-encapsulated hepatocytes, whereas the avascular ECM-encapsulated hepatocytes showed suppressed function in their core³⁵⁸.

One last approach for 3D wall patterning of hydrogel-coated multi-layer microchannels could be categorized as **photoreactive biomaterial-based methods** that utilize either photocrosslinkable or photodegradable biomaterials as key components in their fabrication protocols, as shown in **(Fig. 24d)**^{348, 359, 360}. These methods often hybridize with other fabrication techniques as well to generate the final microvascular model. For instance, Zhang *et al.* used a photocrosslinkable and biodegradable polymer known as poly(octamethylene maleate (anhydride) citrate) (POMaC), in combination with a 3D stamping technology to fabricate a scaffold of a multi-layer microchannel network that was applied for surgical anastomosis in rat hindlimbs, as shown in **(Fig. 24d1)**³⁴⁸. The 3D microchannel structure was cultured with a surrounding of parenchymal cells, and its inner lumen was coated with an EC monolayer³⁴⁸. The researchers further incorporated nanopores and micro-holes in the design, which enhanced permeability, crosstalk with neighboring cells, and extravasation of monocytes across the microvessel³⁴⁸. The scaffold, termed the AngioChip, demonstrated capacity for drug testing as well³⁴⁸.

Other innovative approaches also utilized photoreactive biomaterials, such as the use of a photodegradable polymer in combination with multi-photon technology to directly 3D print microvascular networks, as shown in **(Fig. 24d2)**³⁵⁹, and the use of photocrosslinkable polymer with hydrodynamic focusing to engineer microvessels lined with ECs and an outer layer of SMCs³⁶⁰.

Overall, employing wall patterning methods to construct *in vitro* microvessel models offers the advantage of engineering a clear microvessel structure with well-defined lumens that are generally

straightforward to characterize in terms of geometry²⁵⁶. In addition, parameters such as shear stress are easy to control and calculate based on channel dimensions and the chosen flow rate. While the ability to easily tailor the microvessel geometry through the fabrication method represents an advantage, it is also constrained by the walls surrounding the structure. Once fabricated, the final microvessel design is generally inflexible, which excludes applications that require modeling *in vivo* vascular morphogenesis and remodeling²⁵⁶. Even wall patterning methods that involve hydrogel-coated microchannels, the process of angiogenesis appeared mainly limited to the first sprouting step of angiogenesis³⁴⁸, or to a few sprouts³⁵⁷, or was not demonstrated.

Modeling angiogenesis and vasculogenesis also greatly depends on the resolution of the fabrication method. For instance, *in vitro* microvessels patterned too far apart, which could be due to limitations of 3D printing resolution, would not receive the biochemical cues secreted by other ECs required for anastomosis. Moreover, certain wall patterning methods have been proposed as more suitable for constructing microvessels that are larger than 100 μm due to concerns of microchannel blockage when the cells are loaded into the device²⁵⁶. This size limitation and the inflexibility of geometry makes wall patterning methods difficult to adapt for vascularizing tissue constructs on the scale of spheroids (200-500 μm), or developmental models such as organoids, which are small in size at the beginning of the protocol but change during culture. However, more recent and advanced wall patterning methods such as photoreactive biomaterial-based methods, shown in **(Fig. 24d)** have been successful in fabricating features that are below 100 μm , and could potentially be useful for tissue vascularization applications.

Other concerns have been cited for wall patterning methods such as possible hurdles with coating a microchannel surface with ECs fully and uniformly in order to model truly endothelialized channels²⁵⁶. However, methodical evaluation of uniformity and reproducibility of endothelialization is often lacking in articles of newly proposed methods. Overall, wall-patterning methods have been informative in organ-on-a-chip studies. Nonetheless, researchers must carefully match microvascular tissue engineering methods to the appropriate application by considering the specific questions the model aims to address.

5.3.4.2 3D self-morphogenesis methods

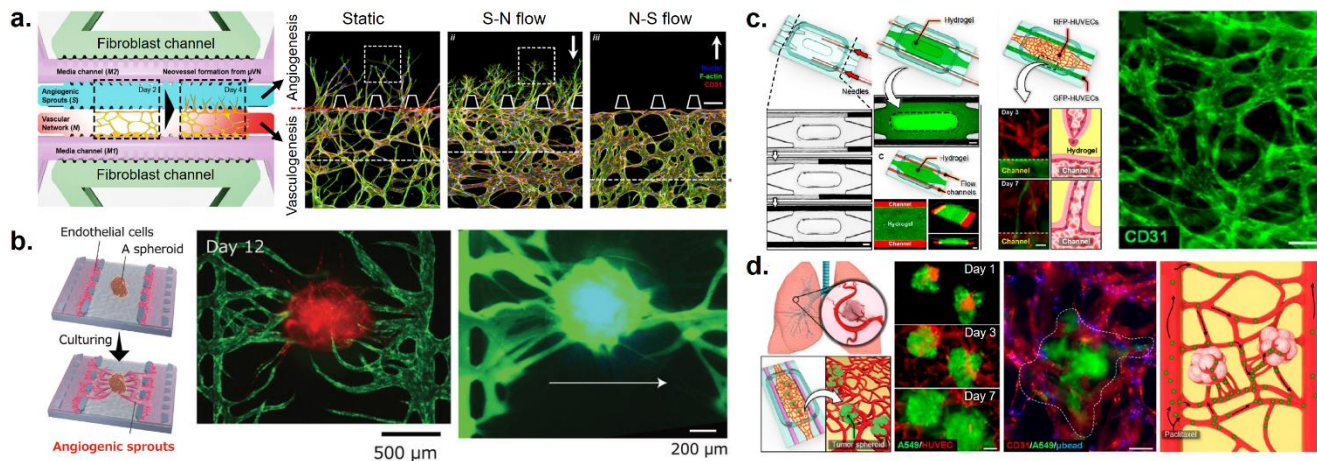


Fig. 25: Self-morphogenesis methods for *in vitro* microphysiological systems of the microvasculature (Lee *et al.* 2018), Ref (256). (a) Microfluidic device for vasculogenesis and angiogenesis of HUVECs in co-culture with fibroblasts. The device allows application of interstitial flow using hydrostatic pressure, which induces angiogenic sprouting in the direction (S-N) that is opposite to sprout formation, and inhibit angiogenesis in the (N-S) direction (Kim *et al.*, 2016), Ref (361). (b) Microfluidic device for vascularization of human lung fibroblast-HUVEC spheroids. The device comprised microgrooves that allowed GFP-HUVECs to sprout into a fibrin hydrogel-filled chamber and connect with RFP-HUVECs co-cultured within the spheroid beforehand. The vascularized spheroid formed perfuseable lumens that was tested using a fluorescent dye (Nashimoto *et al.*, copyrights 2017), Ref (25). (c) Microfluidic device setup that incorporates a hydrogel-filled middle chamber where a vascular bed forms via vasculogenesis in co-culture with fibroblasts within the middle chamber. EC-lined side channels allow anastomosis with the vascular bed. The hydrogel is patterned in the middle chamber by temporarily blocking the side channels using needle tips. CD31 (green) immunofluorescent staining shows vascular network formation (Paek *et al.*, copyright 2019, American Chemical Society), Ref (26). (d) The same device in (c) was used to vascularize tumor spheroids made of A549 cells (green) and RFP-HUVECs (red) which was used to test the chemotherapeutic paclitaxel (Paek *et al.*, 2019), Ref (26). All images were reproduced or republished by permission from their respective publishers.

Self-morphogenesis methods were used to model the microvasculature *in vitro* using microfluidic cell culture, as compiled in (Fig. 25)^{256, 261}. These methods focus on replicating two key vascular processes: vasculogenesis and angiogenesis in microfluidic systems by recreating properties of the *in vivo* 3D microenvironment that lead to each process^{256, 261}. These methods allow ECs to naturally assemble into a 3D microvasculature by testing and applying knowledge on how key components including angiogenic factors, biomechanical cues, ECM hydrogel, and cell-cell signaling, influence microvessel parameters such as sprouting, lumen formation, barrier function, microvessel size, perfusability, and microvessel stabilization^{256, 261}.

Fabrication of microfluidic devices used for modeling the microvasculature using self-morphogenesis are generally straightforward and include the use of cleanroom microfabrication and photolithography^{25, 27, 117, 260}, or less frequently 3D printing²⁶, for fabricating the positive mold for the device. Subsequently, soft lithography is used for fabricating a replica of the mold that will represent the final device. The device is then sealed using a cover made of a transparent material that allows

observation such as glass or PDMS or thin polymer membrane. While the design of devices used for self-morphogenesis differ based on the application of interest, they typically include common features in their overall design. Key design features in microfluidic devices for self-morphogenesis models of the microvasculature commonly include a 3D hydrogel-filled chamber where vasculogenesis or angiogenesis take place, and this hydrogel-filled chamber is often connected to side channels that are kept vacant for growth media, ECs, other cell types of interest, or drug agents to be loaded. The number and purpose of microfluidic chambers differs according to each application. The device can also be designed to include other features such as pressure regulators, media reservoirs, or perfusion ports.

In terms of culture conditions that promote microvascular morphogenesis, fibroblasts are traditionally co-cultured with ECs to provide a secretome that induces angiogenesis^{25, 117, 256, 260, 319}. Microfluidic platforms for *in vitro* models of the microvasculature that incorporated fibroblasts have been successful in achieving perfusable lumens^{25, 117, 260}. For instance, Kim et al. developed a cleanroom microfabricated device with five parallel channels partitioned by PDMS microposts, as illustrated in **(Fig. 25a)**²⁶⁰. The surface tension between the microposts in this design allowed selectively patterning HUVECs that were pre-mixed in a fibrin hydrogel into the central channel, and patterning fibrin-embedded human lung fibroblasts (hLFs) into the outer-most two side channels, while maintaining the two remainder channels vacant for growth media and cell communication between the opposing channels²⁶⁰. This configuration reproduced vasculogenesis on-a-chip and showed its dependence on fibroblast co-culture. The authors also tested an alternative configuration where only one outer channel was filled with fibrin-embedded hLFs, and HUVECs were added to the device such that they would only cover the edge of the central channel, which is achieved by tilting the device 90 degrees after loading the HUVECs. In a later publication, the same configuration enabled them to test and demonstrate the effect of directional flow on angiogenic sprouting of HUVECs from the central channel towards the pro-angiogenic stimulus from the hLFs³⁶¹.

The 3D microvascular networks formed using this method were functional, well interconnected, and perfusable²⁶⁰. The perfusable characteristic of the device is enabled not only because of lumen formation but also because the open lumens were connected to the inner side channels that have inlets, which is an engineering feature rather than a biological one. Essentially, the

side channels mimic two accessible microvessels that could give the user access to the microvascular network for drug testing, characterization of permeability, and testing the effect of shear stress²⁶⁰. Upon application of luminal fluid flow, which yields wall shear stress, the authors reported F-actin reorganization and increased NO production compared to static culture²⁶⁰. The authors also used the model to test endothelial interactions with pericytes and cancer cells, which is advantageous for studying phenotypic and biochemical features in vascular stabilization and destabilization in response to cancer. Another benefit of perfusable microvessels is the ability to use them for transendothelial migration studies²⁵⁶. For instance, the authors used their device to study migration of HL-60 cells; a neutrophil cell line, from the microvessel's lumen to its outer part, which simulates interactions between leukocytes and the endothelium during inflammatory responses²⁶⁰.

Another application of microfluidic systems of the microvasculature is to utilize them for spheroid vascularization²⁵. Nashimoto *et al.* developed a microfluidic device using cleanroom microfabrication that included 100- μ m microgrooves spaced between PDMS microposts, which connect a middle chamber with two side channels, for hLF spheroid vascularization, as shown in **(Fig. 25b)**²⁵. The hLF spheroid is prepared for vascularization by mixing HUVECs and hLFs prior to aggregation²⁵. The spheroid is then embedded in fibrin and loaded into the middle chamber for polymerization²⁵. The device is then tilted to allow HUVECs to attach to the fibrin hydrogel, similarly to the angiogenesis configuration proposed by Kim *et al.*²⁶⁰, except that this step is repeated for both side channels. Using this configuration, the authors observed angiogenic sprouting from the side channels towards the spheroids, followed by vascular invasion into the spheroid²⁵. The HUVECs formed an inter-connected microvascular network that was perfusable after 14-19 days in culture²⁵. The platform was proposed as analogous to *in vivo* angiogenesis that occurs in response to hypoxic signaling²⁵. The spheroid diameter upon seeding into the device was 500 μ m; exceeding diffusion limit of oxygen and nutrients²⁵. However, the authors did not test expression of hypoxic markers, which could differ based on how densely packed the cells are within an engineered tissue. Therefore, the cause for vascularization in this case is does not discern hLF secretome from hypoxic signaling.

Nonetheless, the overall configuration is applicable for vascularization of tumor spheroids²⁶,²⁶¹, spheroids of other healthy cell types^{25-27, 256}, or organoids. Moreover, the ability to maintain tissues

perfused in culture through continuous nutrient perfusion has the potential for establishing long-term viability, which is valuable for developmental models of organs or studying prolonged exposure to drugs and toxins.

Researchers are motivated to develop vascularized tumor spheroids in order to study cancer metastasis and anti-cancer therapeutics *in vitro*^{26, 117}. Similarly to fibroblasts, cancer cells possess strong pro-angiogenic secretomics³⁶². Therefore, tumor spheroids are good candidates for self-morphogenesis microvascularization methods using microfluidic systems²⁶¹. Paek *et al.* developed a PDMS microfluidic device replicated from 3D printed molds, which contained a middle open chamber connected to two side channels, shown in **(Fig. 25c)**²⁶. In this configuration, instead of microposts that prevent hydrogel overflow from the middle chamber to the side channels, the authors use needles to block the side channels temporarily²⁶. The middle chamber is then loaded with a pre-aggregated lung cancer spheroid with ECs within it, mixed with additional individual primary ECs and hLFs embedded in a collagen-fibrin hydrogel precursor. Once the hydrogel is polymerized at 37°C, the needles are removed; creating hollow microchannels that are then seeded with ECs to form an endothelialized lumen that is connected to the middle chamber. The ECs self-assembled into a well-interconnected perfusable microvascular network through vasculogenesis and invaded the lung cancer spheroid, as shown in **(Fig. 25d)**. The configuration was used to evaluate efficacy and toxicity of chemotherapeutic agents perfused through the microvasculature²⁶.

Additionally, the researchers used the same platform to create a microvascular bed through vasculogenesis and subsequently seeded iPSC-derived human retinal pigment epithelial cells (RPEs) on top to create a microengineered model of the outer blood-retinal barrier²⁶. Interestingly, the researchers used primary human retinal microvascular ECs and primary human choroidal fibroblasts instead of HUVECs and hLFs for this application and were able to demonstrate successful vasculogenesis and pigmentation of RPEs which indicates their maturation²⁶. The authors did not report whether or not this composition of cells produced perfusable lumens.

Moreover, the same device was used to model the microvasculature of white adipose tissue (WAT), which would be relevant for studying metabolic regulation of systemic energy levels²⁶. The authors used human adipose-derived stem cells (hASCs) and primary human adipose microvascular endothelial cells (hAMECs) that were co-cultured for an extended period, which induced adipogenesis and vasculogenesis²⁶. The authors did not test perfusable lumen formation in the vascularized WAT model. Interestingly, the authors observed phenotypic differences in size and network density between microvessels created using HUVECs and those formed using hAMECs, which could highlight organ-specific endothelial properties that are worth further appreciation by tissue engineers^{22, 26}.

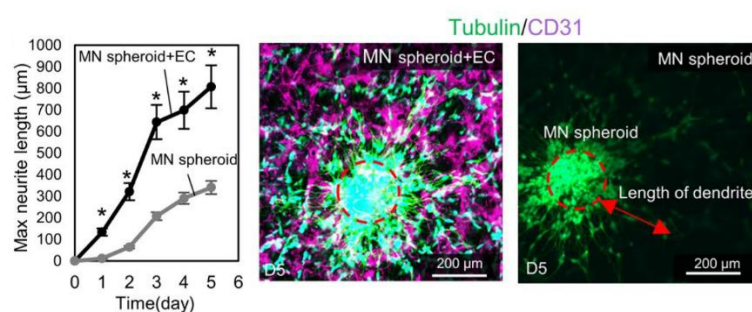


Fig. 26: Motor neuron (MN) spheroids co-culture with HUVECs in microfluidic device leads to vascular network formation and increased neurite length over the course of culture, compared to monocultured MN spheroids. HUVECs are immunostained for CD31 (purple) and MNs are immunostained for Tubulin (green) (Osaki *et al.* 2018), Ref (27). Reprinted with permission from publisher.

Osaki *et al.* used iPSC-derived ECs to vascularize motor neuron spheroids using a similar micropost configuration reported by others^{27, 260}. However, the device design in this work included multiple parallel channels where multiple spheroids were seeded in each chamber in co-culture with ECs²⁷. The authors reported formation of perfusable microvascular networks that mostly surrounded the motor neuron spheroids and partially invaded outer layers of the spheroids²⁷. Interestingly, the authors also reported using spheroids were less than 200 μm in diameter to avoid necrotic cell death at their core²⁷. Therefore, vascular network formation in this model was likely not attributed to hypoxic signaling nor attributed to fibroblasts which were absent in this model. Instead, the authors supplemented the co-culture with a 1:1 mix of endothelial and stem cell media that was supplemented with BDNF and GDNF. As previously stated, BDNF plays a key role in neuronal migration and growth, and has been recently implicated in secretion of angiogenic mediator angiogenin in ECs³²², which is consistent with the findings in this work. Additionally, the authors showed paracrine secretion of BDNF, and expression of signaling molecules involved in cell-cell interactions via the delta-notch pathway, which fosters secretion of VEGF and neuroprotection²⁷. The authors also demonstrated enhanced maturation and connectivity of neurons as measured by Ca^{2+} oscillation, and showed

increased neurite growth upon co-culture with ECs, as shown in **(Fig. 26)**²⁷, which supports the concept of the NVU and the reciprocal angiocrine role of ECs^{22, 363}.

Shin *et al.* developed a microfluidic platform for angiogenesis that enables testing the effect of controlled gradients of VEGF and ANG-1 on the number of tip cells and their migration during sprouting process³⁶⁴. The device allows testing these angiogenic factors in departmentalized or combinatorial fashion, which highlights one of the strengths of microfluidic systems in simplifying a system with the purpose of elucidating a mechanism of interest^{256, 364}.

Wang *et al.* developed a perfusable microvascular *in vitro* model that incorporated a diamond-shaped tissue chamber where ECs are loaded in mixture with hLFs in a fibrin hydrogel, and the chamber is connected to two microchannels on either side that represent an artery and vein³⁶⁵. The configuration allows formation of perfusable microvascular networks within the tissue chamber, and models the hierarchy of blood vessels that descends from artery to a capillary bed and then ascends again to veins^{261, 365}. The formation steps of the microvascular networks combined several steps of vascular development that occur on the platform in proper sequence including vasculogenesis, EC lining, angiogenesis, and anastomosis^{261, 365}. EC lining along the side channels models a main microvessel that can give rise to new microvessels through sprouting angiogenesis. This angiogenic process from the microvessels of the side channels was stimulated by applying transendothelial flow and a positive VEGF gradient that allowed the lined ECs to sprout into the 3D fibrin hydrogel after 24 hours of lining. Subsequently, anastomosis took place between the capillary network formed within the chamber via vasculogenesis and the newly formed angiogenic sprouts, thus creating an interconnected microvascular network. The authors confirmed the microvascular network was perfusable. In subsequent work, the authors further optimized the platform design such that it was compatible with high-throughput drug screening¹¹⁷. The microvascular tissue chamber was also seeded with cancer cells and vascular morphology was evaluated in response to perfusion of anti-cancer therapeutics¹¹⁷. This platform could also be considered an example of a hybrid approach between 3D wall patterning and self-morphogenesis methods for microvascular tissue engineering, although it predominantly operates via the latter.

Revisiting the example of kidney organoid vascularization following flow-induced shear

stress in an organoid-on-a-chip platform, shown in **(Fig. 11, Section 5.1.4.1)**, the vascularization method in the model is thought to occur via self-morphogenesis. However, the device setup still does not enable perfusion of the vascular lumen itself; it only enables perfusion of the chamber where the vascularized organoids are residing. In order to show lumen formation, the authors introduced fluorescent beads to the media in the whole culture and studied its co-localization with the vasculature. The authors did not characterize cell death and hypoxia in the vascularized kidney organoids, therefore, it is not clear if this method of vascularization could resolve cell death at the core of avascular organoids. Although, the fact that it was found to enhance maturation of the kidney organoid is a promising indicator. Design modifications of the proposed platform that may allow lining ECs with the perfusion inlets and outlets could enable studying the effect of luminal shear stress on the kidney's microvasculature, direct perfusion of drugs into the kidney, and modeling urinary output in response.

Overall, the strength of self-morphogenesis methods lies in ability to study vascularization processes in a 3D microenvironment recreated *in vitro* with capacity to control the parameters influencing vasculogenesis and angiogenesis, and thus study the effect of each parameter more clearly^{256, 261}. The ability of microfluidic methods to spatially pattern cells, hydrogels, and gradients of growth factors is useful for understanding cellular decision-making in a 3D context^{260, 366}. In addition, self-morphogenesis enables microvessels to integrate with an organ or tissue of interest dynamically rather than artificially. This is valuable for studying biological phenomena without enforcing a certain paradigm about the *in vivo* process by engineering assumptions or bias. Given that various organs and tissues possess extremely diverse architecture, the ability to adapt 3D wall patterning methods to vascularize a tissue of interest could be challenging without compromising certain features of the original tissue, whereas self-morphogenesis could allow vascularization of tissues in an *in vivo* resembling manner. Extreme 3D phenotypic changes and biological processes such as development and cancer progression, can occur in a parallel timely fashion that require a dynamic 3D system to study them, which could be enabled by self-morphogenesis methods²⁶.

Self-morphogenesis of microvessels using traditional 3D cell culture in well plates was achieved for brain organoids. However, such traditional 3D cell culture methods do not enable easy, sterile, and quick access to the microvasculature for analysis, perfusion tests, application of shear

stress, or continuous nutrient supply during live culture because identifying the inlets to the microvascular network within the intact structure would be challenging. Microfluidic-based vascularization methods based on self-morphogenesis have solved this issue for 3D spheroid culture where ECs lined to edge of the hydrogel form open lumens that connect a user-accessible inlet to the microvascularized spheroid^{25, 26}, which could be adapted to brain organoids as well.

5.4 Summary

Despite the promising applications of human brain organoids, a major challenge that hinders their further advancement is their lack of vasculature^{1, 4}. Several recent attempts to vascularize brain organoids in traditional well plates have generated promising results^{3, 5, 6, 24}. However, control over the distribution and access to the formed vascular network within these brain organoids is lacking. Vascularization of spheroids has been successful using microphysiological systems that enable spatial control of EC patterning to allow perfusion through defined inlets^{25, 26}. However, opportunities for brain organoid vascularization using microphysiological systems have not been fully explored. To explore this opportunity, we aimed to develop a microfluidic device for studying vascularization of midbrain organoids, which we present in the following chapter.

6. Microfluidic-based organoid vascularization in PDMS devices replicated from 3D printed molds

Alia Alameri^{1,2}, Molly Shen^{1,2}, Meghna Mathur³, Camille C. D. Camps^{1,4}, Andy Ng^{1,2}, Timothy Kennedy³, Christopher Moraes^{1,4}, Thomas Durcan³, David Juncker^{1,2,3}

¹Department of Biomedical Engineering, McGill University, Montreal, Quebec, Canada

²Genome Quebec Innovation Center, McGill University, Montreal, Quebec, Canada

³Montreal Neurological Institute, McGill University, Montreal, Quebec, Canada

⁴Department of Chemical Engineering, McGill University, Montreal, Quebec, Canada

6.1 Abstract

Brain organoids are three-dimensional multicellular structures capable of faithfully recapitulating the *in vivo* brain¹. Brain organoids grown from human induced pluripotent stem cells constitute promising tools for investigating mechanisms that underlie human neurodegenerative diseases and neurodevelopment^{1, 2}. A major challenge that hinders applications of brain organoids is their lack of

vasculature, which leads to cell death at their core due to insufficient delivery of oxygen and nutrients once they exceed the diffusion limits that enable oxygenation and nutrient supply^{3, 4}. Attempts to vascularize brain organoids often include differentiation protocols performed in traditional well plates^{3, 5, 6}, which do not provide a straightforward access to the vascular networks for live *in vitro* perfusion, due to a lack of spatial control of ECs within the culture. To address the need for spatially controlled vascularization systems, we developed a ‘Microfluidic-based Organoids Vascularization’ (MOV) device. The device leverages microfluidic principles by incorporating capillary stop valves that prevent hydrogel overflow from a middle channel, where the organoid is added, to side channels where HUVECs are introduced. Digital light processing 3D printing was chosen to fabricate positive molds for fast and cost-effective fabrication of the PDMS device. MOV devices enabled monitoring vascular events during live culture, which we tested using midbrain organoids (MOs) and HUVECs that were either expressing fluorescent proteins or were labeled using CellTracker. Our results showed vascular sprouting of HUVECs in co-culture with MOs, and partial formation of a vascular-like wall within MOV devices. Additionally, to determine the timeframe for vascularization, we characterized the progression of hypoxia and cell death in MOs at four time points by staining for HIF1 α and CC3, and for extensive DNA degradation using TUNEL assay. Our results showed that a dead core develops when MOs reach 1 month in culture, and expression of CC3 is directly proportional to the distance from the surface to the core of MOs. Additionally, we identified a ring-like pattern of hypoxia that surrounded necrotic areas within MOs. Our report demonstrates a cost-effective device for studying midbrain vascularization with spatially controlled patterning of hydrogel and defined inlets and outlets, which has potential implications for future neurobiological studies.

6.2 Introduction

A main challenge of biomedical research has been the inaccessibility of human tissues and organs⁷. 2D cell culture methods provide an accessible *in vitro* platform to study organ function at tissue and cellular levels, and have tremendously enhanced our understanding of physiology and disease⁷. Yet, the lack of a physiologically relevant microenvironment (*e.g.* cell-cell interactions, cell-matrix interactions, gradients of gas and biomolecules), has been widely recognized as a limitation that significantly reduced biological relevance of 2D cell culture^{7, 8, 14}. Animal models have been

extensively used for decades as models that provide physiological context^{14, 129, 139}. However, it is well recognized now that species differences between animals and humans caused a large gap in clinical translation of drugs screened using animal models^{1, 8}. Reports estimate that over 80% of drug candidates fail during phase II and phase III clinical trials mainly due to a lack of efficacy or safety issues unidentified during preclinical screens³⁶⁷. Clinical trials for CNS diseases and disorders represent the second highest percentage of failed trials after oncology^{1, 367}. Therefore, development of effective biological models that mimic highly complex and inaccessible organs such as the human brain is highly necessary. Three-dimensional (3D) cell culture technologies developed to bridge the gap between *in vitro* and *in vivo* biological models by providing accessible *in vitro* platforms that also mimic the multi-cell spatial organization and biochemical and mechanical cues present *in vivo*^{1, 80}. The most recently adapted format of 3D cell culture used in neuroscience research is hiPSC-derived brain organoids; multi-cellular structures capable of self-organizing in 3D space to recapitulate various aspects of human brain development¹. Brain organoids are advantageous as *in vitro* models due to their ability to recapitulate brain cytoarchitecture, multi-source derivability, and ability to tailor them for specific research questions by developing either whole-cerebral organoids¹⁰ or region-specific organoids^{1, 165, 201}. Derivability of brain organoids from hiPSCs allows for modeling human neurological diseases and disorders that are difficult to achieve in animal models due to complex genetic backgrounds and age and species differences^{1, 10}. Even when human disease mutations are introduced, symptoms do not develop with the same severity in the animal as it does in humans^{1, 10}. Additionally, brain organoids are embedded in an ECM-based hydrogel, which further establishes their value in mimicking 3D microenvironmental *in vivo* cell-matrix interactions that drive many biological processes including differentiation, gene expression, and cell survival⁸⁰. Brain organoids can, therefore, complement 2D cell culture and animal models in answering neurophysiological questions, and potentially reduce fruitless animal experimentation and suffering¹³⁵. The aforementioned features established hiPSC-derived brain organoids as promising, clinically relevant neuroscience tools that have been used to model neurodevelopment^{18, 19}, neuropsychiatric disorders¹⁶², and neurodegenerative diseases²¹. Nevertheless, further applications of brain organoids are halted by their lack of maturity, heterogeneity, and missing cell types (*e.g.* immune cells and endothelial cells)⁸. The lack of maturity

of current brain organoids has been widely attributed to their lack of vascularization which leads to the development of a necrotic core inside organoids once their size exceeds the limits of oxygen and nutrient diffusion^{10, 20, 135, 183, 368}.

In recent years, several attempts were made to vascularize brain organoids. Those reports mainly include an *in vivo* approach in which cerebral organoids are implanted in immunodeficient mice to drive *in vivo* vascularization¹⁰², and *in vitro* approaches^{3, 5, 6, 24, 325}. *In vitro* approaches for brain organoid vascularization include 1) premixing methods^{3, 5}, where ECs or stem cell-derived ECs are premixed with the brain organoid before induction, and 2) shell methods⁶, where ECs are added as a hydrogel-embedded shell surrounding the organoid, and 3) fusion methods, where vascular organoids³²⁵ or EC aggregates²⁴ are co-cultured with the brain organoid. First, the *in vivo* method for brain organoid vascularization has generated functional perfusable vascular networks¹⁰². The functional vasculature contributed to significantly reduced cell death in implanted brain organoids compared to non-vascularized *in vitro* organoids¹⁰². However, vascularization via implantation in immunodeficient mice renders the organoid inaccessible, does not eliminate animal suffering as promised by brain organoid culture, and is not representative of the human brain microenvironment, which includes a full functioning immune system and interactions with other human cells. Additional difficulties include cost of animal housing, and requirement for advanced microscopy systems to image through mice brains^{102, 134}. Second, the *in vitro* methods described for brain vascularization, although very promising, have yet to create completely vascularized networks within the whole organoid or enable controlled perfusion of the organoid from one side to the other. One aspect that hinders further progress of *in vitro* vascularized brain organoids is the lack of spatial control over endothelial cell patterning, which makes it difficult to identify an inlet where the vasculature can be accessed in order to prepare organoids for live perfused culture. Therefore, an unmet need exists for a straightforward method for developing accessible inlets and outlets for *in vitro* vascularized brain organoids, which could ultimately have application for neurophysiological studies and drug screening application.

Recent microfabrication technologies enabled the construction of micrometer- to few millimeter-sized features for various biomedical engineering applications^{97, 105, 118, 256}. Those advances fostered the development of microfluidic-based 3D microvasculature models using two main

approaches: 3D wall patterning, and 3D self-morphogenesis^{25, 256}. 3D wall patterning methods, including sacrificial molding^{358, 369}, multi-photon laser patterning³⁵⁹, and assembly of multiple patterned hydrogel layers³⁵⁷, are advantageous due to providing ready-to-use 3D lumenized vessels after fabrication^{25, 256}. However, it is not feasible for these vascular structures to fit into a pre-existing environment if cultured with complex tissues, which prevents vascular remodeling and vasculogenesis²⁵. 3D self-morphogenesis vascularization approaches on the other hand, rely on spontaneous vascularization of ECs through angiogenesis²⁵ or vasculogenesis¹¹⁷, in response to gradients of growth factors³⁷⁰, matrix properties⁷⁶, and co-culture with certain cell types^{25, 26, 256}. Several groups were able to employ 3D self-morphogenesis complemented by microfluidic design to generate perfusable fully connected vascular networks for angiogenesis studies, high-throughput drug screening, and spheroid vascularization^{25-27, 117, 260, 371}.

Microfluidic-based spheroid vascularization platforms that rely on self-morphogenesis have been successful in generating perfusable vasculature that invades the spheroids and connects its lumen to side channels with defined inlets/outlets, but these platforms are yet to be explored for brain organoid vascularization^{25, 26, 117, 372, 373}. In the hLF spheroid model by Nashimoto *et al.*, spheroids; clumps of cell mixtures of HUVECs and hLFs, are suspended in a hydrogel and added to a middle channel where they reside²⁵. The middle channel is separated with microgrooves from a side channel where additional HUVECs are introduced, which is a common design for *in vitro* vascularization systems^{25, 260, 372}. Fabrication of the microgrooves using cleanroom microfabrication allowed high enough resolution to fabricate 100- μ m microgrooves that were small enough to create tension that prevents hydrogel overflow from the middle channel to side channels to keep them vacant for HUVECs^{25, 260, 372}. However, cleanroom microfabrication is costly, and time consuming, and it is unclear if the system is compatible with brain organoids which are larger in size and less uniform than spheroids^{105, 374}. Paek *et al.* developed a tumor vascularization 3D printed platform where needles inserted in side channels block liquid overflow from a middle channel where spheroids suspended in a hydrogel are introduced²⁶. The hydrogel is then polymerized, needles are removed, and ECs are added to the side channels²⁶. This configuration also supported the formation of perfusable vascular networks, however, the workflow is complicated by the needle insertion/removal step, which is

laborious and halts experimental throughput.

Additionally, in most examples of *in vitro* vascularization such as the two examples above, cell types with strong angiogenic profiles (*i.e.* cancer cells and fibroblasts)³⁷⁵ are incorporated in co-culture with the ECs and/or the spheroid to induce vascularization^{25, 26}. Introducing those cell types might not enable investigating factors that influence vascular events in microenvironments where those cell types may not be available such as early vascular development³²⁰. In addition, deparameterized investigation of pro-angiogenic pathways activated by human neuronal cell secretions could be elucidated via co-culture of HUVECs and neuronal spheroids or organoids using *in vitro* microphysiological systems of the vasculature. For instance, Osaki *et al.* developed a microfluidic platform for vascularization of motor neuronal spheroids (MNS) that showed enhanced neuronal activity and increased neurite length upon co-culture of MNS with iPSC-derived ECs. The authors attributed the findings to paracrine signaling of BDNF and juxtacrine signaling of delta-notch pathway within their co-cultures, which play a role in VEGF secretion and neuroprotection and maturation²⁷. While the ECs formed perfusable vascular networks, most of which however, surrounded the MNS outer space instead of fully invading them. In comparison to brain organoids, which are typically larger in diameter than spheroids and capable of unique 3D self-organization^{10, 27, 140}, the MNSs were specifically chosen to be no larger than 200 μm in order to prevent hypoxia and cell death that could develop in their core if they exceed that theoretical size limit. Vascularization of hypoxic brain organoids within microphysiological systems of the vasculature requires further investigation.

Here we report an “organoid-on-a-chip” PDMS devices made from 3D printed molds for microfluidic-based organoid vascularization (MOV) of MOs. The MO model was chosen for this proof of concept study because it is one of the less heterogeneous and more uniform shaped brain organoid models in our experience. Additionally, MOs are promising models to study neurodegeneration and vascular pathology is a key contributor to two most common neurodegenerative diseases; AD and vascular dementia^{15, 135}. The MOV device comprises a middle chamber where the organoid is added, connected by capillary stop valves (CSVs) to side channels where ECs are introduced. CSVs; microfluidic elements that prevent liquid flow when there is an abrupt change in channel height, are incorporated to prevent hydrogel overflow from the organoid channel to the side channels to keep them

vacant for ECs. Our group previously demonstrated the ability to fabricate functional CSVs using 3D printing and have characterized height difference effect on CSV success rate^{105, 376}. The significance of our approach in using 3D printed CSVs is by offering a robust, cost-effective, and time efficient fabrication that can be applied for hydrogel patterning with a universally applicable workflow for microfluidic vascularization platforms for various types of organoids or spheroids. We show that 3D printed CSV structures are capable of retaining fibrin-collagen hydrogels with and without the addition of microgrooves and remain functional while tolerating 3D printing resolutions greater than a 100 μm , thus overcoming the need for highly precise cleanroom fabrication or laborious hydrogel patterning steps.

In addition, we fabricated PDMS funnel structures from 3D printed molds to overcome challenges identified with loading organoids safely into MOV devices. The funnel structures prevented hydrogel leakage from the pipette tip due to misalignment with the middle chamber well, and protected against organoid damage, and organoid floating during the loading process. These challenges have not been discussed in literature to our knowledge and we suspect that they may be unique to organoid-on-a-chip applications given that the 3D self-organizational abilities of organoids change their cellular density compared to spheroids and other tissue constructs.

Additionally, we tested vascularization protocols for MOs by modifying previously published protocols by our collaborators and others^{6, 201}. First, as a priming step MOs were embedded with a hydrogel shell with suspended HUVECs for two weeks before introducing them into MOV devices for co-culture with additional HUVECs in side and/or middle channels. We tested media formulations that included the addition of VEGF as a pro-angiogenic factor, and/or Alk-fc1 to a mix of endothelial and MO media³⁷⁷. Alk-fc1 was added as a potential neuroangiogenic molecule given its involvement in the TGF β pathway that is necessary during vascular development and CNS vascularization³⁷⁷.

Our results showed partial integration of CellTracker-labeled HUVECs into GFP-expressing MOs when cultured in a hydrogel-shell format. Additionally, vascular sprouting was observed in response to co-culture of HUVECs with MOs in MOV devices, which was not observed in monocultures of HUVECs in the device. Partial formation of vascular-like walls that temporarily retained 40-kDa dextran was possible upon co-culture using this approach. Vascular-like lumens were

connected to the side channels, which allowed partial perfusion.

In addition, time-course characterization for hypoxia and necrosis development in control MOs showed development of a necrotic core once organoids reached 1 months in culture. Overall, 3D printing technology coupled with microfluidic CSV elements is a promising avenue for developing a vascularization platform for brain organoids. Our results demonstrate that MOV devices allow for monitoring phenomena related to vascularization events.

6.3 Methods and Materials

6.3.1 Fabrication of microfluidic-based organoid vascularization devices

Design of microfluidic-based organoid vascularization devices: 3D positive molds of the device were designed using SOLIDWORKS 2018. The design includes a middle chamber ($h=150\text{ }\mu\text{m}$, $w=2.7\text{ mm}$) where the organoid resides, and two side channels ($h=450\text{ }\mu\text{m}$, $w=300\text{ }\mu\text{m}$, $l=9\text{ mm}$) where HUVECs are introduced, where h is height, w is width, and l is length of those features. Each channel is connected to one side of the middle chamber through five microchannels of CSVs of dimensions ($h=150\text{ }\mu\text{m}$, $w=150\text{ }\mu\text{m}$, $l=300\text{ }\mu\text{m}$). CSVs are necessary for confining hydrogel patterning to the middle chamber where the organoid resides and vascular sprouting occurs in 3D, while preventing undesired hydrogel overflow to side channels, thus maintaining the side channels vacant for subsequent introduction of HUVECs and growth media. An alternative design of the same device but with a continuous capillary stop valve (cnCSV) instead of the five individual CSVs to test a cnCSV version of the MOV device (cnCSV-MOV) configured with seal surfaces of either glass or PDMS, as shown in configurations D and E in (Table 5). Height difference ($450\text{ }\mu\text{m}-150\text{ }\mu\text{m}=300\text{ }\mu\text{m}$) between the middle chamber and the side channels for both MOV and cnCSV-MOV devices was chosen based on previous work, which showed that the optimal height difference between two adjacent microfluidic channels required for CSVs is $300\text{ }\mu\text{m}$ ¹⁰⁵. The width of CSVs in the main design was set to $150\text{ }\mu\text{m}$ to minimize the time required for HUVECs to coat the walls of the CSVs before sprouting into the hydrogel, while operating at the lowest reliable resolution of our 3D printer. The molds were designed to have a 3.5-mm thick base, which was necessary to avoid upward warping during the post-treatment process of the 3D printed mold.

3D printing and post-treatment of positive molds: A digital light processing 3D printer

(MiiCraft Ultra 100, MiiCraft) was used with BV-002A resin (MiiCraft BV-002A Black, Creative CAD Works) to 3D print positive molds of MOV and cnCSV-MOV devices. 3D printing settings were optimized through printing a range of channel diameters and varying exposure time. The final optimized settings used to 3D print the molds include: 50 μm layer thickness, slow speed, 1.32 s exposure time per layer, 4 buffer layers, 1 base layer, and 65 s base exposure time. 3D printed molds were then post-treated to remove excess uncured resin, as follows. Molds were cleaned with isopropanol/IPA (A416P-4, Fisher Scientific) then dried using a nitrogen (N_2) spray gun. Molds were then immersed in IPA, placed on a shaker for 15 mins, and dried again with the N_2 spray gun. This IPA cleaning process was repeated three times. Dried molds were then placed in a UV chamber (InterllyRay 600, UViTron International) and exposed to UV light at 100% power for 2 mins on each side of the mold, to polymerize any small amounts of excess resin that could not be removed using IPA. Molds were then placed in a 60°C oven for 12-16 hrs to evaporate and/or polymerize any residual chemicals from the cleaning process. This final step was crucial for successful PDMS replication from 3D printed molds and prevented the formation of a sticky layer of uncured PDMS on top of the mold and PDMS device.

PDMS replication from 3D printed molds: Next, MOV and cnCSV-MOV devices were fabricated by replica modeling of PDMS devices from the 3D printed molds. PDMS (SYLGARD™ 184 Silicone Elastomer Kit, DOW) was prepared with 1:10 crosslinker to base ratio, mixed, and poured onto the molds. PDMS was then degassed using vacuum desiccation until bubbles disappeared and was left to cure in a 60°C oven for >12 hours. Cured PDMS devices were released from the mold using a blade knife and 7-mm inlets/outlets for side channels were punched according to the layout in (**Fig. 27a**) using limited reuse biopsy punches (World Precision Instruments). The organoid well and inlets/outlets of the middle chamber were punched using heavy duty 2-mm and 3-mm reusable rapid biopsy punches (World Precision Instrument), respectively, to ensure cutting smooth cylindrically uniform wells, which was difficult to achieve for small punch sizes with limited reuse biopsy punches. Edges of the PDMS devices were then trimmed using a paper cutter (Swingline Paper Cutter 12" 9312, Amazon) to enable trimming multiple devices at once and to ensure flat edges of the device, which, if not flattened, can prevent a tight bond when sealing the devices.

Sterilization and plasma bonding MOV-devices with a seal cover: To prepare devices for assembly and seeding, scotch tape was used to remove dust or PDMS specs from devices. Devices were then sonicated in 70% ethanol solution at RT for 15 minutes to rinse off residual specks. The solution was then replaced with new 70% ethanol and devices were immersed in it for 12-16 hrs to extract uncured PDMS oligomers. Next, devices were placed in MilliQ-water and wet autoclaved at 120°C with a 15-min sterilization cycle. All subsequent steps were done under a biosafety cabinet and devices were kept covered in sterile boxes if placed outside the BSC. Devices were then dried using an N₂ spray gun. Three devices and three 25×75mm pre-cleaned plain glass microscope slides (12-550-A3, Fisher Scientific) were placed in a lid-covered petri dish, with device features side up, and plasma treatment (PE-50, Plasma Etch) was performed for 2 min and 30 s at 100% power. Covering the petri dish during plasma treatment (PT) did not prevent surface functionalization, although longer PT was needed than when the dish was left uncovered. Immediately after PT, PDMS devices were bonded to glass slides, and placed in pipette boxes for dry autoclaving at 120°C with a 15-min sterilization cycle. Autoclaved devices were left at RT for 24 hrs to allow sufficient time for hydrophobic recovery of PDMS.

Alternative assembly of MOV and cnCSV-MOV devices with various seal covers: As alternatives to bonding a glass slide seal with MOV devices as previously described, we tested the use of PDMS-spin coated glass slides to seal either MOV devices or cnCSV-MOV devices, and the use of glass slides to bond cnCSV-MOV devices, and tested fluidics for each configuration. To spin coat PDMS onto glass slides, a 1:20 crosslinker to base PDMS mixture was prepared, and poured on the middle of a 25×75mm glass slide. The slide was placed in a spin coater (WS-650-23B Spin Coater, Laurell) and spun at 500 RPM for 20 s. Spin-coated slides were then cured at 60°C for >12 hrs. Devices were then assembled by placing each PDMS device on top of a cured PDMS-spin coated glass slide, relying on physical interaction of the two PDMS layers to seal the device.

6.3.2 Fabrication of funnel structures for organoid pipetting

The same process of design, 3D printing, post-treatment, PDMS replica molding, and sterilization process used to generate MOV devices, excluding plasma treatment and bonding steps, was applied to fabricate PDMS funnel structures from a positive mold of an array of 20 funnel

structures (**Fig. 28d and Fig. S1**). The middle of each PDMS replicated funnel was punched using a 2-mm reuse biopsy punch, to create an inlet for pipetting an organoid into the middle well.

6.3.3 Fluidic tests and diffusion experiments

Fluidic properties of fabricated and assembled MOV and cnCSV-MOV devices were tested for five configurations of device and seal treatments (**Table 5**). To determine functionality of CSVs and cnCSVs, a fibrin-collagen hydrogel was prepared on ice, with the same concentrations used for device co-culture and shell embedding experiments throughout this report: 2.5 mg/mL fibrinogen (F3879, Sigma Aldrich), 0.5 U/mL thrombin (T6634, Sigma Aldrich), 0.2 mg/mL collagen I (354249, Corning), and 0.15 IU/mL aprotinin (A3428, Sigma Aldrich). A mixture of red food dye and growth media was used for the final top up volume when preparing the hydrogel to visualize its flow into devices. The hydrogel was pipetted into the middle chamber and left to polymerize for 30 mins at 37°C. Zoomed images were acquired using a digital camera to document hydrogel retention within the middle chamber for each configuration.

To characterize diffusion of molecules from side channels into the fibrin-collagen hydrogel network, experiments were performed using a fluorescent dextran molecule (Dextran Texas Red MW 40,000, Invitrogen™ D1829) prepared with PBS at a final concentration of 30 µg/mL. A fibrin-collagen hydrogel of the same composition used throughout this report was introduced into the middle chamber of MOV and cnCSV-MOV devices of configurations A and D, respectively, and left to polymerize for 30 minutes at 37°C. Subsequently, PBS was added to one side channel and the fluorescent dextran solution was added to the other side channel. Live imaging of the device was performed using widefield microscopy to record diffusive transport of fluorescent dextran through the hydrogel. Time-lapse images of dextran diffusion were generated and analyzed.

To calculate the diffusion coefficient of 40-kDa dextran through fibrin-collagen, fluorescent signal was measured using ImageJ by drawing vertical lines on the hydrogel region, during diffusive transport, starting at the edge of the side channel to the middle of the hydrogel-filled chamber. Measurements were taken at a fixed time point ($t=400$ s) and signal intensity (grey value) was exported in relation to position within the hydrogel (µm). Grey values were converted to concentration (µg/mL) using the fluorescent signal of dextran at the first second it filled the side channel as reference for the

dimensional analysis, assuming the initial concentration (C_0) is 30 $\mu\text{g/mL}$, which is highest prior to diffusion. Background signal was measured from the point furthest to the side channel at the first instant of introducing the dye, and subtracted from sample grey values prior to plotting. Quantification of the diffusion coefficient was performed by fitting signal intensity using the error function for 1D diffusion (**Fig. S2b**).

6.3.4 Endothelial cell culture

HUVECs were purchased from Lonza (C2519AS and C2519A, Lonza) and HUVECs expressing mCherry- α -tubulin (mChr-HUVECs) were provided by our collaborator (A. Hayer, McGill University, Montreal, Canada). HUVECs were cultured in EGM-2 (CC-3162, Lonza) unless stated otherwise for co-culture experiments, and passages 4-6 were used for experiments. mChr-HUVECs were cultured in EGM-2 supplemented with 50 $\mu\text{g/mL}$ Hygromycin B Gold (ant-hg-1, InvivoGen) as a selective agent against non-transduced cells, and passages 10-12 were used for experiments. Cell maintenance and subculture were performed according to HUVEC culture protocols provided by Lonza, using EGM-2 and ReagentPackTM Subculture Reagents (CC-5034, Lonza).

6.3.5 Midbrain organoid generation

Control MOs: Midbrain organoids (MOs) were generated from two independent healthy control iPSC lines, including: AIW00202 iPSC line reprogrammed from Peripheral Blood Mononuclear Cells (Montreal Neurological Institute, McGill University), and a fluorescent ACIS36 iPSC lines expressing EGFP inserted at safe harbor locus (AAVS1), reprogrammed from fibroblasts (GM25256, Coriell). **Control MOs** generated from the AIW00202 iPSC line (AIW-MO) and MOs generated from the ACIS36 iPSC line (GFP-MO) were differentiated according to the same established protocol by our collaborators (Montreal Neurological Institute, Montreal, Canada) as follows²⁰¹: iPSC lines were cultured and maintained in mTeSRTM1 medium (05851/05852, STEMCELL Technologies). At 70% confluency, iPSCs were dissociated and seeded into an ultra-low attachment 96 well U-bottomed plate (CLS7007, Corning), at 10,000 cells per well, with neural induction medium to form EBs. After 48 hrs media was switch to neural induction medium without ROCK inhibitor and maintained for additional 48 hrs. On day 4 of the protocol, media was switched to midbrain patterning medium and EBs were maintained until day 7. Next, EBs were embedded in growth factor-reduced

Matrigel® (356230, BD Biosciences). On day 8, embedded EBs were transferred to final differentiation medium (FDM) and maintained with orbital shaking at 70 RPM (Mini-100 Orbital-Genie, SI-M100, Scientific Industries) for the rest of the culture period. Composition of FDM is provided in **(Table S1)**. Composition of neural induction medium and midbrain patterning medium is detailed in previous published work²⁰¹. Given previous results by our collaborators Vi *et al.* that neuroepithelium becomes more developed on day 8 using this protocol²⁰¹, counting of midbrain organoid days in culture in this work starts with day 8 which is the first day in FDM, referred to as FD-1.

MOs for vascularization: MOs used for vascularization experiments followed the same protocol as control MOs up to day 7, where instead of Matrigel® embedding, MOs were maintained without any hydrogel embedding up to FD-9, with orbital shaking at 40 RPM. Similarly to control MOs, FDM was added to non-embedded MOs on FD-1 (day 8 of the protocol) and maintained up to FD-9, to allow sufficient time in FDM to develop midbrain identity prior to vascularization experiments. On FD-10, non-embedded MOs were used in two experimental formats: **1) MOs were directly introduced into devices with HUVECs or mCh-HUVECs:** MOs were prepared with a mixture of fibrin-collagen and HUVECs or mCh-HUVECs, and immediately introduced to MOV devices for co-culture with additional HUVECs or mCh-HUVECs added to side channels. **2) MOs were cultured with a shell of HUVECs first then introduced to devices:** MOs were embedded in a 30 µL mixture of fibrin-collagen made with the composition previously described but with added HUVECs (100,000 cells per hydrogel) to form a “vascular shell” surrounding MOs (shell-MO). The mixture of organoid, HUVECs, and fibrin-collagen was seeded in an ultra-low attachment 96 well U-bottomed plate, and incubated for 1 hr at 37°C/5% CO₂ to allow the hydrogel to polymerize and for HUVECs to adhere to the hydrogel/organoid mix. Next, 200 µL of growth media was added to top up polymerized shell/MOs. The top media compositions tested for this step include a 1:1 ratio of FDM to EGM-2 supplemented with 15, 20, and 30 ng/mL of VEGF (01-185, EMD Millipore). Two days after the initial seeding, shell/MOs were placed on an orbital shaker at 40 RPM and cultured for ~2 weeks (up to FD-22), and were then introduced to MOV devices for co-culture with additional HUVECs.

Bright field micrographs for size tracking were collected for organoids at FD3, FD7, FD14, FD18, and FD22. Measurements were taken in ImageJ using the measure function and drawing two

lines in the shape of an X across the middle long axis of the organoid. The two line measurements for each organoid were averaged and final measurements of n=3 organoids per conditions were averaged and plotted chronologically. Growth rates for organoids were calculated from slope values of linearly approximated trend lines for each condition.

6.3.6 Midbrain organoid and endothelial cell seeding in MOV devices

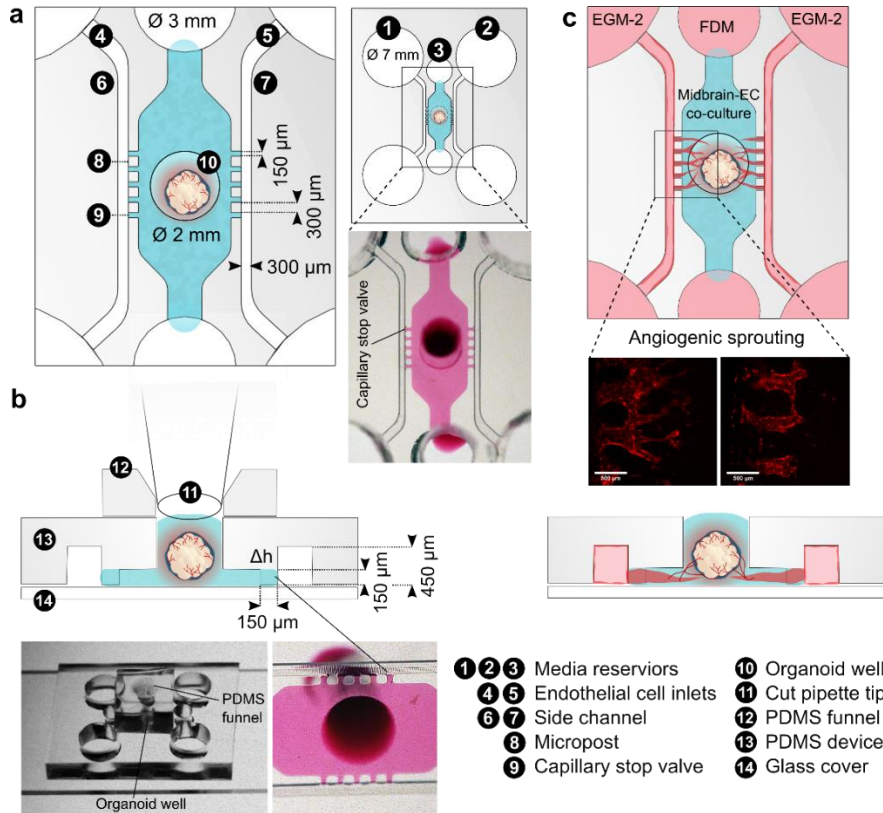


Fig. 27: overview of MOV device design and operation. (a, b) MOV device design enables loading a hydrogel-MO mixture into a middle chamber through a middle well #10, as a first step. Capillary stop valves #9 and surface properties of the device, characterized by a glass slide #13 plasma-bonded to PDMS #14, and hydrophobic recovery, prevent hydrogel overflow to side channels #4 and #5. A cut-tip pipette #11 fits tightly into a PDMS funnel #12 positioned on top of the middle well, allowing successful loading of MOs into the middle chamber. (c) HUVECs are loaded into each side channels and allowed to adhere to the hydrogel-filled microchannels, followed by addition of media (EGM-2 and FDM) or desired media combinations to each channel. Vascular sprouting of HUVECs into the middle chamber is monitored and long-term co-culture of MOs and HUVECs is maintained.

MOs or shell/MOs were seeded in MOV devices (configuration A) either at FD-9 or at FD-22 after co-culture with a shell of HUVECs in fibrin-collagen, respectively. In both culture formats, using a pipette with a cut tip, MOs or shell/MOs were added to a tube, and prepared with a 20 µL fibrin-collagen hydrogel of the composition previously mentioned in (Section 6.3.3.) mixed either with or without additional HUVECs (50,000 cells per hydrogel) to be added to the middle chamber. The organoid/HUVEC hydrogel mixture was prepared on ice to prevent the hydrogel from polymerizing prematurely. PDMS funnels were aligned on top of organoid wells prior to seeding, and were stably fixed on top due to physical interaction of PDMS from the funnel and device.

As illustrated in (Fig. 27), a cut-tip pipette was used to introduce the organoid into the device

by tightly positioning the cut tip in the PDMS funnel before releasing the organoid/HUVEC hydrogel mixture into the middle chamber. Devices were incubated for 1 hr at 37°C/5% CO₂ to allow cells to settle and the hydrogel to polymerize. Next, a 10 uL suspension of HUVECs (100,000 cells in 10 uL of EGM-2) were added to the inlet edge of one side channel. Due to hydrophobicity of the device, the cell suspension solution remains at the inlet edge initially. The glass slide-bonded device is then oriented vertically, and gently tapped twice on a plastic flat surface to provide a small mechanical force that allows flow of the cell suspension into the channel. Next, MOV devices were tilted 90° and incubated for 1 hr at 37°C/5% CO₂ in the horizontal direction, such that the HUVEC cell suspension would be positioned on top of hydrogel-filled CSVs. This incubation method promotes attachment of HUVECs to the hydrogel side, in order for them to sprout promptly in that direction. The same method was repeated to add HUVECs to the other side channel. Finally, media was added to fill the inlets of the device, and was left to drain to fill the outlets before refilling the inlet again. **Media introduced to MOV devices includes either: 1)** 1:1 ratio of EGM to FDM supplemented with 15, 20, or 30 ng/mL VEGF and/or supplemented with 15, 20, or 30 ng/mL ALK-1 Fc (370-AL, R&D systems) introduced to all inlets, **or 2)** adding FDM to the middle channel inlets and placing a droplet of FDM on top of the organoid well, while adding EGM-2 to side channels. MOV devices were kept in sterile 4-well rectangular well plates (1228D90, Thomas Scientific), and incubated flat without tilting for the rest of the culture period. Media change was done every 48 hrs by removing media from outlets and allowing it to completely drain before refilling inlets.

6.3.7 Freezing and cryosectioning organoids

Freezing and cryosectioning MO samples was done according to established protocols²⁰¹. Prior to freezing, MOs were fixed in a 4% PFA solution (28906, Thermo Scientific), for 12-16 hrs at 4°C. Next, MOs were washed 3 times in PBS 1x. Samples were then incubated with a 20% (w/v) sucrose (84097, Sigma-Aldrich) solution at 4°C for 1 day, where sucrose acts as a cryoprotectant agent and enables organoids to sink to the bottom of cryomolds. Next, organoids were transferred to cryomolds (22-363-553, Fisher Scientific) using a cut-tip pipette. Excess sugar solution was pipetted out of cryomolds and residual droplets was dried using KimTech™ wipes. To embed MOs in blocks, Tissue-Plus™ optimal cutting temperature (OCT) medium (23-730-571, Fisher Scientific) was poured

onto the cryomold in a concentric motion from the center. When required, a needle with a bent-tip was used to adjust the position of organoids. To freeze OCT blocks, liquid N₂ was poured to fill 1/3rd of a Styrofoam box with a levitated part, where cryomolds were placed in the gas phase. Within 15 mins, OCT blocks froze completely and were transferred to a -80°C freezer for long-term storage.

Cryosectioning was performed using a Thermo Scientific CryoStar NX70 Cryostat at the (EDDU, Montreal Neurological Institute, Montreal, Canada). Cryomolds were removed from -80°C and were left to equilibrate temperature in the cryostat for 30 mins. To mount blocks on the sample holder, OCT was poured on the holder and the block was pressed on the OCT, with the side closer to organoids facing up. Once frozen, excess OCT was trimmed from the mount using a razorblade. The mount was then placed in the microtome head and 16 µm sections were cut, and picked up on RT Superfrost™ Plus microscope slides (12-550-15, Fisher Scientific). Slides were left to dry for 1-12 hrs at RT then moved to a -20°C freezer for storage.

6.3.8 Immunofluorescence staining and live cell labeling

Immunofluorescence staining was performed according to published work²⁰¹. To summarize, slides were first labeled using a hydrophobic barrier pen to surround cryosections that will be immunostained. Next, cryosections were rehydrated in PBS 1x for 15 mins. PBS was then removed and samples were incubated at RT for 1 hr with a blocking/permeabilizing buffer with the following components: 5% normal donkey serum (017-000-121, Jackson ImmunoResearch), 0.05% bovine serum albumin (821006, Sigma-Aldrich), and 0.2% Triton X-100 (T9284, Sigma-Aldrich), prepared in PBS 1x. Subsequently, primary antibodies were prepared in a blocking buffer of the aforementioned composition and incubated with samples at 4°C for 12-16 hrs. Samples were then washed three times in PBS 1x, for 15 mins each time. Next, samples were incubated with secondary antibodies prepared in blocking buffer for 1 hr at RT. Samples were washed again, three times in PBS 1x, for 15 mins each time. Nuclear stains (either Hoechst or DAPI) were prepared in PBS 1x and incubated with samples for 10 mins, followed by washing once in PBS for 5 mins. Next, Aqua-Poly mounting media (18606, polysciences) was added on top of cryosections and a coverslip was placed on top of the mounting media. Bubbles were removed by gently pressing on the coverslip using tweezers and mounting media was left to dry overnight.

For hypoxia and cell death characterizations, immunofluorescence staining was performed as aforementioned using the following primary antibodies: HIF1 α ; goat polyclonal IgG (AF1935, R&D systems) at 10 μ g/mL, and CC3; rabbit monoclonal IgG (9664L, cell signaling) prepared at 1:200. Secondary antibodies used for detection include: Chicken anti-goat IgG; Alexa Fluor[®] 647 (A-21469, Thermo Fisher); prepared at 10 μ g/mL to detect goat anti-HIF1 α , and donkey anti-rabbit IgG; Dylight[®] 488 (ab96891, Abcam); prepared at 1:200 to detect rabbit anti-CC3. Characterization of cellular DNA fragmentation was performed using Click-iT[™] Plus TUNEL Assay; Alexa Fluor[®] 647 (C10619, Thermo Fisher), according to provider manual. Hoechst 33342 (62249, Thermo Fisher) and DAPI (62248, Thermo Fisher) were used as counterstains, according to provider recommendations.

Live cell labeling was performed using CellTracker[™] (CT) dyes (Thermo Fisher) according to provider instructions. For co-culture experiments, and prior to introducing a HUVEC shell to MOs, where mentioned, FD-9 AIW-MOs were labeled using 1- μ M CT Green CMFDA dye (C2925, Thermo Fisher) prepared in 37°C FDM, incubated for 45 mins in a 37°C/5% CO₂ incubator while shaking at 40 RPM. The dye solution was then replaced with fresh FDM. Where mentioned, HUVECs comprising the fibrin-collagen shell surrounding MOs were labeled using 1- μ M CT Orange CMRA dye (C34551, Thermo Fisher), and HUVECs comprising side channels and additional HUVECs added to the middle chamber were labeled using 1.5- μ M CT Deep Red dye (C34565, Thermo Fisher). To label HUVECs, 80% confluent HUVECs that were plated in T25 or T75 flasks were washed once with HEPES (CC-5022, Lonza), followed by adding the CT dye prepared in 37°C FBS-free EGM-2 to flasks, and incubating cells for 45 mins at 37°C/5% CO₂. The dye was then replaced with fresh EGM-2. Labeled HUVECs or MOs were used for experiments within 24 hrs of labeling.

6.3.9 Hypoxia and cell death characterization

Characterization of hypoxia and cell death was performed for AIW-MOs at 4 time points: EBs at day 4 of differentiation protocol, 1-week MOs (FD-7), 1-month MOs (FD-28), and 1.5-month MOs (FD-43). For positive controls of hypoxia, 1-week AIW-MOs were cultured in FDM supplemented with 100 μ M Cobalt (II) Chloride (15862, Sigma-Aldrich) for 12-16 hrs in a 37°C/5% CO₂ incubator. Samples were fixated and cryosectioned, as previously described. Hypoxia was characterized by immunostaining for HIF1 α , and cell death was characterized by immunostaining for

CC3 and TUNEL assay. Cryosections from the inner largest part of the organoid, where cell death is expected to be highest were chosen for characterization. Samples (n=3 MOs per time point) were immunofluorescence-stained according to the previously described protocol, and imaged using confocal microscopy (Nikon Eclipse Ti2 Microscope). Lasers: 647 nm, 448 nm, 405 nm, were used to visualize fluorescent signal from HIF1 α , CC3, and DAPI, respectively. Lasers: 647 nm and 405 nm were used to visualize fluorescent signal from TUNEL and Hoechst, respectively.

To determine the spatial distribution of HIF1 α and CC3 within MOs, samples >1.6 mm in diameter that were positive for both HIF1 α and CC3 were chosen for analysis. The samples chosen were from two time points (n=4; 2 organoids per time point); 1 month and 1.5 month in culture, to determine if a spatial trend for hypoxia and necrosis is notably present regardless of time in culture. To determine fluorescence signal of HIF1 α /647 and CC3/448, z-stack max projection tiff images of the two channels were analyzed using the line scan function in ImageJ. Six scan lines per organoid were drawn from different directions across the organoid section to measure fluorescence intensity (y-axis) in terms of distance (x-axis). Intensity values from all six line scans were averaged according to their corresponding distance measurements. Given that organoids are not perfectly symmetrical, certain line scans were longer in one direction across the organoid than other line scans. Thus, Intensity values from longer line scans past a certain distance that does not correspond to any value from other line scans were excluded from analysis. Intensity values with the same distance from the surface of the organoid were averaged for all six line scans per organoid. The final average intensity values for each organoid were binned by averaging intensity values within every 50- μ m distance into one value. Binned intensity values were averaged for all organoids and were graphed against distance ranges of 0-800 μ m and 0-1600 μ m. The same analysis was performed for HIF1 α and CC3.

6.3.10 Fluorescent dye perfusion

To test dye retention within vascular wall-like structures MOV devices, fluorescent 40-kDa Dextran 550 dye (100 μ g/mL) was introduced to one side channel and live-imaged using widefield microscopy. Perfusion experiments were performed for GFP shell-MO co-cultured with HUVECs maintained in 1:1 FDM to EGM-2 media supplemented with 30 ng/mL VEGF for the shell and device stages of culture. Prior to perfusion experiments, Hoechst nuclear counter-staining was performed on

samples that were fixed at FD34 (day 12 post device seeding).

6.4 Results and Discussion

6.4.1 Device fabrication, characterization and optimization

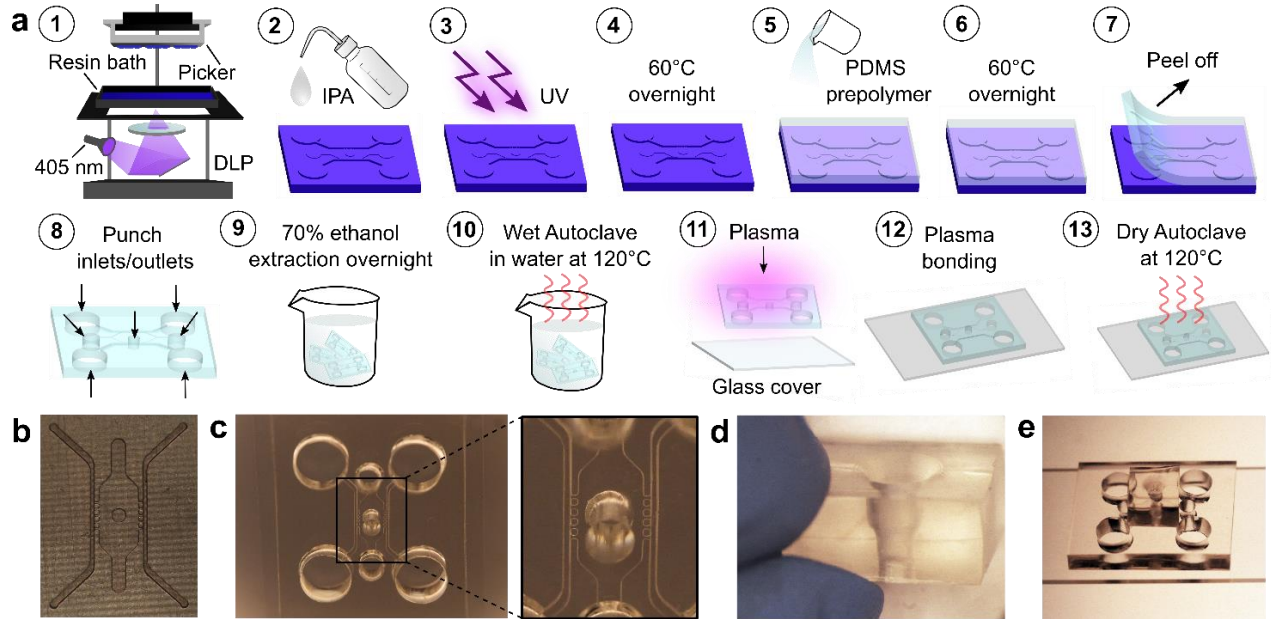


Fig. 28: fabrication, sterilization, and assembly of MOV devices. (a) positive molds are 3D printed (step 1), and post-treated (steps 2-4) to remove residual resin. PDMS is poured on top of devices, cured, peeled, and inlets/outlets are punched (steps 5-8), uncured PDMS is ethanol extracted and devices are sterilized and plasma bonded to a 25×75 mm glass slides (9-13). (b) 3D printed positive mold of MOV devices. (c) glass slide plasma-bonded PDMS device. (d) PDMS funnel structure fabricated from 3D printed positive funnel molds. (e) Final assembled device.

MOV devices, cnCSV-MOV devices, and funnel structures were successfully fabricated by PDMS replica molding from 3D printed positive molds, as shown in (Fig. 28, and Fig. S1). The average size of CSVs of the final MOV device measured from PDMS replicas post-fabrication and post-treatment is 158 μm ($n=3$ devices, 10 CSV measurements per device), which has a 5.5% error from the theoretical value aimed for; 150 μm . Nonetheless, fluidic tests for two configurations of CSVs and one configuration of cnCSVs out of five tested configurations were successful in retaining liquid despite 3D printing errors in microchannel size, as illustrated in (Table 5, Fig. 27b). Success or failure of each configuration was based on each device's ability to retain the hydrogel in all CSVs or cnCSVs of both side channels, for all devices tested ($n=4$). Success of CSVs of MOV devices, despite lower resolution of 3D printed devices compared to cleanroom fabricated ones reported in literature^{25, 260}, suggests that CSV functionality tolerates 3D printing resolution, which allows for advantageous cost-effective fast fabrication of vascularization devices that would otherwise be costly and time-consuming

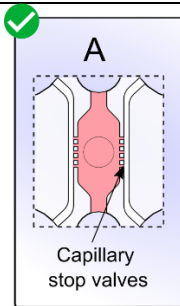
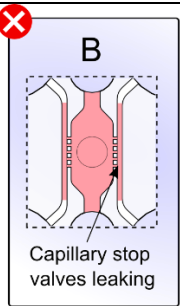
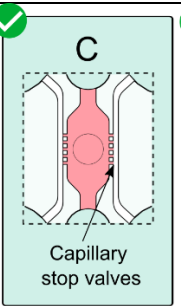
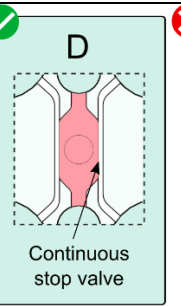
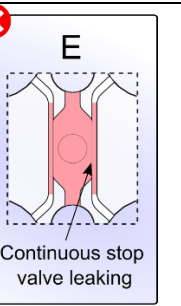
to fabricate using cleanroom methods¹⁰⁵.

Liquid retention in CSVs is a function of both geometry and surface properties of microfluidic channels¹⁰⁵. Since the geometrical property of height difference between the middle chamber and the side channels was consistent across all configurations, the outcome from each variation shown in **(Table 5)** is mainly a reflection of surface properties that allow generating successful CSVs and cnCSVs. Configurations A, C, and D that had either successful CSVs or cnCSVs had alternating hydrophilic properties between the seal covering the device and the PDMS device itself. To alternate surface properties between device and seal for configurations (A-E), we used either a glass slide to allow for a hydrophilic seal, or PDMS spin-coated glass slides for a hydrophobic seal. Hydrophobicity is defined in literature by a water contact angle with a surface that is greater than 90 degrees, and hydrophilicity or wettability of a surface is defined by a contact angle less than 90 degree¹⁰⁵. Assembled devices had differential plasma treatment and/or differential hydrophobic recovery periods of the seal and PDMS device, which further altered surface properties of glass and PDMS across the configurations tested.

Configurations A and B follow the same format where the PDMS device and glass-slide seal are plasma bonded together. However, CSVs of device B failed due to their shorter hydrophobic recovery period. Given that plasma treatment merely increases hydrophilicity of already-hydrophilic glass³⁷⁸, the ‘hydrophobic recovery’ period only restores the hydrophilic level of glass to its original state. On the other hand, plasma-treated PDMS loses approximately 50% of its hydrophilicity 12 hours-post treatment, and restores approximately 80% of its original hydrophobic state by 24 hours^{379, 380}. The surface properties of the PDMS device after the hydrophobic recovery period contribute to liquid retention within CSVs of the middle chamber, while the hydrophilic nature of glass facilitates initial liquid flow into the middle chamber, which prevents liquid trapping due to the low surface energy of PDMS. Had both PDMS device and the seal been hydrophobic, liquid flow into the device would not be possible because the liquid would be trapped in the middle well. Alternatively, when both the PDMS device and glass slide are hydrophilic, as shown in configuration B, where hydrophobic recovery was not applied, the device does not possess sufficient tension to trap the liquid within the middle chamber, due to the high surface energy of both plasma treated PDMS and glass. This

highlights the role of tailored surface properties of microfluidic channels for hydrogel patterning applications.

Table 5: Capillary stop valve function in response to various device configurations

Configuration (A-E)					
	Glass slide seal	Glass slide seal	PDMS spin-coated glass slide seal	PDMS spin-coated glass slide seal	Glass slide seal
Device plasma treated	Yes	Yes	Yes	Yes	Yes
Seal plasma treated	Yes	Yes	No	No	Yes
Hydrophobic Recovery	>12 hrs	<12 hrs	No	No	> or <12 hrs
Capillary stop valves	Succeed	Fail	Succeed	Succeed	Fail

**Note:* Configurations A-C follow the general ‘MOV device’ chip design. The final assembled MOV device throughout this report follows configuration A, unless stated otherwise. Configurations D and E follow the ‘cnCSV-MOV device’ chip design. Capillary stop valve failure was determined based on leakage from at least one capillary stop valve on either sides for any of n=4 devices. Success rate was determined based on full hydrogel retention in capillary stop valves connected to both channels for all n=4 devices.

In configurations C and D, either a CSVs or a cnCSVs plasma treated PDMS device was assembled with a PDMS spin-coated glass slide seal. The two configurations were used for fluidic testing within one-hour of fabrication without extended periods of hydrophobic recovery. In this format, the PDMS spin-coated seal contributes to liquid retention, and high surface energy of the plasma treated PDMS device contributes to the initial liquid flow into the middle chamber.

Although similar in design to configuration D, the PDMS device in configuration E is instead plasma bonded to a glass slide. The hydrophilic glass slide leads to leakage to side channels regardless of the hydrophobic recovery period. Given that configuration A where the glass seal and device were similarly plasma bonded was successful, configuration E failure after >12 hrs of hydrophobic recovery indicates that microgrooves in CSVs contribute to improved liquid retention, suggesting that the cnCSV format is potentially less versatile in terms of seal covers that could be used. Additionally, PDMS spin coating on glass slides creates an additional, albeit thin, layer between the bottom of the device and the magnification lens used during microscopy, which slightly reduces the maximum z-plane that can be reached while imaging intact brain organoids. Imaging through the z-plane is valuable for experiments involving brain organoid vascularization given that organoids could grow to a

millimeter-range size, and the need for monitoring vascular invasion into the organoid at various planes.

Nonetheless, a possible biological benefit of the cnCSVs format, as opposed to microgrooves, is the larger hydrogel surface area for ECs to attach to during the first step of seeding. This could potentially accelerate vascularization by increasing the number of sprouting ECs that interact with factors secreted by organoids in the middle chamber early in the protocol. Additionally, an increased number of ECs would have a higher amount of secreted biomolecules per milliliter of media should that be of interest for drug testing or biomarker discovery applications. Biological significance of cnCSV-MOV device design in comparison to microgroove CSVs is yet to be demonstrated, as no report has compared the two formats methodically to our knowledge.

Separate reports of both microgroove CSVs and a continuous EC side channel were able to induce vascular sprouting of ECs²⁵⁻²⁷. However, while the design reported by Paek *et al.* achieves the same outcome of the cnCSV-MOV device in terms of hydrogel patterning, it does not represent a cnCSV in its technical definition since the authors used needle tips to block the side channels to prevent hydrogel leakage²⁶. Whereas, a true cnCSV is able to prevent hydrogel overflow to side channels autonomously. The presented cnCSV-MOV device design concept thus offers the advantage of simpler hydrogel patterning steps and potential for high-throughput applications that would be challenging to achieve with complicated seeding steps.

Further improvements of the cnCSV-MOV device could include optimizing hydrophobic surface functionalization while eliminating the PDMS-spin coating, which can improve optical properties of the device. In addition, fabricating a permanently hydrophilic PDMS device would allow longer storage periods of the device without requiring plasma treatment prior to seeding. While fabrication of MOV device of configuration A requires an additional day to allow hydrophobic recovery, cnCSV-MOV device of configuration D and MOV device of configuration C have a shorter fabrication protocol since they do not require a 12-hour hydrophobic recovery period. However, MOV device of configuration A was chosen over configurations C and D for co-culture experiments in this report because the hydrophobic recovery period can be extended to 72 hrs post-fabrication without influencing CSV fluidics, allowing more flexible experiment scheduling that is advantageous when

working with multiple cell types that proliferate according to different protocols.

Funnel structures were fabricated using PDMS replicated from 3D printed molds, to facilitate loading MOs safely into MOV devices, as illustrated in (**Fig. 28d, and Fig. S1**). Pipetting MOs into the middle chamber using a cut-tip pipette directly without using funnels caused MOs to break apart in two out of four co-cultures in MOV devices, as shown in (**Fig. S1a**). Further challenges in pipetting organoids safely without a funnel support caused by slight misalignment of the pipette with the middle well inlet, occasionally resulted in overflow of the hydrogel to the top layer of the PDMS device. This could lead to loss of cells embedded in the hydrogel, overflow of the organoid outside the well, or cause the organoid to float within the middle well instead of sedimenting to the bottom of the device, as illustrated in (**Fig. S1a**). The PDMS funnel, when positioned on top of the middle well prior to seeding, remained stable, due to the slightly adherent tendencies in physical interaction between the two PDMS layers. A cut-pipette tip was able to fit tightly into the funnel well, which prevented hydrogel overflow to the top of the PDMS device. MOs pipetted with support of funnels did not break apart and sedimented to the bottom of the device. Sedimentation to the bottom of the device is essential for vascularization because it allows the organoid to remain in close proximity to HUVECs that sprout from the bottom part of the device upwards, as shown in (**Fig. 27c**). Since long-term culture of brain organoids without vascularization leads to cell death at their core^{10,20,216}, vascular invasion must occur in a timely fashion before cell death occurs, which must be permitted by device design.

To determine diffusivity of molecules, such as growth factors and signaling biomolecules, within the fibrin-collagen hydrogel network, 40-kDa fluorescent dextran (Texas Red) was used for diffusion experiments. Molecular weight of 40-kDa was chosen for dextran to mimic the size of VEGF (~44 kDa)³⁸¹; a crucial pro-angiogenic growth factor. Approximating diffusion of dextran in the hydrogel-filled middle chamber to 1D diffusion is justified given that middle chamber is relatively shallow ($h = 150 \mu\text{m}$), the length of the two channels is relatively infinite compared to the region-of-interest where line scan measurements were taken, and the side channel exposed to the hydrogel fills up with the dye solution somewhat instantaneously. However, a short delay in filling the channel causes an initial inclined diffusion front that equilibrates over time in MOV devices, as shown in (**Fig. S2a**). Similar reported models of diffusion in rectangular shallow hydrogel-filled channels have

followed the same 1D approximation³⁷¹. By the 2-hour mark, fluorescent dextran reaches ~2 mm distance through the middle chamber of MOV device, as shown in **(Fig. S2a)**. Importantly, during co-culture of MOs with HUVECs, the hydrogel-MO mixture introduced to the middle chamber is prepared by adding FDM for the top-up volume. Growth factors comprising FDM remain trapped within the hydrogel. Therefore, the MO is not deprived of media during the first hour of diffusive transport, shown in **(Fig. S2a)**. A cnCSV-MOV device of configuration D was chosen to measure dextran diffusion because it was able to avoid signal distortion caused by optical reflection of fluorescence on the CSVs. The diffusion coefficient for dextran in fibrin-collagen was ($D = 35 \mu\text{m}^2/\text{s}$). The diffusion coefficient was quantified by fitting the error function solution for 1D diffusion using the measured fluorescent signal relative to position within the hydrogel at a fixed time point, shown in **(Fig. S2b)**. The diffusion coefficient obtained is on the same order of magnitude of literature values of 40-kDa dextran diffusion in fibrin³⁸².

6.4.2 CellTracker-labeled HUVECs integrate into midbrain organoids

Generation of control and shell-MOs follows previously described protocols, as illustrated in **(Fig. 29a)**. Size tracking of shell-MOs prior to embedding, and Matrigel-embedded controls, showed a more rapid growth rate of a 37% size increase for controls, compared to a 13% size increase for non-embedded MOs, from FD3 to FD7. The size difference between non-embedded MOs and Matrigel-embedded controls becomes significant by FD7. Post-embedding from FD14 to FD22, shell-MOs' sizes remained smaller in comparison to Matrigel-embedded controls, as shown in **(Fig. 29c)**. Growth rate for shell-MOs of condition 3 was 19%, which was comparable to Matrigel-embedded controls that had a 21% growth rate, and nearly double the growth rate for conditions 1 and 2, which were 11% and 8% respectively. Nonetheless, condition 3 MOs were smaller at FD14 compared to the other conditions from start. The increased size of Matrigel-embedded controls compared to non-embedded MOs is also expected since Matrigel provides organoids with a stem cell niche that supports cell attachment and proliferation by facilitating cell-matrix interactions and biophysical signaling^{177, 383, 384}. Size disparities between Matrigel-embedded controls and non-embedded MOs continue after shell embedding, which

is expected given the initially halted growth during the stage where embedding is absent.

Table 6: Media formulations for HUVEC shell/MO conditions shown in (Fig. 29)

Conditions	Media Formulation	Organoid	Shaking
Condition 1	1:1 FDM to EGM +15 ng/mL VEGF	HUVEC shell/MO	40 RPM
Condition 2	Week 1: EGM +15 ng/mL VEGF, week 2: 1:1 FDM to EGM +15 ng/mL VEGF	HUVEC shell/MO	40 RPM
Condition 3	1:1 FDM to EGM +30 ng/mL VEGF	HUVEC shell/MO	40 RPM
Control	FDM Control MO	Matrigel embedded	70 RPM

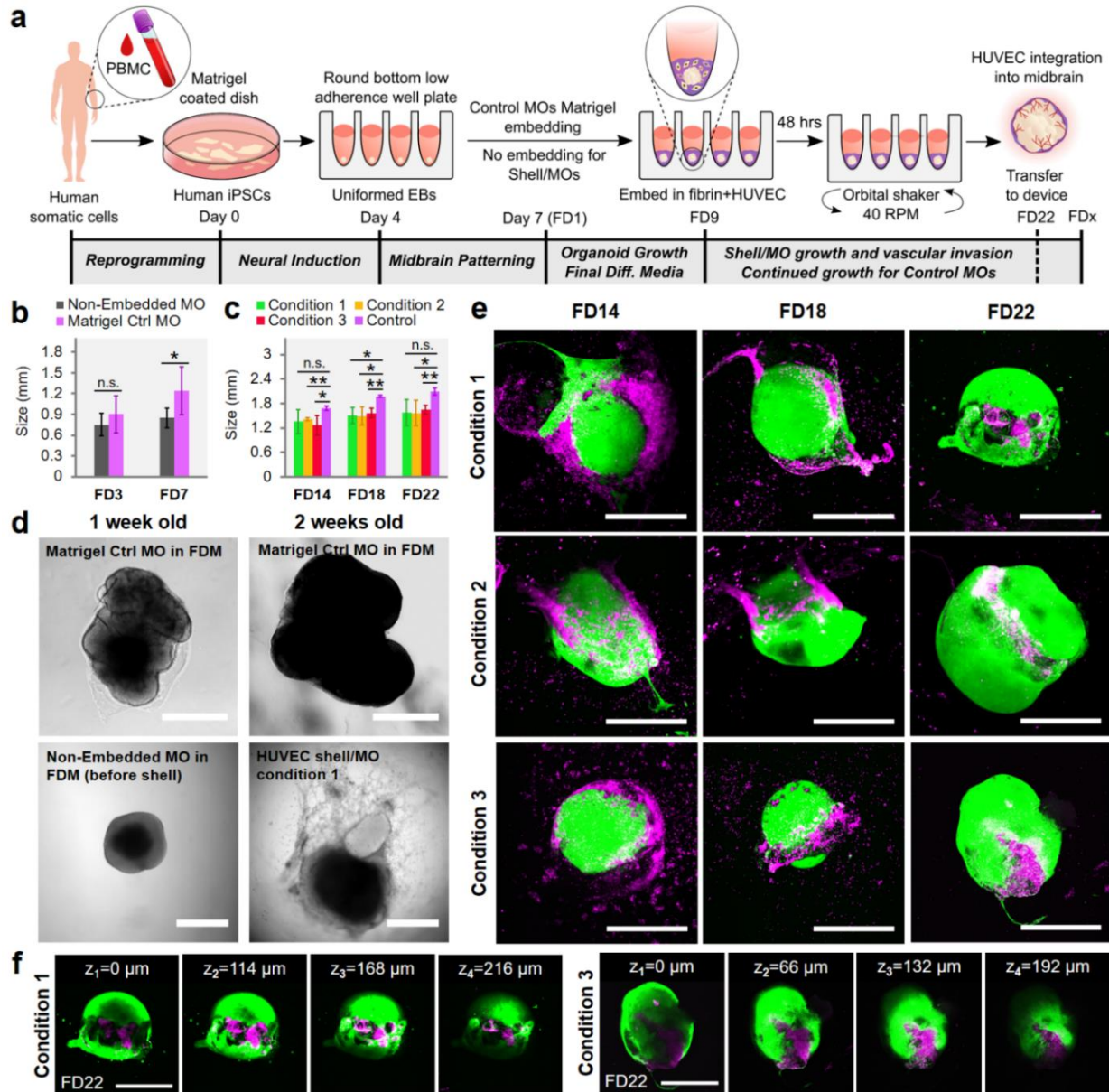


Fig. 29: Characterization of control and shell/MOs for size and HUVEC integration. (a) Protocol for generating Matrigel-embedded control MOs and shell/MOs. *Note:* FD9 and FD22 steps are applicable to shell/MOs for vascularization experiments. Matrigel-embedded control MOs were grown with 70 RPM shaking from FD1 to end of culture. (b) Size comparison of controls, and non-embedded MOs prior to HUVEC shell embedding at FD3 and FD7. (c) Size of shell/MOs under different conditions listed in (Table 2). (d) Bright field micrographs of control MOs, non-embedded MOs, and HUVEC shell/MOs. (e) Z-axis maximum projection of HUVEC shell/MOs at FD14, 18, and 22 under media conditions 1-3. **Fluorescence signal:** GFP-MO (green), CellTracker-CMRA stained HUVECs (magenta). (f) Confocal micrographs of shell/MOs at FD22 shown at separate z planes from bottom to top (z setting: 6-μm steps), showing increased CellTracker-HUVEC signal at the central plane. (b, c) t-test: (*p<0.5, **p<0.01), no significance (n.s). **Scale bars (all):** 1 mm.

Furthermore, FD1 non-embedded MOs cultured without any shaking were observed to completely dissociate into floating cell debris within 72 hrs in culture. This highlights the role of orbital shaking or other means of facilitating mass transport in maintenance of MOs and suggests contribution of higher speed shaking to the increased size of Matrigel-embedded controls compared non-embedded MOs. High speed shaking was avoided for non-embedded MOs to avoid inducing damage to the organoid. The reduced size of non-embedded MOs and shell-MOs compared to controls is not necessarily disadvantageous because hypoxia-induced cell death at the core of brain organoids is proportional to their size^{4, 216}. Smaller sized MOs generated using an accelerated patterning protocol showed reduced central cell death, compared to traditionally generated larger MOs, while preserving midbrain identity²¹⁶.

Animal origin of Matrigel causes high batch-to-batch variability in brain organoids^{252, 384, 385}, which was also observed in our midbrain organoid cultures. Size measurements for both Matrigel-embedded controls and non-embedded MOs were averaged from two separate batches for FD3 and FD7. Matrigel-embedded controls showed higher standard deviation in size than non-embedded controls, as shown in (**Fig. 29b**). Matrigel-induced variability pushed for development of matrix-free brain organoid protocols or synthetic hydrogel embedding protocols with reduced variability^{252, 384, 385}. Brain organoid protocols^{166, 220}, including MO protocols^{21, 207}, successfully replicated molecular identity of each brain organoid model in matrix-free 3D cultures. Protocols for generating matrix-free MOs, only used 2D Matrigel coating during progenitor or iPSC expansion stage similarly to our method for generating ‘matrix-free’, non-embedded MOs^{21, 207}. In this report, non-embedded MOs were able to maintain GFP signal, grow in size, and induce vascular sprouting after device co-culture with HUVECs (**Fig. 30a**). Further work is needed to explore the effects of matrix-free MO culture on organoid identity. However, the sustained growth of non-embedded MOs observed is part of preliminary results exploring matrix-free MO protocols for downstream vascularization attempts. The low growth rate of non-embedded MOs is to be further explored as a method to delay hypoxia and cell death at the core of MOs until vascularization is achieved.

Prior to MOV device co-culture, shell-MOs were embedded in a fibrin-collagen hydrogel in mixture with HUVECs. Fibrin constructs have been shown to enhance survival of neural populations

derived from stem cells^{266, 386}, and support formation of vascular networks in co-cultures^{25, 260}. Fibrin-collagen hydrogels were prepared with defined concentrations for all protein component, which could contribute to reduced variability, despite animal origin of the proteins. On the other hand, concentration of protein components in Matrigel is merely provided in terms of percentage approximations of the expected composition. However, in the presented fibrin-collagen shell embedding method, a unique variability factor could arise from introducing HUVECs into the hydrogel mixture. While the number of HUVECs is counted prior to embedding, pipetting errors could lead to variable numbers of cells introduced to each MO, which represents a potential limitation of the shell-embedding method and other reported brain organoid vascularization methods that require mixing two different cell types prior to long-term culture^{3, 6}.

Three test conditions of shell-MOs were tested along with Matrigel-embedded control MOs, with media variations shown in **(Table 6)**. Integration of CellTracker-CMRA labeled HUVECs into shell-MOs was observed for all test conditions by FD22 with variable degrees, which is two weeks post shell embedding, as shown in **(Fig. 29e, 29f)**. HUVEC integration into shell-MOs is likely to play a role in the reduced size of shell-MOs in comparison to Matrigel-embedded controls through means of MMP induced basement membrane degradation, which is a precursor for vascular invasion *in vivo*. However, further work is needed to elucidate such mechanism for brain organoids.

After seeding MOs with the fibrin-HUVEC shell, vascular-like networks of HUVECs and elongated fibrin structures were observed surrounding MOs for all three conditions, an example of which is illustrated in **(Fig. 29d, bottom right)**. This phenomenon was not observed with Matrigel-embedded controls nor non-embedded MOs. However, further work is needed to characterize the identity of the vascular-like structures. At FD14, CellTracker-CMRA labeled HUVECs, shown in **(Fig. 29e, magenta)**, appeared to surround parts of the surface of MOs. At this stage, HUVECs were either fused to the surface of MOs with minimal integration into MOs, or attached to the surrounding fibrin network. The initial integration of HUVECs into the MO was observed at this point by the small overlap of green and magenta, and the overlap signal is displayed by ImageJ in white in **(Fig. 29e)**. As the co-culture continued to FD18, the white overlap signal remained minimal but HUVECs surrounding MOs decreased, which is likely due to continued shaking and media change. By FD22,

CellTracker-CMRA labeled HUVECs displaced considerable regions of the GFP-MO by integrating into its central regions and dispersing away from the surface of the MO. This phenomenon was observed for all three conditions but with variable ratios of HUVEC to MO signal, as condition 2 had smaller regions of integrated HUVECs relative to the GFP-MO size. Therefore, in subsequent MOV-device co-culture experiments that included shell-MOs we mainly pursued conditions 1 and 3 in our co-cultures.

Inspection of the CMRA and GFP signal through the z-stack for shell-MOs of conditions 1 and 3, shown in (**Fig. 29f**), showed an initial intense GFP signal at the lowest z stack, followed by increased intensity of CMRA signal in an intermediate stack, followed by fading of the CMRA signal and reoccurring GFP signal at the highest z stack. Interestingly, in conditions 1 and 3, hollowing of inner regions in the MO was observed, which could occur due to possible formation of lumens by maturing HUVEC.

While the presented results provide a preliminary indication of possible vascular invasion of HUVECs into MOs, which has not been previously reported, further work is needed to determine endothelial function. This can be achieved by immunostaining for VE-Cadherin as an endothelial-specific adhesion molecule located at junctions of neighboring ECs, and testing vascular wall permeability²⁶⁰. Additionally, molecular identity of integrated HUVECs and MOs must be determined to ensure faithful replication of the *in vivo* developing midbrain.

The ability to vascularize MOs using HUVECs represents an attractive option for engineering cost-effective vascularized midbrain organoids because HUVECs are widely available and do not involve the same cost of maintenance as iPSC-derived ECs. The use of HUVECs was explored by others for cortical organoid vascularization⁵, but has not been demonstrated for midbrain organoid vascularization. Additionally, in a recent study, iPSC-derived ECs showed a five-fold reduction in capillary network formation compared to HUVECs, but it was attenuated by addition of hLFs³⁸⁷. Nonetheless, an advantage of iPSC-derived ECs is the ability to transfect them prior to differentiation with fluorescent protein markers that facilitate easy long-term live-cell tracking without losing passage count as the case is with HUVECs. One key challenge of using CellTracker-labeled HUVECs for live long-term studies of vascularization is fading of the signal as the culture continues. This is problematic

because as HUVECs proliferate, dividing cells retain progressively less signal, and vascular sprouting and subsequent invasion that require formation of tip-stalk morphology become more challenging to observe. Tip cells have narrow sprouting extensions. Since these narrow extensions cannot retain a high volume of live tracking dye while stalk cells can, it becomes difficult to resolve tip cells microscopically.

Vascularization of the human fetal brain *in vivo* begins with the formation of a capillary plexus that surrounds the brain around 5 weeks of gestation²¹³. By week 7 of gestation, angiogenesis begins from the pre-existing plexus occurs in response to increased metabolic demands by the developing brain²¹³. In comparison to previously reported methods of brain organoid vascularization, this shell method for vascularizing MOs, the fusion of vascular organoids with neuronal organoids³²⁵, and the Matrigel shell method previously reported for vascularization of cerebral organoids⁶, are conceptually more reminiscent of neurovascular invasion during embryonic development²¹³. However, whether or not this recapitulation of the process would translate into more beneficial outcome for alleviating cell death in brain organoids and improving their quality as tissue-engineered constructs compared to pre-mixing methods of brain organoid vascularization remains unclear. Previously reported methods that require pre-mixing of HUVECs within cortical organoids⁵, or pre-mixing of *etv2*-transfected iPSC-derived ECs within cortical organoids prior to long-term culture³, although might not fully mimic the developmental steps of *in vivo* vascularization, they are still quite impressive in generating improved brain organoids with minimized cell death at the core. Although, caution must be exercised when inferring developmental pathways that govern vascularization of the brain using these models. Further work is needed to elucidate the role of vascularization in influencing functional or anatomical properties of midbrain organoid models.

6.4.3 Monitoring vascular sprouting of mCherry-HUVECs and CellTracker-HUVECs

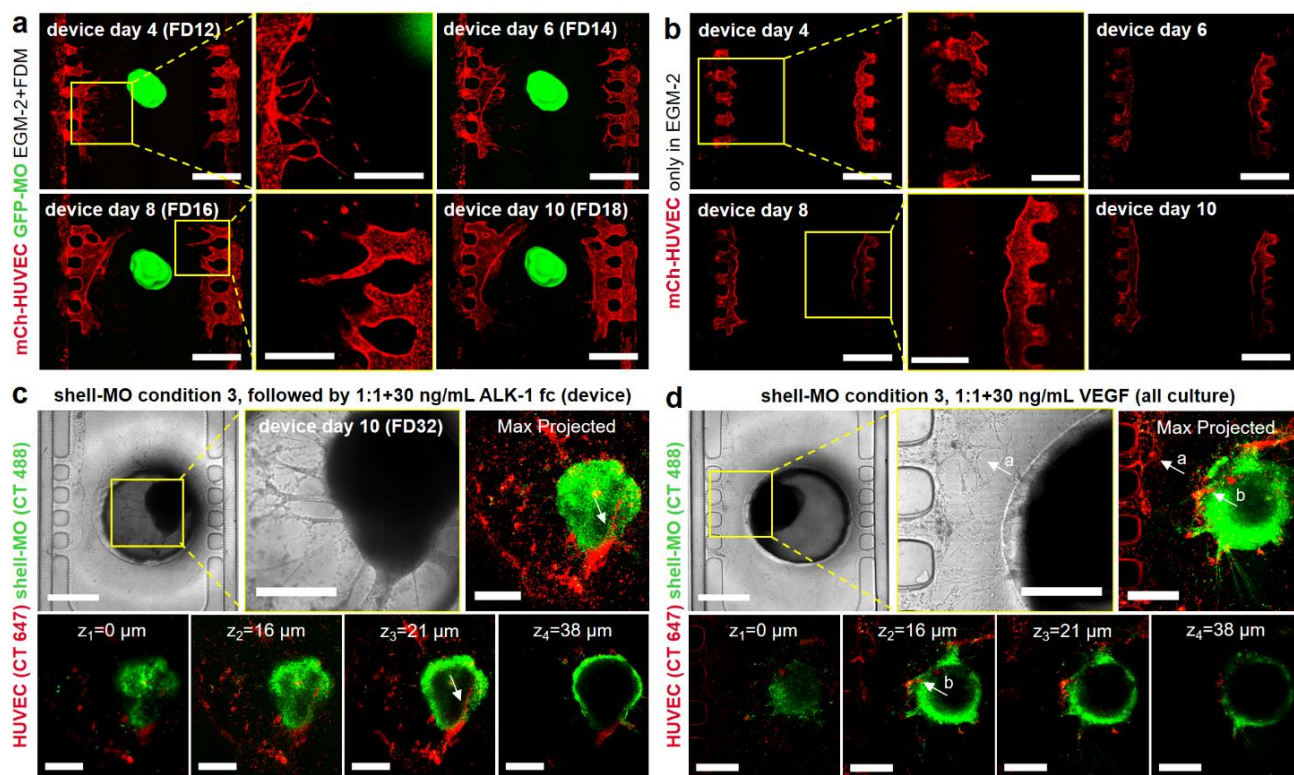


Fig. 30: MOV device co-culture. (a) Z-maximum projection micrographs of GFP-MO (green) on-chip co-culture with mCh-HUVECs (red) cultured with EGM-2 added to side channels and FDM added to the middle chamber. (b) Z-maximum projection on-chip culture of mCh-HUVECs only in EGM-2. (c, d) AIW shell-MO (condition 3) stained for CellTracker CMFDA dye (green) co-cultured with primary HUVECs stained for CellTracker Deep Red dye (red), maintained in (c) 1:1 FDM to EGM-2 media supplemented with 30 ng/mL ALK-1 fc, introduced on device day 1, and (d) 1:1 FDM to EGM-2 media supplemented with 30 ng/mL VEGF all culture. (c, d) Top row displaying BF micrographs and maximum projection fluorescent image of the MO. Bottom row displaying individual Z-planes through the MO (bottom to top plane). **Scale bars:** (a,b) device micrographs: 1 mm, zoomed micrographs: 500 μ m. (c, d) BF device micrographs: 1 mm, zoomed BF and fluorescent micrographs: 500 μ m.

To test if MOV devices permit monitoring vascularization events, fibrin-collagen suspended GFP-MOs were co-cultured with mCh-HUVECs in MOV devices, as previously described. By day 4, vascular sprouts formed from the pre-existing layer of mCh-HUVECs lining each side of the hydrogel, in a process that mimics *in vivo* angiogenesis²⁷¹, as shown in (Fig. 30a). The vascular sprouts extended through the hydrogel-filled middle chamber, and branching of some vascular sprouts was observed; a process by which two vascular sprouts fuse and bridge together to form a lumen²⁷¹. As the co-culture continued, vascular sprouts proliferated further into the hydrogel, and formed additional branches. By day 8, vascular sprouts and branches appeared larger in diameter than earlier time point. By day 10 in co-culture, vascular sprouting decreased and the HUVECs comprising the vascular wall adopted a quiescent morphology characterized by a cobblestone shape that mostly lacks tip-stalk phenotype²⁸¹. Quiescence of HUVECs indicates terminated angiogenesis that prevents subsequent vascular invasion

of the MO, which is a key step required for vascular perfusion of the MO.

To understand the role of GFP-MOs in inducing vascular sprouting, we prepared control mono-cultures of mCh-HUVECs seeded in both side channels of fibrin-collagen filled middle chambers of MOV device without introducing GFP-MOs, as shown in **(Fig. 30b)**. While mCh-HUVECs initially formed vascular sprouts, these sprouts did not proliferate to the same distance into the hydrogel as they did when in co-culture with GFP-MOs. Branching events in this condition were minimal and mostly appeared near the CSVs on day 4. Additionally, quiescence of the vascular wall for mCh-HUVECs on one side of the device occurred as early as day 6. By day 10 of culture, mCh-HUVECs on both sides of the device had stabilized vascular walls and angiogenesis events mostly ceased. Importantly, the immortalized state of mCh-HUVECs due to transfection could be a contributor to premature stabilization of vascular wall-like structures in both mono- and co-cultures shown in **(Fig. 30a, 30b)**.

In the condition presented in **(Fig. 30b)**, mCh-HUVECs are cultured in EGM-2 which contains a proprietary low concentration of VEGF, among other pro-angiogenic factors²⁵. On the other hand, mCh-HUVECs in co-culture with GFP-MOs shown in **(Fig. 30a)** are cultured in EGM-2 that becomes diluted with low volume of FDM introduced into the inlet of the middle chamber to feed the organoid. Additionally, GFP-MOs co-cultured with mCh-HUVECs in **(Fig. 30a)** did not contain a pre-cultured shell of HUVECs. Therefore, the differential vascular sprouting pattern between the two conditions **(Fig. 30a, 30b)** could suggest the contribution of GFP-MO secreted factors to signaling events that induced vascular sprouting, branching, and proliferation of mCh-HUVECs. This is consistent with hypoxia expression that was observed in MOs as early as FD7, shown in **(Fig. 32a)**. Expression of HIF1 α is known to trigger a signaling cascade for VEGF expression, among other pro-angiogenic genes, which can initiate angiogenesis³¹¹. Moreover, the distance between mCh-HUVECs on one side channel and the closest signaling molecules secreted by other HUVECs or other cell types plays a key role in inducing vascular sprouting^{260, 364}. Previously described reports of successful vascularization of spheroids in microphysiological systems were characterized by a smaller middle chamber than our report and thus a shorter distance between the two side-channels that contained ECs, which meant ECs were able to sense stronger angiogenic signaling earlier in culture^{25, 27, 256, 260}. However, given that organoids are larger than spheroids, increasing the size of the middle chamber is unavoidable in order

to accommodate the larger size of organoids while allowing the user to study their vascularization.

Sprouting HUVECs have been shown to connect to other HUVECs in their vicinity through anastomosis^{25, 365}. Therefore, to reduce the distance between HUVECs in the side channel and the MO in the middle well, we tested the role of shell-MOs in inducing vascular network formation in MOV devices. Furthermore, to avoid premature stabilization of mCh-HUVECs due to their immortalized state, we used CellTracker-labeled HUVECs as opposed to immortalized HUVECs in co-culture with shell-MOs, as shown in (**Fig. 30c, 30d**). Given that shell-MO experiments previously discussed (**Fig. 29e, 29f**), showed integration of CellTracker-labeled HUVECs into GFP-MOs, this could suggest that the requirement for vascularizing MOs is now reduced to branching HUVECs with previously existing HUVECs in the shell surrounding MOs as opposed to vascular invasion directly from the side channels.

In the condition shown in (**Fig. 30c**) CellTracker-labeled shell-MOs from shell condition 3 (**Table 6, and Fig. 29**) were co-cultured with CellTracker-labeled HUVECs added to both the hydrogel filling the middle chamber and side channels. In this condition, only Alk-fc1 was added to a 1:1 ratio of FDM to EGM-2 media combination with no additional VEGF, in order to test the effect of Alk-fc1 on angiogenesis in neurovascular co-culture, given its poorly understood role in TGF β signaling during neurovascular development³⁷⁷. The addition of Alk-fc1 to media was accompanied with vascular sprouting, and preliminary evidence for vascular invasion into MOs, as shown in fluorescent micrographs of zoomed maximum projection of z planes and individual z planes of the co-culture at day 10 in device (**Fig. 30c**). Control co-culture experiments of CellTracker-labeled MOs with CellTracker-labeled HUVECs in 1:1 ratio of FDM to EGM-2 without the addition of Alk-fc1 or VEGF did not show any evidence of vascular invasion into MOs. Nonetheless, further work and statistical analysis is required to determine if Alk-fc1 has a possible role in inducing vascularization of neuronal tissues.

In the condition shown in (**Fig. 30d**), CellTracker-labeled shell-MOs of shell condition 3 were similarly co-cultured with CellTracker-labeled HUVECs added to the middle and side channel, with the 1:1 FDM to EGM-2 media was supplemented with VEGF instead of Alk-fc1. Similarly to the condition in (**Fig. 30c**), vascular invasion of HUVECs into the shell-MO was observed through

confocal imaging through the z-axis of the organoid in the condition in **(Fig. 30d)**. However, the distance vascular sprouts traveled from the surface to the center of the organoid showed disparities between the conditions tested as shown in **(Fig. 30c, 30d)**. Nonetheless, in both conditions shown in **(Fig. 30c and 30d)**, the cells did not become prematurely quiescent as was the case with mCh-HUVECs cultured with MOs that did not contain a shell of HUVECs. Bright field micrographs of shell-MOs of both conditions shown in **(Fig. 30c and 30d)** showed continued vascular sprouting of HUVECs at day 10 in device, which was not the case for mCh-HUVECs that ceased to sprout as early as day 6 in mono-culture. Importantly, the current work does not claim any conclusions regarding a possible mechanism for vascular sprouting or invasion into MOs, but rather aims to determine the utility of the proposed platform for monitoring possible vascular events such as sprouting and invasion during live culture.

Visualization of Deep Red CellTracker-labeled HUVECs for vascularization studies was more challenging in comparison to mCh-HUVECs. CellTracker dyes are retained in the cytosol of cells and decrease as cells proliferate, while mCherry transfection leads to continuous expression of the fluorescent protein at all actin filaments by the dividing cells³⁸⁸. CellTracker-labeling of shell-MOs using the CMFDA dye, shown in green in **(Fig. 30)**, was also tested. The dye was not able to penetrate to the core of MOs, which makes it difficult to determine morphological changes within the core of the organoid in response to co-culture or presence of cell debris in the core due to cell death.

6.4.4 Vascular-like networks are partially perfusable

Experimental variation was observed in the extent of which vascular network formation occurred among repeats of the same condition. For instance, co-cultures in MOV devices of the same condition formed more extended and connected vascular networks with branched lumens as shown in **(Fig. 31a)** than the experimental repeat of the same condition shown in **(Fig. 30d)**. However, perfusion of the vascular network for this condition did not retain the fluorescent dextran dye solution added. This is likely due to incomplete vascular network formation or inconsistent HUVEC coating on the hydrogel-filled CSVs connecting the network formed in the middle chamber to side channels, shown in **(Fig. 31a)**. Given that the fluorescent dye is added to one side channel in order to perfuse the network, full coating of the CSVs with vascular lumens without gaps is a pre-requisite to perfuse the

dye through any vascular network that forms. On the other hand, one co-culture condition where 1 to 1 FDM to EGM-2 supplemented with both 30 ng/mL Alk-fc1 and 30 ng/mL VEGF was added after device seeding, was able to partially retain the 40-kDa fluorescent dextran dye solution as shown in (**Fig. 31b**), despite lacking the extensive sprout formation and branching observed in other conditions. While retention of the fluorescent dye could suggest possibility for formation of vascular wall-like structures, further work is needed to optimize growth media conditions in order to develop a formulation that reproduces multiple vascular functions in one condition.

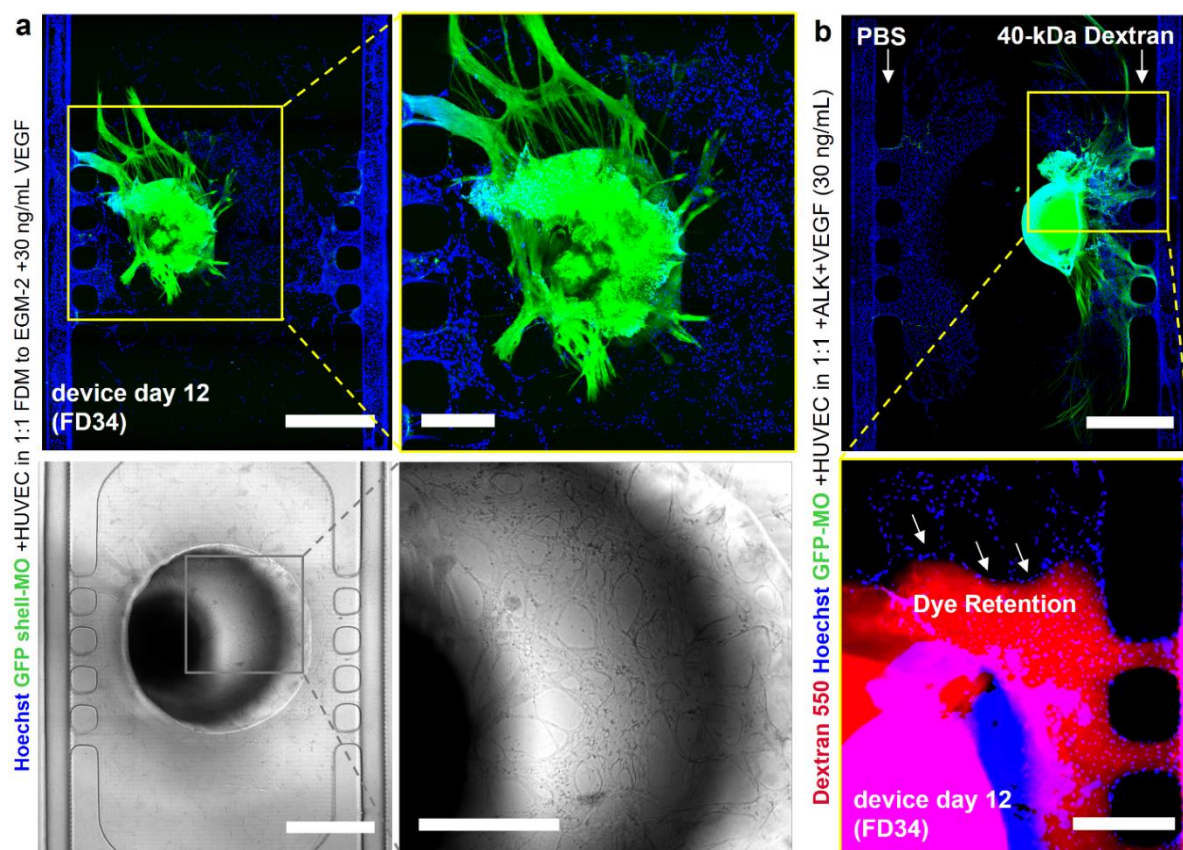


Fig. 31: Nuclear staining, imaging, and dye perfusion for HUVECs in co-culture with GFP shell-MOs at FD34, device day 12. (a) On-chip co-culture in 1:1 FDM to EGM-2 media supplemented with 30 ng/mL VEGF (all culture) displaying extensions from the organoid (top row), and vascular-like networks (BF micrographs, bottom row). (b) On-chip co-culture of GFP shell-MO stage (condition 3), maintained in 1:1 FDM to EGM-2 media supplemented with 30 ng/mL VEGF+ 30 ng/mL ALK-1 fc starting device day 1. Bottom micrographs displaying retention of Dextran 550 (MW: 40-kDa) within vascular wall-like structures. **Fluorescence signal:** GFP-MO (green), Hoechst (blue), Dextran 550 (red). **Scale bars:** full device micrographs: 1 mm, zoomed micrographs: 500 μ m.

6.4.5 Midbrain organoids express hypoxia and cell death markers

We aimed to characterize spatiotemporal expression of hypoxia and cell death markers in control MOs. Immunostaining MOs showed that HIF1 α appeared as ‘ring-like pattern’ surrounding the core of MOs starting week 1 of culture in FDM, as shown in (**Fig. 32a**). The observed pattern

appears as a hypoxic ring in the 2D view of the cryosections, but it is more likely that the expression pattern would adopt a ‘hypoxic shell-like pattern’ that surrounds the core of the organoid if analyzed in 3D view. 3D analysis of hypoxia pattern in intact MOs could be performed in future work by fluorescent-protein transfection tagging HIF1 α . The same pattern continued to appear at 1 month in culture surrounding a CC3+/TUNEL+ core of MOs; which signified onset of cell death. At 1.5 month in culture, HIF1 α expression appeared more dispersed, while MOs maintained a CC3+/TUNEL+ core. Furthermore, irregular shaped MOs such as organoid 2 in (**Fig. 32b**), showed two dead cores at different organoid regions that extended in size and each dead core was surrounded with its own hypoxic ring-like pattern. TUNEL staining for DNA degradation appeared to localize at core of MOs similarly to CC3+, which further confirms cell death at the core.

HIF1 α expression trend inversely localized with CC3+ expression as shown in (**Fig. 32a**, **32c**). This could suggest that as MOs grow in size, hypoxic cells displace from the core of MOs to their outer layers while hypoxic cells at the core of MOs reach a fatal point where hypoxia is beyond rescue and begin to experience cell death due to persistent oxygen deprivation^{235, 236}. Average intensity values of HIF1 α and CC3 plotted against the distance from the surface to the core of MOs shown in (**Fig. 32b**) and distance across the whole diameter of MOs as shown in (**Fig. 32c**), show that hypoxia is highest at 300 μ m distance, while CC3 expression is highest at 650 μ m distance from surface to core. This suggests that oxygenation of MOs with orbital shaking in traditional culture becomes less efficient as organoids grown in size and that cells comprising MOs are able to withstand hypoxia without cell death for a greater distance than the theoretical limit of oxygen diffusion. This is consistent with a previously reported mathematical model for oxygen diffusion in cerebral organoids, which suggested that as brain organoids grow, cells become displaced from the core to outer layers, which decreases cell density at the core of organoids and therefore decreases oxygen consumption⁴. The mathematical model provides an explanation for the reason organoids grow in size despite cell death at their core. Increasing size of MOs is not necessarily an indicator of healthy growth, as the results presented demonstrate increased expression of cell death markers as the distance from surface to core increases. The results underscore the need to vascularize brain organoids.

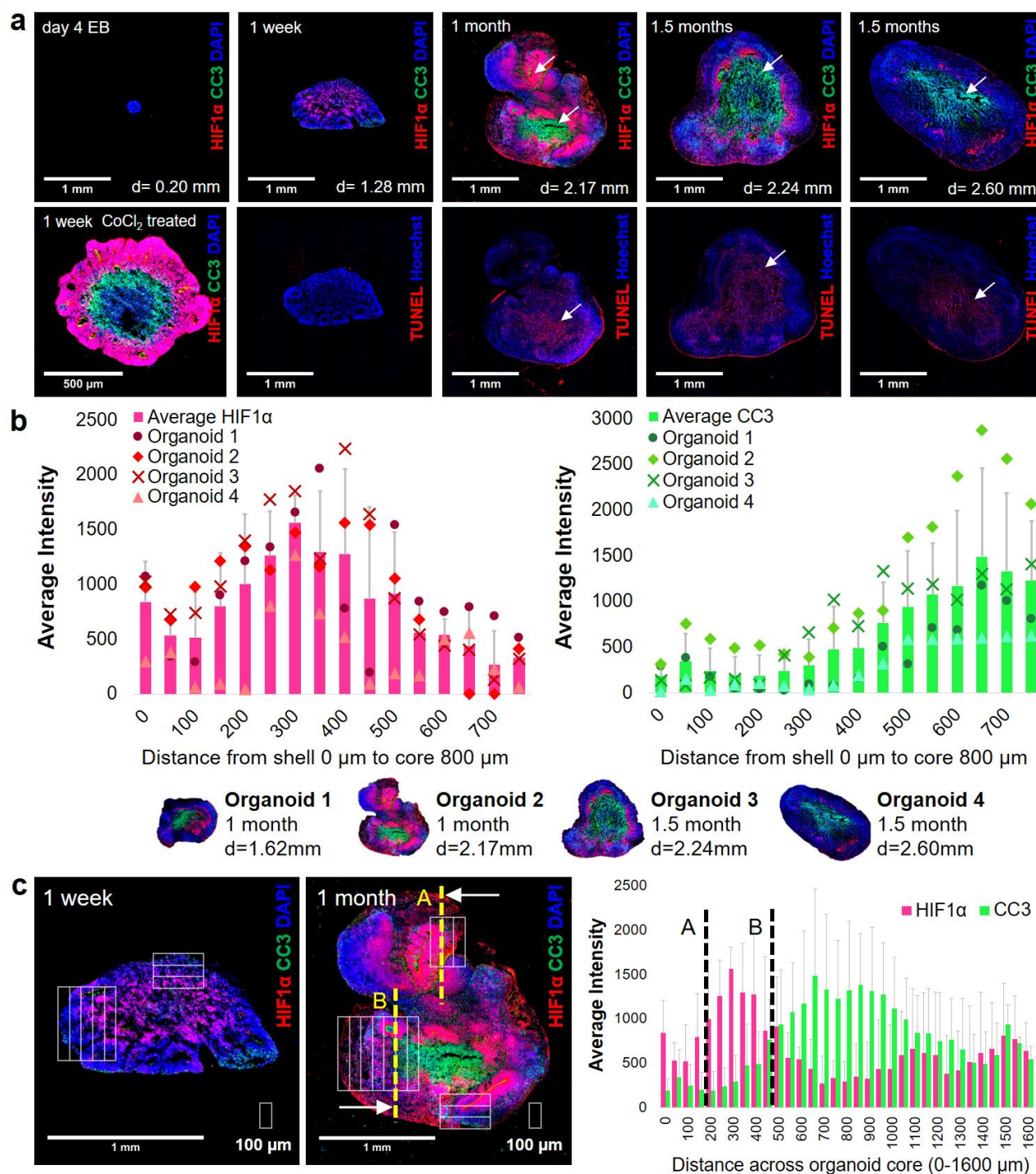


Fig. 32: (a) Immunohistochemical analysis of AIW-MOs and 100 μM Cobalt (II) Chloride-treated AIW-MOs, cultured in FDM, at day 4, FD7 (1 week), FD28 (1 month), and FD43 (1.5 months), showing dead core development (CC3 and TUNEL signal, indicated with white arrows), and expression of hypoxia marker (HIF1 α). Same look-up tables were applied to the same markers for all sections. **(b)** Average intensity (grey value) mapped against distance in μm from the outer shell to the core of HIF1 α ⁺/CC3⁺ MOs (n=4 MOs, 6 line scans per MO). **(c)** Average intensity mapped against distance across full MO sections (organoids 1-4), showing corresponding points A and B in micrograph (left) of HIF1 α ⁺/CC3⁺ MO, where hypoxia and necrosis signals appear intensified, respectively.

6.5 Conclusion

The presented work reports a PDMS microfluidic device replicated from 3D printed molds for

studying midbrain organoid vascularization. Modification of surface properties of the PDMS device and seal enabled patterning a fibrin-collagen hydrogel in two formats; a capillary stop valve that comprises spaced microgrooves, and a continuous capillary stop valve format. This work explored various aspects pertaining to the development and operation of a microphysiological system for studying vascularization of midbrain organoids-on-a-chip. The platform enabled monitoring and imaging several vascular processes including vascular sprouting, branching, invasion, and formation of vascular wall-like structures. Characterization of hypoxia and cell death in MOs provided an approximate time frame for vascularization to take place before onset of cell death. The time frame is between the one week to the one month mark for MOs in FDM. Further work to advance this system will be carried to optimize vascularization of the MO and characterize features of the vasculature.

Many devastating neurological disorders including AD, PD, ischemic stroke, epilepsy, and multiple sclerosis occur due to breakdown or dysfunction of the BBB²⁵⁶. The reported device can be applicable for vascularization of other types of organoids including other types of brain organoids, and could have valuable implications for modeling neurovascular interactions, neurological disorders, and drug testing applications.

6.6 Supplementary information

6.6.1 3D positive molds and PDMS replicas of funnel structures

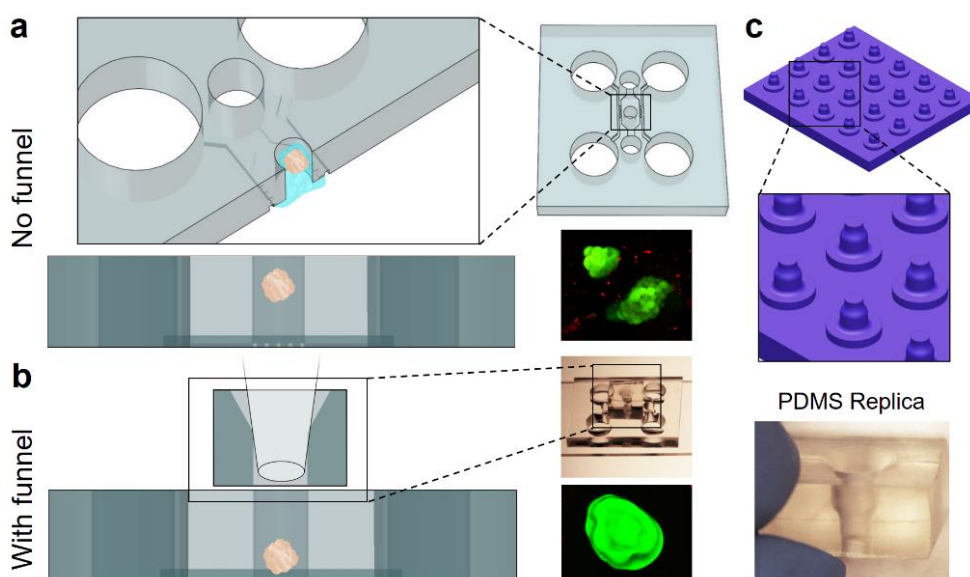


Fig. S1: Funnel structures enable safe loading of MOs into MOV devices. (a) MO introduction into devices without funnels breaking up organoids and prevents MO sedimentation to the bottom of the device. (b) cut-tip pipette fits tightly into the PDMS funnel and enables loading MOs safely in the middle chamber and their sedimentation to the bottom of the device. (c) Design of an array of positive molds of funnels for 3D printing, and the final PDMS funnel replicated from 3D printed molds.

6.6.2 Characterization of diffusion in a fibrin-collagen filled chamber

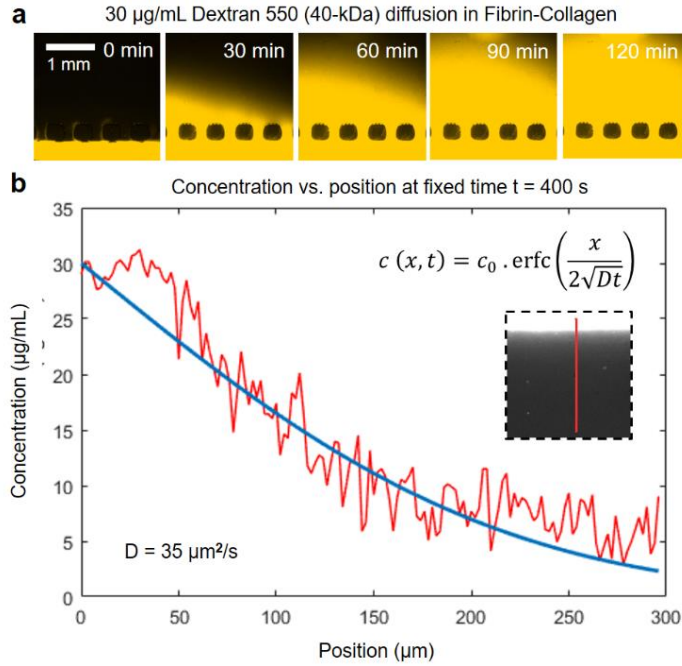


Fig. S2: Diffusion of 40-kDa dextran in fibrin-collagen filled MOV device. (a) Time-lapse micrographs at 30-min intervals of 100 µg/mL Dextran 550 (40-kDa) dye diffusion through a fibrin-collagen filled middle chamber of MOV device (without cell culture). Dye signal reaches a 2-mm distance in the device by 120 mins. (b) Concentration (µg/mL), represented by grey value is mapped against position (µm) from the edge of capillary stop valves where the hydrogel surfaces to the center of the middle chamber in the vertical direction. Dye signal (red) in relation to position is fitted and plotted (blue curve) using the error function for 1D diffusion. The diffusion coefficient (left bottom corner) was quantified by fitting the error function solution for 1D diffusion. (a, b) Widefield microscopy: 200 ms exposure time, 4X magnification.

6.6.3 Final differentiation medium composition

Table S1: final differentiation medium composition

Media Component	Vendor/Cat no.	Concentration
Neurobasal Media	Thermo Fisher, 21103-049	1:1
N-2 supplement (100X)	Gibco, 17502048	1:100
B-27™ (50X), minus vitamin A	Invitrogen, 12587010	1:50
GlutaMAX™ (100X)	Gibco, 35050-061	1%
MEM-NEAA (100X)	Invitrogen, 11140050	1%
2-mercaptoethanol (1000X)	Gibco, 21985023	35:1e ⁶
Penicillin-Streptomycin (100X)	Millipore Sigma, P0781	1:1000
BDNF	PeproTech, 450-02	10 ng/mL
GDNF	PeproTech, 450-10	10 ng/mL
Ascorbic acid	Millipore Sigma, A5960	100 µM
db-cAMP	Millipore Sigma, D0627	125 µM

7. Extended discussion

This part is written as an extension to the discussion (Section 6.4) in the manuscript chapter.

7.1 Device fabrication and design

3D printing represents a more cost-effective and faster fabrication method than traditional cleanroom microfabrication¹⁰⁵. While principles of cleanroom microfabrication have been long established in the field, the fabrication steps remain labor-intensive and require specialized training¹⁰⁵. On the other hand, commercially available DLS 3D printing technology is highly accessible to non-

expert users. This is advantageous because it offers to bridge the gap between bioengineers, and biologists or clinicians, which could improve opportunities for translational applications in the future such as drug testing using patient-derived samples²⁵⁶.

Moreover, 3D printing allows faster iterations between design and device fabrication¹⁰⁵, which is not only advantageous for early stages of project development, but also because it could enable flexible engineering strategies when working with unpredictable biological outcomes. For instance, brain organoids are notorious for their shape-irregularity and batch-to-batch variability. Depending on the logistics and time-frame by which brain organoids are grown in labs prior to seeding into the device, the user could analyze organoids in terms of size and choose to re-tailor the design features to better suit the size of the organoid. For example, organoids could grow in culture to be smaller in diameter than expected due to inherent protocol variability or disease modeling¹⁰. In such case, it would be beneficial to decrease the dimensions of the middle chamber, thereby reducing the distance between the organoid and ECs on the side channels. A reduced distance between the organoid and ECs would enhance vascular sprouting in response to secreted factors diffusing from the organoid³⁶⁴, and could speed up vascular invasion into the organoid.

Additionally, the microfluidic configurations tested allowed hydrogel patterning using two formats of capillary stop valve; one characterized by microgrooves and another characterized by a continuous capillary stop valve, as shown in **(Table 5)**. The continuous capillary stop valve format eliminates the needle-blocking step previously reported²⁶, which simplifies the protocol, and could potentially have biological implications since it increases the surface area coated by ECs compared to the microgroove format. Importantly, eliminating unnecessary steps by automating a desired functional feature during the development of a microfluidic system has been one of the main goals of the microfluidic field^{104, 105, 256}. Simplification of steps is valuable for optimization of a microfluidic platform for future use by non-experts as well as scaling-up applications that may increase testing throughput^{104, 108, 256}. In addition, reducing device handling steps and duration during cell culture is a cell friendly-practice for sterility purposes and because cell viability could be compromised by prolonged room-temperature incubation³⁸⁹.

7.2 Cell and organoid seeding

The development and use of PDMS funnel structures represented an unexpected requirement for seeding the midbrain organoids in MOV-devices. Given that pipette tips are manually cut to increase their diameter for organoid seeding and handling, the performed cut could occur at an angle, which introduces a source of error when attempting to pipette organoids directly on top of the middle well. Misalignment of angled pipette tips occasionally results in overflow of the EC-organoid hydrogel mixture to the top layer of the PDMS device, which can lead to seeding the wrong number of cells or floating of the organoid. Such challenges would introduce variability in the seeding method, which could affect the vascularization process. The funnels provided a tight seal with the pipette tip, which prevented misalignment of the pipette with the middle well where the organoid is introduced. Additionally, in certain cases prior to using the funnels, organoids broke apart during the seeding process, as shown in **(Fig. S1)**, and the use of funnels enabled gentle pipetting of organoids that prevented such damage. These seeding challenges have not been widely discussed in microphysiological systems for spheroid vascularization. Therefore, these challenges could be due to user experience, or could be unique to midbrain organoids or other types of organoids due to differences in how densely packed cells are within organoids compared to spheroids.

Seeding a shell of HUVECs surrounding the MOs showed that HUVECs could integrate with the organoid. While the HUVECs during this step did not show a clear vascular network-like structure within the organoid, the results were similar in phenotype to those reported by Shi *et al.* for vascularized cortical organoids⁵. Additionally, the length of our protocol was shorter than those reported in literature which likely affected the maturation and morphogenesis of the vasculature.

7.3 Vascular network formation

Overall, MOV devices supports live *in vitro* observation and imaging of several key steps reminiscent of *in vivo* angiogenesis including sprouting, branching, and possible vascular invasion. However, the results do not prove the mechanism by which these processes occurred in this specific setup. Partial dye retention within the vascular-like network, shown in **(Fig. 31)**, is a preliminary indicator that suggests potential for future optimization of the platform for perfusable vascularized midbrain organoids in continuous live culture. Connection of open lumens between the middle chamber and the side channels is required for perfusion, and was only achieved asymmetrically in the

devices. Formation of well inter-connected vascular networks that are also connected to the lumens of the side channels remains a work-in-progress and requires further optimization of the microenvironment by better mimicking the conditions during *in vivo* midbrain vascularization.

Variability of midbrain organoid culture could hinder progress with vascularization attempts and biological studies that assess mechanisms underlying human brain vascularization. Further work is needed to reduce batch-to-batch variability, which would improve reproducibility of vascularization protocols.

7.4 Hypoxia and cell death in midbrain organoids

Characterization of hypoxia and cell death in MOs provides a time window for when vascularization is most urgent. As shown in (**Fig. 32**), expression of the hypoxic marker HIF1 α in MOs was observed as early as one week in FDM, and onset of cell death was observed at the one month mark. HUVEC integration into the shell-MOs was observed prior to the cell death time point, which could suggest that the protocol is compatible with the progression of hypoxic signaling. Yet, further characterization is needed to determine viability of HUVECs once they have integrated within MOs, to determine if they are also at risk of hypoxia and cell death as MOs grow in culture.

While perfusion of MOs once vascularized is necessary for maturation of MOs and the vasculature, introducing flow into the platform prematurely risks diluting hypoxic signaling²³, which could prevent continued sprouting of HUVECs towards MOs in the device. Additionally, characterization of MOs post HUVEC-integration and invasion can determine whether vascular invasion prior to perfusion could reduce or delay cell death at the core of MOs. For instance, Cakir *et al.* reported reduced cell death and increased growth of vascularized cortical organoids even without continuous perfusion live culture. This finding could be explained by the formation of vascular lumens that reduce organoid density and allow media to penetrate newly hollowed parts within the organoid, thus enhancing mass transport to the core. Moreover, it would be worth investigating whether cell death that has already occurred in midbrain organoids be rescued by vascularization since the neurovascular link is implicated in neuronal growth^{23, 363}.

Variability in hypoxic signaling was also observed, as indicated by SD values reported in (**Fig. 32b, 32c**). Variable hypoxic signaling is also a possible contributor to variability in vascularization of

MOs given its direct effect on VEGF-mediated angiogenic signaling. Given that organoid diameter is an important parameter for hypoxia and cell death, methods that increase organoid size homogeneity through automation and microtechnology could offer to reduce this source of variability^{390, 391}.

Some methods previously cited in the introduction (**Section 5.2.3.1**) have attempted to reduce cell death and hypoxia and/or reduce variability using approaches that involved: spinning mini-bioreactors²⁰⁶, accelerated patterning²¹⁶, slicing²¹⁸, and millifluidics²¹⁷, in addition to more traditional approaches such as shaking and bioreactors^{147, 183}.

The slicing was successful in eliminating cell death but the method was applicable for a specific study of cortical layer development²¹⁸. The bioreactor method reported by Quadrato *et al.* was also impressive in extending viability to 9 months without hypoxia and cell death²⁰⁶. However, the other methods either reduced cell death or delayed it but did not eliminate it. Additionally, slicing and the mini-bioreactor method do not account for the role of the endothelium during development. Vascularization methods on the other hand were successful in reducing cell death even without live perfusion in some cases³, and do account for neuroangiocrine factors reciprocated between neuronal populations and the endothelium. Therefore, vascularization will likely remain a key step for improving quality of brain organoids. Other methods that reduce cell death and hypoxia would be beneficial for delaying cell death until vascular morphogenesis is achieved during the culture period.

8. Conclusion and Future Work

The presented work reports a PDMS microfluidic device replicated from 3D printed molds for studying midbrain organoid vascularization. Three successful configurations of device surface properties were reported for patterning a fibrin-collagen hydrogel in two formats; a capillary stop valve that comprises spaced microgrooves, and a continuous capillary stop valve format. This work explored various aspects pertaining to the development and operation of a microphysiological system for studying vascularization of midbrain organoids-on-a-chip.

Development and use of funnel structures circumvented seeding challenges such as damage to the organoid and hydrogel overflow outside the middle chamber where it is pipetted. The platform enabled monitoring and imaging several vascular processes including vascular sprouting, branching, invasion, and formation of vascular wall-like structures.

Connecting vascular lumens to side channels with defined inlets and outlets would represent a valuable advancement for developing vascularized midbrain organoids. Traditional brain organoid vascularization methods that use well plates do not support straightforward and simplified perfusion of organoids. Further optimization of the platform presented in this work could advance solution to this problem.

Characterization of hypoxia and cell death in MOs provided an approximate time frame for vascularization to take place before onset of cell death. The time frame is between the one week to the one month mark for MOs in FDM.

Future work to advance this system will be carried by first optimizing media formulation and vascularization protocol. Second, characterization of endothelial and midbrain markers will be carried to determine the identity of cell populations and their functional properties. Third, the device design will be modified for live continuous perfusion culture, which would allow studying the vascular remodeling step that occurs after angiogenesis as the vasculature matures. Additionally, the platform could accommodate the addition of astrocytes and microglia which could be explored for modeling the permeability of the BBB, and drug testing applications. Many devastating neurological disorders including AD, PD, ischemic stroke, epilepsy, and multiple sclerosis occur due to breakdown or dysfunction of the BBB²⁵⁶. Therefore, a brain organoid vascularization microphysiological system would be valuable.

Moreover, the neurovascular link has been predominantly studied in animal models due to the inaccessibility of the human brain. Current work is ongoing to characterize the secretome and exosome profile of the co-culture using supernatant collected from MOV devices and control mono-cultures of HUVECs and MOs at different time points. Such characterization would be beneficial for studying the neurovascular link in a clinically relevant context by using human-derived MOs and human ECs, and could provide opportunities towards biomarker discovery and drug development for neurovascular diseases.

9. References

1. Di Lullo, E. & Kriegstein, A.R. The use of brain organoids to investigate neural development and disease. *Nature Reviews Neuroscience* **18**, 573 (2017).
2. Qian, X., Song, H. & Ming, G.-l. Brain organoids: advances, applications and challenges. *Development* **146**, dev166074 (2019).
3. Cakir, B. et al. Engineering of human brain organoids with a functional vascular-like system. *Nature methods*, 1-7 (2019).
4. McMurtry, R.J. Analytic models of oxygen and nutrient diffusion, metabolism dynamics, and architecture optimization in three-dimensional tissue constructs with applications and insights in cerebral organoids. *Tissue Engineering Part C: Methods* **22**, 221-249 (2016).
5. Shi, Y. et al. Vascularized human cortical organoids (vOrganoids) model cortical development in vivo. *PLoS biology* **18**, e3000705 (2020).
6. Pham, M.T. et al. Generation of human vascularized brain organoids. *Neuroreport* **29**, 588 (2018).
7. Shamir, E.R. & Ewald, A.J. Three-dimensional organotypic culture: experimental models of mammalian biology and disease. *Nature reviews Molecular cell biology* **15**, 647-664 (2014).
8. Fatehullah, A., Tan, S.H. & Barker, N. Organoids as an in vitro model of human development and disease. *Nature cell biology* **18**, 246 (2016).
9. Chen, H.I., Song, H. & Ming, G.I. Applications of human brain organoids to clinical problems. *Developmental Dynamics* (2018).
10. Lancaster, M.A. et al. Cerebral organoids model human brain development and microcephaly. *Nature* **501**, 373 (2013).
11. Guan, Y. et al. Human hepatic organoids for the analysis of human genetic diseases. *JCI insight* **2** (2017).
12. Eiraku, M. et al. Self-organizing optic-cup morphogenesis in three-dimensional culture. *Nature* **472**, 51-56 (2011).
13. Yip, H.Y.K., Tan, C.W., Hirokawa, Y. & Burgess, A.W. Colon organoid formation and cryptogenesis are stimulated by growth factors secreted from myofibroblasts. *PLoS one* **13** (2018).
14. Chen, H.I., Song, H. & Ming, G.I. Applications of human brain organoids to clinical problems. *Developmental Dynamics* **248**, 53-64 (2019).
15. Grenier, K., Kao, J. & Diamandis, P. Three-dimensional modeling of human neurodegeneration: Brain organoids coming of age. *Molecular psychiatry*, 1-21 (2019).
16. Forsberg, S.L., Ilieva, M. & Michel, T.M. Epigenetics and cerebral organoids: promising directions in autism spectrum disorders. *Translational psychiatry* **8**, 1-11 (2018).
17. Trujillo, C.A. & Muotri, A.R. Brain organoids and the study of neurodevelopment. *Trends in molecular medicine* **24**, 982-990 (2018).
18. Watanabe, M. et al. Self-Organized Cerebral Organoids with Human-Specific Features Predict Effective Drugs to Combat Zika Virus Infection. *Cell Reports* **21**, 517-532 (2017).
19. Mariani, J. et al. FOXP1-dependent dysregulation of GABA/glutamate neuron differentiation in autism spectrum disorders. *Cell* **162**, 375-390 (2015).
20. Raja, W.K. et al. Self-organizing 3D human neural tissue derived from induced pluripotent stem cells recapitulate Alzheimer's disease phenotypes. *PLoS one* **11** (2016).
21. Smits, L.M. et al. Modeling Parkinson's disease in midbrain-like organoids. *NPJ Parkinson's disease* **5**, 1-8 (2019).
22. Rafii, S., Butler, J.M. & Ding, B.-S. Angiocrine functions of organ-specific endothelial cells. *Nature* **529**, 316-325 (2016).
23. Iadecola, C. The neurovascular unit coming of age: a journey through neurovascular coupling in health and disease. *Neuron* **96**, 17-42 (2017).
24. Ahn, Y. et al. Human Blood Vessel Organoids Penetrate Human Cerebral Organoids and Form a Vessel-Like System. *Cells* **10**, 2036 (2021).
25. Nashimoto, Y. et al. Integrating perfusable vascular networks with a three-dimensional tissue in a microfluidic device. *Integrative Biology* **9**, 506-518 (2017).
26. Paek, J. et al. Microphysiological Engineering of Self-Assembled and Perfusable Microvascular Beds for the Production of Vascularized Three-Dimensional Human Microtissues. *ACS nano* (2019).
27. Osaki, T., Sivathanu, V. & Kamm, R.D. Engineered 3D vascular and neuronal networks in a microfluidic platform. *Scientific reports* **8**, 5168 (2018).
28. Sano, E. et al. Engineering of vascularized 3D cell constructs to model cellular interactions through a vascular network. *Biomicrofluidics* **12**, 042204 (2018).
29. Wang, Y., Wang, L., Zhu, Y. & Qin, J. Human brain organoid-on-a-chip to model prenatal nicotine exposure. *Lab on a Chip* **18**, 851-860 (2018).
30. Duval, K. et al. Modeling physiological events in 2D vs. 3D cell culture. *Physiology* **32**, 266-277 (2017).
31. Kapalczyńska, M. et al. 2D and 3D cell cultures—a comparison of different types of cancer cell cultures. *Archives of medical science: AMS* **14**, 910 (2018).
32. Lovitt, C.J., Shelper, T.B. & Avery, V.M. Advanced cell culture techniques for cancer drug discovery. *Biology* **3**, 345-367 (2014).
33. Li, F., Shen, A. & Amanullah, A. Cell culture processes in monoclonal antibody production. *Pharmaceutical Sciences Encyclopedia: Drug Discovery, Development, and Manufacturing*, 1-38 (2010).
34. Montomoli, E. et al. Cell culture-derived influenza vaccines from Vero cells: a new horizon for vaccine production. *Expert review of vaccines* **11**, 587-594 (2012).
35. Daley, G.Q. & Scadden, D.T. Prospects for stem cell-based therapy. *Cell* **132**, 544-548 (2008).
36. Hussein, K.H., Park, K.-M., Kang, K.-S. & Woo, H.-M. Biocompatibility evaluation of tissue-engineered decellularized scaffolds for biomedical application. *Materials Science and Engineering: C* **67**, 766-778 (2016).

37. Gomes, M.E., Rodrigues, M.T., Domingues, R.M. & Reis, R.L. Tissue engineering and regenerative medicine: new trends and directions—a year in review. *Tissue Engineering Part B: Reviews* **23**, 211-224 (2017).
38. Jin, R. & Dijkstra, P.J. in Biomedical applications of hydrogels handbook 203-225 (Springer, 2010).
39. Leijten, J. et al. Spatially and temporally controlled hydrogels for tissue engineering. *Materials Science and Engineering: R: Reports* **119**, 1-35 (2017).
40. Yao, T. & Asayama, Y. Animal-cell culture media: history, characteristics, and current issues. *Reproductive medicine and biology* **16**, 99-117 (2017).
41. Hosoya, K., Takahashi, K., Oya, K. & Iwamori, S. Simultaneous process of surface modification and sterilization for polystyrene dish. *Vacuum* **148**, 69-77 (2018).
42. Lerman, M.J., Lembong, J., Muramoto, S., Gillen, G. & Fisher, J.P. The evolution of polystyrene as a cell culture material. *Tissue Engineering Part B: Reviews* **24**, 359-372 (2018).
43. Stone, N.L., England, T.J. & O'Sullivan, S.E. A Novel Transwell Blood Brain Barrier Model Using Primary Human Cells. *Frontiers in Cellular Neuroscience* **13** (2019).
44. van Duinen, V., Trietsch, S.J., Joore, J., Vulto, P. & Hankemeier, T. Microfluidic 3D cell culture: from tools to tissue models. *Current Opinion in Biotechnology* **35**, 118-126 (2015).
45. Taylor, M.W. Viruses and man: A history of interactions. (Springer, 2014).
46. Jedrzejczak-Silicka, M. History of cell culture. (InTech, 2017).
47. Kuo, C.-T. et al. Three-dimensional spheroid culture targeting versatile tissue bioassays using a PDMS-based hanging drop array. *Scientific Reports* **7**, 4363 (2017).
48. Murali, A., Ramlogan-Steel, C.A., Andrzejewski, S., Steel, J.C. & Layton, C.J. Retinal explant culture: A platform to investigate human neuro-retina. *Clinical & experimental ophthalmology* **47**, 274-285 (2019).
49. Jackson, R. et al. Isolation of human explant derived cardiac stem cells from cryopreserved heart tissue. *PloS one* **12** (2017).
50. Castiaux, A.D., Spence, D.M. & Martin, R.S. Review of 3D cell culture with analysis in microfluidic systems. *Analytical Methods* **11**, 4220-4232 (2019).
51. Bai, C. et al. Associations of chemo-and radio-resistant phenotypes with the gap junction, adhesion and extracellular matrix in a three-dimensional culture model of soft sarcoma. *Journal of Experimental & Clinical Cancer Research* **34**, 58 (2015).
52. Soares, C.P. et al. 2D and 3D-organized cardiac cells shows differences in cellular morphology, adhesion junctions, presence of myofibrils and protein expression. *PloS one* **7** (2012).
53. Frega, M., Tedesco, M., Massobrio, P., Pesce, M. & Martinoia, S. Network dynamics of 3D engineered neuronal cultures: a new experimental model for in-vitro electrophysiology. *Scientific reports* **4**, 5489 (2014).
54. Alberts, B. et al. in Molecular Biology of the Cell. 4th edition (Garland Science, 2002).
55. Matter, K. & Balda, M.S. Signalling to and from tight junctions. *Nature reviews Molecular cell biology* **4**, 225-237 (2003).
56. Zihni, C., Balda, M.S. & Matter, K. Signalling at tight junctions during epithelial differentiation and microbial pathogenesis. *Journal of cell science* **127**, 3401-3413 (2014).
57. Balda, M.S. & Matter, K. Tight junctions and the regulation of gene expression. *Biochimica Et Biophysica Acta (BBA)-Biomembranes* **1788**, 761-767 (2009).
58. Zihni, C., Mills, C., Matter, K. & Balda, M.S. Tight junctions: from simple barriers to multifunctional molecular gates. *Nature reviews Molecular cell biology* **17**, 564 (2016).
59. Xu, Z., Chen, Y. & Chen, Y. Spatiotemporal regulation of Rho GTPases in neuronal migration. *Cells* **8**, 568 (2019).
60. Braga, V.M. Cell–cell adhesion and signalling. *Current opinion in cell biology* **14**, 546-556 (2002).
61. Maeda, S. & Tsukihara, T. Structure of the gap junction channel and its implications for its biological functions. *Cellular and Molecular Life Sciences* **68**, 1115-1129 (2011).
62. Labernadie, A. et al. A mechanically active heterotypic E-cadherin/N-cadherin adhesion enables fibroblasts to drive cancer cell invasion. *Nature cell biology* **19**, 224-237 (2017).
63. Abbott, N.J., Rönnbäck, L. & Hansson, E. Astrocyte–endothelial interactions at the blood–brain barrier. *Nature Reviews Neuroscience* **7**, 41-53 (2006).
64. Alberts, B. et al. in Molecular Biology of the Cell. 4th edition (Garland Science, 2002).
65. Davidson, M., Kukla, D. & Khetani, S. Microengineered cultures containing human hepatic stellate cells and hepatocytes for drug development. *Integr. Biol.* **9** (2017).
66. Foster, E. et al. Heparin hydrogel sandwich cultures of primary hepatocytes. *European Polymer Journal* **72**, 726-735 (2015).
67. Huh, D. et al. Reconstituting organ-level lung functions on a chip. *Science* **328**, 1662-1668 (2010).
68. Kolahi, K.S. et al. Effect of substrate stiffness on early mouse embryo development. *PloS one* **7** (2012).
69. Cox, T.R. & Erler, J.T. Remodeling and homeostasis of the extracellular matrix: implications for fibrotic diseases and cancer. *Disease models & mechanisms* **4**, 165-178 (2011).
70. Butcher, D.T., Alliston, T. & Weaver, V.M. A tense situation: forcing tumour progression. *Nature Reviews Cancer* **9**, 108-122 (2009).
71. Handorf, A.M., Zhou, Y., Halanski, M.A. & Li, W.-J. Tissue stiffness dictates development, homeostasis, and disease progression. *Organogenesis* **11**, 1-15 (2015).
72. Ariza de Schellenberger, A., Bergs, J., Sack, I. & Taupitz, M. in Quantification of Biophysical Parameters in Medical Imaging. (eds. I. Sack & T. Schaeffter) 123-150 (Springer International Publishing, Cham; 2018).
73. Humphrey, J.D., Dufresne, E.R. & Schwartz, M.A. Mechanotransduction and extracellular matrix homeostasis. *Nature reviews Molecular cell biology* **15**, 802-812 (2014).

74. Lu, P., Takai, K., Weaver, V.M. & Werb, Z. Extracellular matrix degradation and remodeling in development and disease. *Cold Spring Harb Perspect Biol* **3**, a005058 (2011).
75. Engler, A.J., Sen, S., Sweeney, H.L. & Discher, D.E. Matrix elasticity directs stem cell lineage specification. *Cell* **126**, 677-689 (2006).
76. LaValley, D.J. & Reinhart-King, C.A. Matrix stiffening in the formation of blood vessels. *Advances in Regenerative Biology* **1**, 25247 (2014).
77. Hanjaya-Putra, D. et al. Vascular endothelial growth factor and substrate mechanics regulate in vitro tubulogenesis of endothelial progenitor cells. *Journal of cellular and molecular medicine* **14**, 2436-2447 (2010).
78. Thorne, J.T. et al. Dynamic reciprocity between cells and their microenvironment in reproduction. *Biol Reprod* **92**, 25-25 (2015).
79. Baker, B.M. & Chen, C.S. Deconstructing the third dimension—how 3D culture microenvironments alter cellular cues. *Journal of cell science* **125**, 3015-3024 (2012).
80. Langhans, S.A. Three-dimensional in vitro cell culture models in drug discovery and drug repositioning. *Frontiers in pharmacology* **9**, 6 (2018).
81. De Mori, A., Peña Fernández, M., Blunn, G., Tozzi, G. & Roldo, M. 3D Printing and Electrospinning of Composite Hydrogels for Cartilage and Bone Tissue Engineering. *Polymers (Basel)* **10**, 285 (2018).
82. Fennema, E., Rivron, N., Rouwkema, J., van Blitterswijk, C. & de Boer, J. Spheroid culture as a tool for creating 3D complex tissues. *Trends in biotechnology* **31**, 108-115 (2013).
83. Carter, S.-S.D., Liu, X., Yue, Z. & Wallace, G.G. Three-dimensional neuronal cell culture: in pursuit of novel treatments for neurodegenerative disease. *MRS Communications* **7**, 320-331 (2017).
84. Edmondson, R., Broglie, J.J., Adcock, A.F. & Yang, L. Three-dimensional cell culture systems and their applications in drug discovery and cell-based biosensors. *Assay and drug development technologies* **12**, 207-218 (2014).
85. Chen, Y.-W. et al. A three-dimensional model of human lung development and disease from pluripotent stem cells. *Nature cell biology* **19**, 542-549 (2017).
86. Workman, M.J. et al. Engineered human pluripotent-stem-cell-derived intestinal tissues with a functional enteric nervous system. *Nature medicine* **23**, 49-59 (2017).
87. Ma, Z. et al. Self-organizing human cardiac microchambers mediated by geometric confinement. *Nature communications* **6**, 1-10 (2015).
88. Clevers, H. Modeling development and disease with organoids. *Cell* **165**, 1586-1597 (2016).
89. Kunz-Schughart, L.A., Freyer, J.P., Hofstaedter, F. & Ebner, R. The use of 3-D cultures for high-throughput screening: the multicellular spheroid model. *Journal of biomolecular screening* **9**, 273-285 (2004).
90. Jung, Y. et al. Scaffold-free, human mesenchymal stem cell-based tissue engineered blood vessels. *Scientific reports* **5**, 15116 (2015).
91. Rodenhizer, D., Dean, T., Xu, B., Cojocari, D. & McGuigan, A.P. A three-dimensional engineered heterogeneous tumor model for assessing cellular environment and response. *Nature protocols* **13**, 1917-1957 (2018).
92. Suzuki, N. et al. Neuronal Cell Sheets of Cortical Motor Neuron Phenotype Derived from Human iPSCs. *Cell Transplant* **26**, 1355-1364 (2017).
93. Ishigami, M. et al. Human iPS cell-derived cardiac tissue sheets for functional restoration of infarcted porcine hearts. *PloS one* **13**, e0201650 (2018).
94. Catto, V., Farè, S., Freddi, G. & Tanzi, M.C. Vascular tissue engineering: recent advances in small diameter blood vessel regeneration. *ISRN Vascular Medicine* **2014** (2014).
95. Vunjak-Novakovic, G. & Radisic, M. in *Biopolymer Methods in Tissue Engineering* 131-145 (Springer, 2004).
96. Qasim, M., Haq, F., Kang, M.-H. & Kim, J.-H. 3D printing approaches for cardiac tissue engineering and role of immune modulation in tissue regeneration. *International journal of nanomedicine* **14**, 1311 (2019).
97. Li, N., Tourovskaia, A. & Folch, A. Biology on a chip: microfabrication for studying the behavior of cultured cells. *Critical Reviews™ in Biomedical Engineering* **31** (2003).
98. Li, X., Valadez, A.V., Zuo, P. & Nie, Z. Microfluidic 3D cell culture: potential application for tissue-based bioassays. *Bioanalysis* **4**, 1509-1525 (2012).
99. Ermis, M., Antmen, E. & Hasirci, V. Micro and Nanofabrication methods to control cell-substrate interactions and cell behavior: A review from the tissue engineering perspective. *Bioactive Materials* **3**, 355-369 (2018).
100. Huang, X. et al. Monitoring the intracellular calcium response to a dynamic hypertonic environment. *Scientific Reports* **6**, 23591 (2016).
101. Chaicharoenaudomrung, N., Kunhorm, P. & Noisa, P. Three-dimensional cell culture systems as an in vitro platform for cancer and stem cell modeling. *World Journal of Stem Cells* **11**, 1065 (2019).
102. Mansour, A.A. et al. An in vivo model of functional and vascularized human brain organoids. *Nature Biotechnology* **36**, 432 (2018).
103. Whitesides, G.M. The origins and the future of microfluidics. *Nature* **442**, 368-373 (2006).
104. Beebe, D.J., Mensing, G.A. & Walker, G.M. Physics and applications of microfluidics in biology. *Annual review of biomedical engineering* **4**, 261-286 (2002).
105. Olanrewaju, A., Beaugrand, M., Yafia, M. & Juncker, D. Capillary microfluidics in microchannels: from microfluidic networks to capillary circuits. *Lab on a Chip* **18**, 2323-2347 (2018).
106. Coluccio, M.L. et al. Microfluidic platforms for cell cultures and investigations. *Microelectronic Engineering* **208**, 14-28 (2019).
107. Du, G., Fang, Q. & den Toonder, J.M.J. Microfluidics for cell-based high throughput screening platforms—A review. *Analytica Chimica Acta* **903**, 36-50 (2016).

108. Young, E.W. & Beebe, D.J. Fundamentals of microfluidic cell culture in controlled microenvironments. *Chemical Society Reviews* **39**, 1036-1048 (2010).
109. Eijkel, J.C. & Van Den Berg, A. Water in micro-and nanofluidics systems described using the water potential. *Lab on a Chip* **5**, 1202-1209 (2005).
110. Eijkel, J.C. & Van Den Berg, A. Young 4ever-the use of capillarity for passive flow handling in lab on a chip devices. *Lab on a Chip* **6**, 1405-1408 (2006).
111. Green, J., Holdø, A. & Khan, A. A review of passive and active mixing systems in microfluidic devices. *The International Journal of Multiphysics* **1** (2007).
112. Gökaltun, A., Kang, Y.B.A., Yarmush, M.L., Usta, O.B. & Asatekin, A. Simple Surface Modification of Poly(dimethylsiloxane) via Surface Segregating Smart Polymers for Biomicrofluidics. *Scientific reports* **9**, 7377-7377 (2019).
113. Parittotokkaporn, S. et al. Make it simple: long-term stable gradient generation in a microfluidic microdevice. *Biomedical microdevices* **21**, 77 (2019).
114. Skafte-Pedersen, P. et al. A self-contained, programmable microfluidic cell culture system with real-time microscopy access. *Biomedical microdevices* **14**, 385-399 (2012).
115. Komeya, M. et al. Pumpless microfluidic system driven by hydrostatic pressure induces and maintains mouse spermatogenesis in vitro. *Scientific reports* **7**, 1-8 (2017).
116. Wang, Y.I. & Shuler, M.L. UniChip enables long-term recirculating unidirectional perfusion with gravity-driven flow for microphysiological systems. *Lab on a Chip* **18**, 2563-2574 (2018).
117. Phan, D.T. et al. A vascularized and perfused organ-on-a-chip platform for large-scale drug screening applications. *Lab on a Chip* **17**, 511-520 (2017).
118. Huh, D., Hamilton, G.A. & Ingber, D.E. From 3D cell culture to organs-on-chips. *Trends in cell biology* **21**, 745-754 (2011).
119. Park, S.E., Georgescu, A. & Huh, D. Organoids-on-a-chip. *Science* **364**, 960-965 (2019).
120. Bhatia, S.N. & Ingber, D.E. Microfluidic organs-on-chips. *Nature biotechnology* **32**, 760 (2014).
121. Homan, K.A. et al. Flow-enhanced vascularization and maturation of kidney organoids in vitro. *Nature Methods* **16**, 255-262 (2019).
122. Harms, V. & Elias, L. in *Encyclopedia of Behavioral Medicine*. (eds. M.D. Gellman & J.R. Turner) 262-263 (Springer New York, New York, NY; 2013).
123. Ahn, S.I. et al. Microengineered human blood-brain barrier platform for understanding nanoparticle transport mechanisms. *Nature Communications* **11**, 175 (2020).
124. van Der Helm, M.W., Van Der Meer, A.D., Eijkel, J.C., van den Berg, A. & Segerink, L.I. Microfluidic organ-on-chip technology for blood-brain barrier research. *Tissue barriers* **4**, e1142493 (2016).
125. Wong, A. et al. The blood-brain barrier: an engineering perspective. *Frontiers in neuroengineering* **6**, 7 (2013).
126. Takebe, T., Zhang, B. & Radisic, M. Synergistic engineering: organoids meet organs-on-a-chip. *Cell Stem Cell* **21**, 297-300 (2017).
127. Wang, Y., Wang, L., Guo, Y., Zhu, Y. & Qin, J. Engineering stem cell-derived 3D brain organoids in a perfusable organ-on-a-chip system. *RSC advances* **8**, 1677-1685 (2018).
128. Kim, J.A., Hong, S. & Rhee, W.J. Microfluidic three-dimensional cell culture of stem cells for high-throughput analysis. *World journal of stem cells* **11**, 803 (2019).
129. Götz, J., Bodea, L.-G. & Goedert, M. Rodent models for Alzheimer disease. *Nature Reviews Neuroscience* **19**, 583-598 (2018).
130. Thomson, J.A. et al. Embryonic stem cell lines derived from human blastocysts. *science* **282**, 1145-1147 (1998).
131. Takahashi, K. & Yamanaka, S. Induction of Pluripotent Stem Cells from Mouse Embryonic and Adult Fibroblast Cultures by Defined Factors. *Cell* **126**, 663-676 (2006).
132. Gibbons, H.M. & Dragunow, M. Adult human brain cell culture for neuroscience research. *The international journal of biochemistry & cell biology* **42**, 844-856 (2010).
133. Ellenbroek, B. & Youn, J. Rodent models in neuroscience research: is it a rat race? *Disease models & mechanisms* **9**, 1079-1087 (2016).
134. Jorfi, M., D'Avanzo, C., Kim, D.Y. & Irimia, D. Three-dimensional models of the human brain development and diseases. *Advanced healthcare materials* **7**, 1700723 (2018).
135. Kelava, I. & Lancaster, M.A. Dishing out mini-brains: current progress and future prospects in brain organoid research. *Developmental biology* **420**, 199-209 (2016).
136. Pound, P., Ebrahim, S., Sandercock, P., Bracken, M.B. & Roberts, I. Where is the evidence that animal research benefits humans? *Bmj* **328**, 514-517 (2004).
137. Yang, N., Ng, Y.H., Pang, Z.P., Südhof, T.C. & Wernig, M. Induced neuronal cells: how to make and define a neuron. *Cell stem cell* **9**, 517-525 (2011).
138. Al-Ali, H., Blackmore, M., Bixby, J.L. & Lemmon, V.P. in *Assay Guidance Manual* [Internet] (Eli Lilly & Company and the National Center for Advancing Translational Sciences, 2014).
139. Humpel, C. Organotypic brain slice cultures: A review. *Neuroscience* **305**, 86-98 (2015).
140. Lee, C.-T., Bendriem, R.M., Wu, W.W. & Shen, R.-F. 3D brain Organoids derived from pluripotent stem cells: promising experimental models for brain development and neurodegenerative disorders. *Journal of biomedical science* **24**, 59 (2017).
141. Qian, X. et al. Brain-region-specific organoids using mini-bioreactors for modeling ZIKV exposure. *Cell* **165**, 1238-1254 (2016).
142. Tomaskovic-Crook, E. & Crook, J.M. in *Organoids: Stem Cells, Structure, and Function*. (ed. K. Turksen) 13-22 (Springer New York, New York, NY; 2019).
143. Gordon, J., Amini, S. & White, M.K. in *Neuronal Cell Culture* 1-8 (Springer, 2013).

144. McGraw, C.M., Ward, C.S. & Samaco, R.C. in American Journal of Medical Genetics Part C: Seminars in Medical Genetics, Vol. 175 368-379 (Wiley Online Library, 2017).
145. Dezone, R.S. et al. Derivation of Functional Human Astrocytes from Cerebral Organoids. *Scientific Reports* **7**, 45091 (2017).
146. Ravi, V.M. et al. Human organotypic brain slice culture: a novel framework for environmental research in neuro-oncology. *Life science alliance* **2** (2019).
147. Ormel, P.R. et al. Microglia innately develop within cerebral organoids. *Nature Communications* **9**, 4167 (2018).
148. Hall, A.A. et al. Delayed treatments for stroke influence neuronal death in rat organotypic slice cultures subjected to oxygen glucose deprivation. *Neuroscience* **164**, 470-477 (2009).
149. Ham, O., Jin, Y.B., Kim, J. & Lee, M.-O. Blood vessel formation in cerebral organoids formed from human embryonic stem cells. *Biochemical and Biophysical Research Communications* **521**, 84-90 (2020).
150. Farahany, N.A. et al. The ethics of experimenting with human brain tissue. *Nature* **556**, 429-432 (2018).
151. Adams, J.W., Cugola, F.R. & Muotri, A.R. Brain organoids as tools for modeling human neurodevelopmental disorders. *Physiology* **34**, 365-375 (2019).
152. Megiorni, F., Mora, B., Indovina, P. & Mazzilli, M.C. Expression of neuronal markers during NTera2/cloneD1 differentiation by cell aggregation method. *Neuroscience Letters* **373**, 105-109 (2005).
153. Nolan, G.P. What's wrong with drug screening today. *Nature Chemical Biology* **3**, 187-191 (2007).
154. Daub, A., Sharma, P. & Finkbeiner, S. High-content screening of primary neurons: ready for prime time. *Curr Opin Neurobiol* **19**, 537-543 (2009).
155. Bahmad, H. et al. Modeling human neurological and neurodegenerative diseases: from induced pluripotent stem cells to neuronal differentiation and its applications in neurotrauma. *Frontiers in molecular neuroscience* **10**, 50 (2017).
156. Chestkov, I.V., Vasilieva, E.A., Illarioshkin, S.N., Lagarkova, M.A. & Kiselev, S.L. Patient-Specific Induced Pluripotent Stem Cells for SOD1-Associated Amyotrophic Lateral Sclerosis Pathogenesis Studies. *Acta Naturae* **6**, 54-60 (2014).
157. Minami, N. et al. Organotypic brain explant culture as a drug evaluation system for malignant brain tumors. *Cancer Med* **6**, 2635-2645 (2017).
158. Alberdi, E. et al. Amyloid β oligomers induce Ca^{2+} dysregulation and neuronal death through activation of ionotropic glutamate receptors. *Cell Calcium* **47**, 264-272 (2010).
159. Cavaliere, F., Dinkel, K. & Reymann, K. The subventricular zone releases factors which can be protective in oxygen/glucose deprivation-induced cortical damage: An organotypic study. *Experimental Neurology* **201**, 66-74 (2006).
160. Daviaud, N., Garbayo, E., Schiller, P.C., Perez-Pinzon, M. & Montero-Menei, C.N. Organotypic cultures as tools for optimizing central nervous system cell therapies. *Experimental Neurology* **248**, 429-440 (2013).
161. Kovács, R., Papageorgiou, I. & Heinemann, U. Slice Cultures as a Model to Study Neurovascular Coupling and Blood Brain Barrier In Vitro. *Cardiovascular Psychiatry and Neurology* **2011**, 646958 (2011).
162. Quadrato, G., Brown, J. & Arlotta, P. The promises and challenges of human brain organoids as models of neuropsychiatric disease. *Nature medicine* **22**, 1220 (2016).
163. Eiraku, M. et al. Self-organized formation of polarized cortical tissues from ESCs and its active manipulation by extrinsic signals. *Cell stem cell* **3**, 519-532 (2008).
164. Kadoshima, T. et al. Self-organization of axial polarity, inside-out layer pattern, and species-specific progenitor dynamics in human ES cell-derived neocortex. *Proceedings of the National Academy of Sciences* **110**, 20284-20289 (2013).
165. Sakaguchi, H. et al. Generation of functional hippocampal neurons from self-organizing human embryonic stem cell-derived dorsomedial telencephalic tissue. *Nature Communications* **6**, 8896 (2015).
166. Muguruma, K., Nishiyama, A., Kawakami, H., Hashimoto, K. & Sasai, Y. Self-organization of polarized cerebellar tissue in 3D culture of human pluripotent stem cells. *Cell reports* **10**, 537-550 (2015).
167. Li, Y. et al. Induction of Expansion and Folding in Human Cerebral Organoids. *Cell Stem Cell* **20**, 385-396.e383 (2017).
168. Otani, T., Marchetto, M.C., Gage, F.H., Simons, B.D. & Livesey, F.J. 2D and 3D stem cell models of primate cortical development identify species-specific differences in progenitor behavior contributing to brain size. *Cell stem cell* **18**, 467-480 (2016).
169. Arzua, T. et al. Modeling alcohol-induced neurotoxicity using human induced pluripotent stem cell-derived three-dimensional cerebral organoids. *Translational psychiatry* **10**, 1-21 (2020).
170. Depla, J.A. et al. Cerebral Organoids: A Human Model for AAV Capsid Selection and Therapeutic Transgene Efficacy in the Brain. *Molecular Therapy-Methods & Clinical Development* **18**, 167-175 (2020).
171. Alić, I. et al. Patient-specific Alzheimer-like pathology in trisomy 21 cerebral organoids reveals BACE2 as a gene dose-sensitive AD suppressor in human brain. *Molecular Psychiatry*, 1-23 (2020).
172. Daviaud, N., Chevalier, C., Friedel, R.H. & Zou, H. Distinct vulnerability and resilience of human neuroprogenitor subtypes in cerebral organoid model of prenatal hypoxic injury. *Frontiers in cellular neuroscience* **13**, 336 (2019).
173. Gabriel, E. et al. Recent Zika Virus Isolates Induce Premature Differentiation of Neural Progenitors in Human Brain Organoids. *Cell Stem Cell* **20**, 397-406.e395 (2017).
174. Qiao, H. et al. Herpes simplex virus type 1 infection leads to neurodevelopmental disorder-associated neuropathological changes. *PLoS Pathogens* **16**, e1008899 (2020).
175. Zhang, B. et al. Differential antiviral immunity to Japanese encephalitis virus in developing cortical organoids. *Cell Death & Disease* **9**, 719 (2018).
176. Song, E. et al. Neuroinvasion of SARS-CoV-2 in human and mouse brain. *Journal of Experimental Medicine* **218** (2021).
177. Wang, H. Modeling neurological diseases with human brain organoids. *Frontiers in synaptic neuroscience* **10**, 15 (2018).

178. Mehrjardi, M.Z. Is Zika virus an emerging TORCH agent? An invited commentary. *Virology: research and treatment* **8**, 1178122X17708993 (2017).
179. Organization, W.H. WHO Coronavirus (COVID-19) Dashboard <https://covid19.who.int/>. (2021).
180. Lai, C.-C., Shih, T.-P., Ko, W.-C., Tang, H.-J. & Hsueh, P.-R. Severe acute respiratory syndrome coronavirus 2 (SARS-CoV-2) and coronavirus disease-2019 (COVID-19): The epidemic and the challenges. *International Journal of Antimicrobial Agents* **55**, 105924 (2020).
181. Mao, L. et al. Neurologic Manifestations of Hospitalized Patients With Coronavirus Disease 2019 in Wuhan, China. *JAMA Neurology* **77**, 683-690 (2020).
182. Smith, J.C. & Sheltzer, J.M. Cigarette smoke triggers the expansion of a subpopulation of respiratory epithelial cells that express the SARS-CoV-2 receptor ACE2. *bioRxiv*, 2020.2003.2028.013672 (2020).
183. Monzel, A.S. et al. Derivation of Human Midbrain-Specific Organoids from Neuroepithelial Stem Cells. *Stem Cell Reports* **8**, 1144-1154 (2017).
184. Dalrymple, N.A. & Mackow, E.R. Endothelial cells elicit immune-enhancing responses to dengue virus infection. *J Virol* **86**, 6408-6415 (2012).
185. Heinz, U.E. & Rollnik, J.D. Outcome and prognosis of hypoxic brain damage patients undergoing neurological early rehabilitation. *BMC Res Notes* **8**, 243-243 (2015).
186. Bray, N.J. & O'Donovan, M.C. The genetics of neuropsychiatric disorders. *Brain and neuroscience advances* **2**, 2398212818799271 (2018).
187. Gratten, J., Wray, N.R., Keller, M.C. & Visscher, P.M. Large-scale genomics unveils the genetic architecture of psychiatric disorders. *Nature neuroscience* **17**, 782-790 (2014).
188. Sanders, S.J. et al. De novo mutations revealed by whole-exome sequencing are strongly associated with autism. *Nature* **485**, 237-241 (2012).
189. Wray, S. Modelling neurodegenerative disease using brain organoids. *Seminars in Cell & Developmental Biology* **111**, 60-66 (2021).
190. Seo, J. et al. Inhibition of p25/Cdk5 attenuates tauopathy in mouse and iPSC models of frontotemporal dementia. *Journal of Neuroscience* **37**, 9917-9924 (2017).
191. Pérez-Brangulí, F. et al. Human SPG11 cerebral organoids reveal cortical neurogenesis impairment. *Human Molecular Genetics* **28**, 961-971 (2018).
192. Gonzalez, C. et al. Modeling amyloid beta and tau pathology in human cerebral organoids. *Molecular psychiatry* **23**, 2363-2374 (2018).
193. Yan, Y. et al. Modeling neurodegenerative microenvironment using cortical organoids derived from human stem cells. *Tissue Engineering Part A* **24**, 1125-1137 (2018).
194. Conforti, P. et al. Faulty neuronal determination and cell polarization are reverted by modulating HD early phenotypes. *Proc Natl Acad Sci U S A* **115**, E762-E771 (2018).
195. Kim, H. et al. Modeling G2019S-LRRK2 sporadic Parkinson's disease in 3D midbrain organoids. *Stem Cell Reports* **12**, 518-531 (2019).
196. Kawada, J. et al. Generation of a motor nerve organoid with human stem cell-derived neurons. *Stem cell reports* **9**, 1441-1449 (2017).
197. Choi, S.H. et al. A three-dimensional human neural cell culture model of Alzheimer's disease. *Nature* **515**, 274-278 (2014).
198. Meyer, K. et al. REST and neural gene network dysregulation in iPSC models of Alzheimer's disease. *Cell reports* **26**, 1112-1127. e1119 (2019).
199. Galet, B., Cheval, H. & Ravassard, P. Patient-Derived Midbrain Organoids to Explore the Molecular Basis of Parkinson's Disease. *Frontiers in Neurology* **11**, 1005 (2020).
200. Hegarty, S.V., Sullivan, A.M. & O'Keefe, G.W. Midbrain dopaminergic neurons: A review of the molecular circuitry that regulates their development. *Developmental Biology* **379**, 123-138 (2013).
201. Mohamed, N.-V. et al. Generation of human midbrain organoids from induced pluripotent stem cells. *MNI Open Research* **3** (2019).
202. Chesselet, M.-F., Fleming, S., Mortazavi, F. & Meurers, B. Strengths and limitations of genetic mouse models of Parkinson's disease. *Parkinsonism & Related Disorders* **14**, S84-S87 (2008).
203. Kriks, S. et al. Dopamine neurons derived from human ES cells efficiently engraft in animal models of Parkinson's disease. *Nature* **480**, 547-551 (2011).
204. Miller, J.D. et al. Human iPSC-based modeling of late-onset disease via progerin-induced aging. *Cell stem cell* **13**, 691-705 (2013).
205. Restelli, L.M. et al. Neuronal mitochondrial dysfunction activates the integrated stress response to induce fibroblast growth factor 21. *Cell reports* **24**, 1407-1414 (2018).
206. Quadrato, G. et al. Cell diversity and network dynamics in photosensitive human brain organoids. *Nature* **545**, 48-53 (2017).
207. Tieng, V. et al. Engineering of midbrain organoids containing long-lived dopaminergic neurons. *Stem cells and development* **23**, 1535-1547 (2014).
208. Jo, J. et al. Midbrain-like organoids from human pluripotent stem cells contain functional dopaminergic and neuromelanin-producing neurons. *Cell stem cell* **19**, 248-257 (2016).
209. Kwak, T.H. et al. Generation of homogeneous midbrain organoids with in vivo-like cellular composition facilitates neurotoxin-based Parkinson's disease modeling. *Stem Cells* **38**, 727-740 (2020).

210. Ahfeldt, T. et al. Pathogenic pathways in early-onset autosomal recessive Parkinson's disease discovered using isogenic human dopaminergic neurons. *Stem cell reports* **14**, 75-90 (2020).
211. Smits, L.M. & Schwamborn, J.C. Midbrain Organoids: A New Tool to Investigate Parkinson's Disease. *Frontiers in Cell and Developmental Biology* **8** (2020).
212. Teichberg, V.I., Cohen-Kashi-Malina, K., Cooper, I. & Zlotnik, A. Homeostasis of glutamate in brain fluids: An accelerated brain-to-blood efflux of excess glutamate is produced by blood glutamate scavenging and offers protection from neuropathologies. *Neuroscience* **158**, 301-308 (2009).
213. Matsui, T.K., Tsuru, Y., Hasegawa, K. & Kuwako, K.-i. Vascularization of human brain organoids. *Stem Cells* **39**, 1017-1024 (2021).
214. Lovett, M., Lee, K., Edwards, A. & Kaplan, D.L. Vascularization strategies for tissue engineering. *Tissue Eng Part B Rev* **15**, 353-370 (2009).
215. Ao, Z. et al. Tubular human brain organoids to model microglia-mediated neuroinflammation. *Lab on a Chip* (2021).
216. Nickels, S.L. et al. Reproducible generation of human midbrain organoids for in vitro modeling of Parkinson's disease. *Stem Cell Research* **46**, 101870 (2020).
217. Berger, E. et al. Millifluidic culture improves human midbrain organoid vitality and differentiation. *Lab on a Chip* **18**, 3172-3183 (2018).
218. Qian, X. et al. Sliced Human Cortical Organoids for Modeling Distinct Cortical Layer Formation. *Cell Stem Cell* **26**, 766-781.e769 (2020).
219. Kroemer, G. et al. Classification of cell death: recommendations of the Nomenclature Committee on Cell Death 2009. *Cell Death Differ* **16**, 3-11 (2009).
220. Paşca, A.M. et al. Functional cortical neurons and astrocytes from human pluripotent stem cells in 3D culture. *Nature methods* **12**, 671-678 (2015).
221. Lee, C.-T. et al. CYP3A5 mediates effects of cocaine on human neocorticalogenesis: studies using an in vitro 3D self-organized hPSC model with a single cortex-like unit. *Neuropsychopharmacology* **42**, 774-784 (2017).
222. Bian, S. et al. Genetically engineered cerebral organoids model brain tumor formation. *Nature Methods* **15**, 631-639 (2018).
223. Cai, H. et al. Intelligent acoustofluidics enabled mini-bioreactors for human brain organoids. *Lab on a Chip* **21**, 2194-2205 (2021).
224. Boisvert, E.M., Means, R.E., Michaud, M., Madri, J.A. & Katz, S.G. Minocycline mitigates the effect of neonatal hypoxic insult on human brain organoids. *Cell Death & Disease* **10**, 325 (2019).
225. Harbuzariu, A. et al. Modelling heme-mediated brain injury associated with cerebral malaria in human brain cortical organoids. *Scientific Reports* **9**, 19162 (2019).
226. dos Reis, R.S., Sant, S., Keeney, H., Wagner, M.C.E. & Ayyavoo, V. Modeling HIV-1 neuropathogenesis using three-dimensional human brain organoids (hBORGs) with HIV-1 infected microglia. *Scientific Reports* **10**, 15209 (2020).
227. Greijer, A.E. & van der Wall, E. The role of hypoxia inducible factor 1 (HIF-1) in hypoxia induced apoptosis. *J Clin Pathol* **57**, 1009-1014 (2004).
228. Velasco, S. et al. Individual brain organoids reproducibly form cell diversity of the human cerebral cortex. *Nature* **570**, 523-527 (2019).
229. Xiang, Y. et al. hESC-Derived Thalamic Organoids Form Reciprocal Projections When Fused with Cortical Organoids. *Cell Stem Cell* **24**, 487-497.e487 (2019).
230. Forristal, C.E., Wright, K.L., Hanley, N.A., Oreffo, R.O.C. & Houghton, F.D. Hypoxia inducible factors regulate pluripotency and proliferation in human embryonic stem cells cultured at reduced oxygen tensions. *Reproduction* **139**, 85-97 (2010).
231. Studer, L. et al. Enhanced proliferation, survival, and dopaminergic differentiation of CNS precursors in lowered oxygen. *J Neurosci* **20**, 7377-7383 (2000).
232. Pistollato, F., Chen, H.-L., Schwartz, P.H., Basso, G. & Panchision, D.M. Oxygen tension controls the expansion of human CNS precursors and the generation of astrocytes and oligodendrocytes. *Molecular and Cellular Neuroscience* **35**, 424-435 (2007).
233. Mazumdar, J. et al. O₂ regulates stem cells through Wnt/ β -catenin signalling. *Nature cell biology* **12**, 1007-1013 (2010).
234. Prado-Lopez, S. et al. Hypoxia Promotes Efficient Differentiation of Human Embryonic Stem Cells to Functional Endothelium. *STEM CELLS* **28**, 407-418 (2010).
235. Wang, Q., Yang, L. & Wang, Y. Enhanced differentiation of neural stem cells to neurons and promotion of neurite outgrowth by oxygen-glucose deprivation. *International Journal of Developmental Neuroscience* **43**, 50-57 (2015).
236. Nalivaeva, N.N., Turner, A.J. & Zhuravin, I.A. Role of Prenatal Hypoxia in Brain Development, Cognitive Functions, and Neurodegeneration. *Front Neurosci* **12**, 825-825 (2018).
237. Xiang, Y., Cakir, B. & Park, I.-H. in *Seminars in cell & developmental biology*, Vol. 111 40-51 (Elsevier, 2021).
238. Del Dosso, A., Urenda, J.-P., Nguyen, T. & Quadrato, G. Upgrading the physiological relevance of human brain organoids. *Neuron* **107**, 1014-1028 (2020).
239. Mansour, A.A., Schafer, S.T. & Gage, F.H. in *Seminars in Cell & Developmental Biology*, Vol. 111 32-39 (Elsevier, 2021).
240. Nutma, E., van Gent, D., Amor, S. & Peferoen, L.A.N. Astrocyte and Oligodendrocyte Cross-Talk in the Central Nervous System. *Cells* **9**, 600 (2020).
241. Chukwurah, E., Osmundsen, A., Davis, S.W. & Lizarraga, S.B. All together now: modeling the interaction of neural with non-neural systems using organoid models. *Front Neurosci* **13**, 582 (2019).
242. Renner, M. et al. Self-organized developmental patterning and differentiation in cerebral organoids. *The EMBO journal* **36**, 1316-1329 (2017).
243. Madhavan, M. et al. Induction of myelinating oligodendrocytes in human cortical spheroids. *Nature Methods* **15**, 700-706 (2018).

244. Marton, R.M. et al. Differentiation and maturation of oligodendrocytes in human three-dimensional neural cultures. *Nature Neuroscience* **22**, 484-491 (2019).
245. Abud, E.M. et al. iPSC-derived human microglia-like cells to study neurological diseases. *Neuron* **94**, 278-293. e279 (2017).
246. Haenseler, W. et al. A highly efficient human pluripotent stem cell microglia model displays a neuronal-co-culture-specific expression profile and inflammatory response. *Stem cell reports* **8**, 1727-1742 (2017).
247. Lin, Y.-T. et al. APOE4 Causes Widespread Molecular and Cellular Alterations Associated with Alzheimer's Disease Phenotypes in Human iPSC-Derived Brain Cell Types. *Neuron* **98**, 1141-1154.e1147 (2018).
248. Faravelli, I., Costamagna, G., Tamanini, S. & Corti, S. Back to the origins: Human brain organoids to investigate neurodegeneration. *Brain research* **1727**, 146561 (2020).
249. Espuny-Camacho, I. et al. Human pluripotent stem-cell-derived cortical neurons integrate functionally into the lesioned adult murine visual cortex in an area-specific way. *Cell reports* **23**, 2732-2743 (2018).
250. Bhaduri, A. et al. Cell stress in cortical organoids impairs molecular subtype specification. *Nature* **578**, 142-148 (2020).
251. Tang, Y., Liu, M.-L., Zang, T. & Zhang, C.-L. Direct reprogramming rather than iPSC-based reprogramming maintains aging hallmarks in human motor neurons. *Frontiers in molecular neuroscience* **10**, 359 (2017).
252. Lancaster, M.A. et al. Guided self-organization and cortical plate formation in human brain organoids. *Nature Biotechnology* **35**, 659-666 (2017).
253. Rouwkema, J. & Khademhosseini, A. Vascularization and angiogenesis in tissue engineering: beyond creating static networks. *Trends in biotechnology* **34**, 733-745 (2016).
254. Devillard, C.D. & Marquette, C.A. Vascular Tissue Engineering: Challenges and Requirements for an Ideal Large Scale Blood Vessel. *Frontiers in Bioengineering and Biotechnology*, 913 (2021).
255. Chang, W.G. & Niklason, L.E. A short discourse on vascular tissue engineering. *NPJ Regenerative medicine* **2**, 1-8 (2017).
256. Lee, S. et al. Microfluidic-based vascularized microphysiological systems. *Lab on a Chip* **18**, 2686-2709 (2018).
257. Vajda, J., Milojević, M., Maver, U. & Vihar, B. Microvascular Tissue Engineering—A Review. *Biomedicines* **9**, 589 (2021).
258. Yuan, S.-Y. & Rigor, R.R. in Colloquium Series on Integrated Systems Physiology: From Molecule to Function, Vol. 3 1-146 (Morgan & Claypool Life Sciences, 2011).
259. Beare, J.E., Curtis-Whitchurch, L., LeBlanc, A.J. & Hoying, J.B. in Encyclopedia of Cardiovascular Research and Medicine. (eds. R.S. Vasan & D.B. Sawyer) 349-364 (Elsevier, Oxford; 2018).
260. Kim, S., Lee, H., Chung, M. & Jeon, N.L. Engineering of functional, perfusable 3D microvascular networks on a chip. *Lab on a Chip* **13**, 1489-1500 (2013).
261. Wang, X., Sun, Q. & Pei, J. Microfluidic-Based 3D Engineered Microvascular Networks and Their Applications in Vascularized Microtumor Models. *Micromachines* **9**, 493 (2018).
262. Serbo, J.V. & Gerecht, S. Vascular tissue engineering: biodegradable scaffold platforms to promote angiogenesis. *Stem cell research & therapy* **4**, 1-8 (2013).
263. Wang, Z., Mithieux, S.M. & Weiss, A.S. Fabrication techniques for vascular and vascularized tissue engineering. *Advanced healthcare materials* **8**, 1900742 (2019).
264. Yang, G., Mahadik, B., Choi, J.Y. & Fisher, J.P. Vascularization in tissue engineering: fundamentals and state-of-art. *Progress in Biomedical Engineering* **2**, 012002 (2020).
265. Andrejcsk, J.W. & Hughes, C.C. Engineering perfused microvascular networks into microphysiological systems platforms. *Current Opinion in Biomedical Engineering* **5**, 74-81 (2018).
266. Chandrababu, K., Senan, M. & Krishnan, L.K. Exploitation of fibrin-based signaling niche for deriving progenitors from human adipose-derived mesenchymal stem cells towards potential neural engineering applications. *Scientific Reports* **10**, 7116 (2020).
267. Teebken, O.E. & Haverich, A. Tissue engineering of small diameter vascular grafts. *European journal of vascular and endovascular surgery* **23**, 475-485 (2002).
268. Peck, M., Gebhart, D., Dusserre, N., McAllister, T.N. & L'Heureux, N. The evolution of vascular tissue engineering and current state of the art. *Cells Tissues Organs* **195**, 144-158 (2012).
269. Song, H.H.G., Rumma, R.T., Ozaki, C.K., Edelman, E.R. & Chen, C.S. Vascular Tissue Engineering: Progress, Challenges, and Clinical Promise. *Cell stem cell* **22**, 340-354 (2018).
270. Osaki, T., Sivathanu, V. & Kamm, R.D. Vascularized microfluidic organ-chips for drug screening, disease models and tissue engineering. *Current opinion in biotechnology* **52**, 116-123 (2018).
271. Logsdon, E.A., Finley, S.D., Popel, A.S. & Gabhann, F.M. A systems biology view of blood vessel growth and remodelling. *Journal of cellular and molecular medicine* **18**, 1491-1508 (2014).
272. Andrique, L., Recher, G., Nassoy, P. & Bikfalvi, A. in Tumor Vascularization. (eds. D. Ribatti & F. Pezzella) 101-112 (Academic Press, 2020).
273. Ribatti, D., Vacca, A., Nico, B., Roncali, L. & Dammacco, F. Postnatal vasculogenesis. *Mechanisms of Development* **100**, 157-163 (2001).
274. Vailhé, B., Vittet, D. & Feige, J.-J. In Vitro Models of Vasculogenesis and Angiogenesis. *Laboratory Investigation* **81**, 439-452 (2001).
275. Drake, C.J. Embryonic and adult vasculogenesis. *Birth Defects Research Part C: Embryo Today: Reviews* **69**, 73-82 (2003).
276. Goldie, L.C., Nix, M.K. & Hirschi, K.K. Embryonic vasculogenesis and hematopoietic specification. *Organogenesis* **4**, 257-263 (2008).
277. Adair, T. & Montani, J. (
278. Matsumoto, K., Yoshitomi, H., Rossant, J. & Zaret, K.S. Liver organogenesis promoted by endothelial cells prior to vascular function. *Science* **294**, 559-563 (2001).

279. Lammert, E., Cleaver, O. & Melton, D. Induction of pancreatic differentiation by signals from blood vessels. *Science* **294**, 564-567 (2001).
280. Bauer, A.L., Jackson, T.L. & Jiang, Y. Topography of extracellular matrix mediates vascular morphogenesis and migration speeds in angiogenesis. *PLoS computational biology* **5**, e1000445 (2009).
281. De Smet, F., Segura, I., De Bock, K., Hohensinner, P.J. & Carmeliet, P. Mechanisms of vessel branching: filopodia on endothelial tip cells lead the way. *Arteriosclerosis, thrombosis, and vascular biology* **29**, 639-649 (2009).
282. Bentley, K., Mariggi, G., Gerhardt, H. & Bates, P.A. Tipping the balance: robustness of tip cell selection, migration and fusion in angiogenesis. *PLoS computational biology* **5**, e1000549 (2009).
283. Davis, G.E., Bayless, K.J. & Mavila, A. Molecular basis of endothelial cell morphogenesis in three-dimensional extracellular matrices. *The Anatomical Record: An Official Publication of the American Association of Anatomists* **268**, 252-275 (2002).
284. Kamei, M. et al. Endothelial tubes assemble from intracellular vacuoles in vivo. *Nature* **442**, 453-456 (2006).
285. Moreira-Soares, M., Coimbra, R., Rebelo, L., Carvalho, J. & D. M. Travasso, R. Angiogenic Factors produced by Hypoxic Cells are a leading driver of Anastomoses in Sprouting Angiogenesis—a computational study. *Scientific Reports* **8**, 8726 (2018).
286. Stratman, A.N. et al. Interactions between mural cells and endothelial cells stabilize the developing zebrafish dorsal aorta. *Development* **144**, 115-127 (2017).
287. Garcia, M.D. & Larina, I.V. Vascular development and hemodynamic force in the mouse yolk sac. *Frontiers in Physiology* **5** (2014).
288. Siafakas, N.M., Antoniou, K.M. & Tzortzaki, E.G. Role of angiogenesis and vascular remodeling in chronic obstructive pulmonary disease. *Int J Chron Obstruct Pulmon Dis* **2**, 453-462 (2007).
289. Hofer, I.E., den Adel, B. & Daemen, M.J.A.P. Biomechanical factors as triggers of vascular growth. *Cardiovascular Research* **99**, 276-283 (2013).
290. Morton, S.U. & Brodsky, D. Fetal Physiology and the Transition to Extrauterine Life. *Clin Perinatol* **43**, 395-407 (2016).
291. Liu, F. et al. Pathophysiologic Role of Molecules Determining Arteriovenous Differentiation in Adult Life. *Journal of Vascular Research* **57**, 245-253 (2020).
292. Adamo, L. et al. Biomechanical forces promote embryonic haematopoiesis. *Nature* **459**, 1131-1135 (2009).
293. Chien, S. Mechanotransduction and endothelial cell homeostasis: the wisdom of the cell. *American Journal of Physiology-Heart and Circulatory Physiology* **292**, H1209-H1224 (2007).
294. Lucitti, J.L. et al. Vascular remodeling of the mouse yolk sac requires hemodynamic force. (2007).
295. Heiss, C., Rodriguez-Mateos, A. & Kelm, M. Central role of eNOS in the maintenance of endothelial homeostasis. *Antioxid Redox Signal* **22**, 1230-1242 (2015).
296. Clark, E.R. Studies on the growth of blood-vessels in the tail of the frog larva—by observation and experiment on the living animal. *American Journal of Anatomy* **23**, 37-88 (1918).
297. Krogh, A. The number and distribution of capillaries in muscles with calculations of the oxygen pressure head necessary for supplying the tissue. *The Journal of physiology* **52**, 409 (1919).
298. Pries, A.R., Reglin, B. & Secomb, T.W. Modeling of angioadaptation: insights for vascular development. *Int J Dev Biol* **55**, 399-405 (2011).
299. karthik, S. et al. Synergistic interaction of sprouting and intussusceptive angiogenesis during zebrafish caudal vein plexus development. *Scientific Reports* **8**, 9840 (2018).
300. Egginton, S. In vivo shear stress response. *Biochemical Society Transactions* **39**, 1633-1638 (2011).
301. Galie, P.A. et al. Fluid shear stress threshold regulates angiogenic sprouting. *Proceedings of the National Academy of Sciences* **111**, 7968-7973 (2014).
302. Song, J.W. & Munn, L.L. Fluid forces control endothelial sprouting. *Proceedings of the National Academy of Sciences* **108**, 15342-15347 (2011).
303. Akbari, E., Spychalski, G.B., Rangharajan, K.K., Prakash, S. & Song, J.W. Competing fluid forces control endothelial sprouting in a 3-D microfluidic vessel bifurcation model. *Micromachines* **10**, 451 (2019).
304. Colgan, O.C. et al. Regulation of bovine brain microvascular endothelial tight junction assembly and barrier function by laminar shear stress. *American Journal of Physiology-Heart and Circulatory Physiology* **292**, H3190-H3197 (2007).
305. Bernardo-Castro, S. et al. Pathophysiology of Blood–Brain Barrier Permeability Throughout the Different Stages of Ischemic Stroke and Its Implication on Hemorrhagic Transformation and Recovery. *Frontiers in Neurology* **11** (2020).
306. Potente, M., Gerhardt, H. & Carmeliet, P. Basic and therapeutic aspects of angiogenesis. *Cell* **146**, 873-887 (2011).
307. Styp-Rekowska, B., Hlushchuk, R., Pries, A. & Djonov, V. Intussusceptive angiogenesis: pillars against the blood flow. *Acta physiologica* **202**, 213-223 (2011).
308. Fraisl, P., Mazzone, M., Schmidt, T. & Carmeliet, P. Regulation of angiogenesis by oxygen and metabolism. *Developmental cell* **16**, 167-179 (2009).
309. Ramírez-Bergeron, D.L. et al. Hypoxia affects mesoderm and enhances hemangioblast specification during early development. (2004).
310. Uno, K., Merges, C.A., Grebe, R., Luty, G.A. & Prow, T.W. Hyperoxia inhibits several critical aspects of vascular development. *Dev Dyn* **236**, 981-990 (2007).
311. Krock, B.L., Skuli, N. & Simon, M.C. Hypoxia-induced angiogenesis: good and evil. *Genes & cancer* **2**, 1117-1133 (2011).
312. Shan, F., Huang, Z., Xiong, R., Huang, Q.Y. & Li, J. HIF1 α -induced upregulation of KLF4 promotes migration of human vascular smooth muscle cells under hypoxia. *Journal of Cellular Physiology* **235**, 141-150 (2020).
313. Barrs, R.W., Jia, J., Silver, S.E., Yost, M. & Mei, Y. Biomaterials for bioprinting microvasculature. *Chemical Reviews* **120**, 10887-10949 (2020).

314. Jang, S., Collin de l'Hortet, A. & Soto-Gutierrez, A. Induced Pluripotent Stem Cell-Derived Endothelial Cells: Overview, Current Advances, Applications, and Future Directions. *Am J Pathol* **189**, 502-512 (2019).
315. Wiseman, E. et al. Integrated multiparametric high-content profiling of endothelial cells. *SLAS DISCOVERY: Advancing Life Sciences R&D* **24**, 264-273 (2019).
316. Heng, B.C. et al. Effect of cell-seeding density on the proliferation and gene expression profile of human umbilical vein endothelial cells within ex vivo culture. *Cytotherapy* **13**, 606-617 (2011).
317. Kilpinen, H. et al. Common genetic variation drives molecular heterogeneity in human iPSCs. *Nature* **546**, 370-375 (2017).
318. Manev, H. & Manev, R. 5-Lipoxygenase (ALOX5) and FLAP (ALOX5AP) gene polymorphisms as factors in vascular pathology and Alzheimer's disease. *Medical hypotheses* **66**, 501-503 (2006).
319. Newman, A.C., Nakatsu, M.N., Chou, W., Gershon, P.D. & Hughes, C.C. The requirement for fibroblasts in angiogenesis: fibroblast-derived matrix proteins are essential for endothelial cell lumen formation. *Molecular biology of the cell* **22**, 3791-3800 (2011).
320. Raybaud, C. Normal and abnormal embryology and development of the intracranial vascular system. *Neurosurgery Clinics* **21**, 399-426 (2010).
321. Gijtenbeek, M. et al. First trimester size charts of embryonic brain structures. *Human Reproduction* **29**, 201-207 (2014).
322. Mori, A. et al. Brain-derived neurotrophic factor induces angiogenin secretion and nuclear translocation in human umbilical vein endothelial cells. *Pathology - Research and Practice* **214**, 521-526 (2018).
323. Zacchigna, S., Lambrechts, D. & Carmeliet, P. Neurovascular signalling defects in neurodegeneration. *Nature Reviews Neuroscience* **9**, 169-181 (2008).
324. Wälchli, T. et al. Wiring the vascular network with neural cues: a CNS perspective. *Neuron* **87**, 271-296 (2015).
325. Wörsdörfer, P., Rockel, A., Alt, Y., Kern, A. & Ergün, S. Generation of vascularized neural organoids by co-culturing with mesodermal progenitor cells. *STAR protocols* **1**, 100041 (2020).
326. Dantzer, R. Neuroimmune Interactions: From the Brain to the Immune System and Vice Versa. *Physiol Rev* **98**, 477-504 (2018).
327. Li, Y.N. et al. The $\gamma 3$ chain of laminin is widely but differentially expressed in murine basement membranes: expression and functional studies. *Matrix Biol* **31**, 120-134 (2012).
328. La, J.-H., Feng, B., Kaji, K., Schwartz, E.S. & Gebhart, G.F. Roles of isolectin B4-binding afferents in colorectal mechanical nociception. *Pain* **157**, 348-354 (2016).
329. Sawai, T., Sakaguchi, H., Thomas, E., Takahashi, J. & Fujita, M. The ethics of cerebral organoid research: being conscious of consciousness. *Stem Cell Reports* **13**, 440-447 (2019).
330. Hyun, I., Scharf-Deering, J. & Lunshof, J.E. Ethical issues related to brain organoid research. *Brain research* **1732**, 146653 (2020).
331. Lavazza, A. 'Consciousnessoids': clues and insights from human cerebral organoids for the study of consciousness. *Neuroscience of Consciousness* **2021**, niab029 (2021).
332. Dehaene, S., Changeux, J.-P. & Naccache, L. The global neuronal workspace model of conscious access: from neuronal architectures to clinical applications. *Characterizing consciousness: From cognition to the clinic?*, 55-84 (2011).
333. Trujillo, C.A. et al. Complex oscillatory waves emerging from cortical organoids model early human brain network development. *Cell stem cell* **25**, 558-569. e557 (2019).
334. Reardon, S. Lab-grown 'mini brains' produce electrical patterns that resemble those of premature babies. *Nature* **563**, 453-454 (2018).
335. Koch, C., Massimini, M., Boly, M. & Tononi, G. Neural correlates of consciousness: progress and problems. *Nature Reviews Neuroscience* **17**, 307-321 (2016).
336. Lagercrantz, H. in *Seminars in Fetal and Neonatal Medicine*, Vol. 19 300-305 (Elsevier, 2014).
337. Birch, J. & Browning, H. Neural organoids and the precautionary principle. *The American journal of bioethics* **21**, 56-58 (2021).
338. Mashour, G.A., Roelfsema, P., Changeux, J.-P. & Dehaene, S. Conscious processing and the global neuronal workspace hypothesis. *Neuron* **105**, 776-798 (2020).
339. Merker, B. Consciousness without a cerebral cortex: A challenge for neuroscience and medicine. *Behavioral and brain sciences* **30**, 63-81 (2007).
340. Aru, J., Suzuki, M., Rutiku, R., Larkum, M.E. & Bachmann, T. Coupling the state and contents of consciousness. *Frontiers in Systems Neuroscience* **13**, 43 (2019).
341. Northoff, G. & Huang, Z. How do the brain's time and space mediate consciousness and its different dimensions? Temporo-spatial theory of consciousness (TTC). *Neuroscience & Biobehavioral Reviews* **80**, 630-645 (2017).
342. Lavazza, A. & Massimini, M. Cerebral organoids: ethical issues and consciousness assessment. *Journal of Medical Ethics* **44**, 606-610 (2018).
343. Giandomenico, S.L. et al. Cerebral organoids at the air-liquid interface generate diverse nerve tracts with functional output. *Nature neuroscience* **22**, 669-679 (2019).
344. Chen, H.I. et al. Transplantation of human brain organoids: revisiting the science and ethics of brain chimeras. *Cell Stem Cell* **25**, 462-472 (2019).
345. Żuradzki, T. Against the precautionary approach to moral status: the case of surrogates for living human brains. *The American Journal of Bioethics* **21**, 53-56 (2021).
346. Carvalho, C., Gaspar, A., Knight, A. & Vicente, L. Ethical and scientific pitfalls concerning laboratory research with non-human primates, and possible solutions. *Animals* **9**, 12 (2018).
347. Li, X., Xu, S., He, P. & Liu, Y. In vitro recapitulation of functional microvessels for the study of endothelial shear response, nitric oxide and [Ca²⁺]_i. *PLoS one* **10**, e0126797 (2015).

348. Zhang, B. et al. Biodegradable scaffold with built-in vasculature for organ-on-a-chip engineering and direct surgical anastomosis. *Nature materials* **15**, 669-678 (2016).
349. Zilberman-Rudenko, J. et al. Utility of microfluidic devices to study the platelet–endothelium interface. *Platelets* **28**, 449-456 (2017).
350. Lee, H., Park, W., Ryu, H. & Jeon, N.L. A microfluidic platform for quantitative analysis of cancer angiogenesis and intravasation. *Biomicrofluidics* **8**, 054102 (2014).
351. Folkman, J. & Haudenschild, C. Angiogenesis in vitro. *Nature* **288**, 551-556 (1980).
352. Kubota, Y., Kleinman, H.K., Martin, G.R. & Lawley, T.J. Role of laminin and basement membrane in the morphological differentiation of human endothelial cells into capillary-like structures. *The Journal of cell biology* **107**, 1589-1598 (1988).
353. Li, Y.-H. & Zhu, C. A modified Boyden chamber assay for tumor cell transendothelial migration in vitro. *Clinical & experimental metastasis* **17**, 423-429 (1999).
354. Sharma, D. et al. Upgrading prevascularization in tissue engineering: a review of strategies for promoting highly organized microvascular network formation. *Acta Biomaterialia* **95**, 112-130 (2019).
355. Park, T.H. & Shuler, M.L. Integration of cell culture and microfabrication technology. *Biotechnology progress* **19**, 243-253 (2003).
356. Wong, K.H., Truslow, J.G., Khankhel, A.H., Chan, K.L. & Tien, J. Artificial lymphatic drainage systems for vascularized microfluidic scaffolds. *Journal of Biomedical Materials Research Part A* **101**, 2181-2190 (2013).
357. Zheng, Y. et al. In vitro microvessels for the study of angiogenesis and thrombosis. *Proceedings of the national academy of sciences* **109**, 9342-9347 (2012).
358. Miller, J.S. et al. Rapid casting of patterned vascular networks for perfusable engineered three-dimensional tissues. *Nature Materials* **11**, 768-774 (2012).
359. Arakawa, C.K., Badeau, B.A., Zheng, Y. & DeForest, C.A. Multicellular Vascularized Engineered Tissues through User-Programmable Biomaterial Photodegradation. *Adv Mater* **29**, 10.1002/adma.201703156 (2017).
360. DiVito, K.A., Daniele, M.A., Roberts, S.A., Ligler, F.S. & Adams, A.A. Data characterizing microfabricated human blood vessels created via hydrodynamic focusing. *Data in brief* **14**, 156-162 (2017).
361. Kim, S., Chung, M., Ahn, J., Lee, S. & Jeon, N.L. Interstitial flow regulates the angiogenic response and phenotype of endothelial cells in a 3D culture model. *Lab on a Chip* **16**, 4189-4199 (2016).
362. Ritchie, S., Reed, D.A., Pereira, B.A. & Timpson, P. The cancer cell secretome drives cooperative manipulation of the tumour microenvironment to accelerate tumourigenesis. *Faculty Reviews* **10** (2021).
363. Paredes, I., Himmels, P. & Ruiz de Almodóvar, C. Neurovascular Communication during CNS Development. *Developmental Cell* **45**, 10-32 (2018).
364. Shin, Y. et al. In vitro 3D collective sprouting angiogenesis under orchestrated ANG-1 and VEGF gradients. *Lab on a chip* **11**, 2175-2181 (2011).
365. Wang, X. et al. Engineering anastomosis between living capillary networks and endothelial cell-lined microfluidic channels. *Lab on a Chip* **16**, 282-290 (2016).
366. Chung, S. et al. Cell migration into scaffolds under co-culture conditions in a microfluidic platform. *Lab on a Chip* **9**, 269-275 (2009).
367. Arrowsmith, J. & Miller, P. Phase II and Phase III attrition rates 2011–2012. *Nature Reviews Drug Discovery* **12**, 569-569 (2013).
368. Place, T.L., Domann, F.E. & Case, A.J. Limitations of oxygen delivery to cells in culture: An underappreciated problem in basic and translational research. *Free Radic Biol Med* **113**, 311-322 (2017).
369. Wang, X.-Y. et al. Engineering interconnected 3D vascular networks in hydrogels using molded sodium alginate lattice as the sacrificial template. *Lab on a Chip* **14**, 2709-2716 (2014).
370. Seo, H.-R. et al. Intrinsic FGF2 and FGF5 promotes angiogenesis of human aortic endothelial cells in 3D microfluidic angiogenesis system. *Scientific reports* **6**, 1-11 (2016).
371. Chan, J.M. et al. Engineering of in vitro 3D capillary beds by self-directed angiogenic sprouting. *PloS one* **7**, e50582 (2012).
372. Jeon, J.S. et al. Human 3D vascularized organotypic microfluidic assays to study breast cancer cell extravasation. *Proceedings of the National Academy of Sciences* **112**, 214-219 (2015).
373. Ko, J. et al. Tumor spheroid-on-a-chip: a standardized microfluidic culture platform for investigating tumor angiogenesis. *Lab on a Chip* **19**, 2822-2833 (2019).
374. Tasoglu, S. & Folch, A. 3D printed microfluidic devices. (MDPI, 2019).
375. Kalluri, R. The biology and function of fibroblasts in cancer. *Nature Reviews Cancer* **16**, 582-598 (2016).
376. Olanrewaju, A., Robillard, A., Dagher, M. & Juncker, D. Autonomous microfluidic capillary circuits replicated from 3D-printed molds. *Lab on a Chip* **16**, 3804-3814 (2016).
377. Mancuso, M.R., Kuhnert, F. & Kuo, C.J. Developmental angiogenesis of the central nervous system. *Lymphatic research and biology* **6**, 173-180 (2008).
378. Kabot, L., Worden, T., Matsushita, A., Hernandez, R. & Abramzon, N. Inquiry base experiment: The effect of plasma on glass surface properties. (2016).
379. Fritz, J.L. & Owen, M.J. Hydrophobic recovery of plasma-treated polydimethylsiloxane. *The Journal of adhesion* **54**, 33-45 (1995).
380. Tan, S.H., Nguyen, N.-T., Chua, Y.C. & Kang, T.G. Oxygen plasma treatment for reducing hydrophobicity of a sealed polydimethylsiloxane microchannel. *Biomicrofluidics* **4**, 032204 (2010).
381. Myoken, Y. et al. Vascular endothelial cell growth factor (VEGF) produced by A-431 human epidermoid carcinoma cells and identification of VEGF membrane binding sites. *Proceedings of the National Academy of Sciences* **88**, 5819-5823 (1991).

382. Leonidakis, K.A. et al. Fibrin structural and diffusional analysis suggests that fibers are permeable to solute transport. *Acta Biomaterialia* **47**, 25-39 (2017).
383. Yin, X. et al. Engineering stem cell organoids. *Cell stem cell* **18**, 25-38 (2016).
384. Oksdath, M. et al. Synthetic scaffolds to control the biochemical, mechanical, and geometrical environment of stem cell-derived brain organoids. *APL bioengineering* **2**, 041501 (2018).
385. Chen, C., Rengarajan, V., Kjar, A. & Huang, Y. A matrigel-free method to generate matured human cerebral organoids using 3D-Printed microwell arrays. *Bioactive Materials* **6**, 1130-1139 (2021).
386. Robinson, M., Douglas, S. & Michelle Willerth, S. Mechanically stable fibrin scaffolds promote viability and induce neurite outgrowth in neural aggregates derived from human induced pluripotent stem cells. *Scientific reports* **7**, 6250-6250 (2017).
387. Bezenah, J.R., Kong, Y.P. & Putnam, A.J. Evaluating the potential of endothelial cells derived from human induced pluripotent stem cells to form microvascular networks in 3D cultures. *Scientific reports* **8**, 1-14 (2018).
388. Hayer, A. et al. Engulfed cadherin fingers are polarized junctional structures between collectively migrating endothelial cells. *Nature cell biology* **18**, 1311-1323 (2016).
389. Wang, J. et al. The analysis of viability for mammalian cells treated at different temperatures and its application in cell shipment. *PLoS One* **12**, e0176120 (2017).
390. Jiang, S. et al. An Automated Organoid Platform with Inter-organoid Homogeneity and Inter-patient Heterogeneity. *Cell Reports Medicine* **1**, 100161 (2020).
391. Velasco, V., Shariati, S.A. & Esfandypour, R. Microtechnology-based methods for organoid models. *Microsystems & nanoengineering* **6**, 1-13 (2020).